

Compaction of Asphalt Road Pavements

Samenstelling promotiecommissie:

Voorzitter

Prof. dr. ir. H.J. Grootenboer

Universiteit Twente

Promotoren en assistent promotoren;

Prof. dr. ir. M.F.A.M. van Maarseveen

Universiteit Twente

Prof. dr. ir. A.A.A. Molenaar

Technische Universiteit Delft

Ir. M.F.C. van de Ven

Technische Universiteit Delft

Prof. dr. ir. J. Huetink

Universiteit Twente

Prof. dr. ir. A. van Harten

Universiteit Twente

Prof. dr. ir. E.C. van Berkum

Universiteit Twente

Dr. ir. C.A.P.M. van Gurp

Koac wegmeetsdienst

Publisher: H.L. ter Huerne, CT&M Department,
University of Twente, P.O. Box 217, 7500 AE, Enschede, the Netherlands

Cover: design: Lieske Stevens and Maarten van Bentum
Print: Febodruk BV, Enschede

H.L. ter Huerne, Enschede, 2004

No part of this work may be reproduced by print, photocopy or any other means without the permission in writing from the publisher.

ISBN 90-365-2027-4

Compaction of Asphalt Road Pavements

USING FINITE ELEMENTS AND CRITICAL STATE THEORY

PROEFSCHRIFT

ter verkrijging van
de graad van doctor aan de Universiteit Twente,
op gezag van de rector magnificus,
prof.dr. F.A. van Vught,
volgens besluit van het College voor Promoties
in het openbaar te verdedigen
op vrijdag 5 maart 2004 om 15.00 uur

door

Hendrikus Lodewikus ter Huerne

geboren op 12 april 1961

te Enschede

Dit proefschrift is goedgekeurd door de promotoren
prof.dr.ir. M.F.A.M. van Maarseveen
prof.dr.ir. A.A.A. Molenaar

en de assistent-promotor
ir. M.F.C. van de Ven

Preface

In September 1992 I started working at the University of Twente in the Civil Engineering and Management (CT&M) department. With an academic background in structural engineering from TU-Delft (Delft University of Technology), and experience working in the design of steel and concrete structures at DHV, it was more of a lateral move to the Traffic and Transportation group of the University of Twente. To apply the knowledge and techniques from the domain of structural engineering to areas such as: underground infrastructure construction, monitoring and maintenance of traffic and transport systems, and design renewal procedures for improving infrastructure

Due to increased travel demands, and increased environmental awareness, it is becoming increasingly difficult to construct by-pass lanes for maintenance. A maintenance regime was developed where work was done at night with partial lane closures. A relevant and interesting question then arose, concerning the technical suitability of roads that were constructed under such adverse conditions.

Upon beginning this investigation it was soon realised that to obtain meaningful results a comprehensive study had to be conducted into other adverse circumstances under which construction took place like cold weather, rain, time constraints, passing traffic, etc.. This expanded mandate was then followed for a couple of months before we realised that the compaction quality was an element that merited attention in its own right. We therefore began a detailed study into asphalt compaction and its effect on the quality of the final product.

Perhaps due to the fact that at this time a joint co-operation began with the Road and Railroad Laboratory (RRL) of André Molenaar at the TU-Delft, it became possible to follow the study of compaction due to the resources this co-operation availed. Together with the RRL group I investigated in great detail the processes of asphalt and I am grateful to all the members that assisted me where necessary. Although I came from Twente (a competing University) they treated me as a full member of their own group within a very brief space of time.

The start of the new project coincided with a crucial time for CT&M as it was defining its profile in terms of teaching and research direction. I recall a lot of discussion about the profile of the CT&M study and what the research should be exactly. I can still hear the voices of colleagues Kraan, Witbreuk, Jasperse, Bossink and others contributing or even arguing about which new areas our department would stand out in. These are pleasant memories that will always be dear to me.

This thesis project has involved several sub-projects. A significant part of these were done by students either as part of their practical training, master thesis projects and student assistantships. I am grateful to all the students who took on various elements of these sub projects and in doing so helped me achieve the main goal. To Rogier van Dee, Jeroen Roeloffzen, Erik van de Laan and also Hans van de Kooij I am grateful. Although not really a student I want to acknowledge Ad Klompenmaker. He is a very enthusiastic roller operator who sent me lots of letters about the merits of compaction processes of asphalt achieved by rolling.

I would also like to mention the companies that assisted me in completing this thesis. I want to mention Shell who mixed the used fake bitumen, DWW which shared with me a substantial amount of data about productions checks (DIAK data) and NBM which supplied the base materials for testing and for building the experimental compaction test section.

Additionally, I would like to acknowledge the support of friends and colleagues who contributed in various ways to this thesis project. In particular I want to thank my office-buddy and friend Maarten van Bentum, Collins Makoriwa, my sister Erna Rubens-ter Huerne and my wonderful brother-in-law Paul Rubens who made the English texts more readable. Also a big thank you to Gerrit Snellink who was always available to help out with any interesting job. Finally of course I would like to express my appreciation for the support of my thesis advisors Martin van Maarseveen, André Molenaar and Martin van de Ven. They were of great value in pointing out avenues to pursue and helping make this thesis what it is now.

I want to thank my parents who always made it possible to study, and also motivated me when necessary. To them some of my actions were associated with madness, but that possibly had more to do with my hobbies and who I am.

This thesis was born in a time of important changes in my personal life. Ali and I got married in 1992, about the time the thesis begun. Anne was born soon after our marriage and the move from Amersfoort to Enschede. My second daughter, Lotte joined us two years later. I now realise that doing a Ph. D. allows all these changes but has perhaps influenced the quality of time I spend with them. To Lotte, Anne and Ali, who missed a lot of hours that I should have spent with them completing this “boekje”, I promise to mend my ways. Thank you for your patience and love.

Enschede, 6 februari 2004

Table of contents

Preface	i
Table of contents	iii
Summary	v
Samenvatting	x
1. Introduction	1
1.1. The socio-economic relevance of roads	2
1.2. Practice of road construction in the Netherlands	6
1.3. The process of constructing roads	10
1.4. Towards improvement of the road construction process	17
1.5. Problem analysis, questions and scope	22
1.6. The research design	25
1.7. Outline of the thesis	28
2. Compaction of granular materials and Hot Mix Asphalt	31
2.1. Introduction	31
2.2. Compaction, the benefits and the way to achieve it	32
2.3. Quantities to determine compaction levels and compactibility	37
2.4. Resemblance HMA and unbound materials	45
2.5. Critical State theory	51
Summary	60
3. Modelling HMA material behaviour	61
3.1. Introduction	61
3.2. Modification of the Hveem Stabilometer	63
3.3. Conducting an MHSM test	71
3.4. Material measuring programme	77
3.5. Testing the MHSM suitability	81
3.6. The main test programme	88
Summary	99
4. A FEM analysis of the rolling process	101
4.1. Introduction	101
4.2. General FEM theory	102
4.3. Simulating rolling with FEM	111
4.4. FEM simulation of HMA compaction processes	119
Summary	131

5	The compaction test section.	133
5.1	Introduction	133
5.2	Experiments with a constructed test section	135
5.3	Analysis of the test section results	143
5.4	Estimation of VMA and temperature profiles of the HMA layer	160
	Summary	163
6	Results of the FEM analyses	165
6.1	Introduction	165
6.2	Simulation of an individual roller pass	166
6.3	Subsequent roller passes	181
	Summary	186
7	Conclusions and recommendations	187
7.1	Conclusions	187
7.2	Recommendations	189
7.3	Final conclusions and reflections	192
	Appendix A	195
	Appendix C	209
	Appendix D	211
	Appendix E	217
	Appendix F	219
	Appendix G	221
	Appendix H	225
	Appendix I	233
	Appendix J	237
	Appendix K	247
	Appendix L	249
	Appendix M	253
	Appendix N	263
	Appendix O	283
	Abbreviations and symbols	289
	References	293
	Curriculum Vitae	299

Summary

The past decades have shown an exponential increase in the use of the road network. The increased loading on road structures requires more frequent maintenance work, whereas on the other hand the demand for undisturbed traffic flows restricts the opportunity for doing roadwork. It is believed that these operating conditions can have a detrimental effect on the quality of roadworks. If this hypothesis is correct then the increased maintenance requirement in combination with a lower quality of work may result in a vicious circle of road network degradation.

At the beginning of this project the conditions under which roadworks in the Netherlands are executed was not clear. It was also not known whether these conditions affect the quality of the work. From preliminary work done during this project it was concluded that i.) a reasonable amount of roadwork carried out in the Netherlands is done under adverse conditions, and ii.) many of these conditions could have a detrimental effect on the quality of the road constructed.

The next step of the project investigated the effect of technical conditions on the quality of the final product. In terms of asphalt roads the following processes were discussed; production and transport of asphalt mixes, laying and pre-compaction of the layer and final compaction by different types of rollers.

A workshop with road technicians has been organised to estimate the magnitude of the effect of various aspects on the final quality of road construction. Based on the results of the workshop a causal model has been developed describing relevant variables and dependencies between these variables and indicating particular problem areas. This information proved to be very useful in the final design of the core of the project.

It was concluded that in practice the compaction process is the key element in establishing the final quality of the road. Compaction of asphalt is mainly based on experimental knowledge. From experiences with compaction of asphalt mixes gained in the past, one can estimate what results to expect when comparable mixtures are compacted under similar circumstances. If we operate outside the experience domain the results of compaction are uncertain. At present this is often the case since regularly roads are maintained under adverse conditions and new types of mixtures are being used.

The ability of simulating the compaction process for asphalt roads has several advantages. It allows one to estimate a priori under what conditions a particular mixture can be used. Moreover it provides an indication as to what rollers are suitable for specific mixtures and how the rolling process should be managed in order to reach

a desired compaction level. Finally, simulation can show the impacts of constructing under adverse conditions.

The objective of this research was *“to investigate whether it is possible to develop a tool that enables simulation of a compaction process of asphalt for construction of roads, and how this is best done”*.

The research therefore focuses on the compaction processes of asphalt and addresses the following issues:

- a.) identifying a constitutive model that is able to describe the behaviour of asphalt mixes during the compaction process (by studying the analogy with soil mechanics)
- b.) identification, design and composition of equipment that is able to quantify the parameters for a material model as a result of a.) and deduction of those parameters for an asphalt mixture by performing a laboratory test programme,
- c.) identification of a suitable FEM tool that is able to simulate the compaction process of asphalt by rolling while employing the relationships and parameter values resulting from a.) and b.),
- d.) validation of the simulation results using measurements from a compaction process of a test section.

Constitutive model

The constitutive model for asphalt is adopted from soil mechanics. A comparison between soil and asphalt (during compaction) is made. Both materials (mixtures) consist of solid particles, fluid (water or bitumen) and pores filled with air. During loading of the initially loosely compacted material the particle matrix changes (proximity of the particle skeleton) and air filled voids are driven out. The material compacts. The fluid in the mixture lubricates the contact surfaces between the particles and makes movement of the particles easier. The material behaviour can be characterised as elastic (until the particles start to move) and plastic (when the particle move). The critical state theory offers a model that, based on those particle movements, expresses a relationship between the specific volume of the material and the stress situation inside the material.

The behaviour of soil and asphalt indicates that, despite the differences in fluids involved (water does have a higher viscosity than bitumen even during compaction), the soil model is capable of describing the behaviour of warm asphalt materials during compaction.

The laboratory test programme

For quantification of the adopted material model one requires suitable equipment to measure the model parameters. Certain elements of the Hveem Stabilometer were selected as appropriate because during a test the equipment does subject the sample to load conditions that are very similar to the conditions the material experiences during compaction in the road. However, the Hveem offers only limited control on the volume of the sample during a test, and the load conditions (axial versus radial stress)

can change during the course of a test. Thus, as part of the project, a modification of the Hveem was developed to; i.) ensure better control with regard to the sample's volume during a test, and ii.) to maintain the ratio between axial and radial stress on the sample at a fixed level. The result of the modification process is referred to as the Modified Hveem Stabilometer (MHSM). By means of the MHSM a laboratory test programme is conducted to determine whether both the critical state model and the MHSM could be used for modelling and quantifying the properties of asphalt mixtures during compaction.

Unfortunately it is not possible to test hot samples inside the MHSM. However, by using bitumen particularly manufactured for this purpose, i.e. bitumen that at room temperature imitates common bitumen at compaction temperature, a laboratory measuring regime can be conducted and material parameters were obtained. The laboratory test programme contained:

- i. testing of mixtures with round and crushed sand,
- ii. testing of mixtures with more and less bitumen,
- iii. testing of mixtures at lower and higher temperatures (different bitumen viscosities),
- iv. testing of mixtures subjected to different loading combinations.

The results of the test programme have been analysed and where possible compared to known information on the behaviour of asphalt mixtures or known compaction mechanisms. In general the results obtained appealed to reason except for those from the experiment with the variation in temperature. The test results indicate that hotter mixtures (lower bitumen viscosity) are more difficult to compact. These results do contradict the engineering judgement; however, no literature addressing this issue could be found.

The compaction test section

The compaction test section was constructed to gather information for doing the FEM simulations and to be able to validate those simulations. The test section of 30 m length was compacted by using, in turn, either 8 or 16 passes of a static steel roller drum with a mass of 8 tonne. The test section consisted of two layers of Dense Asphalt Concrete 0/16 of ca. 50 mm thick after compaction. During compaction accurate temperature measurements were taken, and compaction progression was measured at 16 (layer thickness) plus 4 (nuclear density) positions. From the figures obtained an accurate course of the compaction progression as a function of the number of roller passes could be established. The values for bulk density and layer thickness were obtained from cores drilled after compaction was completed.. These values were used as a check for the previous readings.

During construction the material temperature was monitored at three levels inside the layer. The figures were used as an input for the FEM simulations. Two sub-sections of the test section were compacted at different material temperatures. The results were surprising; between both sub-sections there was no difference in compaction progression as a function of the number of roller passes. Again, material temperature

proved to have an unexpected effect¹ on the ease with which an asphalt mixture can be compacted e.g. hotter mixtures proved to be harder to compact.

FEM simulations

To develop simulations of the compaction process a FEM approach was used. With regards to the type of the problem and the material behaviour that has to be simulated, particular demands must be made on the approach. During compaction the material can suffer large deformations and also the contact between roller and drum must be correctly modelled. The material involved behaves partly as a solid and partly as a liquid. A suitable material model should be available for use inside the FEM. A suitable approach for the problem was the ALE method; a mixed approach between Eulerian (for modelling structural problems) and Lagrangian (for fluid mechanical problems). At the Twente University the DiekA application is often used as a FEM tool to do simulations of the rolling process of steel. Within DiekA a material model is implemented that was developed for describing the behaviour of soft rock. The model behaves reasonably similarly to critical state behaviour. For the plastic behaviour it is accurate, for elastic behaviour it could be improved. Further, it is possible to use within DiekA a rotated coordinate system for specific nodes and elements. This feature offers advantages when the rollers drum has to be modelled.

Results

A substantial amount of calculations were performed to find a suitable FEM set up. The simulations employed indicated the stress levels in the material in the vicinity of the roller drum. Other results obtained were: plastic strains of the material, material flow through the mesh (corresponding to the material speed caused by rolling), information about the contact properties between drum and asphalt (stress and size of contact surface), etc. The simulations gave a good insight in what happens inside the material as a result of static steel rolling. To keep the numerical process stable, the layer thickness reduction was pre-described in our calculations, instead of the subjected roller drum force as is the case in a real rolling process. Furthermore, because the elastic part of the Rock model did not correspond to the equivalent part of the critical state model, the ultimate validation, a comparison between test section and simulations achieved, could not be done.

The simulations of subsequent rolling passes also gave advanced insight in how compaction takes place during successive roller passes. Compaction progression can be expressed as a process of averaging. As a result of the first roller pass the most compaction progression takes place at a height where the stresses are the largest; in the upper part of the layer. The stiffness in the upper part of the layer also increased due to these high stresses. Therefore during the next pass a major part of the compaction progression occurs where the material is the most soft: low in the layer. During the third step major compaction progression takes place at the location where the material is still relatively soft and the stresses are relatively high; in the middle of

¹ An expected effect of material temperature related to compaction of asphalt mixtures would be that the hotter the mixture the more compactable it is.

the layer. This process repeats as compaction proceeds, however, the compaction progression becomes less and less. After a reasonable number of passes the compaction is more or less homogeneous throughout. This process is called a process of averaging.

Conclusions

The simulations tests and results in this work have enlarged the body of knowledge in the domain of asphalt compaction. However, there is no simulation tool readily available to deal with the compaction process of asphalt. The method developed in this research project is capable of simulating the compaction process of asphalt, but some topics or features of interest for further development or investigation are:

- i.) the effects of material temperature on compaction behaviour,
- ii.) implementation of a true critical state model inside a suitable FEM tool,
- iii.) modification of a FEM tool in such a way that numerical stable simulations of a force pre-described simulation is possible.

The simulations provide an insight into the compaction process and may be useful in the designing of new mixtures, new rollers, rolling techniques and rolling methods.

Due to the rigour involved in the techniques developed in this work the simulation tool should be applied for developing advanced procedures: procedures for compaction of specific mixtures, procedures for the selection of the roller and procedures for the specification of the roller process under specific working conditions. It would not be feasible to use this approach for any road construction job separately.

Samenvatting

Het gebruik van het wegennet is in de laatste decennia sterk toegenomen. Deze sterke toename in verkeersbelasting vraagt enerzijds om regelmatig onderhoud aan wegen, terwijl anderzijds de wens voor een ongestoorde verkeersafwikkeling de mogelijkheden voor wegonderhoud sterk inperkt. Het vermoeden bestaat dat daardoor wegwerkzaamheden vaker onder minder gunstige omstandigheden dienen plaats te vinden en dat hiervan een negatieve invloed uitgaat op de kwaliteit van het onderhoudsresultaat. Indien deze veronderstelling juist is kan de toegenomen vraag naar onderhoud en de mogelijk lagere kwaliteit van het onderhoudswerk leiden tot een negatieve spiraal voor de toestand voor het wegennetwerk

Om een indruk te krijgen of en in welke mate wegwerkzaamheden onder minder gunstige omstandigheden worden uitgevoerd en of deze omstandigheden doorwerken op de kwaliteit van het uitgevoerde werk is in eerste instantie een inventariserend onderzoek uitgevoerd. Uit dit onderzoek blijkt dat inderdaad een significant deel van het werk aan de weg in Nederland onder relatief ongunstige omstandigheden plaatsvindt, en dat deze uitvoeringsomstandigheden een negatief effect hebben op de kwaliteit van de wegverharding.

Vervolgens is nagegaan hoe de verschillende “technische” omstandigheden invloed uitoefenen op het ontstaan van kwaliteit. Het betreft de volgende processen: productie en transport van het asfalt mengsel, het spreiden van de laag, de voorverdichting door de balk en vervolgens de eindverdichting.

Met direct betrokkenen bij de uitvoering van wegonderhoud in de praktijk is een workshop georganiseerd om een inschatting te maken van invloed en orde grootte van de verschillende aspecten op de kwaliteit van het werk. Aan de hand van de resultaten van de workshop is een causaal model opgesteld, waarin de relevante variabelen zijn beschreven en de afhankelijkheden tussen deze variabelen en waarbij een aantal probleem gebieden in kaart zijn gebracht. De verkregen informatie is erg nuttig gebleken bij het definitieve ontwerp van de kern van dit onderzoek.

De conclusie was, dat in de praktijk het verdichtingsproces cruciaal is voor de kwaliteit van het eindproduct. Het verdichten van asfalt is hoofdzakelijk gebaseerd op ervaringskennis. Uit de ervaring opgedaan met het walsen van asfaltmengsels in het verleden weet men welk resultaat bij benadering mag worden verwacht zodra onder vergelijkbare omstandigheden met vergelijkbare materialen (mengsels) wordt gewerkt. Zodra echter “buiten het ervaringsgebied” gewerkt moet gaan worden, is het te verwachten resultaat onzeker. Tegenwoordig komt dit veelvuldig voor, omdat wegwerkzaamheden dienen plaats te vinden onder minder gunstige omstandigheden en omdat nieuwe mengsels regelmatig hun intrede doen.

Simulatie van verdichtingsprocessen van asfalt voor wegen heeft in dit opzicht een aantal voordelen. Simulatie kan a priori inzicht geven onder welke omstandigheden met een bepaald mengsel kan worden gewerkt. Verder kan worden aangegeven welke specifieke walsen geschikt zijn voor een bepaald mengsel en hoe het walsproces het best kan worden ingericht om een gewenst verdichtingsresultaat te bereiken. Tenslotte kan simulatie de invloed van ongunstige werkomstandigheden zichtbaar maken.

Het doel van dit onderzoek was *“te onderzoeken of het mogelijk is een instrument te ontwikkelen waarmee het verdichtingsproces van asfalt voor wegconstructies kan worden gesimuleerd, en op welke wijze dat het best gedaan kan worden”*.

Het onderzoek richt zich op verdichting van asfalt en behandelt de volgende onderwerpen:

- a.) Identificatie van een geschikt constitutief model voor het gedrag van asfalt tijdens het verdichten (door bestudering van de analogie met grondmechanica,
- b.) Vaststelling, ontwerp en samenstelling van apparatuur waarmee parameters voor het materiaalmodel voortvloeiend uit a.) bepaald kunnen worden en afleiding van de waarden van deze materiaal parameters door het uitvoeren van laboratorium proeven,
- c.) het selecteren van een geschikte Eindige Elementen Methode (EEM) waarmee onder gebruikmaking van model en parameterwaarden uit a.) en b.) de verdichting van asfalt door walsen gesimuleerd kan worden,
- d.) validatie van de simulatie resultaten aan de hand van metingen ontleend aan een verdichtingsproefvak.

Constitutief model

Het constitutieve materiaalmodel voor de beschrijving van het gedrag van asfalt is ontleend aan de grondmechanica. Een vergelijking heeft plaatsgevonden tussen het gedrag van grond en asfalt tijdens verdichting. Beide materialen (mengsels) bestaan uit vaste deeltjes, een vloeistof (bitumen of water) en poriën gevuld met lucht. Tijdens belasting van een initieel relatief onverdichte materiaal verandert de korrelrangschikking (de dichtheid van het deeltjesskelet) en hierdoor wordt de lucht uitgedreven. Het specifieke volume van het materiaal verandert en de dichtheid van het materiaal neemt toe. De vloeistof in het mengsel “smeert” de contactvlakken tussen de korrels en maakt het schuiven van de korrels ten opzichte van elkaar lichter. Het materiaalgedrag kan worden gekarakteriseerd als elastisch (totdat de korrels gaan schuiven) en plastisch (tijdens het schuiven). De critical state theorie biedt een model dat gebaseerd op de korrelverschuivingen, een relatie weergeeft tussen het specifiek volume van het materiaal en de spanningstoestand in het materiaal.

Bestudering van grond en asfalt geeft aan dat, ondanks de verschillen in de vloeistoffase (water heeft een veel lagere viscositeit dan bitumen bij verdichtingstemperaturen), het grondmechanica model goed bruikbaar zou kunnen zijn voor het beschrijven van het gedrag van asfalt tijdens de verdichting.

Test programma

Om het materiaalmodel te parametriseren is gezocht naar een geschikt meetinstrument. Gezien de eigenschappen van de Hveem Stabilometer (HSM) lag een toetsing van de mogelijkheden van het toestel voor dit onderzoek voor de hand. De HSM belast een proefstuk tijdens een test op een manier die in grote mate vergelijkbaar is met de manier waarop het asfalt tijdens de verdichting “in de weg” wordt belast. Echter, de Hveem biedt weinig controle over het volume van het proefstuk tijdens de test en ook de spanningscondities (axiale versus radiale spanningen) veranderen nogal tijdens de test. Als onderdeel van het onderzoeksproject is daarom de Hveem gemodificeerd waardoor i.) de volume controle van het proefstuk tijdens de test beter wordt gewaarborgd, en ii.) de opbouw van de primaire spanningen op het proefstuk nagenoeg lineair verloopt tijdens de test. Aldus ontstond de Modified Hveem Stabilometer (MHSM) en met dit instrument is een laboratorium meetprogramma uitgevoerd om te testen of zowel de MHSM en het critical state model geschikt zijn om het gedrag van asfalt tijdens de verdichting te beschrijven en te kwantificeren.

Met de MHSM kunnen helaas geen warme asfaltmengsels worden getest. Echter, door gebruikt te maken van een specifiek voor dit doeleinde gemaakt “bitumen”, een bitumen die bij kamertemperatuur een viscositeit bezit gelijk aan de viscositeit van een “normale” bitumen bij verdichtingstemperaturen, is een meetprogramma uitgevoerd en zijn materiaalparameters bepaald. Het meetprogramma omvatte:

- i. metingen aan mengsels met rond en gebroken materiaal in de zand fractie,
- ii. metingen aan mengsels met meer en minder bitumen,
- iii. metingen aan mengsels bij verschillende “temperaturen” (verschillende bitumen viscositeiten),
- iv. metingen aan een mengsel onderworpen aan verschillende spanningscondities.

De resultaten van het meetprogramma zijn geanalyseerd en waar mogelijk vergeleken met reeds bekende gegevens over het gedrag van asfaltmengsels of bekende mechanismen. Dit leverde over het algemeen een positief resultaat op met uitzondering van de metingen op de mengsels van verschillende temperaturen (iii). Uit de metingen aan de mengsels bleken de warmere materialen (lagere bitumen viscositeit) zwaarder verdichtbaar. Alhoewel bij de auteur geen literatuur bekend is die op dit specifieke punt uitsluitsel geeft, druist dit toch in tegen het gevoel dat is gebaseerd op praktijkervaring.

Het verdichtingsproefvak

Een verdichtingsproefvak is aangelegd om gegevens te verzamelen voor de simulaties en de resultaten van deze simulaties te kunnen valideren. Het proefvak was ca. 30 m lang en is verdicht met deels 8 en deels 16 passages van een statische wals met een massa van ongeveer 8 ton. Het proefvak bestond uit twee lagen asfalt DAB 0/16 van ca 50 mm dik ieder na verdichting. Tijdens verdichting zijn nauwkeurige temperatuurmetingen uitgevoerd, en is de verdichtingsprogressie gemeten op 20 posities, waarvan 16 laagdikte metingen en 4 (nucleaire dichtheid) posities. Uit de metingen kon nauwkeurig de verdichtingsprogressie als functie van het aantal walspassages worden bepaald. Na voltooiing van het proefvak zijn ter plaatse van de

meetpunten kernen geboord ten behoeve van controle van de laagdikte en dichtheidsmetingen.

Door het continu meten van de materiaalt temperatuur kon tevens vrij nauwkeurig het afkoelingsproces van het materiaal tijdens de verdichting op verschillende diepten in de laag worden bepaald. Deze gegevens werden gebruikt als invoer voor de EEM simulaties. Bewust zijn twee delen van de test sectie verdicht bij verschillende materiaal temperaturen. Uit deze resultaten bleek, zeer verrassend, dat voor beide vakken geen significant verschil in verdichtingsprogressie kon worden vastgesteld. Wederom bleek de materiaal temperatuur niet het verwachte effect² te hebben op het gemak waarmee een asfalt mengsel kan worden verdicht.

EEM simulaties

Voor het uitvoeren van de simulaties is gebruik gemaakt van een EEM benadering. Gezien de aard van het probleem en het te simuleren materiaalgedrag diende specifieke eisen te worden gesteld aan deze benadering: zo kunnen tijdens het walsen in het materiaal grote vervormingen ontstaan en verdient het contact tussen de walsrol en het te verdichten materiaal nadere aandacht. Het materiaalgedrag houdt het midden tussen dat van een vaste stof en het gedrag van een vloeistof. Dit vereist een specifiek materiaalmodel binnen EEM. Een geschikte EEM methode voor het probleem bleek de ALE methode: een gecombineerde methode tussen de Euler benadering (voor vloeistofmechanica problemen) en de Lagrangiaanse benadering (voor constructieproblemen). Als EEM tool is het pakket DiekA gebruikt, dat binnen de Universiteit Twente veelvuldig gebruikt wordt voor simulaties van het walsgedrag van staal. In DiekA is een materiaalmodel geïmplementeerd dat is ontwikkeld voor beschrijving van het gedrag van zacht gesteente. Dit komt redelijk in de buurt van critical state gedrag (voor het plastische deel) maar het gemodelleerde elastische gedrag komt helaas niet volledig overeen met dat van critical state. Bij aanvang van het numerieke werk werd het gebruikte materiaal model echter wel geschikt geacht; een constatering die later diende te worden bijgesteld. Verder beschikt DiekA over de mogelijkheid een geroteerd lokaal coördinatenstelsel te definiëren, een handige optie bij het modelleren van de walsrol.

Resultaten

Door gebruik te maken van de EEM software zijn vele berekeningen uitgevoerd om een geschikte EEM “set up” te bewerkstelligen. De uitgevoerde simulaties leverden een beeld op van de spanningen in het materiaal in de omgeving van de walsrol. Verder ontstond voortgaand inzicht in de plastische rekken in het materiaal, de stroomsnelheden van het materiaal door de mesh (gelijk aan de verplaatsingen van het materiaal door het walsen), en gegevens over het contactvlak (spanning en grootte) tussen de walsrol en het asfalt, etc. De simulaties leveren inzicht in wat er precies gebeurt in het materiaal als gevolg van statische verdichting. Als kanttkening dient te worden geplaatst dat, om het rekenproces numeriek stabiel te houden, wordt gewerkt

² Onder het verwachte effect wordt hier verstaan de in het algemeen in de wegenbouw gangbare gedachte dat naarmate het asfalt warmer is, het makkelijker kan worden verdicht.

met een opgegeven reductie van de laagdikte (voorgeschreven verdichtingstoename) in plaats van met een voorgeschreven walsgewicht. Verder was, doordat het elastische deel van het gebruikte Rock model niet correspondeerde met het elastische deel van het critical state model, de ultieme validatie, een vergelijking tussen testvak en simulatie niet goed mogelijk.

De simulaties van opeenvolgende walspassages geven in detail inzicht in hoe de verdichtingsprogressie in een laag plaatsvindt. De verdichtingstoename is te omschrijven als een soort middelingsproces. Tijdens de eerste walspassage vindt de meeste verdichtingsprogressie plaats op een hoogte in de laag waar de spanningen op het materiaal het grootst zijn: boven in de laag. Hierdoor neemt de stijfheid van het materiaal boven in de laag het meest toe. Als gevolg daarvan ontstaat tijdens de tweede stap de meeste verdichtingstoename op de plek waarop dat moment het materiaal het zachtst is: het meest onder in de laag. Tijdens de derde stap vindt de meeste verdichtingsprogressie plaats daar waar de druk relatief hoog is in combinatie met waar het materiaal nog relatief zacht is: in het midden van de laag. Dit proces gaat door totdat na een aantal walspassages de verdichting weer min of meer homogeen over de hoogte (dikte) verdeeld is.

Conclusies

In zijn totaliteit kan worden geconcludeerd dat de gemaakte simulaties en uitgevoerde testen een aanzienlijke verbreding en verdieping van inzichten hebben opgeleverd van het gedrag van asfalt tijdens de verdichting c.q. onder een statische stalen walsrol. Een alom toepasbaar gereedschap voor simulatie van verdichtingsprocessen van asfalt is evenwel nog niet beschikbaar. Wel geeft het onderzoek aan dat de ingeslagen weg een potentieel succesvolle weg is, alhoewel bepaalde opties nog nader dienen te worden ontwikkeld c.q. onderzocht. Nadere inspanningen dienen te worden verricht naar:

- i.) de effecten van materiaaltertemperatuur op het verdichtingsgedrag van asfalt,
- ii.) implementatie van een critical state model binnen een geschikte EEM code,
- iii.) het aanpassen van de EEM code DiekA om krachtgestuurde berekeningen te kunnen uitvoeren.

De simulaties bieden echter zeer veel inzicht en lijken welhaast onmisbaar in een veranderende wegebouwwereld waar nieuwe mengsels en nieuwe walsen en veranderende omstandigheden in de toekomst meer en meer werkelijkheid zullen worden.

Vanwege de noodzakelijke deskundigheid die nodig is voor het gebruik van de simulatie tool wordt toepassing vooral belangrijk geacht voor het ontwikkelen van geavanceerde procedures: procedures voor de verdichting van specifieke mengsels, procedures voor de selectie van de wals, en procedures voor de inrichting van het walsproces bij minder gunstige omstandigheden. Het lijkt weinig zinvol om deze benadering toe te passen voor elk afzonderlijk wegebouw project.

1. Introduction

Transport of people, cargo and information is crucial to our society. People should be able to make trips for their work, education, personal care, social events and recreation. Cargo should find its way to firms, shops and consumers. Mobility forms a crucial condition for the social and cultural development of humans and society. Infrastructure is an essential condition for prosperity and well-being. Mobility should be possible for all groups in society.

The road network represents an important social and economic value; we must ensure that it is maintained to a standard that it can fulfil its functions. However, despite all investments and effort and because of the intensive use of the road network there is still a lot of damage and road distress, leading to traffic accidents, economical loss and traffic jams (caused by road maintenance).

Continuous traffic growth has led to a dramatic increase in the amount of congestion. Congestion has strong adverse effects on society because of the lack of reliability and increased travel times. More traffic also causes a faster wear of the road pavements, which asks for a higher frequency of road maintenance. Maintenance, however, affects the availability of the road network and can contribute to even more congestion.

Research in road engineering materials resulted so far in a better understanding of which material composition should be used for particular applications. The production and paving methods of asphalt mixes have been improved over the last decades. However, it is still hard to realise road sections that are homogeneously constructed. This is because the production and construction processes are almost completely based on “engineering judgement”. Theoretical knowledge about material behaviour, during e.g. compaction, is limited and it is therefore hard to predict and manage (the effect of) a compaction process.

Since compaction has such a large influence on the quality of asphalt mixtures, knowledge on how to control the compaction process is very important. Unfortunately this knowledge is missing. This thesis therefore is a sound basis for further compaction studies. It focuses on compaction of asphalt pavements, and describes how a loose material behaves when compacted and how this behaviour can be modelled. It further discusses construction of a compaction test section. Furthermore, the results of compaction simulations by means of Finite Element tool are described. It is strongly believed that all this has resulted in a much better understanding of the compaction process.

In this chapter however we will deal with the exploration of the problem field and a justification of the compaction research. We will start with a short presentation of the socio-economic relevance of roads based on figures of traffic and transport in the Netherlands (1.1). The interaction between the use of the road network and the maintenance of it will be discussed. Then we continue with an inventory of the way construction work on roads in the Netherlands is being done and we identified if the way of working really matters (1.2). In section 1.3 the physical process of constructing roads will be examined. What are the important steps in the process

related to achieving quality? As a next step (1.4) we will focus more detailed on relations of the construction process by utilisation of the knowledge of practitioners in the road building industry.

In the second half of this chapter the set up of the research is discussed. Section 1.5 discusses the analysis of the problem, identification of the research objectives, the research questions and the scope and limitations of the project. Section 1.6, the research design, discusses the steps taken during the research to achieve the goal of the project. The last section (1.7) will discuss the outline of this thesis.

1.1. The socio-economic relevance of roads

The road network and the growth of traffic and transport on roads

In 2001 the Dutch administration presented the latest national traffic and transportation plan (Min. v VWS, 2001). It postulates that at the start of the 21st century humanity is more mobile than ever, that growth of mobility has not come to an end and probably will not end in the near future. The change in policy between the former (Min. v VWS, 1992) and the latter plan is that car mobility is tolerated more than ever before. Growth of car mobility is accepted, as part of modern society.

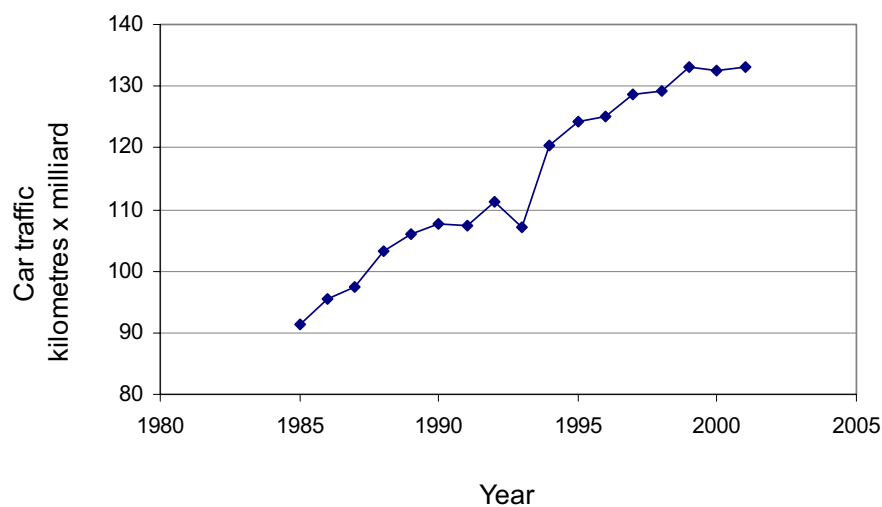


Figure 1.1 The growth of car kilometres in the Netherlands over the years 1985-2001 (SWOV, 2003).

For the NVVP study the Transport Research Centre of the Dutch Ministry of Transport, Public Works and Water Management (AVV) explored three scenarios in order to estimate the growth of traffic and transport in the following order; Divided Europe (DE), European Coordination (EC) and the Global Competition (GC) (Min. v VWS, 2001). The expected growth of slow traffic (bikes, pedestrians, etc.), public road transport and car traffic until 2020 are estimated for the three scenarios at respectively 19%, 29% and 22%, related to the reference year 1995 (1995 = 100%). Key factors for mobility growth were demographic, economic, technological and

spatial developments. The growth of traffic (car) kilometres over the years 1985-2001 is illustrated in Figure 1.1.

Besides the increase in car traffic, development of road cargo is also relevant. The growth of road cargo is almost comparable to the growth of car traffic. The AVV did explorative research into the growth of road transport by using the three earlier mentioned scenarios (DE, EC and GC). The EC scenario is the one that can be seen as “the most probable” if the Dutch and/or European authorities do not take any measures to regulate the growth of traffic and transport in any way.

Figure 1.2 illustrates the growth of road cargo that has occurred over the years 1994-2000. in the EC scenario the growth of road cargo is even more dramatic; it will double from 38 milliard tonne kilometre in 1995 to 76 milliard tonne kilometre in 2020.

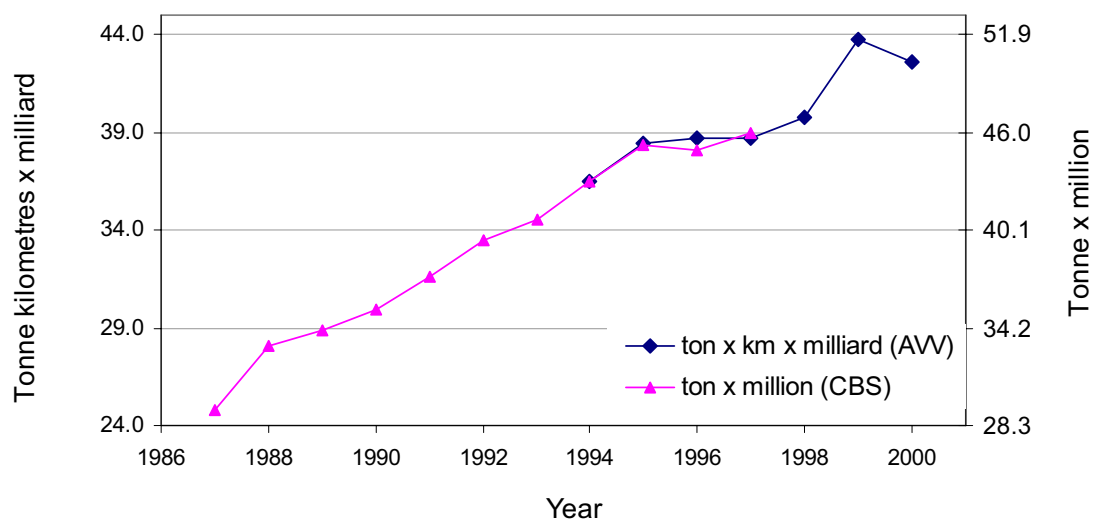


Figure 1.2 The growth of road cargo in the Netherlands over the years 1987-2000 (Min. v. VWS., 2002 and CBS, 2003).

The growth of traffic and transport became clear in the previous sub-sections just as the benefit of the infrastructure for the society. However to give idea about the number of roads and what they costs the society, some figures will be given.

In 1997 the total length of roads in the Netherlands was about 115.617 km (CBS, 2003). The length of motorways in the Netherlands was about 3188 km in 2001 (Min. v. VWS, 2002). In 1996 the distribution of roads over the different administrations was as follows; 3,206 km (2.8%) of the road length was under authority of the National Dutch administration, 6,910 km (6.1%) was under authority of the regional (province) administration and the remaining part 103,304 km (91.1%) was other (private or municipal administration). In the Netherlands still around 90% of the roads are paved with asphalt which number is not very different from other western countries in the world. In the United States for example 94% of the total amount of paved roads 3,466,000 kilometres are surfaced with asphalt (Asphalt Institute, 1989).

The replacement-value of the whole Dutch road network was in 1995 estimated at about 45 milliard Euro (Jacobs, 1995). In 2000 the money the government spent on road construction and maintenance was approximately 4.6 milliard Euro (CBS, 2003).

Because the road network is so important in social and economic terms, we must ensure that it is maintained to a standard that it can fulfil its functions. However, despite all investments and effort and because of the intensive use of the road network there is still a lot of damage and road distress, leading to traffic accidents, economical loss and traffic jams (caused by the road maintenance). It would be much more efficient if the number and frequency of distress and road maintenance works could be reduced. This would also improve the road safety and the availability of the road network to traffic.

Recent developments in road construction

In the last quarter of the 20th century there were many developments in the road engineering practice. Decker published in 1999 a paper that gives an overview of the developments in the road-engineering branch achieved in the years 1974 – 1999. Decker made clear that many mixture design methods, quality systems and all kind of new equipment were developed that can assist the road construction process. However, he also made clear that research that contributes to the production processes of HMA roads constitute a small minority related to the total amount of research and development.

It is widely accepted that for realisation of good HMA roads adequate compaction of the material is a prerequisite. In most of the research however, the attention is focussed on mechanical characteristics of the asphalt mix at an achieved compaction level, whereas for instance the compaction process itself and how to get a homogeneous compacted road section are underexposed and sometimes even absent¹.

The interaction between road use and road maintenance

In 2001 the total number of congestions was almost 35 thousand. About 1100 of them were caused by road works during the day while approximately 780 were caused by road works at night time. This means that about 1880 of the congestions (i.e. 5.4 percent) were caused by road maintenance works (AVV, 2002). To relieve this problem major maintenance road works are currently being planned outside traffic peak periods. Indeed, a lot of maintenance work is done at night and outside the season that can be marked as “favourable” for such a task. If the hypothesis is valid that these unfavourable conditions for road maintenance affect the quality of road construction in a negative way, then the frequency of road maintenance has to increase and a vicious circle could be born (Figure 1.3).

¹ With respect to asphalt compaction there exists one exception on this generality; the research done by Abd El Halim after a new type of a static roller called the Asphalt Multi-Integrated Roller (AMIR). The roller should avoid roller cracks and is based on the revolutionary Hot Iron Process Asphalt Compaction (HIPAC) principle.

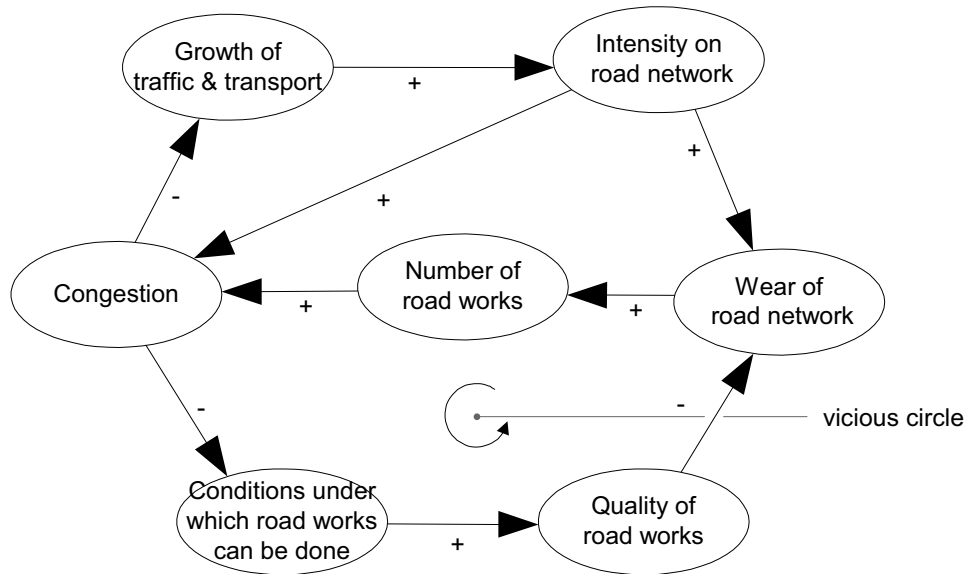


Figure 1.3 The interaction between traffic growth, the availability of the road network and road maintenance quality.

The shift of road maintenance works from day to night times causes a deterioration of labour conditions for the roadmen. Working at night also puts rigorous time constraints on the work itself. The work has to be finished before the morning rush hour starts. In many cases the work also has to be performed “under traffic”, putting even more stress on the roadmen. Road maintenance is coming increasingly “under pressure”, not just by the increase of traffic volumes but also because of a matter of poor planning by the road authorities. In the Netherlands there has always been an unequal spreading of maintenance works that are tendered over a calendar year. It results in discontinuity of work in stock for the contractors and considerable work pressure in the last few months of the calendar year. At these times the meteorological conditions for HMA paving are, in the Netherlands, usually unfavourable. These unfavourable conditions are a threat to the quality of road maintenance work.

Caused by the pressure on infrastructure, road network maintenance works are increasingly done at night, under less favourable weather conditions and under traffic. It is thought that these circumstances do affect the roadwork and therefore the quality of roads. The question remains whether it is possible to achieve good quality roadwork under these severe conditions? Because of this question it would be interesting to achieve better insight in the circumstances that affect (re-) construction processes of HMA roads.

Knowledge, however, of the construction process and the behaviour of the relevant mixtures during construction is still merely empirical and based on experience. When new material mixtures are introduced, or construction is shifted to outside the experience domain, such a change in the existing procedure(s) can result in undesirable effects and it is uncertain how to manage such situations.

If a contribution could be made to quality improvement (by being able to manage the construction process more efficiently) this would be an asset to a more efficient administration of a valuable treasure as the infrastructure network. It would be better

possible to find the balance between conditions of working and quality needed. In specific situations it might be the case that a small quality drop is preferable in exchange to long unavailability of (a part of) the road network. When better knowledge becomes available about the origination of quality during construction such decisions can be made on a more solid basis. Currently, the limited and empirical knowledge of the construction process itself seems to be the weakest link, in the strongly mechanised process of asphalt road engineering. It is probably extremely efficient to improve this weak link by further development of procedures, knowledge and/or tools.

To get better insight in this problem area of achieving higher quality relating to construction processes of roadwork, a pilot study was done looking into how and in what extent environmental (external) conditions can affect the quality of roadwork. It would be much better if the relationship between “conditions under which roadwork can be done ”and “quality of the roadwork” (see Figure 1.3), can be transformed in such a way that the interchanging parts are not a vicious circle (circle reasoning) anymore. The following paragraphs will focus on explorative information obtained on this issue.

1.2. Practice of road construction in the Netherlands

In the previous section it has been concluded that in the last decade a.) knowledge of methods of producing asphalt road constructions is still mainly empirical, and, b.) the pressure on road maintenance works has gradually been built up by various factors. Practitioners in the road building industry know that the quality of maintenance work strongly depends on the conditions under which the work is carried out. Furthermore they know that there is a strong correlation between achieved compaction level and the resistance of the road against failure. Therefore, in the first phase of this thesis a pilot inquiry, described in this section, and a workshop (section 1.4) have been organised to gain insight into the road building practice and to test these hypotheses.

The pilot inquiry contains two stages. In the first stage it has been investigated how often (substantial) road maintenance works are done under unfavourable conditions. This stage uses interviews and literature study and subsequently a simple causal model was built. In the second stage of the pilot it was investigated whether any evidence could be found that working under unfavourable conditions affects road quality.

It was assumed that a suitable approach to find out what really affects quality of road works was to combine three types of research: a.) field study, b.) interviewing branch organisations, and, c.) interviewing road administrations. In the field study three visits to road construction sites were made. In the Netherlands there are two large branch organisations (NVWB and VBW-Asfalt), both of which were interviewed on this topic. Finally the Dutch administration for road building works (DWW) was interviewed.

From the interviews and field research a simple theoretical model was developed (Figure 1.4). Originally we indicated that three categories of non-technical factors exist that can result in a quality decrease of road building works. The model describes

the relationships between the three categories of causal factors and quality specifications for constructing roads. The first category consists of extraneous factors, mainly meteorological conditions. They affect the construction process although these factors cannot be controlled. An example of such a factor is a “low environmental air temperature”. This condition cools the mixture rapidly, which may cause bad compaction. This category is called a “meteorological factors”.

The second category we will call “logistic factors”. It concerns the planning of work processes. Just like the extraneous factors they have a direct effect on the process of construction. However, these “logistic factors” can be affected by several factors surrounding the planning stage and the implementations stage. An example is “discontinuity in the HMA transport from the plant to the site”. This may cause an adjustment of the driving speed of the paver, and thereby result in discontinuities in the pre-compaction stage.

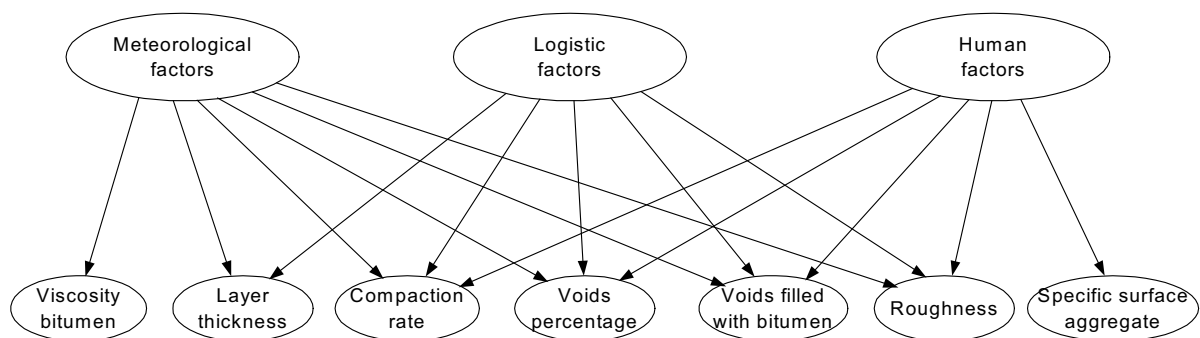


Figure 1.4 The relation between several clustered factors during compaction and quality specification at a global level, (Ter Huerne, 1996).

The third category consists of “human factors”. These factors are related to working conditions, and the impact that these conditions have on the physical, emotional or psychological state of the road workers. They have an indirect impact on the construction process since the well-being of the worker has an effect on his/her work. The effect depends on the person involved and therefore can vary substantially. For example, work stress can cause a paver operator to drive at a high speed. Given the nature of the screed this can easily result in less pre-compaction. When the available set of rollers on site is not adjusted to that lower pre-compaction level, then there might arise a problem. More details and examples about these categories and their relation to quality specifications can be found in Ter Huerne (1996).

Additionally, based on the model illustrated in Figure 1.4, two topics were considered:

- a. how often do road works take place under adverse circumstances in the Netherlands
- b. does working under adverse conditions really deteriorate the quality?

How many road works are achieved under adverse conditions?

In 1995 a preliminary investigation was done at the University of Twente to examine under what conditions road works are constructed in the Netherlands. The objective of that investigation was “quantification of the circumstances under which road (maintenance) works are done”. The investigation only looked at roads that are owned by the Dutch government. The roads that were investigated were categorised into three groups:

- motorways with an intensity larger than 40.000 vehicles a day (i.e. high intensity),
- motorways with intensity less than 40.000 vehicles a day (i.e. low intensity),
- dual carriage ways (i.e. major roads).

A sample was drawn from all road sections on which maintenance was completed in between 1992 and 1995. In 1995 the Dutch road administration consisted of 8 districts and 26 regional divisions (AVV, 1995). Three of these regional divisions were selected as a representative sample. From each of these three regional divisions about 6 roadwork projects were selected. Altogether the sample contained 19 road sections which were analysed for the 3 previously mentioned categories of roads. We were mainly interested to see under what conditions the road maintenance work was carried out. Part of the analysis was: a.) whether the work was done at day or at night, b.) whether the work was done while the road was completely free of traffic or whether the work was done “under traffic”, and c.) whether the work was done under favourable or unfavourable weather conditions. The results of the analysis are expressed in Table 1.1.

INVENTORY OF CONDITIONS OF ROADWORK	
Conditions while paving	Percentage of the work
At night time	56%
At daytime	44%
Under traffic	100%
Without traffic	0%
Shower	17%
Wind speed (m/s) above temperature (°C)	6%

Table 1.1 Circumstances under which roadwork is carried out in the Netherlands between 1992 and 1995, (Ter Huerne, 1997).

The results indicate that 56 percent of the road works were constructed at night. The timing of the work depends on the type of the road and the intensity of the traffic. On motorways with a high intensity of traffic, road works were always carried out at

night. On motorways with low traffic intensity approximately half of the work was carried out at night and on dual carriageways that percentage was 17%.

For all the selected sections (19) road works were done “under traffic”, which means that part of the road was closed to allow roadwork to proceed (traffic was diverted). In 17 percent of cases it was raining while paving work was going on whereas in 6 percent of cases the wind speed in m/sec was higher than the environmental temperature² in °C. Until 1995 these circumstances were noted in the legislation as not very suitable for doing paving jobs.

Effects of roadwork construction under unfavourable conditions.

From the model illustrated in Figure 1.4, hypotheses were extracted. In order to test these hypotheses, information from a project enforced by the Road and Hydraulic Engineering Institute of the (Dutch) Directorate General of public Works (DWW/RWS) was used. In 1994 they recorded data about the quality of the work that was completed from 1991 to 1993. They used data from five road reconstruction projects with a paving area bigger than 40.000 square meter. Besides all kind of other information they also recorded road quality specifications from drilled cores and circumstances under which the road construction work was done. There are 339 records of information available about construction circumstances. From 237 records the information from cores available was: voids content, bulk density, Voids Filled with Bitumen (VFB) and compaction level. Information from different sources had to be linked. After linking these sources there were 192 records available with both core information and construction conditions information. However, inside these 192 records, different (i.e. not comparable) mixtures were used (DAC, porous asphalt etc). There was no information available on the roughness and evenness of the road after rolling was finished. After grouping the different materials logically, 12 to 20 records remained for testing the following hypotheses:

- H1 Meteorological circumstances do significantly affect the quality parameters for compaction level, voids percentage filled with bitumen and the voids percentage.
- H2 Achieving road works “under traffic” does significantly affect the quality parameters for compaction level, voids percentage filled with bitumen and the voids percentage.
- H3 Achieving road works at night does significantly affect the quality parameters for compaction level, voids percentage filled with bitumen and the voids percentage.

Lower compaction level

The average compaction level of the sections paved at poor meteorological conditions proved to be 1.6 percent lower than the road sections paved under good conditions.

² It is clear that mathematical it is not correct that a wind speed in m/sec is compared to a temperature in °C. However, until around the 90's this was a commonly used rule of thumb for judging if the weather conditions were suitable for doing a HMA paving job.

Due to the small sample size and the standard deviation of the measures the difference is significant at a reliability level of 87 percent.

Further testing hypothesis H2 and H3 proved that road works done at night and “under traffic” do achieve a 2.0 percent lower compaction level than equal sections paved during the day and without traffic. In combination with the size of the sample and the standard deviation in the obtained results this takes the reliability level of the statement to 95 percent. Both hypotheses must be tested simultaneously because in our sample there was a full correlation between the category road works done at night and road works done “under traffic”. Therefore the responsible factor (working at night or working “under traffic”) for the lower compaction level could not be discriminated. A correlation between environmental conditions and the time of paving (day/night time) seems reasonable (possible) but is not tested here. It is recommended to check this in future research works.

1.3. The process of constructing roads

In the previous section it was shown that high traffic volumes put additional pressure on road maintenance works. Road maintenance activities are today carried out in off-peak periods. Common belief in the road construction industry is that building or maintaining roads under varying conditions does have an effect on the quality of work. In section 1.2 it was shown that already in the period 1992-1995 a substantial amount of roadwork was performed under less favourable conditions. This situation has only worsened. A statistical analysis indicated a correlation between the conditions during paving and the corresponding quality of the construction. Furthermore, because it is thought that a significant part of decreasing road quality does originate on site during road construction, it is useful to study construction and maintenance processes of asphalt roads in more detail.

Production process of (re-)constructing asphalt roads.

The process of constructing HMA roads consists of different stages: production of the mixture, transport of the mixture to the site, possibly cold milling of (a part of) the old construction, spraying of a tack coat, filling remaining cracks (if necessary), paving of the new material, manually correcting the spread material (if necessary), compaction of the layer, and finally splitting the fresh asphalt surface. All the process steps will be discussed, and, because this project focuses on compaction, this will be discussed in particular.

Factors affecting the compaction process

The mixing temperature of the asphalt concrete is determined by the requirements for achieving dry aggregate, for good particle coating, and for paving and compacting. The contractors ask for a mixture as hot as possible; it is important to minimise cooling of the mixture during transport and transshipment. It is also important to avoid local temperature differences in the bulk material. A hot storage silo is used to store the production of hot mix temporarily before being hauled.

Trucks are used to transport the mixture to the site. The bodies of the truck bed should be insulated and covered if necessary to maintain the mixture temperature within specification requirements. As a rule, the asphalt mix that has been brought to the paving site is deposited directly into the paver. Allowable mixture temperatures can be found in the RAW Standard Conditions of Contract for Works of Civil Engineering Construction, 2002. Good planning of logistics and fine-tuning of transport capacity to paving capacity are crucial for achieving an even working temperature in the paver. A homogeneous material temperature is a prerequisite for homogeneous pre-compaction and spreading of the material. During transshipment of the material (from the silo into the truck and from the truck into the paver) slight segregation may take place, which affects the quality of the construction negatively.

When paving a new HMA layer on an existing road construction a tack coat (usually emulsified bitumen) has to be used to ensure a good bond between the new and the old layer. The three essential requirements of a tack are: it must be very thin, it must cover uniformly the entire surface of the paved area, and it must be allowed to break or cure before the hot mix asphalt is applied. A light tack coat does no harm and bonds the surfaces, which is needed for adequate road construction. Tack coats, having a surplus of bitumen over the surface, may form a slip plane. It deteriorates the bearing capacity of the construction and may harm compaction because the bottom of the new (upper) layer meets little frictional resistance against movements.

There are several reasons for applying an overlay on an existing road pavement. If the surface of the new layer has to be smooth, then the surface of the lower layer has to be smooth as well. To ensure smoothness of the base, milling may be necessary. Proper milling can increase homogeneity of the thickness of the new layer, which is a prerequisite for achieving a homogeneous compaction level.

Laying and pre-compaction

Laying of a new asphalt layer is done with a paving machine. A paver, as shown in Figure 1.5 is the prime mover that receives the mixture from the truck, stores it on board and has a conveying system that transports and dumps it on the prepared surface. The paver comprises a tractor part and a screed unit. The most critical feature of the paver is the self-levelling screed unit, which determines the profile and pre-compaction level of the material being placed. The main forces that determine the level of the screed are speed of the paver, the resistance of the material under compaction and the weight of the screed. Detailed aspects that affect the screed level can be found in NCAT (1991). Compaction force from the screed can be applied by tamping bars or vibrators or both. The HMA in front of the screed is loose whereas the material discharged behind the screed is already reasonably compacted. The screed weight plus its vibrating and tamping energy which it imparts, produces an increase in density. In order to make adjustments in the thickness of the material, there is a screed depth crank at the rear end of the screed, which can be lowered or raised. Electronic measuring and adjustment systems continuously control the level of the paved layer.

Homogeneity of pre-compaction level and layer thickness are sensible for the “stiffness” of the material being placed. Non-homogeneities of mixture resistance (caused by mixture composition and temperature), varieties in paving speed, varieties in layer thickness and screed adjustments may cause variations in compaction achieved by the screed.

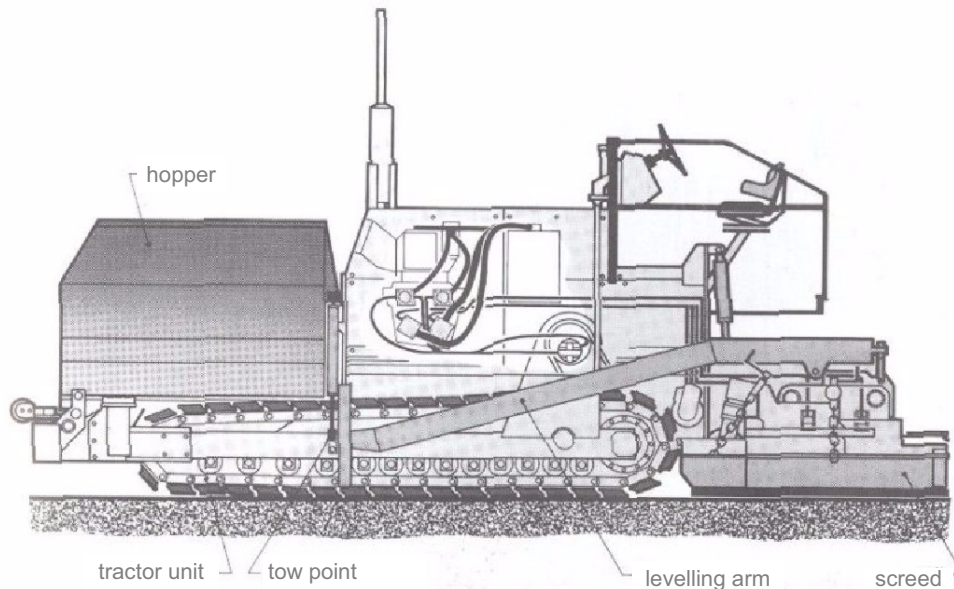


Figure 1.5 A schematic view of a paver, containing a hopper, a screed and tractor unit (VBW, 2000).

The pre-compaction level achieved by the screed only partly affects the final level of the achieved compaction layer. This final compaction level is primarily determined by rolling. Adequate pre-compaction is important for the final smoothness of the upper surface, since the rolling process starts on a more stable layer. If pre-compaction by the screed is low, more compaction effort is needed by rolling to meet the required level of compaction. If the available rolling equipment is just sufficient, then poor compaction may be the result at local spots (because of unavoidable in-homogeneity in compaction effort applied), which results in inferior final compaction. A variety in pre-compaction level achieved by the screed usually also produces varieties in the final compaction level.

Finally it may be mentioned that equipment producers in screeds do innovate their equipment in order to achieve higher pre-compaction levels. So producers of paving equipment recognise the importance of pre-compaction.

Compaction process

Compaction reduces the volume of air in the HMA mixture through the application of external forces. The expulsion of air enables the mix to occupy less volume, thereby increasing the density of the mass. Self-propelled compactors provide these external forces that deliver the compaction energy. Usually a compaction train consists of more rollers the objectives of which are:

1. to achieve the required density to meet the specifications,
2. to provide a smooth surface.

These objectives can be met by the use of different types of rollers. The choice of roller depends on the type of job: e.g. construction or maintenance, the compactibility of the mixture, the width of the roller, the width of the paving lane, the speed of the roller and the cooling rate of the material.

Roller types available for HMA compaction can roughly be divided into three categories; static-steel-wheel rollers, vibratory-steel-wheel rollers and pneumatic-tire rollers. The term static/vibratory relates to the nature of the drums connected to the roller. In vibratory rollers an unbalanced mass is mounted inside the drum, which causes the drum to work as a hammer on the asphalt, which can improve the compaction effect substantially. Both types of steel-wheel rollers are quite common in the Netherlands whereas the pneumatic-tired roller is only occasionally used.

Static-steel-wheel rollers

As a rule static-steel-wheel rollers are of the tandem or three-wheel type and come in a variety of weights and configurations. The three-wheel tricycle rollers weigh between 8 and 14 tons. The two rear wheels are between 1.40 and 1.75 m in diameter and between 0.46 and 0.51 m in width. The front wheel is between 1.0 and 1.20 m in diameter and between 0.85 and 1.10 m in width. This roller is often used as a breakdown roller in the initial part of the rolling operation. Its main advantage is the ability to apply high pressure due to the large back wheels. The diameter and pressure between the front and rear wheels differ considerably. This may cause large differences in compaction progression achieved by both wheels. There is a small overlap between the track of the front and rear wheels. Tandem rollers are two axle rollers where both drums have the same width. They weigh between 5 to 14 tons and can be ballasted to add weight. Usually, the drums vary from 1.22 to 1.52 m in diameter and are 1.07 to 1.40 m width. A three-wheel static steel roller is shown in Figure 1.6.



Figure 1.6 A three wheel static steel roller (VBW, 2000).

The contact pressure between the steel drum and the HMA mixture being compacted determines the actual compaction effort supplied by steel-wheel rollers. The diameter of the drum and the depth of penetration of the drum into the HMA material determine the contact area. If the penetration depth increases for a given roller, the contact pressure decreases since the contact area is larger. For a given contact pressure, larger drums have lower angles of contact than smaller drums. Since larger drums have smaller contact angles, they also have a lower component of horizontal force that tends to push against the material being compacted. During the rolling the drums of steel-wheel rollers become slightly sprayed with water to avoid adherence of the asphalt mix to the drum.

Vibratory steel-wheel rollers

Vibratory rollers are the only type of HMA compactors that have a dynamic load component and are lighter than non-vibratory steel-wheel rollers. The total, compactive effort is the sum of the static and dynamic loads. Geller (1984) reports that vibration reduces the mechanical friction between the particles during compaction. This may result in an increased mechanical interlock afterwards. The vibration is especially effective to harsh mixtures, mixtures that express high volume concentrations of coarse aggregate. Vibratory rollers can be far more effective than static steel-wheel rollers, but on the other hand they require more operator discipline in carrying out the roller pattern. Selecting the incorrect (dynamic) force level, rolling too fast, and making too many passes with the vibrator engaged can cause problems because a too heavy load on the soft material can cause shearing of the material (fissures). In general the vibratory roller is produced as a tandem compactor. The roller can then be used in both the static and the vibration mode. A tandem roller is shown in Figure 1.7.



Figure 1.7 A static or vibratory steel wheel tandem roller.

Pneumatic-Tired Rollers

Nowadays it is assumed that Pneumatic-Tired Rollers (PTRs, see Figure 1.8) achieve better kneading action to the HMA than steel drum rollers do. Typical configurations of PTRs provide 4, 5, 6 or 7 tyres on the front of the roller and 3, 4, 5 or 6 tires on the rear with the rear tire aligned in such a way that compaction of the material passing between the front tires is provided. The tires are smooth, i.e. they have no tread and the wheels are individually mounted to the frame of the roller. For compaction purposes the tire inflation pressures of the PTR should be as high as the behaviour of the HMA will permit without severe rutting which could be difficult to remove by the finish roller. PTRs can be used for breakdown or intermediate rolling. In the breakdown mode, PTRs usually cause deformation that may or may not be removed with finish rolling. Therefore, the mix behaviour determines whether a PTR can be effectively used as a breakdown roller. Traditionally PTRs have been used in the intermediate position. PTRs are reported to offer several advantages when compacting dense graded HMA:

1. they provide a more uniform degree of compaction than steel-wheel rollers,
2. they provide a tighter, more dense surface, and thus decrease the permeability of the layer,
3. they provide increased density that in many occasions cannot be obtained with steel-wheel rollers,
4. they compact the mixture without causing checking and they help to remove any checking that is caused with steel-wheel rollers.



Figure 1.8 A Pneumatic Tired Roller compacting an asphalt road mat (VBW, 2000).

The AMIR or HIPAC compactor.

Commonly, in order to compact asphalt for building roads, use is made of compactors with steel roller drums. However, it is thought that the incompatibility of the hard, round steel drum and the soft, flat asphalt pavement should be the cause for roller cracks. Because steel drums are round, only a very small area of contact is presented to the asphalt surface for compaction. As the roller travels along the pavement, the

asphalt in front of the drum is pushed ahead, causing a pulling force in the asphalt behind the drum. This pushing and pulling action should cause the asphalt to crack. To avoid roller cracks when rolling HMA for compaction, around 20 years ago a revolutionary type of compactor has been developed. It was the Asphalt Multi-Integrated Roller (AMIR) based on the Hot Iron Process Asphalt Compaction (HIPAC) principle see Figure 1.9.

An AMIR/HIPAC roller replaces the cylindrical stiff shaped roller drums with a moving flat, soft plate (a wide rubber belt around the cylinders) that should produce a crack free asphalt layer because of the uniform compaction surface along and across the mat. The AMIR/HIPAC compactor applies its compaction energy to the asphalt mix in a way that differs from existing vibratory, pneumatic or static steel rollers. The rubber belt should, because of the continuous contact, load the mat, 30 times longer than a steel roller drum and should apply a lower loading stress. It is claimed that, although this type of compactors work with very little contact pressure, they can easily meet the demands on required compaction level.



Figure 1.9 A roller built in accordance with HIPAC specifications (Abd El Halim, 2004).

After final compaction

Compaction is finished when the required compaction level is achieved. Now the road construction should cool down to the environmental temperature and when necessary a split layer for skid resistance should be added and/or lines should be drawn. Nevertheless both measures do not affect bearing capacity. The road construction is finished now.

1.4. **Towards improvement of the road construction process**

The pilot inquiry, discussed in section 1.2, revealed how serious the impact of the conditions during construction could be for the quality of the mixture produced. The production process of asphalt roads was discussed in section 1.3. Both sections show that in the production process the produced road quality can be affected significantly, both positively and negatively. It has been argued that better knowledge of the (in-between) factors and their mutual relationships can lead to a substantial improvement of the asphalt road specifications.

Because of a lack of literature on road construction processes in practice a workshop was organised to investigate which variables are really important during (re-) construction processes of asphalt roads. Since road construction processes in practice are strongly based on experience, a broad group of practitioners was invited to the workshop to discuss quality control during HMA road construction. In the workshop the focus was also on how circumstantial conditions during road construction can affect quality.

Organisation of the workshop

The workshop was organised with the following objective; *“utilisation of knowledge of professionals relating to road construction processes”*. In section 1.2 three categories of causes are distinguished that can have an impact on road quality during construction. The workshop took place, all day from 9.00 till 17.00 hours. It turned out that it took a complete day working it to model all effects of one group of causal factors (i.e. about one third of the global model as illustrated in Figure 1.4). It was decided to focus primarily on working “during unfavourable weather conditions” because in this category causal relationships could be derived with most certainty. It is believed that severe meteorological conditions during paving HMA’s result in an accelerated cooling of the mixture under construction. Specialists assume that this accelerated cooling results in a lower compaction result.

The following officials were selected to attend the workshop; a foreman, a screed operator, a roller operator, a consultant, a quality control supervisor, and a desk officer of DWW (i.e. the Dutch road administration).

Approach

The workshop started with a short briefing on the topic of the research, the relationship between the workshop and the project, and the approach that ideally should be followed during the day. At first an inventory was made of the causal variables that can affect the road quality and of the indicators of relevant road quality specifications. All the variables (causes and specifications) were written on cards, one variable per card. During the session the cards were glued on a wall in a specific order, the causes were positioned at the upper part of the wall and the specifications at the lower part. The position of the cards could be changed easily if necessary. In the next stage relationships between the variables were identified. Where necessary in-between variables or factors were defined. Following this procedure, a model was

built that expresses the effects of unfavourable conditions on the quality of roadwork under construction.

Discussion of the results

Although the focus was on constructing asphalt roads under unfavourable weather conditions and the effects on road construction quality, the attendees translated this in a relationship between material temperature and achieved compaction level. This opinion was based on the assumption that unfavourable weather conditions do primarily affect the temperature of the material as well as the material workability and the achieved compaction level. The final compaction level was seen as the most important element for quality of an asphalt road construction.

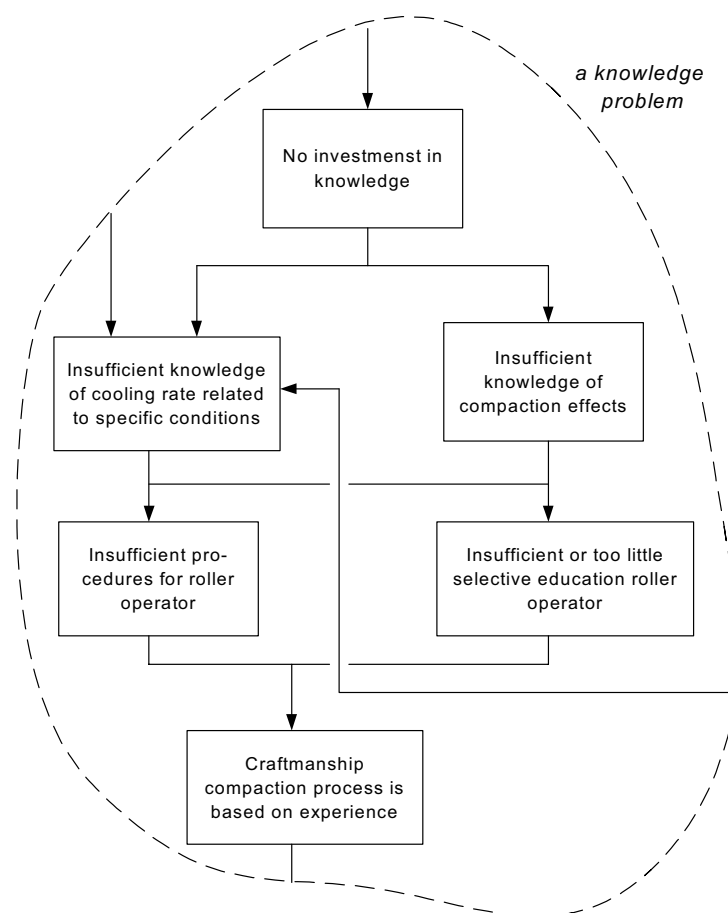


Figure 1.10 Listing of effects that can occur when working under severe conditions, and their causal relations; a knowledge problem. This knowledge problem represents a set of variables selected from the workshop model, see appendix A.

After the workshop the first concept of the model was worked out in detail and this version of the model has been sent to all participants, together with a questionnaire focussing on potential obscurities. Based on the reactions of the attendees the model was improved. The final version of the model contained 58 variables and 89 modelled relationships. The model is illustrated in the appendix A.

Inside the model “problem areas” can be defined. These problem areas consist of a coherent set of variables. An example of such a problem area is presented in Figure 1.10. This problem area indicates how (along which route) the participants think that “no investment in knowledge” can lead to “craftsmanship of the compaction process is based on experience”.

The argumentation for this problem area can be described in more detail as: the problem of not achieving the required compaction level arises because the roller operator does not know how far compaction has progressed during the rolling process. He (or she) also does not know how workable the mixture exactly is, and what the temperature of the material is. Therefore the task of achieving the target compaction level is carried out based on “experience”.

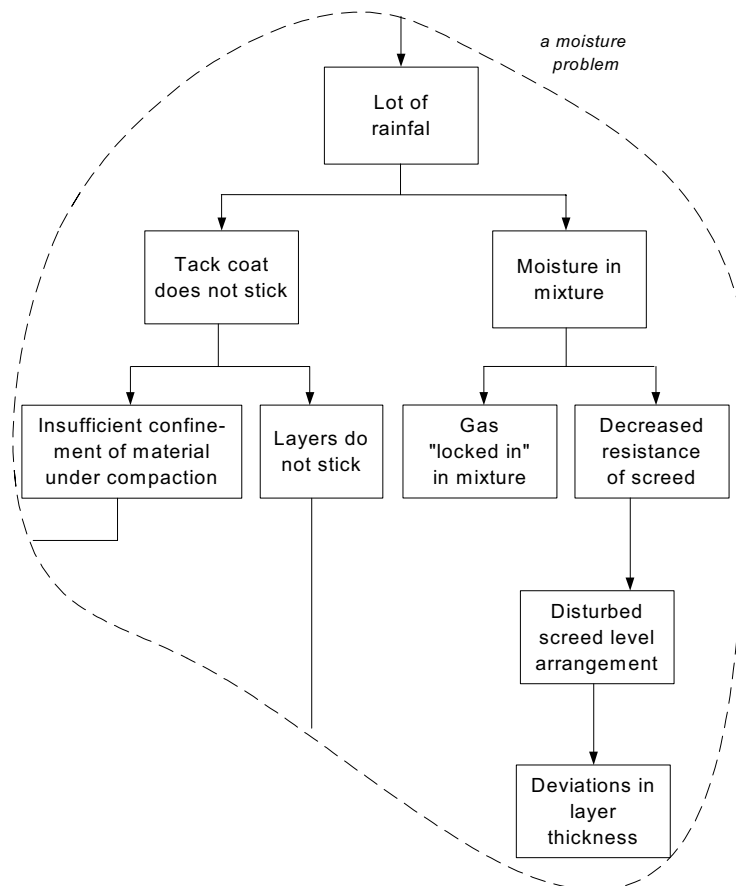


Figure 1.11 Listing of effects that can occur when working under severe conditions, and their causal relations; a moisture problem. This moisture problem represents a set of variables selected from the workshop model, see appendix A.

When the roadwork is achieved under normal conditions such an approach can work satisfactory. When conditions are normal and stable, the roller operator uses his experience with compacting such materials. However, when due to severe weather conditions various combinations of ambient temperature, wind and even showers can occur, the experience of the roller operator becomes inadequate. Not knowing how far compaction has progressed, not knowing the temperature of the material and not

knowing the current material workability, the rolling operator is then strongly handicapped.

A second example of an interesting problem area is illustrated in Figure 1.11, it deals with “the moisture problem”. The illustration of this problem area makes clear how the participants think that “a lot of rainfall” can lead to “insufficient confining of the rolled material”, “layers that do not stick”, “gas that is locked inside the material” or “deviations in layer thickness”.

The workshop model expresses what the participants think about the relationships between variables in the HMA compaction process. It expresses the links between causes and results. Participant’s opinions on the variables are between “it is expected” and “relatively sure”.

Translation of the workshop information into a causal model

The model developed in the workshop contains versatile and highly valuable information. Nevertheless, the model is not suitable for straightforward application in the research project (paving under severe weather conditions). Therefore based on the workshop model a second, causal model was developed. The model is illustrated in Figure 1.12. The model focuses on HMA compaction because the workshop model indicated that compaction forms the central issue in the quality control of the road construction process. The causal model also incorporates relations from road building practice, literature and physics. Representation of the workshop model on the causal model is not one to one. Some information from the workshop model is not expressed in the causal-model since the information is not related to compaction.

The model comprises evident relations such as the effects of sun-radiation, wind-speed, showers etc. on the temperature of the material; however, to what extent these weather conditions do affect the course of temperature is still left open. Both the effects of “transport time of the mixture” and “layer thickness” on the temperature of the material during compaction, appear to be evident but there is no research known by the author that studied the magnitude of these effects. Here the nature of the relationships also varies between “it is expected” and “relatively sure”. From some relationships one assumes that they exist but in fact they are not demonstrated or validated (e.g. “*temperature of the mixture on compactibility of the mixture*” and “*first roller pass after paving on temperature of the mix during compaction*”). From other relationships it is very clear they exist and sometimes they are even demonstrated and validated by research (e.g. “*composition of the mixture on compactibility, Nijboer 1948*” or “*type of bitumen on viscosity of the bitumen, Shell, 1990*”).

Moreover, a distinction is made explicitly between design parameters, external factors (i.e. meteorological conditions), key variables, control variables and quality specifications. The key variables have a dominant role in the compaction process. The design parameters are choices made by the designer during the engineering process and cannot be adjusted during the paving job. The external factors are the non-adjustable factors, enforced from the outside; conditions under which the paving job has to be done (meteorological conditions, time, roadblock possibilities etc). The

control variables are the variables that can be manipulated during the construction process and that have directly or indirectly an impact on the quality. These variables are of major importance in this research.

The causal model as developed here (Figure 1.12) forms a useful source of information for the sequel of this research project.

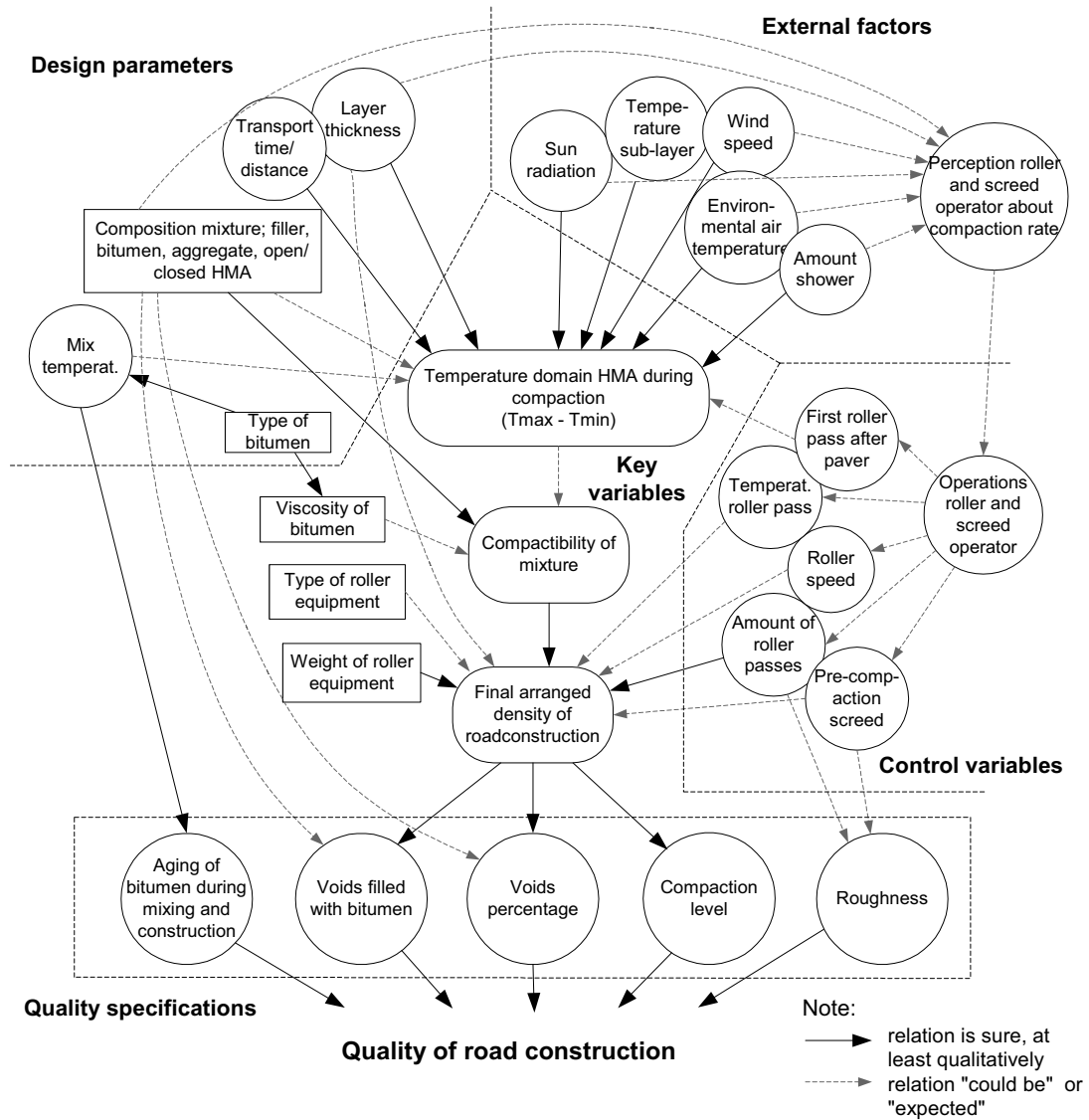


Figure 1.12 The causal model about HMA compaction based on the workshop information.

1.5. **Problem analysis, questions and scope**

Problem analysis

From the previous sections the following conclusions can be recapitulated;

The socio-economic relevance of roads (1.1).

- The road network for traffic and transport forms an important financial and social resource.
- Due to the growth of mobility the pressure on the road maintenance is growing. It is expected that this growth will not end in the nearby future.
- To maximise the availability of (parts of) the road network in order to avoid road jams and economical losses, road maintenance is shifted to time frames outside peak periods (especially at night).
- The increase in night work and the overall pressure on the roadwork itself has led to less favourable conditions for road maintenance. In the road construction industry there is a widespread belief that this has a negative impact on the quality and bearing capacity of road constructions.

Practice of road construction in the Netherlands (1.2).

- Pilot investigations confirm that nowadays a significant amount of road maintenance on the motorway network is done under unfavourable conditions such as at night, under traffic and under poor weather conditions.
- The research indicates further that working under unfavourable weather conditions as well as at night and in combination with “working under traffic” affects road quality negatively.

The road construction process (1.3).

- During the construction process of asphalt roads, the paver (pre-compaction) and rollers (final compaction) achieve compaction of the HMA.
- During storage, transshipment and transport of the mixture and also in the paver, segregation of the mixture can occur. This segregation can introduce discontinuities in the mixture composition.
- The pre-compaction level achieved by the paver, depends on several factors like paving speed, material resistance, applied level of compaction energy. A poor pre-compaction level may affect the final compaction level. Variations in pre-compaction within a road section may result also in variations in final compaction level.
- For the phase of final compaction, rollers can be used of different type (dynamic/static, steel/tired wheels), different weight, and roller drum dimensions. All kind of combinations are possible but all combinations do result in different compaction progression rates.

Towards improvement of the road construction process (1.4).

- Compaction of HMA mixtures to a prescribed level is crucial for achieving an adequate durability and bearing capacity of a road construction.

- There are many factors, in-between variables, conditions and design parameters that influence the compaction process and the final result of that process.
- It is acknowledged that there are several elements that play a role in determining the quality of the final product. For some of these elements, extensive research has led to a profound understanding of the role they play in the quality of the final product (e.g. between type and temperature of the bitumen and the viscosity of the bitumen), while for others more research skill has to be undertaken to demonstrate their importance (e.g. it may be possible that the rate of HMA temperature drop is a function of the time difference between laying the asphalt and the first roller pass applied).
- The relative importance of the various relations is unclear (e.g. does bright sunshine in combination with wind, increase or decrease the cooling rate?)

View on the particular problem field:

At present fundamental knowledge about the material behaviour of HMA during compaction hardly exists. In practice compaction of asphalt pavements, homogeneously and to a target level, is mainly achieved “based on experience” and sometimes with assistance of nuclear equipment³. This way of working can still provide acceptable compaction results if the rolling operator is very experienced and familiar with the conditions and the involved mixture. If this is not the case (and practice clearly indicates that this question is surely not just hypothetical) the job may fall outside the experience domain and realisation of homogeneous and sufficient compaction is doubtful. Moreover, without adequate knowledge efficient fine-tuning of the compaction progress is out of the question.

From a social-economic perspective, improvement of the quality of road constructions is desirable. The quality of the road construction is very dependent on the compaction process. Therefore, to be able to improve this quality significantly, it is essential to have close control over the compaction process. This requires detailed knowledge on material behaviour during compaction in practice and on how this behaviour is affected by all kinds of factors, conditions and actions (see Figure 1.12). This knowledge is not yet available and has to be acquired. Because of the complexity of interactions within the compaction process it would also be very desirable to incorporate this knowledge in a simulation model. With such a model one could perform all kind of simulations (e.g. conditions, roller schemes, etc.) to investigate the impacts on the compaction results. In this way, one would gain the necessary insight to control the compaction process and to create HMA road constructions with a compaction level that is homogeneous and close to the design value. Therefore it was decided to investigate the route for development of such a simulation tool. The investigations of the different steps necessary for a complete simulation tool, is the main objective of this research.

³ When using nuclear equipment the compaction level of asphalt can be monitored while the compaction process is ongoing. Without nuclear measurements the compaction level as a rule is only measured at the end of the process, so adjustments cannot be made anymore.

Research objectives

The objective of this research is “*assess the suitability of various options to simulate the compaction process of HMA, to identify and select the most promising option and refine the selected option into a working model capable of accurately simulating the compaction process of HMA*”. Such a tool should be capable of predicting the effect of different variables on compaction during rolling of an arbitrary HMA mixture. Important modelling aspects are: the development of a suitable material model, testing such a model, implementation of the model inside a simulation tool, deduction of HMA material parameters by doing laboratory tests and comparing obtained (simulated) results to compaction processes at full scale. Furthermore it is important to have the input information available that is required for achieving a complete rolling simulation (material temperature and compaction progression during the whole rolling process). These latter aspects ask for realisation of a full size rolling experiment.

The research questions

From the research objectives the following main research questions are derived:

- 1 What happens precisely during compaction of HMA's Are there models available that describe the behaviour of asphalt mixes during compaction adequately? Which materials do behave quite similarly and are there material models available? How does a suitable model look like?
- 2 Is there equipment available that is (after modification) suitable to measure the material parameters of HMA mixtures while they are under compaction? Which demands would be made suitable equipment? How can material parameters be measured?
- 3 Given a suitable material model and given a set of material parameters, how is simulation of a HMA compaction process by rolling possible? Which tool can be used for simulation of such a process? What demands would be made of such a simulation tool?
- 4 What information is needed as input for simulation of a HMA compaction process? What information can be used to validate a developed simulation tool for HMA compaction? How can such a simulation tool be validated?

Scope & limitations

The field of interest is rather complex and comprehensive. Consideration of the whole problem field in a single research project would be too ambitious. Therefore restrictions have been made.

The first restriction is to only deduce material parameters for a single mixture being; Dense Asphalt Concrete (DAC). The second restriction is that simulations have only been done for static steel rolling. However, if the system proves to work for this mixture and roller combination then it is plausible to assume that it also works for other mixture-roller combinations as long as they have comparable characteristics.

In reality the rolling process is a three dimensional process. The assumption is made that it is sufficiently to only model the longitudinal and the depth direction of the asphalt material, in order to simulate the process adequate.

1.6. The research design

Project design

This research project aims to investigate the possibilities and develop a tool that can simulate compaction processes of HMA. A project design is useful to organise the desired activities within the research project because it states what has to be done and how it is organised (Verschuren, 1998). The design is built up of two components; a.) the conceptual design: the concept or the idea; it indicates what should be achieved during the research and why, and b.) the technical research design: the way the research is carried out; which indicates how the conceptual design can be achieved, the where, the when and the how.

The problem analysis indicates that for managing the compaction process of HMA adequately, knowledge of the involved material behaviour is crucial. Because this knowledge is currently not available it has to be developed. An existing theory for modelling soil behaviour will be tested for modelling the behaviour of HMA under compaction. In order to do so, adequate equipment for determining HMA material properties has to be selected or developed. As a next step it will be investigated whether such a model can be used in a Finite Element Method (FEM) code to simulate a whole HMA compaction process.

In more detail it would appear that it is not known what forces and/or stresses compaction equipment (mainly rollers) do apply on the material under compaction and how the material behaves (i.e. to what extent it compacts) as a result of these external-loading forces.

In constructing asphalt roads different types of materials and compaction equipment are used. The objective is to investigate whether the chosen conceptual design, i.e. selecting a material model, calibrating material parameters and performing adequate calculations (with an FEM-model), is useful. When the results of these experiments are positive for the selected compactor/material combination, it can be expected that the same procedure can be applied for other combinations.

The asphalt industry states that material behaviour of asphalt mixtures is strongly dependent on its temperature. In addition the asphalt material during construction is strongly dependent on meteorological conditions like temperature, wind and rain during construction, (Daines, 1985 and 1986). Literature states that temperature of the HMA material during compaction affects compaction progression. It implies that the effect of temperature of the material on the material properties and compaction progress has to be investigated during the project.

The research model

A model is important in getting an overview over the different steps that should be taken during the research. Such a model should visualise the steps that will be taken to meet the research objectives. The model illustrates the nature of the research and the results that can be expected. It fulfils a role in the communication about the research project and can help in selecting the relevant literature in the initial phase of the project.

Confrontation

Characteristic for the used method, is the principle of confrontation between the involved items, see Figure 1.13. An encounter in the project is visualised by a horizontal arrow with two arrowheads. In this compaction research model four comparisons are envisaged:

- 1.) A confrontation of the theoretical material model behaviour compared to HMA behaviour measured in a laboratory (i.e. HMA, validation of the material model and quantification of its parameters),
- 2.) It is possible to measure the material properties using standard or slightly modified laboratory equipment, given a specific model of material behaviour,
- 3.) Implementation of measured material properties, using a theoretical material model, to in an FEM approach,
- 4.) A comparison between simulation of a compaction process and measurements taken in the field.

Articulation of the research model

The following articulation of the research set up is useful to get better understanding about the steps that will be made during the research project, see also Figure 1.13.

- (a) Investigation and comparison of the behaviour of soil and asphalt mixtures during compaction should indicate if it is possible to use existing soil mechanical models for describing the behaviour of HMA mixes. (b) To validate whether such a theory is adequate for modelling HMA behaviour and for quantification of the material model parameters. (c) When an appropriate FEM approach is selected, simulations of the rolling process can be achieved. For this task use must be made of the selected and tested material model and the quantified material parameters. (d) For simulating a rolling process the major information about material temperature, layer thickness and compaction progress are gathered by monitoring the construction of a real compaction test section. Monitoring this experimental test section also enables validation of the achieved simulations.

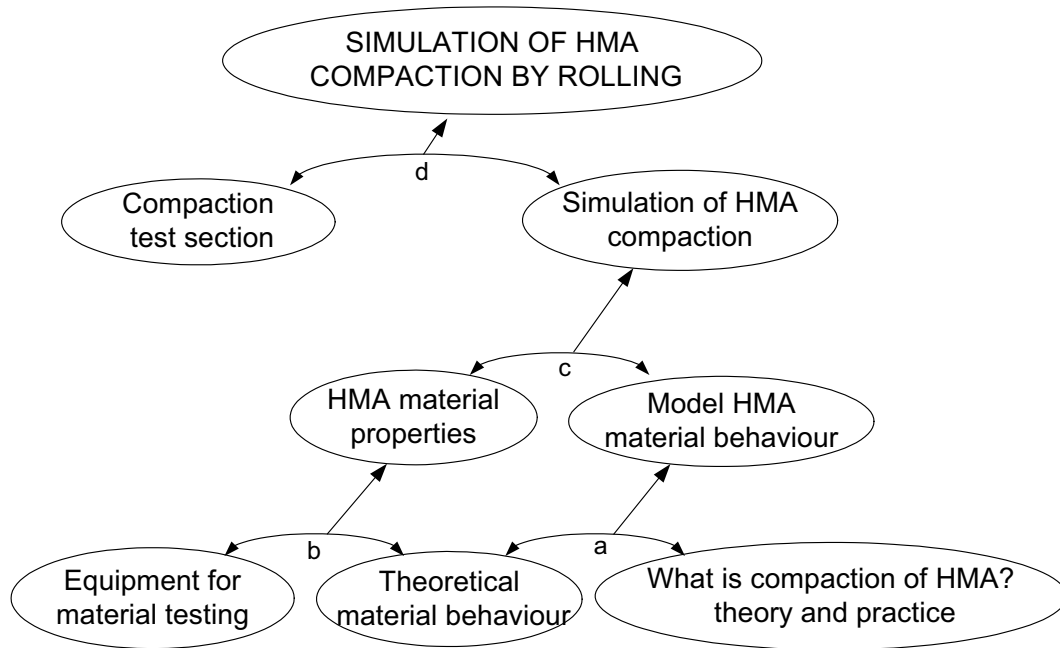


Figure 1.13 The research model and the different interactions.

Hypotheses

Testing hypotheses will help in reaching the research objectives. During the research a view of the problem field can be formulated using the next hypotheses:

- a.) During compaction asphalt mixtures behave quite similar to untreated granular materials. This may imply that the compaction behaviour of asphalt mixes can be described using models developed for soils. The most important item for the two materials (or mixtures) is the movement of particles in or through a fluid/gas mixture,
- b.) The gathered and/or selected laboratory equipment is suitable for measuring the HMA mixture properties in such a way that it characterises its material behaviour during compaction,
- c.) There are suitable FEM approaches that calculate the stress and strain patterns in an asphalt layer that occur when that material is loaded with the pass of a steel-wheel roller drum,
- d.) A relation can be drawn between the results of the FEM simulations of the rolling process and findings measured in the field experiment. This could indicate whether the FEM tool is able to present a good prediction of the compacting effect of a static-steel wheel roller on a dense HMA material.

1.7. Outline of the thesis

The main objective of the research is to develop a reliable tool for simulating HMA rolling processes. Such a tool enables one to do a parameter-study in order to optimise the process. This is particularly important during construction of high quality asphalt roads when environmental circumstances are adverse.

For simulation of such a process a fundamental asphalt material model is needed. Currently such a model does not exist. A reason for this could possibly be the fact the material behaviour is rather complex; it behaves elastic-plastic-viscous. However, if the material composition is analysed one can recognise that HMA mixtures are composed of particles (the aggregate), a fluid (the bitumen) and air (voids) just like soils (e.g. coarse sand). Due to this analogy in composition between hot asphalt mixes and soils, their mechanical behaviour (i.e. their reaction in shape and volume on a loading force) could be comparable.

For modelling the mechanical behaviour of soils reasonable fundamental theories and models were developed in the last decades see also e.g. Atkinson (1993), Wood (1990) or the basic work from 1968 of Schofield at all. An appropriate model that possibly can be used for modelling asphalt can be found in the critical state theory, a theory generally accepted for description of the mechanical behaviour of soils. In chapter 2 the behaviour of granular materials during compaction is discussed. More specifically it is focussed on the soils and HMA materials. The chapter gives insight in the possibilities for using the critical state theory for HMA.

Before using such a model, its suitability should be tested and properties for the “new” material should be determined. For those objectives suitable equipment should be selected and laboratory tests must be done. Suitable equipment did not exist and therefore an existing piece of equipment was modified in such a way that it could do the job. Modifying the Hveem Stabilometer and developing a testing procedure for HMA mixtures became a substantial part of the research. Chapter 3 focuses on modelling the HMA behaviour. It discusses how the Hveem Stabilometer is modified and how the laboratory test programme was achieved. Finally the test results measured from the test programme were analysed.

For simulating a rolling process on asphalt a suitable tool had to be selected. This was found in the DiekA FEM approach. DiekA makes use of an ALE formulation, which can handle contact phenomena, large distortions and materials that behave half as a solid half as a fluid. All aspects do occur in a process as rolling of asphalt. Further, DiekA comprises the “Rock” material model, a model that operates not precisely but sufficiently enough in accordance to critical state principles. In chapter 4 the FEM theory in general is discussed and more in particular the principles of the ALE approach. It discusses also how a simulation of a roller pass in general should be done.

In order to be able to do simulations and for testing the reliability of the developed simulation tool, one needs information about compaction processes achieved in reality. This information was gathered by constructing a compaction test section while monitoring the governing material- and process-parameters. The test section was constructed under laboratory conditions. Chapter 5 focuses on the constructed

experimental test sections, the measured material temperatures and finally the achieved compaction progression. During the analysis of the results of the test section emphasis was placed on the effects of the material temperature on the compaction progress.

After chapter 4, which discusses how by using FEM simulations of compaction processes can be made, and chapter 5 in which construction of a real compaction process is discussed, the focus in chapter 6 is on the results of a series of simulated roller passes. First we will discuss how correctness of the individual roller pass can be tested and how the different results should be interpreted. Secondly the result of a simulated compaction process of a series of roller passes is discussed. Finally the conclusions and recommendations of the complete compaction research project are discussed in chapter 7.

2. Compaction of granular materials and Hot Mix Asphalt

2.1. Introduction

There is hardly any fundamental knowledge about how Hot Mix Asphalt concretes (HMA) behave during compaction processes. Therefore, one has to rely extensively on experience to compact the HMA road constructions homogeneously to the target compaction level. Such experience however is not always available especially not in case of adverse external circumstances (Ter Huerne et al., 1996). Nevertheless, a sufficient compaction of HMA in road constructions is tremendous important for realising a good bearing capacity. This thesis aims to develop a generic tool that employs the Finite Element Method (FEM) approach to simulate the compaction process of HMA. This chapter will focus on the analogy between granular materials and HMA's. In particular strong indications exist that granular materials behave quite similar to HMA's during compaction. For granular materials fundamental models are available describing its behaviour during compaction. A representation of the complete research project is given in Figure 2.1. The specific topic of interest that will be discussed in this chapter is marked grey.

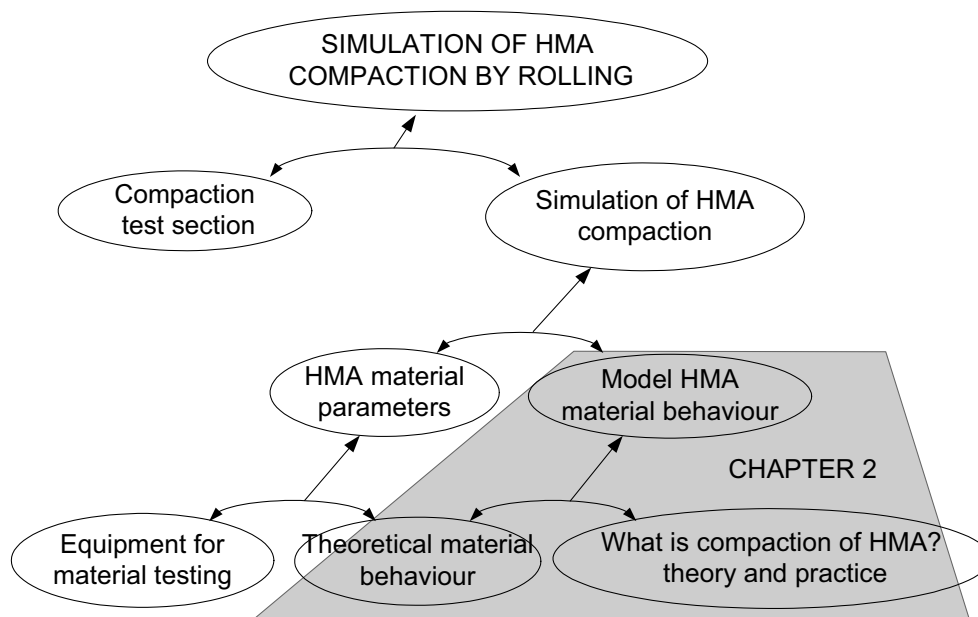


Figure 2.1 The research set up of the overall compaction project, grey shaded the topics of interest in chapter 2.

Section 2.2 describes the process that takes place inside granular materials and HMA during compaction. It investigates the importance of compaction and the changes in measured material properties when the compaction level increases.

During compaction the movement of particles inside the mixture is important. As a result of that movement, frictional forces develop between the individual particles. The section discusses the effect of a liquid in the material matrix, and at what level the liquid influences the friction forces.

In section 2.3 the attention is focussed on methods to measure the level of compaction. Fundamentally five distinct methods can be distinguished all measuring different quantities. However, some of these quantities do not reflect the fundamental state of compaction in terms of particle proximity. Therefore, a selection has been made for use in this research. Compactibility is the ease at which a material can be compacted. There exist different methods that can be used for measuring compactibility. Three of them will be discussed here, it concerns: the *C*-value method, the complex modulus method and the modified Mohr method. All methods will be briefly described and discussed here.

The second part of the chapter focuses on the similarities between asphalt and granular materials. These similarities allow adopting and further development of a soil model to be used for HMA. Section 2.4 presents the arguments for supporting the analogy. In section 2.5 the critical state theory is presented which is commonly used in soil mechanics. It forms the basis for the material model that will be adopted for describing the HMA behaviour during compaction.

2.2. *Compaction, the benefits and the way to achieve it*

Granular materials and concretes are widely used in the construction of roads, dams, locks, (concrete) structures for buildings, foundations, earthwork's, etc. Generally, the materials can be classified into "bound" and "unbound". Unbound materials are materials without a binding agent in the form of cement, bitumen, etc.

Bound materials can further be classified in cement bound and bitumen bound materials. The former refers to cement concrete and the latter to asphalt concrete. The difference between asphalt concrete and cement concrete from a constructive point of view is that the characterisation of the binding agent in asphalt concrete strongly depends on temperature and loading time. For low temperatures the viscosity is so high that its behaviour can be compared to that of a solid. At high temperatures it behaves as a liquid. The binding agent in asphalt concrete can be characterised as visco-elastic. The characteristics of the binding agent in cement concrete (i.e. the cement mixed with sand and water) hardens with all the particles to a solid matrix due to an irreversible chemical reaction. In asphalt concrete the binding agent and the particles are not chemically bound. The bitumen and the particles stay separate components so they can also be separated if necessary.

From a loose to a more dense particle pattern

Building roads or more in broad civil structures is quite different from a general manufacturing process. A road is constructed in situ. Due to the nature of that construction process the granular materials and concretes are often delivered in a “loose state”.

The fact that the particles are in a relatively loose state of packing implies that there are significant voids in the material. That loose state of packing of the material originates from earlier processes, like excavation, mixing, and transportation. In that loose state of packing materials have a poor bearing capacity. To carry loads successfully with little deformation, as e.g. in a road construction, it is necessary to bring the material in a denser state of packing. To achieve that state, particles have to be re-arranged and the voids have to be driven out. In civil engineering this process is known as compaction. Sometimes compaction is also called “densification”.

Initially the particles are rearranged during compaction, the particle skeleton occupies less volume and air voids are driven out. The result is that the same amount of particles occupies a smaller volume, and hence does achieve a higher density. If compaction continues the liquid (binding agent) will be squeezed out of the matrix carrying along with it the fines. For large volumes of bitumen and fines this can happen before an adequate particle skeleton is attained. Such a situation is undesirable in road construction.

From the previous statements it can be concluded that the involved materials (i.e. soils, asphalt concrete and cement concrete) show large differences. However, globally seen the behaviour of the materials, especially in the construction stage where particle matrices change from a loose into a more dense packing, do show large similarities. It concerns the stage in which the movement of particles in the matrix governs the global behaviour. During this stage the presence and type of the fluids in the mixtures (water, bitumen or cement paste) affects the ease of sliding of the particles over each other and therefore the mechanical behaviour of the composed mixture or soil. It is due to this phenomenon that in this research project it is aimed to model the behaviour of an asphalt mixture during rolling by adopting a model from the wider developed knowledge domain of soil mechanics.

The necessity for compaction

Granular based materials do have a low bearing capacity when the particle pattern is relatively loose. It results in large deformations when the material is loaded significantly. This is illustrated in Figure 2.2. On the left side a loose particle pattern is given. Already under little forces, movement of the upper particles will occur. The upper particles “fall” into the spaces between the lower one’s. These deformations result in a denser particle matrix. On the right side of the figure a denser pattern is shown. It is evident that this particle configuration can carry a higher load.

However, civil structures require a stable and strong material. Thus, a granular material with a loose particle matrix as primary product has to be compacted during

construction. A denser particle matrix realises a.) a more stable stacking of the individual particles, b.) more inter particle contact points, and, c.) less voids between the particles.

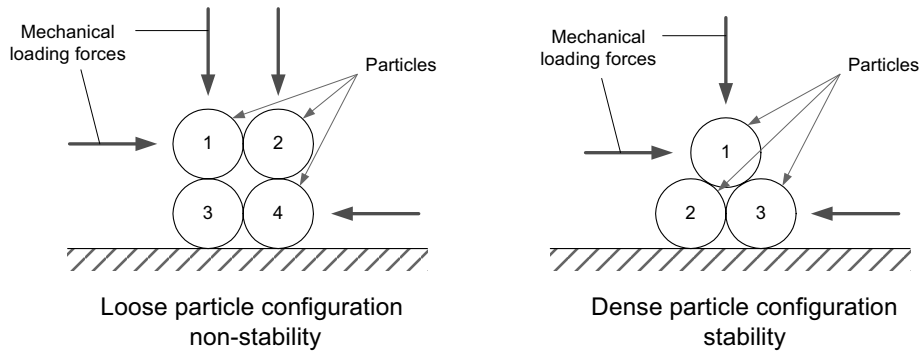


Figure 2.2 Stability of a particle pattern related to its density.

All these phenomena improve asphalt concrete quality because

- a) A more stable packing⁴ of the particles results in less particle re-orientations under loading. Less particle re-orientations means less (unwanted) plastic deformations of the material.
- b) More inter particle contact points⁴ imply, that as a result of a specific load level, the forces are smaller in the inter-particle contact points. It decreases the likelihood of particle crushing. Particle crushing means plastic deformation of the material.
- c) Less voids in the matrix implies that the material is less susceptible to moisture penetration. This criterion is especially important in regions where frost forms a hazard to the integrity of the road construction.

A good compaction is essential for a good bearing capacity with little deformations and a watertight construction. Shell (1990) states in her Bitumen Handbook:

“Compaction is probably the most crucial stage in the construction of any layer within a road pavement. Compaction brings the constituents of a material into an intimate contact, and where this not occurs air voids will remain. The importance of compaction as a decisive influence on the performance of bituminous materials has been recognised for some time ...” and *“Since the structural performance of the whole pavement is largely governed by the level of compaction... .”*

Hveem (1950) explored the importance of the ability of a material to resist a vertical load without generating excess horizontal stresses in a confined situation. He defines that quality as the “stability” of the material. He developed a design method for HMA mixtures that ranked a material between two extremes. On the one side a very stable material that does generate just a negligible horizontal stress when vertically loaded

4 For the sake of completeness it has to be mentioned that the mechanisms under a.) and b.) are only valid for mixtures that make use of a sand and/or stone skeleton. There also exist materials that do not make use of inter-particle contacts for supporting loads as for example Mastic Asphalt or Gussasphalt. In such a case, because of the absence of a particle skeleton, loading forces are supported directly by the bitumen. That makes the use of stiffer bitumen necessary. These type of materials are not widely used in the Netherlands and therefore excluded from this research. It is expected that these materials behave different during compaction.

(e.g. steel), and on the other side the non-stable behaviour of a liquid in which a horizontal stress becomes equal to the vertical one. This method of judging mixtures by testing their stability is still in use in the United States, more detail about it can be found in Asphalt Institute (1989).

Figge (1987) describes the elastic, plastic and viscous material behaviour during compaction with the help of rheological models. He considered the compaction process at a particle level. He describes the ideal situation of an individual particle as *“particles should in the final stage have as little opportunities as possible for movement. The position of the particle should be fixated by a high amount of contact points with the surrounding particles. Apart from providing positional stability, a large number of inter particle contact points is crucial for translating the loading forces from one particle to another without damage. The embedment of the individual particle depends nevertheless on more factors like particle shape, particle surface and particle texture.”*

Factors affecting the compaction of HMA

During compaction of Hot Mix Asphalt (HMA) three important factors affect pavement performance (Asphalt Institute, 1989):

- 1) The squeezing together of the particles increases their inter particle contacts and friction, resulting in a higher material stability and strength.
- 2) Reduction of air voids decreases the material permeability. In an under-compacted material voids are interconnected. This permits intrusion of air and water into the construction. Air oxidises the bitumen and makes it brittle and susceptible to cracks. Water permeating into the material can initiate stripping (i.e. separation of bitumen from the particles).
- 3) Finally, if a high level of compaction is not achieved during construction, subsequent traffic will further consolidate the material. This further consolidation will mainly occur in the wheel paths, which means that rutting is taking place. This rutting decreases the smoothness of the riding surface.

The goal of compacting an asphalt concrete pavement is to achieve an optimum air void content, to provide a smooth riding surface and to increase the bearing capacity of the material under construction. The task of the rollers in the construction process is to reduce the voids content for dense graded mixtures. At that level the voids are usually not interconnected anymore and the unfavourable effects of air and water are avoided. Caution is needed because the material should not be compacted below a minimum void content. Below that certain minimum value there is the danger for flushing and mixture instability when the material expands thermally.

Powell et al (1975, 1982, 1983) investigated more quantitatively the relationship between the compaction level and the performance of bituminous materials. They reported that if the void content of the material rises from 4 to 12 percent, the stiffness of the material decreases with approximately 55%⁵.

⁵ Stiffness modulus was measured by using the three point bending tests and uni-axial loading tests on materials with respectively 5.2, 4.0, 3.0 and 2.7 percent of bitumen. Tests were done at a frequency of 25 Hz and a temperature 25 °C. Stiffness decreased from 2400 MPa to 1080 MPa.

Swanson et al (1966) studied the effect of bitumen viscosity on the compaction of asphalt concrete. They studied compaction processes at different temperatures by compacting rectangular test specimens with a laboratory-rolling machine. By using the temperature viscosity relation of the bitumen they obtained the average viscosity of the binding agent for the specific compaction test. They investigated the level to which the test samples were compacted by checking the void percentage, unit weights and Marshall Stability, and related these to bitumen viscosity. Although the study was not set up to investigate a direct relation between percent of voids in the material and Marshall Stability, it could be derived from the figures that materials compacted to a lower voids level do have a much higher Marshall Stability.

It is evident that compaction is essential for the performance of asphalt concrete road slabs. A high compaction level will result in a stable particle stacking, a high amount of inter-particle contact points and a low void content. All aspects together contribute to a good durability of the road construction. The following paragraph describes in detail what happens during compaction processes.

Interactions of particles, fluid and voids

Realisation of a closer particle pattern must be achieved during the construction process. Compaction can only occur when particles are moved or re-arranged into a closer pattern. Pressure, vibration, kneading or other stimuli can achieve this result. To understand the compaction process on particle level, the findings of Figge (1987), Paulmann (1969) and Nijboer (1942, 1948) are of interest.

Figge studied the possibilities of movement of individual particles during compaction. He postulated that in a non-compacted asphalt mixture the individual particles are reasonably free to move. As compaction progresses, these particle movement possibilities are greatly reduced. The compaction equipment must be able to create such loads on the material that it results in movement of the individual particles. The sooner this is done the faster one will arrive to a situation where no more particle movement can take place. During compaction air is driven out of the mixture. The stress that is needed to realise compaction depends on the resistance that the particles offer before they move. This resistance depends on the inter-particle friction forces. When the compaction of a material proceeds, the forces needed for achieving particle movements arise.

Nijboer and Paulmann investigated the extent to which this friction is determined by the characteristics and amount of the fluid in the mixture. The fluid acts as a lubricating agent between the particles and reduces friction. Nijboer investigated the fluid-air menisci that originate from the three phases in the mixture. He postulated that inside the voids of the mixture fluid-air menisci exist. The surface tension of those fluid-air menisci pulls aggregate particles towards each other. The net result is a pre-compression stress in the particle matrix. This gives the matrix shear strength. The magnitude of this stress in the sample is proportional to the surface tension and inversely proportional to the diameter of the voids between the particles. When the voids are completely filled (saturated material), the stress disappears. In such a situation the material behaves hydraulically. The results of Nijboer indicate that for HMA mixtures the hydraulic region starts at void contents of 2 to 4%.

2.3. Quantities to determine compaction levels and compactibility

For compaction it is important to know how much energy is required and how much time is needed to achieve a desired level. For that purpose modelling of the material behaviour, i.e. finding a relation between the specific volume of the material and the corresponding required stress combination under prevailing circumstances is of great help. Hence, the specific volume of the material corresponds to a specific compaction level. The ease with which this can be achieved (required energy) reveals the compactibility of the mixture.

There are several methods for measuring compaction levels and compactibility. In this research we are interested in selecting a method that expresses the proximity of the particle matrix of the material. It will allow us to express the compaction level in fundamental properties.

Determination of the compaction level

Regrettably, the particle proximity cannot be measured directly. Parameters commonly used in road engineering practice are; *density*, *voids content*, *voids in the mineral aggregate (VMA)* and *degree of compaction*. In soil mechanics, also use is made of the parameter *specific volume of the material*, v . This parameter expresses, just like *VMA*, real particle proximity, but it is a bulk parameter.

Some definitions:

- 1) Voids Content [%]; The volume of voids in the material related to the total volume of material (inclusive voids), or volume voids [mm^3]/ total volume material [mm^3]
- 2) Density, ρ [kg/m^3], the density of the relevant material; weight material [kg] / volume of the material [m^3]
- 3) Degree of Compaction [%], the bulk density of a piece of material (sample) related to the bulk density of the same material after (re)compaction in a standard way (Marshall or Gyratory or refusal) times 100%; = $100 \times$ bulk density existing piece material [kg/m^3] / bulk density Marshall hammer or Gyratory compacted material [kg/m^3]
- 4) Voids in Mineral Aggregate, *VMA* [%], The amount of “space” in mineral aggregate related to the total volume of the material, in the case of asphalt concrete a part of this volume is filled with the bitumen; $100\% \times$ (volume voids + volume bitumen) [mm^3]/ total volume of material [mm^3]
- 5) Specific Volume, v [-/-], the volume of voids in the aggregate skeleton plus the volume of aggregate in the material [mm^3] related to the volume of aggregate in the material [mm^3]; (volume Voids in aggregate skeleton + volume of water [mm^3]) / volume of aggregate [mm^3].

The first three mentioned parameters are in road construction practice commonly used as indicator for the level of compaction. However a problem with them is that they are not a true indicator for particle proximity. Further, is there a direct relation between the bearing capacity of a HMA road construction and that particle proximity. Good measures for the particle proximity in the material are the quantities voids in the mineral aggregate (*VMA*) and specific volume (ν). When the composition of a HMA mixture is known, then the specific volume, ν , can directly be calculated from the *VMA* value and vice versa.

The use of density or voids content to express compacted state (or implicitly bearing capacity) of a HMA road and can lead to erroneous results. Imagine a mixture with a certain particle matrix density (i.e. fixed *VMA* level). Holding that particle arrangement constant, one can increase the bitumen content (replace voids with bitumen) resulting in a higher density in kg/m^3 . Now the specimen would have a lower void content but particle proximity, and thus bearing capacity, has not changed at all. The effects of bitumen content on density and voids content is illustrated in Figure 2.3 under the condition that *VMA* and thus particle proximity is kept equal.

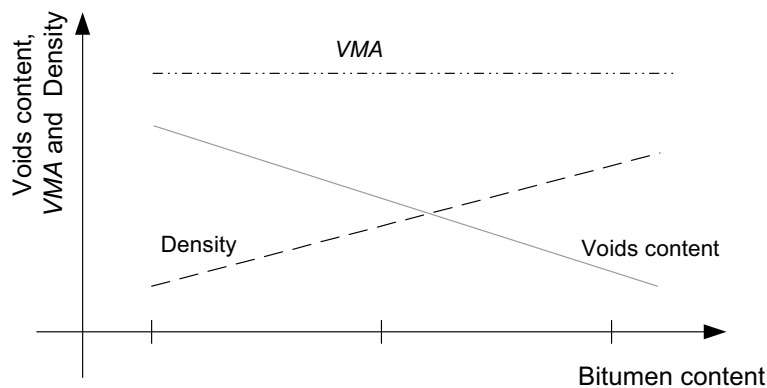


Figure 2.3 The effects of bitumen content on material parameters density and voids content at a fixed *VMA* level. Take that if the voids become filled with bitumen automatically the density increases.

Degree of compaction is a better indicator for particle proximity but does suffer another disadvantage. It is not an absolute but rather a relative measure for particle proximity. Using a reference sample a higher compaction level will always indicate closer particle proximity. However, the problem in road building engineering is that there is no standard reference sample. Hence a compaction level of 98% has no general meaning in terms of density or *VMA*; it is related to a fixed amount of compaction energy applied.

Of the above-mentioned parameters only the *VMA* and the specific volume, ν , give a clear indication about particle proximity of the pattern. All the other parameters do not.

Concluding, both *VMA* and ν , have been found capable to express particle proximity or level of compaction. There is a simple correlation between these two parameters

(Figure 2.4). Hence, there is little advantage in selecting the use of one over the other. We will use *VMA* since this is a well-known parameter in road engineering.

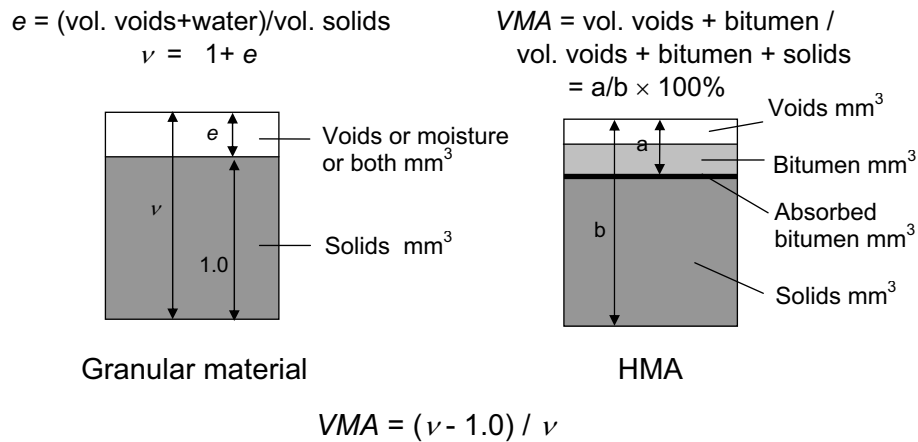


Figure 2.4 The volumetric composition of granular materials and HMA's related to *VMA* and ν .

Measuring compactibility

Compactibility of an HMA is the ease with which a material can be compacted. In this research also compactibility values for different materials/mixtures will be measured and results will be compared with results from literature.

In literature several methods for measuring compactibility can be found. Three methods will be discussed here:

- a) compaction progress described with a exponential formula or sometimes called; *C*-value method,
- b) the complex modulus method,
- c) the modified Mohr method.

In the next paragraph the most capable methods will be evaluated.

Ad a. The *C*-value method is the most frequently used method to measure compactibility. It describes the progress in compaction by using an exponential formula. Kezdi (1969) developed this principle and other researchers (Renken, 1980; Arand 1985,1987) have employed it. The model is based on the assumption that the progress of compaction, expressed in terms of increase in density $d\rho$, due to an added amount of compaction energy, dS , depends on the difference between the current density state and the maximum density, ρ_{∞} . When ρ_0 is the density at the start of the compaction process,

The concept of Kezdi can be formulated as:

$$\rho_A(S) = \rho_{A\infty} - (\rho_{A\infty} - \rho_{A0}) \cdot e^{-\frac{S}{C}} [kg / m^3]$$

The C value in the formula is a measure for the speed the density approaches the asymptotic value ρ_{∞} and thus also for the speed by which the compaction progresses, see Figure 2.5. Analysing the equation above, one can see that materials with lower C -values are more easy to compact compared to materials with higher C -values. Renken (1980) determined C values for asphalt concrete mixtures commonly used in Germany during the eighties. He obtained typical values in between 10 and 30. A study in the Netherlands, (Hopman, 1994) revealed C -values ranging from 18 to 38.

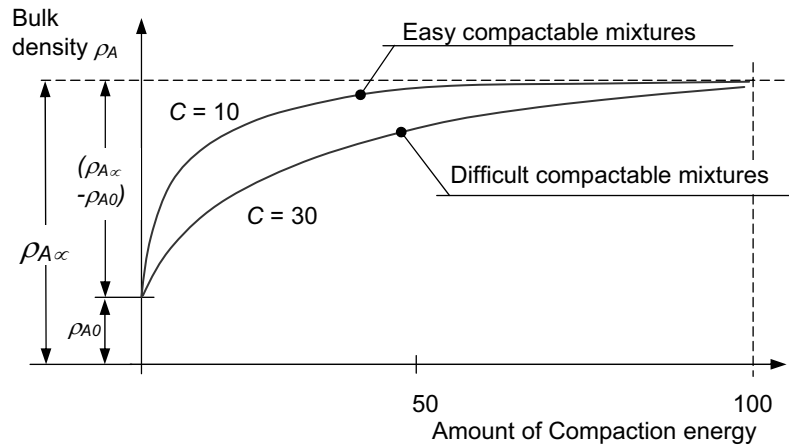


Figure 2.5 The compaction process according to the C -value method.

Ad b. All the mechanical characteristics of mixtures of bitumen and aggregate show a temperature and loading time dependent behaviour (Partl et al, 1998; de Benedetto et al, 1998). This implies that the material behaves partly viscous which makes it difficult to characterise. A useful method is to load the material with a sinusoidal force with small amplitude while measuring the deformation signal. In that case the deformation signal should also be sinusoidal if the material behaves in a linear viscous-elastic manner, (Huet, 1963). When these stress-strain signals are analysed they provide an insight in the mechanical stiffness of the material as a function of temperature and loading time.

Gauer reported in 1975 about research he did after the visco-elastic behaviour of bituminous mixtures at several levels of compaction. For that research he used a gyratory compactor from which he was able to adapt both the pre-described gyratory angle as well as the real (actual) gyratory angle. It seems that signals gathered from such a test (see also Figure 2.6) do correspond largely to signals obtained by other researchers who tested equal materials dynamically as e.g. Huet (1963).

From this dynamical research on HMA materials it is known that a phase shift angle can be deduced when the loading signal is compared to the deformation signal. Along a similar procedure Gauer deduced for the tests with the gyratory compactor on the asphalt mixes also the phase angle φ . He assumed that this φ parameter represents information about the flow ratio and the elastic part of the complex internal resistance of the material.

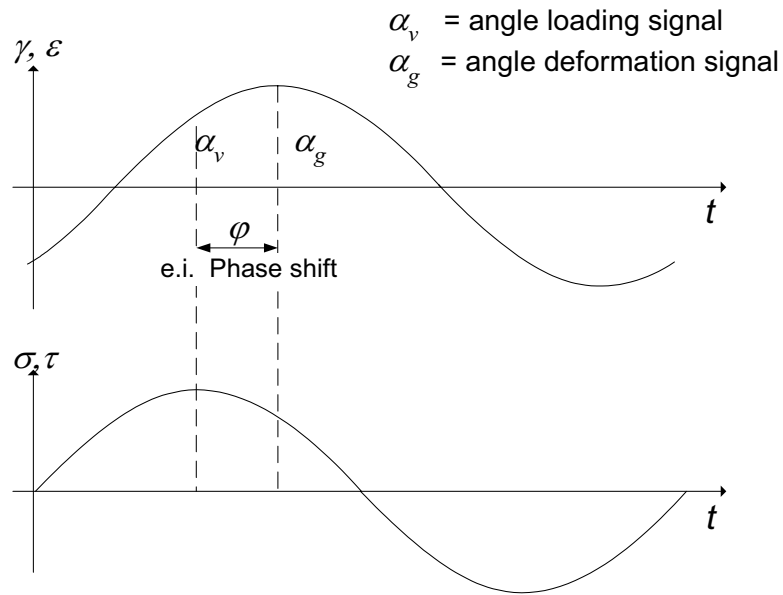


Figure 2.6 Loading and deformation signal of a visco-elastic material when sinusoidal loaded, (Gauer, 1975).

Gauer used the phase shift, φ , from the gyratory compaction tests for deduction of the workability of the materials at several levels of compaction; from un-compacted until compaction was completed. For this task he used the ideas of Fritz (1974) to express the effects on compactibility. Fritz distinguished the imaginary part and the real part of the deformation energy of the material. The real part of the resistance was assumed to be stored inside the material during compaction whereas the imaginary part of the resistance should be transformed into heat. From the phase shift, measured during compacting the material, Gauer deduced what he called the “*complex internal resistance, τ_E* ,”. The surface under the τ_E curve (see Figure 2.7) until a fixed level of the voids content was used as a parameter for the compactibility of the material during compaction.

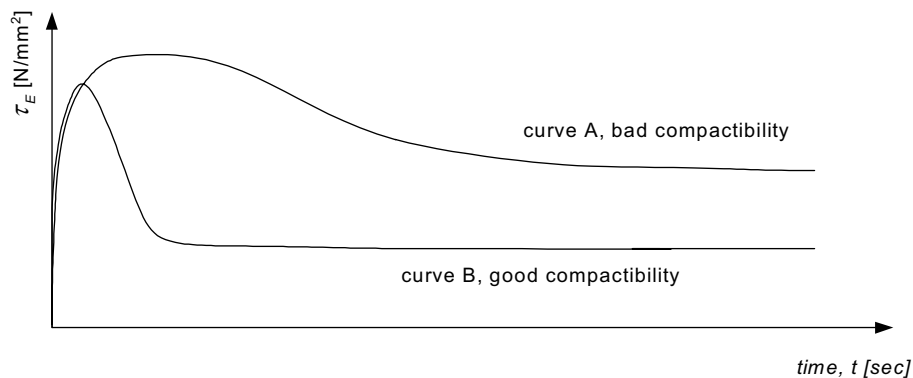


Figure 2.7 The τ_E curve used as a parameter for the compactibility after Gauer (1975).

The complex modulus method makes use of a modern compaction tool that loads the material dynamically in view of mechanical properties and density characteristics.

There is evidence that material samples prepared with a Gyratory compactor systematically better approximate the in situ compacted material than Marshall compacted samples do (VBW-Asfalt, 1997).

Ad c. In the forties of the last century tri-axial testing and characterising the failure behaviour of soils by means of Mohr-Coulomb failure criterion was widely accepted in the soil mechanics field. Based on the expected similarity between HMA and granular materials, Nijboer (1948) characterised HMA's by means of the parameters τ and ϕ (according to the Mohr theory for granular materials). In addition he introduced the parameter η to capture the viscous component of HMA. Nijboer assumed that the resistance against deformation of "bituminous mineral aggregate mixtures" could be represented by three physical quantities (Figure 2.8):

- the angle of internal friction, ϕ ,
- the initial resistance, τ ,
- the viscosity of the mass, η , which denotes the influence of the viscosity on the shear resistance of the bitumen aggregate mixture.

This latter parameter takes into account the fact that the position of the Mohr-Coulomb failure line depends on the viscosity of the mass and thus on the temperature of the material or the loading time.

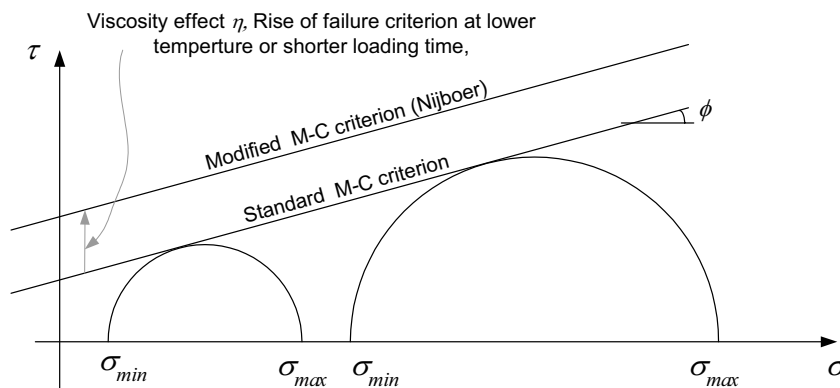


Figure 2.8 The modified Mohr-Coulomb method, by introducing viscosity η (Nijboer, 1948).

Nijboer studied in advance the plastic behaviour of bituminous aggregate mixtures but later on he used a significant part of the gathered knowledge for developing his "rolling theory". He made an inventory of all parameters of which he thought that they were relevant for the progress of HMA compaction. By plausible reasoning he came to the R_f relationship (i.e. relation that calculates the R_f factor); The R_f factor is a parameter that should indicate how far the compaction process of HMA is progressed.

$$R_f = \frac{P}{ID} - C * \tau_{cb} * n * \left(\frac{h}{v}\right)^{0.4} \quad [\text{N}\cdot\text{mm}\cdot\text{sec}]$$

in which;

- P = the weight of the roller drum [N]
- l = the width of the roller drum [mm]
- D = the diameter of the roller drum [mm]
- C = factor for the roller type (i.e. 2.5 for static steel rolling)
- τ_{cb} = the initial resistance of the bituminous mixture [N/mm^2]
- η_m = the viscosity of the mass of the compacted mixture [poise]
- n = the number of roller passes applied [-]
- h = thickness of the layer [mm]
- v = speed of the compactor [mm/sec]

Note that progress of compaction only occurs if the quotient $P/l \times D$ is bigger than $C \times \tau_{cb}$. To check all the ideas Nijboer build a laboratory rolling machine and tested by experiments the effects of a.) layer thickness', b.) roller drum diameter, c.) rolling speed, d.) material temperature, e.) roller drum weights, f.) number of roller passes applied, and, g.) different mixture compositions. Some of his findings are illustrated in Figure 2.9, a figure that represents a part of his basic work.

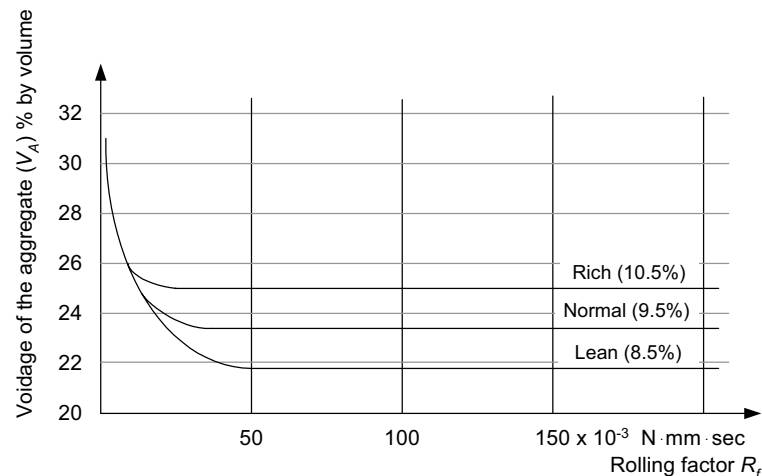


Figure 2.9 One of the basic figures developed by Nijboer (1948), for three types of bitumen aggregate mixtures respectively; Rich (10.5 % of bitumen), Normal (9.5 %) and Lean (8.5 % of bitumen).

Nijboer did tests on already compacted samples to deduce ϕ , τ and η , and processed these quantities successively in a rolling formula for predicting compaction progress. The method is in principle not a “pure” method to measure compactibility but more a method to describe the plastic deformation of HMA’s. During many of his material measurements in the tri-axial apparatus, the governing stress conditions tend the material to shear. During compaction too high shear stress levels must preferably be avoided, because when granular materials shear, they expand, become less compacted and even cracks can develop. This inconsistency makes the method in the authors opinion not fully capable for modelling HMA compaction behaviour.

However, a further developed theory from Nijboer’s work grew when Nijboer worked together with Vizi under auspices of the Studie Centrum Wegenbouw (1978). The theory became relatively well developed for the time it was used (i.e. 40ties till 70ties) it covered already the complete range of involved aspects from quantifying mixtures to calculating the required number of roller passes, (Vizi, 1981). During that time also

a lot of experimental work about compaction processes was done on real road sections outside the laboratory. Based on the “rolling theory” and experience gathered during real road compaction, figures became developed that expresses progress in compaction of asphalt as a result of static steel rolling. The most useful ones express the state of density as function of R_f , see Figure 2.10.

Nijboer used the τ , φ & η method for quantifying the effect of several material parameters on compactibility of the mixture (e.g. bitumen viscosity or material temperature, aggregate angularity, aggregate roughness). The values for the parameters used for different mixture compositions can be found in Vizi (1981) or SCW (1971).

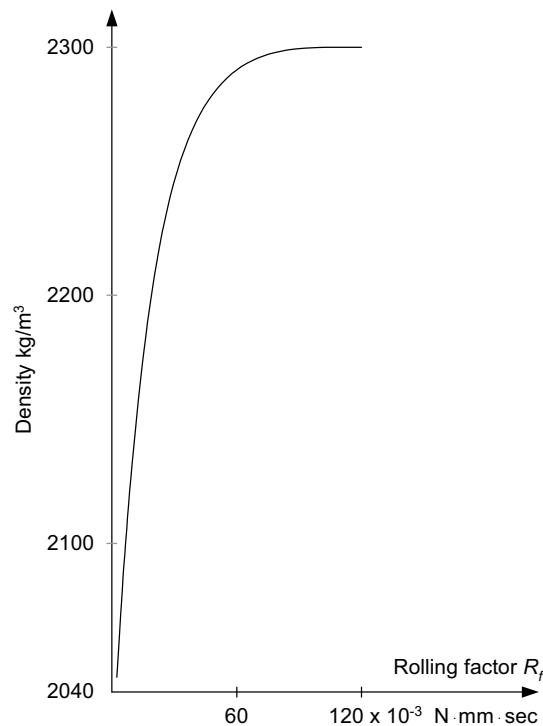


Figure 2.10 The density of the layer as a function of the R_f factor during compaction of a crushed sand asphalt mixture (SCW, 1978).

Evaluating compactibility measuring methods

Exponential formula's or C -value methods are methods that directly measure the compaction progress (density progress or voids decrease) as it occurs. There are no simplifications of the process. The method can be used both for material that is compacted in a mould as well as for describing the compaction process of material at a construction site. The method assumes that compaction progresses exponentially as a function of applied energy. Results are directly related to material parameters and hence can be used for validation.

Both, the complex modulus method and modified Mohr method are not as useful as the C -value method because they do not express the absolute stage of particle proximity. The complex modulus method assumes an elastic-viscous material behaviour throughout the whole regime and completely ignores plastic behaviour.

Figge (1987) found that in initial stages of compaction the material behaviour is predominantly plastic. Supported by these findings this research makes use of a fully elastic-plastic model to describe the relevant material behaviour. Accordingly we are forced to reject the Mohr method because it is based on shear stress situations⁶ in the material as described earlier. Compaction does not take place in the shear regime. However, both methods do provide a reasonable indication of compactibility when compared to the selected (C-value) method.

For this compaction research something like the Mohr approximation is the best suitable because it expresses material behaviour by using relations or models in such a way that it can be implemented in a FEM approach. The problem with the Mohr theory however is that it assumes shearing of the material, therefore instead of the Mohr method it is better to use something like the critical state method. Both the C-value method and the complex modulus method do not express relations between the stress state of a sample and its behaviour in terms of strain.

2.4. Resemblance HMA and unbound materials

This research intends to apply a model from soil mechanics to simulate the behaviour of non-compacted hot HMA⁷ mixes. This section explores the similarities between granular materials and HMA's with respect to compaction. Specifically, the interaction between the particles and the fluid during compaction in both materials is analysed. The starting point is an existing sound theoretical soil mechanics model that describes elastic-plastic behaviour of granular materials. The existing road engineering knowledge about compaction of HMA's is more of a heuristic and practical nature.

It turns out that there is a strong analogy between hot HMA mixtures and granular materials. At low temperatures however, there is little similarity because the fluid in the asphalt mixture is so highly viscous then.

Loading a granular material

Progression during compaction depends on the resistance that particles experience when they are forced to move. When studying the behaviour of a HMA or a granular material and analysing the inter-particle and particle-fluid behaviour four different mechanisms can be distinguished;

1. the hysteresis phenomenon that granular materials express,
2. the fluid content and compaction energy that affects the compactibility,
3. the fluid content that affects inter-particle friction,
4. the rheological models for granular materials, the materials express a combination of elastic, viscous & plastic behaviour.

These mechanisms will be discussed in the sequel.

⁶ During the compaction process of asphalt concrete high shear levels only occur either when the weight of the roller is too high or material is too soft. This normally does not occur when the rolling process is carried out in a proper way.

⁷ The model will be used only for describing the behaviour of continuously dense graded hot asphalt mixtures.

In soil mechanics the resistance from mainly gravel and sandy granular materials is considered as the sum of an initial resistance part and a cohesive part. Huschek (1980) assumed that this mechanism, derived from Coulomb, should also work in a material as asphalt concrete. The frictional resistance is proportional to the normal force that works on the sheared surfaces. The theories indicate that the amount and the qualities of a fluid in a three-phase system, as both wet granular materials and asphalt mixes are, acts upon both phenomena, friction and cohesion. In addition Nijboer (1942) assumed that the friction between particles causes an important part of the resistance against plastic deformation. Fluid content and friction appear to be important aspects in the fluid particle interactions.

Hysteresis of granular materials

In the inter-particle contact points both normal and shear forces will develop when a load is applied on a particle skeleton. Before particle movement starts, the shear force developed in the inter-particle contact surface has to overcome the frictional resistance. After such a particle movement the matrix is rearranged into a new pattern. In case the material is unloaded there is no driving force to get the particles back into the original position. This means that a part of the deformation remains.

This mechanism results in a load-displacement curve as shown in Figure 2.11. This phenomenon is known as hysteresis and most granular mixtures exhibit it. The rebound deformation during unloading is known as elastic. The non-reversible deformation is called compaction of the particle-based material.

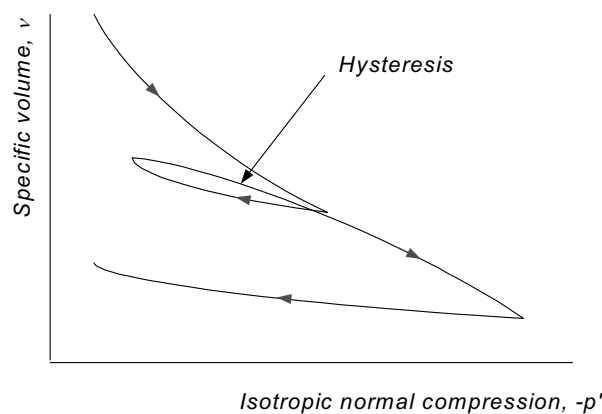


Figure 2.11 The hysteresis phenomenon during loading, unloading, and reloading of particle-based materials.

Fluid content and compaction energy

It is commonly known that fluid in a granular material affects its mechanical behaviour. At least the inter-particle frictional resistance will be different when the amount of fluid in the contact surface changes. From soil mechanics it is known that there exists an Optimum Moisture Content (OMC) and a Critical Moisture Content (CMC) when the relationship between moisture content and achieved dry density (as a

result of an fixed amount of compaction energy) is considered. This mechanism implies that as a result of an increase of moisture content, a.) the dry density decreases below CMC, b.) the dry density increases between CMC and OMC, and, c.) the dry density decreases again above OMC (Figure 2.12).

A general quality of a fluid is that it tries to envelop solids. At low fluid contents this can lead to surface tension stresses that act like cohesion. This depends strongly on the void structure. This is in fact comparable with cohesion of moistured fine graded materials like (wet) clay. This cohesion makes it more difficult to compact.

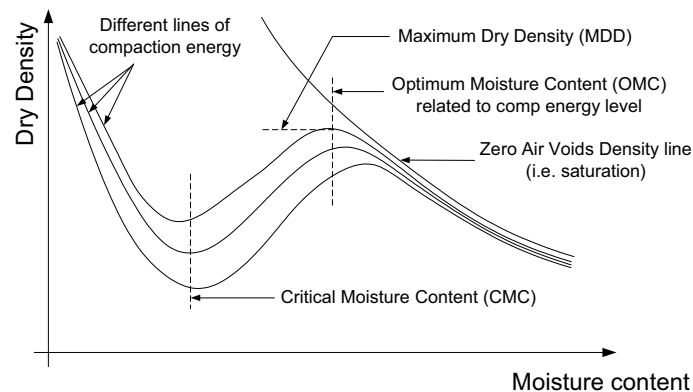


Figure 2.12 Effects of fluid content on achieved density in a granular material (Konig, 1995).

Semmelink (1991) studied the behaviour of unbound granular materials and emphasises the phenomenon of bad compaction related to these low fluid contents. Pike (1972) found that dry materials could be compacted to higher densities than identical slightly moistured material. The moisture content, at which a lowest dry density was found, he called the pessimistic void content. Arquie (1973) reported also about this phenomenon, he called this the “Critical Moisture Content” (CMC). At a just slightly moistened state a granular material absorbs water eagerly. It results in the development of local bonds between the particles.

When fluid content increases the cohesion increases also until all possible bonds have been developed. When moisture content rises further the cohesion decreases due to smaller suction stresses. The cohesion disappears when the material becomes saturated, suction stresses have been neutralised in this case.

Friction affects the movement of particles during compaction. A lubricating fluid in the inter-particle contact surfaces will affect friction resistance. This mechanism becomes dominant when due to the amount of fluid the absorbed film around the particles is developed completely and “free liquid” starts to originate. This free liquid behaves really as a fluid and makes the sliding process of particles, and thus compaction, easier. That specific fluid content, above CMC, results in increased compaction levels related to certain amounts of achieved compaction energy.

This implies that there exists an optimal liquid content coupled to a fixed amount of compaction energy. The phenomenon was object of study of Paulmann (1969), Arand (1972) and Bohmer (1974). They investigated it by measuring density and voids

content of Marshall compacted HMA cores at different bitumen contents. The bitumen content at which the dry density reaches a maximum they called the optimal bitumen content. In soil mechanics the comparable moisture content is known as the “Optimum Moisture Content” (OMC). It is the author not known of there exists also a most “Critical Bitumen Content”.

With an increasing amount of fluid (or fluid and fines, which together form the mortar in an HMA) the available space “in” the aggregate matrix becomes more than “filled”. Now there is more fluid or mortar than there is space in the densest particle matrix. It implies that the particle matrix must become less proxime. This situation is comparable to a “saturated” granular material. At that stage, fluids content above OMC, there are almost no inter-particle contacts and loads have to be carried by the fluid or the mortar. Material behaviour in that stage depends strongly on the stiffness of the fluid or the mortar. Improvement of compaction is difficult because most of the spaces in the mixture are filled. When air voids remain (maximum 2 to 4%), they exist in separated air bubbles that can be driven out.

Suction in the capillary zone

In soil mechanics the effect of moisture in granular materials is extensively studied. In a soil just above the (ground) water table a wet zone (i.e. capillary zone) exists. The water held in the capillary zone (excluding water vapour) can be subdivided into four categories; 1. water chemically bonded in the crystalline structure of the soil particles, 2. water absorbed on the surface of the particles, 3. water held by surface tension forces around the points of contact of the particles, and, 4. water held in the pores between the particles. The mechanisms 3 and 4 cause a negative pressure (i.e. suction) inside the fluid. These negative pressures develop due to a surface tension force acting at the boundary of the solid and the liquid. That force “pulls” so to say the particles together. Investigations from Cronney et al (1991) indicate that the magnitude of the suction depends on the fineness of pore structure in the material, specific weight of the fluid, the surface tension force and the angle of contact between the fluid and the particles.

For a soil this whole system is the cause for the existence of the capillary (wet) zone above the (ground) water table. Since it is plausible that the system can be applied on the particle bitumen mixture; the following analogies can be drawn. Because commonly used HMA mixtures are not “saturated” (they contain air voids) there occurs suction inside the bitumen. These suction stresses (they can be seen as a pre-compression on the particle matrix) can theoretically be the reason that it is possible to enforce a little tensile or shear stress on the material without failure. This suction can also be the reason that the bitumen stays inside the material and doesn’t drop of the particles to the bottom of the layer.

Investigations show that for soils there is a strong correlation between the moisture content and the extent of the suction. When moisture content decreases, suction increases. It is discovered that the extent of the suction can vary widely in extent, from around zero for soils that do not suck up moisture until thousands of MN/m² for oven-dried soils. That large variation makes the use of a logarithmic scale convenient when considering the suction-moisture relationship. Schofield (1968) introduced for

this phenomenon the pF scale, the soil suction is expressed in terms of the length of an equivalent suspended water column and the logarithmic of this length expressed in centimetres of water is referred to as the pF value of the soil moisture.

It is quite plausible that the suction in the fluid in a non-saturated granular material or hot asphalt mixes is the reason for the compactibility behaviour of just slightly “moistened” materials. The phenomenon can be the cause of the mechanism that is illustrated in figure 3.6 between zero moisture and CMC, where the compactibility decreases when the moisture content rises.

Fluid content and inter-particle friction

When a fluid in a granular material does reduce friction between the particles it affects also the ease of particle movement and therefore the ease of compaction. Nijboer (1942, 1948) and Paulmann (1969) studied both the effect of the fluid content on inter-particle friction.

Nijboer did tri-axial tests on respectively dry aggregate samples, samples with only water, samples with oil and samples with bitumen at two temperatures. From these tests he deduced the internal friction of the material ϕ and initial resistance τ (see also Figure 2.8). He concluded that internal friction of the material decreases if there is a fluid added that really lubricates (i.e. oil or bitumen) whereas the internal friction stays equal if a fluid is added that not lubricates. Water proved to be a not lubricating fluid. An assumption in this whole theory is that the inter-particle friction in the mixture determines internal friction. Because the decrease of the internal friction is not very large Nijboer assumed that there is just partly hydrostatic lubrication⁸ between the particles. This implies that between the particles there is partly dry friction and partly lubrication.

Nijboer also found a clear relationship between the initial resistance τ , and the temperature of the material; the initial resistance increased when the material temperature became lower. He assumed that the bitumen viscosity must be the cause for this because it is the only variable in the system that is sensitive to temperature changes.

Paulmann postulated that internal friction should depend on the amount of bitumen in the mixture and developed a relationship between bitumen content, inter-particle friction and compactibility. He concluded that at low bitumen contents the effect of the inter-particle friction is dominant over the effect of the bitumen. Due to the thin bitumen film, lubrication seems to be poor. The particles have almost direct contact and progress in compaction is slow. When bitumen content increases the viscosity of the bitumen starts to play a bigger role. Resistance against compaction becomes smaller because the bitumen film around the particles becomes thicker. Particles can slide more easily and also the compaction progress improves.

⁸ Hydrostatic lubrication is a term normally used in mechanical engineering and also used by Nijboer. It means that there is a fluid film in-between two solid parts. This fluid lubricates the solid surfaces and reduces the dry friction.

When the bitumen content rises further it may happen that the bitumen and the air that is “locked in” presses particles from each other. The particle matrix becomes less proximate, the *VMA* level increases and as a result the total resistance against deformation becomes smaller.

Rheological models for granular materials; Elastic, Viscous & Plastic

It is commonly known that material behaviour of granular materials is mainly plastic especially when the material is virginally compressed (Barnes, 1995). Unloading of a previous loaded granular material and reloading it until the same level will occur mainly elastically. To analyse analogies between HMA and granular material its behaviour during compaction is also investigated in terms of elastic-plastic-viscous behaviour. Figge (1987) studied the HMA material behaviour at an increasing compaction level. His results show that the behaviour at the start of the compaction process is largely plastic and hardly elastic and viscous. When the material becomes compacted this turns over in largely elastic and just little viscous and plastic.

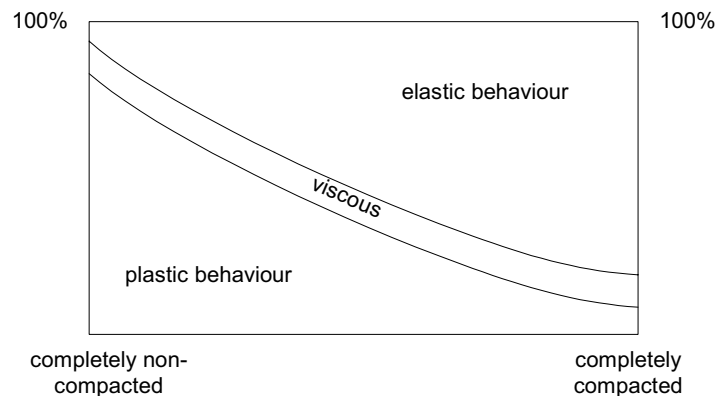


Figure 2.13 Rheological behaviour during compaction, elastic – plastic – viscous, (Figge, 1987).

Figge presented his results in a graph as illustrated in Figure 2.13. The graph shows that the viscous part of the deformation related to the total deformation (i.e. elastic + plastic + viscous), stays approximately equal. The ratio plastic versus elastic behaviour nevertheless decreases considerably during increase of compaction.

Comparing the behaviour of granular materials and HMA

In loose-compacted granular materials and hot, loose-compacted HMA’s similar mechanisms govern the material behaviour during compaction. Both materials are built of solid particles, a fluid and voids. Obviously, the viscosity of the bitumen in an HMA is different from the viscosity of moisture (water) in a granular material. Furthermore the lubricating effect of water in a granular skeleton is different from the lubricating effect of bitumen in an asphalt mixture.

Since asphalt mixtures and granular materials have basically the same behaviour, similar models can be used to describe the compactibility of asphalt mixes and

granular materials. Therefore a soil mechanics model is adopted for modelling the compaction behaviour of asphalt mixes.

2.5. Critical State theory

A suitable soil mechanics model that makes use of elastic-plastic principles is found in the critical state theory, developed at Cambridge University. In this section the main principles of this theory will be presented. The critical state theory describes granular material behaviour by means of a closed yield locus. Different shapes of yield loci are used for different granular materials.

Basic principles in soil mechanics

In soil mechanics, p' and q are often used as stress parameters. p' is the mean effective stress (on the solid parts of the material), it is the stress that is carried by the particles of a granular material. If there is fluid in the material the effective stress is derived by subtracting the fluid pressure in the material from the total stress. q is the deviator stress in the material. If there is no shear stress in the material, $q = 0$; under those conditions the material is “isotropically compressed”.

When a cubical element is subjected to normal and shear stresses, Figure 2.14, the mean effective stress, p' , and the deviator stress, q , are calculated as follows;

$$p' = \frac{\sigma'_{xx} + \sigma'_{yy} + \sigma'_{zz}}{3}$$

$$q = \left[\frac{(\sigma'_{yy} - \sigma'_{zz})^2 + (\sigma'_{zz} - \sigma'_{xx})^2 + (\sigma'_{xx} - \sigma'_{yy})^2}{2} + 3(\tau_{yz}^2 + \tau_{zx}^2 + \tau_{xy}^2) \right]^{1/2}$$

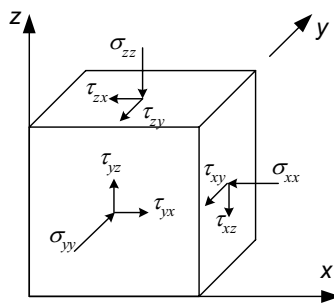


Figure 2.14 A cubic element loaded by normal and shear stresses.

The strains, ϵ_{vol} and ϵ_{sh} , are defined as;

$$\epsilon_v = \epsilon_{xx} + \epsilon_{yy} + \epsilon_{zz}$$

$$\epsilon_{sh} = \frac{1}{3} \left\{ 2[(\epsilon_{yy} - \epsilon_{zz})^2 + (\epsilon_{zz} - \epsilon_{xx})^2 + (\epsilon_{xx} - \epsilon_{yy})^2] + 3(\gamma_{yz}^2 + \gamma_{zx}^2 + \gamma_{xy}^2) \right\}^{1/2}$$

In granular material and HMA mechanics one often deals with axial symmetric samples. For axial symmetrical situations, like a tri-axial test, the equations can be simplified as follows (Figure 2.15):

$$p' = \frac{1}{3}\sigma'_{ax} + \frac{2}{3}\sigma'_{rad}$$

$$q = \sigma_{ax} - \sigma_{rad}$$

In the axial symmetrical situation the strains, ε_{vol} and ε_{sh} , become;

$$\varepsilon_{vol} = \varepsilon_{ax} + 2\varepsilon_{rad}$$

$$\varepsilon_{sh} = \frac{2}{3}(\varepsilon_{ax} - \varepsilon_{rad})$$

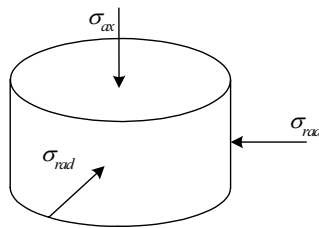


Figure 2.15 An axial symmetrical element supported by effective normal stresses σ_{ax} and σ_{rad} .

Mohr Coulomb, Yield surfaces & critical state

One of the aspects in (elasto-)plasticity theory that makes it appropriate for modelling the compaction process of asphalt concrete is the use of yield loci. A yield locus gives a boundary between stress states that cause elastic (recoverable) deformations and plastic (irrecoverable) deformations. If a stress point falls inside a yield locus, the material behaves elastically, if the stress point falls on the yield locus, the material behaves plastically. However a stress point can never fall outside a yield locus. The yield locus is a limitation of possible stress states.

A well-known example is the yield surface of the Mohr-Coulomb model, which in the principal stress space is an open-ended cone with a hexagonal intersection in the π plane. The basic version of the Mohr-Coulomb model is ideal elastic - ideal plastic. It means that a piece of material is in the elastic phase during loading, until the limit load is reached. When loaded beyond the limit the material behaves plastic. An important limitation of the Mohr Coulomb model (Figure 2.16) is that the cone is open-ended, so that plastic volume changes caused by isotropic compression cannot occur.

Preliminary simulations of the rolling process, (Ter Huerne, 2000), nevertheless showed that during that process high isotropic stress situations occur in the material. This implies that plastic deformations due to these compaction stress situations cannot

be simulated. This makes the Mohr-Coulomb model inadequate for modelling compaction processes of HMA.

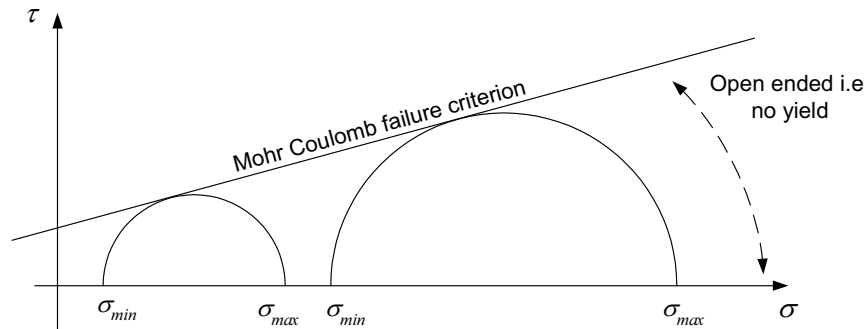


Figure 2.16 The Mohr-Coulomb criterion in the σ , τ stress surface.

There are also models used for describing soil mechanical behaviour that make use of a closed yield locus i.e. they model yield at high isotropic compression stress. Models with a yield locus as a continuous closed curve are used, for example, in the family of critical state models. The Modified Cam Clay model (Roscoe et al, 1968), the model on which all critical state models are based, uses an ellipse as yield locus, with the isotropic p' axis as the symmetry axis.

Stress situations related to critical state

The essence of such a model (or theory) is that it couples the (change in) specific volume of the material to the stress state of that material. The critical state theory distinguishes three stress situations (i.e. critical state itself, left from critical state and right from critical state, see also Figure 2.17) when a material is loaded or deformed plastically. These situations are coupled to the critical state stress situation, which implicitly is one of the situations itself. The critical state situation is defined as the ultimate condition of perfect plasticity in which plastic shearing can continue indefinitely without changes in volume or effective stresses (Wood, 1990). This stress situation is the highest point of the yield locus, see Figure 2.17. When all critical state points for all yield loci for a particular material are connected the critical state line (CSL) is obtained (Figure 2.18).

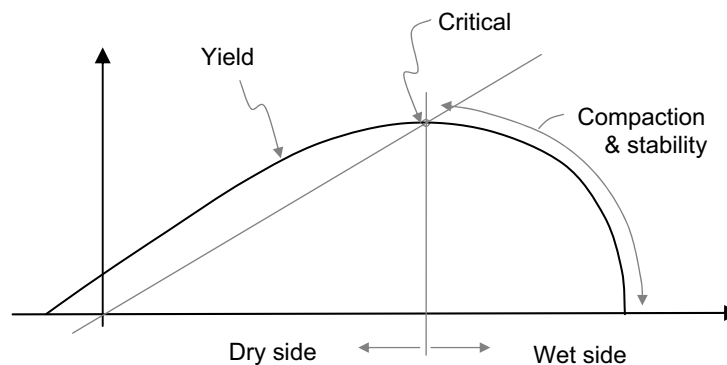


Figure 2.17 The yield locus of an elastic plastic material model.

When the stress situation is left from the critical state and on the yield locus, see Figure 2.17 (i.e. higher q/p' ratio), the material tends to shear. Initially the volume increases and the material becomes less compacted and less strong. Due to this, the yield locus, that represents the material strength, decreases also. A material loaded to this condition (enforced stress level) behaves instable due to the decrease of strength (stress level stays equal whereas strength decreases). The decrease of strength can be modelled with the softening phenomenon.

When the stress situation is at the right of critical state and on the yield locus (i.e. lower q/p' ratio), the material tends to compact as a result of plastic deformation. The volume of the material decreases and the material becomes stronger. Due to the strength increase the yield locus increases too. The material can carry the enforced stress combination or can even carry higher stresses. Hence, the material behaviour is stable. The increase of strength can be modelled with the hardening phenomenon. In soil mechanics the left side of critical state is called the dry side, whereas the right side is called the wet side.

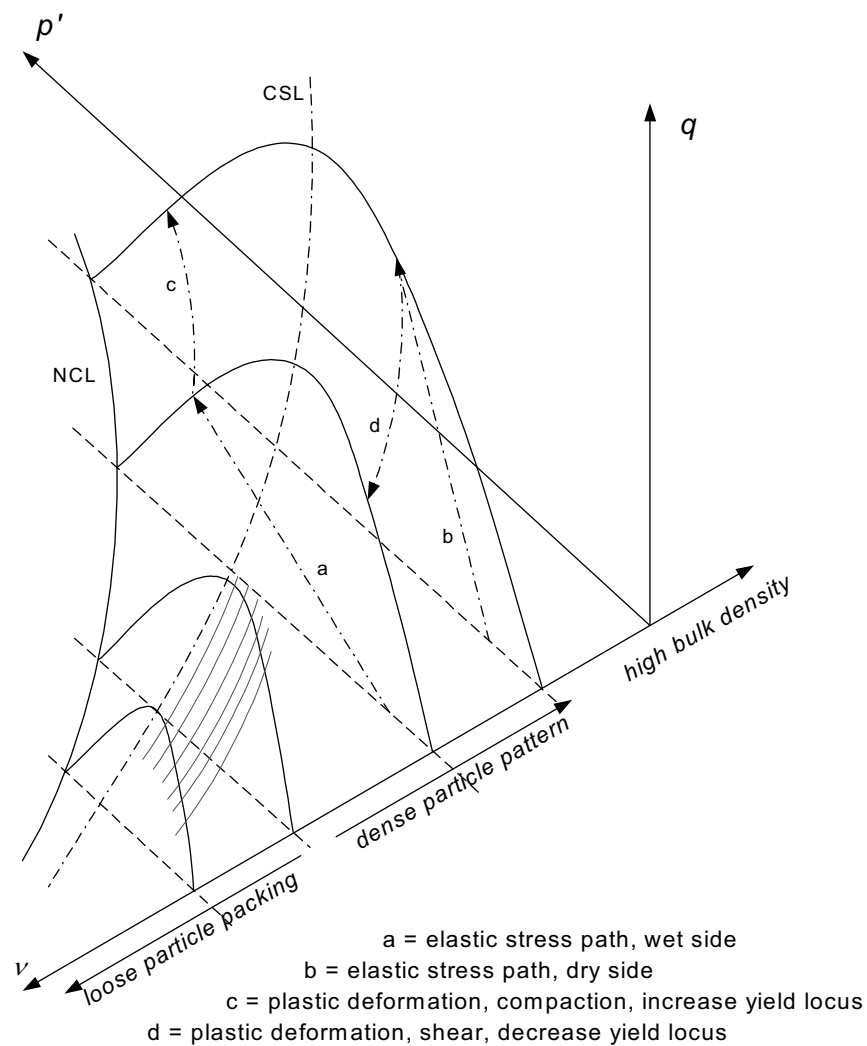


Figure 2.18 Four yield loci for a material as a result of different compacted states and two elastic – plastic stress paths plotted in the p' - q - v space.

A material can also be loaded purely isotropically. In this case there is no deviator stress on it, which implies that $q=0$. A virgin material (no loading history) shows a smooth continuously curved line when the material is loaded isotropically. The line that represents this loading (Figure 2.18 and Figure 2.19) is known as the Normal Compression Line (NCL). The line connects all normal isotropic loading points from succeeding yield loci through a series of specific volumes.

A particular amount of a granular material can have any volume. That volume can be defined as the specific volume of the material in that particular state. For every specific volume the material does have a particular yield locus (i.e. strength). Accordingly the material does have a whole family of yield loci sizes all coupled to a specific volume, v . The size of the yield locus is coupled to the specific volume of the material or the state of compaction of it. Materials in a loose state do have large specific volumes and low strengths; materials in a dense compacted state do have small specific volumes and higher strengths. This theory looks quite suitable for asphalt concrete mixtures for which it is known that better compaction causes a smaller volume and a higher strength up to a certain optimum.

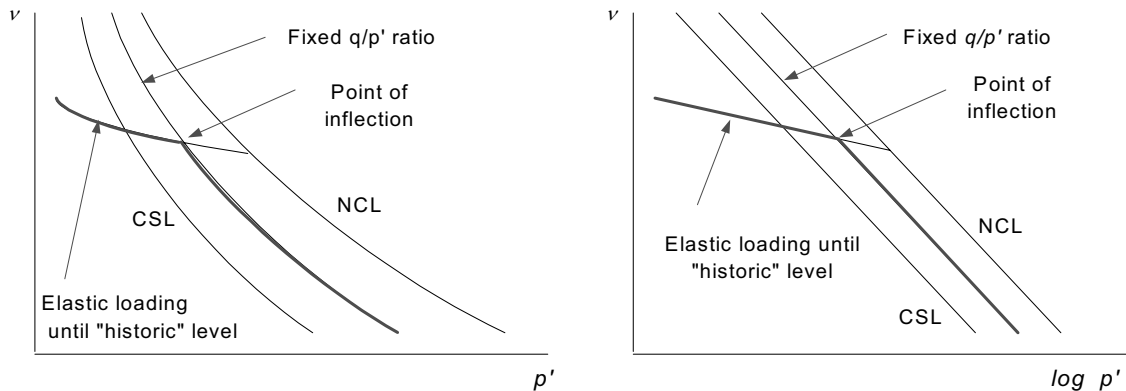


Figure 2.19 CSL and NCL in both the linear $p':v$ plane and the $\log p':v$ plane.

The system is illustrated in Figure 2.18 in which four yield loci are plotted. The system of growth and shrinkage of yield loci is also illustrated in the two dimensional $p':q$ plane in Figure 2.20. The whole curved surface, from the $p'=q=0$ axis, through the CSL line until the NCL line, can be seen as a boundary surface, stresses above that surface cannot exist. During plastic deformation of a material the trajectory of stress follows the surface. When through unloading the stress level comes below the surface the material does not deform plastically anymore but deforms elastically.

Elastic plastic flow behaviour; Stable or Instable

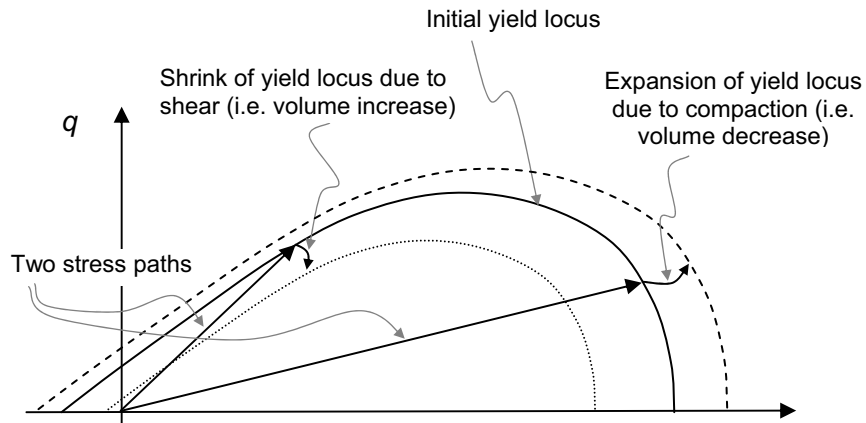


Figure 2.20 Shrink and growth of a yield locus through plastic flow.

During a well-controlled compaction process the compaction energy is turned into an increased material strength caused by stable material behaviour (i.e. no too high shear stresses). However, if compaction is carried out with an extremely heavy roller or the mixture is too soft this could lead to high shear stresses that may cause shear deformations, the system is unstable now, roller fissures or cracks may occur and possibly even shearing of the material. There is no progress in compaction and one can best describe this as a poor compaction process.

In Figure 2.21 stable and instable material behaviour of a particle based material during flow is illustrated. During instable behaviour material strength decreases after a peak strength has been reached (curve B), whereas as a result of stable behaviour the strength increases continuously during plastic deformation (curve A).

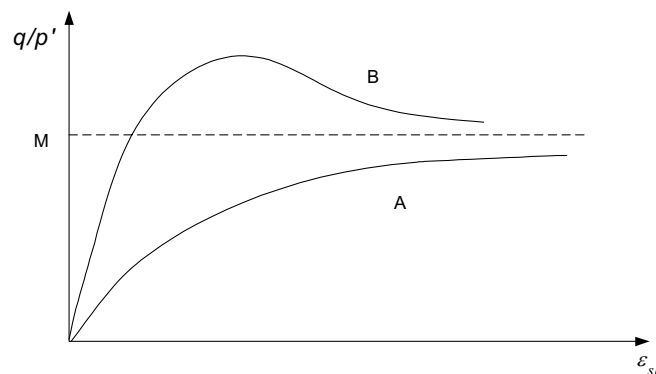


Figure 2.21 Stability and instability of a particle based material during flow.

Loading “in Situ” materials

In reality, materials are almost never in a virgin state but do have a loading history. In that situation the loading line in the $\log p':v$ plane, shows a point of inflection at a certain point, see Figure 2.19. When the material is loaded below this “bending point” deformations are almost completely elastic. This is caused by the (almost) absence of particle rearrangement. Until this loading level, deformations are mainly caused by deformations of the particles themselves. The deformations will recover when the material becomes unloaded. When the loading rises above that “bending point” the particle matrix starts to rearrange itself and due to that deformations it becomes elastic-plastic.

The critical state soil mechanics also shows that for many granular materials the lines of plastic deformation become straight when they are plotted in the $\log p':v$ plane (Wood, 1990). Materials can also be loaded with a fixed q/p' ratio. Critical state soil mechanics shows that these lines are straight and parallel to NCL and CSL lines if plotted in the $\log p':v$ plane. In fact such lines express how easy a material deforms plastically (i.e. compact). This system of representing material behaviour will be used during the analysis of the material testing during the compaction research of HMA. In the chapter 4 material measurements will be discussed. All material measurements will be carried out at a fixed q/p' ratio and compression lines will be presented.

Different yield loci

If one applies the critical state theory to different types of granular materials (powders and probably HMA as well) one will obtain different shapes of yield loci. In the original Cam Clay theory this yield locus was a logarithmic spiral, later on in Modified Cam Clay (MCC) theory it was modified into an ellipse. As an extension to the Cam Clay theory several yield loci have been developed. Some of them provide a better fit with experimental data and others are more practical and lend them-selves to easier mathematical manipulations, (Brekelmans, 1989). Literature studies reveal that many researchers have developed specific shapes of yield loci for these types of models. Shapes of commonly used yield loci are illustrated in Figure 2.22.

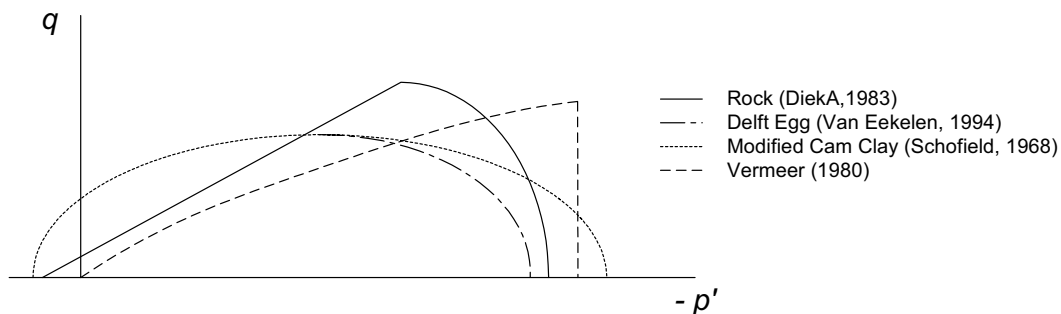


Figure 2.22 Different shapes of yield loci (Teunissen, 1983, Brekelmans, 1989, Van Eekelen, 1994, Schofield, 1968).

In this compaction study we will adopt a yield locus that is implicitly implemented in the “Rock model” which is incorporated in the DiekA FEM approach. This model has several parameters that allow the user great flexibility in selecting the most desired shape. Details about the Rock model and the DiekA approach will respectively be discussed in chapters 3 and 4.

Nature of deformation of asphalt mixes during compaction

The analogy between the behaviour of HMA and that of granular materials holds when the temperature during compaction is constant and homogeneous. A change in temperature of the mixture causes a change in the viscosity of the bitumen. This may affect the slope of the NCL and CSL in the p' versus v plane. In the material measuring programme (chapter 3) this slope was obtained for three bitumen viscosities (equivalent to three temperatures).

Plastic potentials and association of flow rules

Plastic potentials are curves in the $p':q$ effective stress plane to which, by definition, the vectors of plastic strain increment are orthogonal. It is often convenient to make plastic potentials and yield surfaces that coincide. If the plastic potential and the yield surface are identical, then the plastic deformation of this material model obeys an associated flow rule. If the plastic potential and the yield surface do not coincide, plastic deformation obeys non-associated flow. The yield cap of the Rock model obeys associated flow. This implies that with the choice of a shape of the yield locus one also chooses the plastic potential.

Plastic behaviour of powders

Compaction of powders is a forming process that is used during the manufacturing of several ceramic products. To achieve quality of the ceramic product it is necessary to compact the base material homogeneously ensuring that residual stresses remain small.

In 1989 Brekelmans completed his work on compaction of powders in a mould. Brekelmans dilemma was that there were no constitutive models for powders. To solve this he simulated the compaction processes of powders by using a FEM tool. He believed that there was a close similarity between compaction of granular materials and powders. This belief was supported by an extensive research on various yield models such as; Vermeer, Ashton, Suh and Nova. All of them used an “open” Mohr-Coulomb type of criterion together with a second branch of a closed critical state type of “criterion”.

The study of Brekelmans is important for this study because of two aspects. 1.) There is an analogy between this research into the compaction of HMA and that of Brekelmans. For both materials there were no constitutive relations for compaction behaviour available. Hence, the material behaviour had to be simulated with use of a model from a different material discipline. 2.) Brekelmans did an intensive literature

survey after different shapes of yield loci. He presented them graphically, see also Figure 2.22.

Material model “Rock”

Around 1983 the semi two-dimensional “Rock” material model was implemented in the DiekA FEM code. It was originally formulated to study the behaviour of soft rock materials. The model describes elastic-plastic material behaviour by using the critical state principles. For describing elastic material behaviour the model uses the modulus of elasticity, E , and the Poisson’s ratio, ν . For hardening caused by compaction, and, softening caused by shear, two parameters can be defined. The shape of the “Rock” model yield locus is created with help of four zones as illustrated in Figure 2.23. The zones indicate the direction of deformation at the elastic-plastic interface, they regulate associated versus non-associated flow.

The shape of the yield locus in the Rock model is controlled by eight parameters. With the use of these parameters several reasonable yield loci can be formulated. The shape of the plastic potential is not freely adjustable. The way plastic deformation is coupled to the governing stress level depends on the zone of the yield locus that is active.

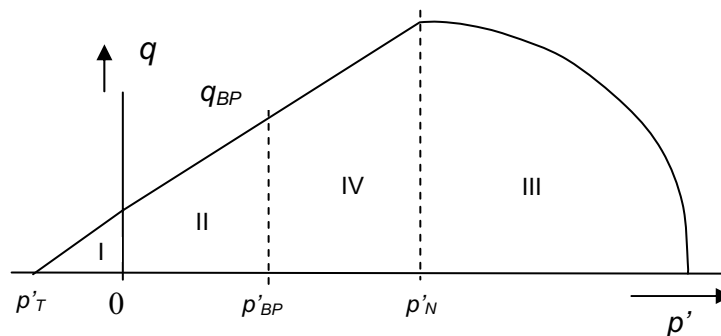


Figure 2.23 The yield locus and four zones of the used “Rock” material model.

The shear branch of the rock model yield locus can be modelled as a curved or straight line. The closure cap is modelled elliptical (eccentricity can be chosen). During this HMA compaction research, attention is mainly focussed on the closure cap of the yield locus. Therefore this part of the model (i.e. the shear branch) is kept simply straight. More details about the Rock model can be found in Section 4.3 and Appendix E.

Summary

Granular materials and HMA are both granular materials consisting mainly of solid particles. The spaces between the particles are partly filled with air and partly with liquid (for HMA; at compaction temperatures). All activities aiming to bring particles into a closer pattern are referred to as compaction. Particles in mixtures are sliding along each other during this activity. Compaction realises a more stable stacking of the particles and a larger number of inter particle contact points, resulting in a higher bearing capacity of the material.

The importance of compaction is underscored by several studies. By well-known research institutes in the road building branch it is even thought that compaction probably could be the most crucial stage in the construction of any layer within a road pavement.

Inside granular materials and HMA, the fluid medium plays a similar role when the particles are sliding along each other. The fluid lubricates the particle faces, reducing inter-particle friction and does make particle movement and compactibility easier. For a certain amount of compaction energy there is both an optimum and a worst fluid content that leads to maximum compactibility versus least compactibility. Due to the analogy between HMA and granular materials it should be possible to adopt soil mechanical constitutive relations for modelling the compaction behaviour of HMA.

Different ways of measuring compaction levels and compactibility values of HMA's and granular materials can be distinguished. This research selected Voids in the Mineral Aggregate (*VMA*) and the *C*-value method for measuring compaction and compactibility respectively.

The critical state theory has found to be suitable for modelling the compaction process of particle based materials. The theory is comprehensive and deals with situations where shear takes place during loading and also where compaction takes place. The theory operates with a yield locus as an interface between plastic and elastic behaviour. Yield loci and specific volumes can grow or shrink due to achieved loading stress combinations.

Compaction has to be optimised. The compressive force (roller properties) has to be suitable to the material being compacted, otherwise unfavourable shear results.

In describing HMA compaction a yield locus that is implicitly implemented in the Rock model is adopted. The "Rock" model makes use of hardening due to compaction and softening if the material is sheared. Because it uses a lot of parameters, the user can select almost any type of shape of the yield locus. The model makes use of associated flow in the compaction i.e. closure branch.

3. Modelling HMA material behaviour

3.1. Introduction

To be able to simulate HMA compaction processes, the mechanical material behaviour during compaction has to be known. However, fundamental constitutive models that describe the behaviour of HMA materials are not available. During compaction the arrangement of the particle pattern inside the HMA matrix changes from loose to dense. This behaviour is similar to that of granular material. From this similarity came the idea to adopt a soil mechanical model for describing the HMA behaviour. To calibrate such a model for HMA, a material measurement programme has been designed.

To be able to simulate HMA compaction processes, the mechanical material behaviour during compaction has to be known. However, fundamental constitutive models that describe the behaviour of HMA materials are not available. During compaction the arrangement of the particle pattern inside the HMA matrix changes from loose to dense. This behaviour is similar to that of a granular material. From this similarity came the idea to adopt a soil mechanical model for describing the HMA behaviour. To calibrate such a model for HMA, a material measurement programme has been designed.

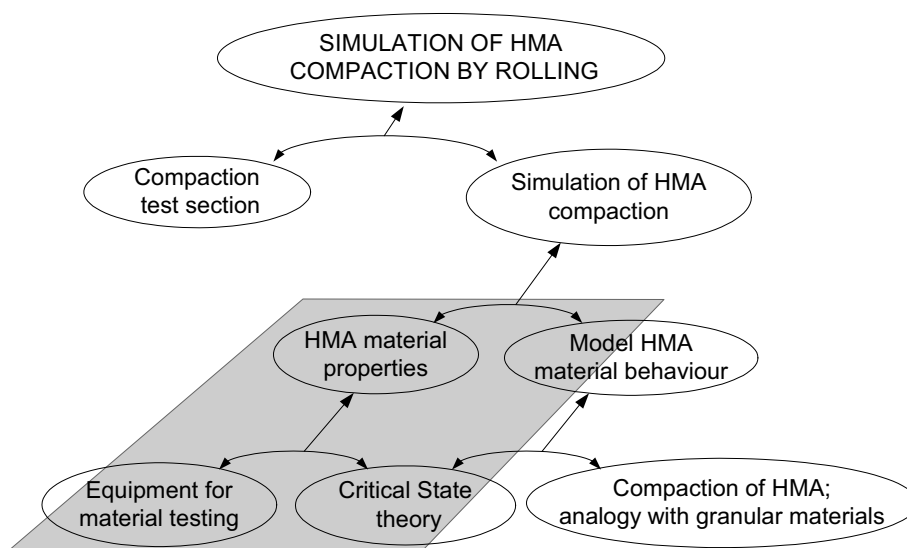


Figure 3.1 Set up of the compaction research with the topics discussed in chapter 3 highlighted.

One of the main goals of this chapter is measuring material properties with respect to critical state principles and transforming those into the selected material model parameters. The information that is required for feeding the material model consists of; a.) the shape of the yield locus, b.) the size of the yield locus as a function of temperature and compaction level, and, c.) hardening and softening properties due to compaction or expansion. Figure 3.1 highlights the topics that will be discussed in this

particular chapter and it shows the purpose of this chapter within the overall research project.

Deduction of the critical state material parameters requires adequate testing equipment. In soil mechanics tri-axial testing is commonly used for that task. It is essential to control the volume of the sample during such tests. The Hveem Stabilometer is also suitable for measuring axial symmetrical sample properties. In such a stabilometer the radial confining pressure on the sample occurs due to radial deformation, which is more or less identical to the way the radial stress develops during compaction. The stabilometer test therefore simulates the conditions during compaction in a realistic way and seems therefore be better suited to the task than triaxial equipment.

However, the Hveem Stabilometer in its standard form does not have adequate control of the sample volume. To achieve the wanted accuracy on volume control over the sample the stabilometer had to be modified. A comparison of the most important aspects of a tri-axial test, a HSM test and a MHSM test is summarised in Table 3.1. The way the stabilometer was modified and the working principles of this Modified Hveem Stabilometer (MHSM) will be discussed in section 3.2. In section 3.3 attention is focussed on doing tests with the MHSM and how the required material properties can be obtained from these tests.

TRI-AXIAL EQUIPMENT COMPARED TO HVEEM			
	Tri axial	HSM	Modified HSM
Confinement medium	Foil & fluid or air under pressure	Air /oil mixture	Oil
Dimensions ratio sample h/d =	2.5	0.6	0.6
Volume control	Difficult	Poor	Reasonable
Confinement stress	Fixed, every predefined quantity possible	Progressive, result of radial deformation, not adjustable	Linear, result of radial deformation, Adjustable
Maximum confinement stress [MPa]	ca. 0.6	ca. 1.1	ca. 1.1
Coupling radial/axial loading stress	Independent	Dependent	Dependent

Table 3.1 Comparing the tri-axial test equipment to original and modified HSM.

An experimental programme has been devised for measuring material properties. In total 6 test series of approximately 6 experiments each were performed. The first two test series were carried out for validating the suitability of the equipment; one with a lower bitumen content and one with a rounder particle shape. After that, the material, Dense Asphalt Concrete (DAC) 0/11, is tested at three “temperatures” and two “stress combinations”. Because the equipment was not suitable to test the materials hot, the minerals were mixed with modified bitumen (viscosity) in such a way that they behave as if they were hot. Accordingly four variables are involved in the

experimental programme; temperature of the material (i.e. bitumen viscosity), confining stress-strain relationship, aggregate angularity and bitumen content. The experimental results are analysed and discussed with relation to the composition of the materials. Since the experiments lead partly to counter intuitive results (higher material temperature causes less compactibility) attention is focussed on mechanisms that can explain this phenomenon. The measurement programme and the results of it are presented in section 3.4. The validity of the MHSM equipment for measuring critical state parameters for HMA mixtures is discussed in section 3.5. The deduction of the critical state parameters from the test results is discussed in section 3.6.

3.2. Modification of the Hveem Stabilometer

In the engineering field uni-axial tests (i.e. tests without lateral “confining” stresses) are used for deduction of material characteristics for materials such as steel and cement concrete. Many granular materials cannot be tested that way due to a lack of cohesion. Without confining pressure they would fall apart during a test, Wood (1990). The same holds for HMA materials especially when they are in a non-compacted state. When testing the material, it should be loaded to the same conditions as it would be in an “in situ” situation. For HMA this requires a radial “confining” stress.

In chapter 2 it was found that for elastic-plastic modelling of hot (or soft) HMA mixtures, a model with a closed yield locus could be suitable. In soil mechanics the tri-axial cell is the basic equipment for deducing critical state material parameters. The device is an axial symmetrical one with two degrees of freedom. It is essential that the volume of the sample is controlled during such a test. Like the tri-axial cell, the Hveem Stabilometer can measure material properties of axial symmetrical samples. An essential difference compared with the tri-axial equipment, however, is the way the radial pressure is applied on the sample. In (most) tri-axial test equipment the radial pressure on the sample is an enforced (fixed) quantity. During a Hveem Stabilometer test the radial pressure on a sample is the result of the radial deformation of the material; that is exactly the same as how radial stress develops during compacting a material under field conditions. That radial deformation in turn depends on the stiffness (of the particle matrix) of the tested material and the vertical load. The Stabilometer test therefore simulates in a realistic way the conditions to which the material is subjected during compaction.

Principles of the Hveem Stabilometer

Hveem designed and developed an apparatus (Figure 3.2) for testing the stability of HMA samples. The fundamental concept behind this apparatus (Stabilometer) was that the characterisation of a granular based material could be achieved by measuring its ability to carry a reasonable axial load without too much radial deformation (Hveem, 1950). A horizontal stress is generated within a rigid sample upon application of a vertical load. The Hveem Stabilometer (HSM) utilises this principle by measuring the horizontal confining stress required to support a given vertical load. That quantity is defined as stability.

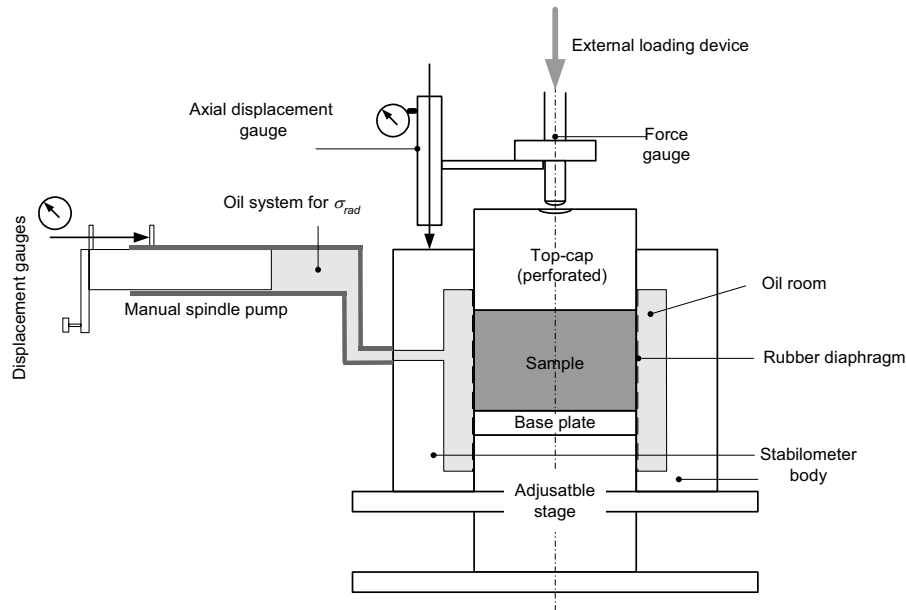


Figure 3.2 The principles of the standard Hveem Stabilometer.

Like other tri-axial test equipment the HSM makes use of axial symmetrical samples. External facilities are required to apply an axial load and to measure the axial deformation. A mixture of oil and air surrounds the sample radially. A rubber diaphragm separates the oil/air mixture and the sample. This oil/air mixture is further enclosed in the rigid stabilometer body and therefore provides sample confinement. The pressure in the oil/air mixture is a function of the radial deformation of the sample. This pressure is measured using a standard pressure gauge. By altering the ratio of oil to air in the mixture one can alter the response of the system to specific deformations.

The main differences between a standard tri-axial cell and the HSM are the way the radial confining stress is applied to the sample and the geometry of the sample. In the tri-axial test equipment the height of the sample is about 2.4 times the diameter whereas in the HSM that ratio is 0.6. In the tri-axial cell therefore, shear surfaces can freely occur in the sample during a test. In the HSM they can not develop as freely because of the sample dimensions. The possibilities for development of shear surfaces in a sample related to its dimensions are illustrated in Figure 3.3. Development of shear surfaces is important if the test sample is loaded to high shear stress conditions. These stress conditions are irrelevant for compaction of the material.

Also a comparison can be made between material samples inside the tri-axial cell, the HSM and in the road. In the road a confining stiffness around the material piece under consideration is not always present. It is only present when a load (roller) is passing the considered piece of material (i.e. when a loading stress is applied on the material). The HSM operates on the same principle. Confining stresses only develop when there is an axial load on the sample, which causes radial deformations. One can see that these two systems match. For the tri-axial cell this is not the case. In the tri-axial cell the confining stress has to be arranged on a fixed level throughout the whole test.

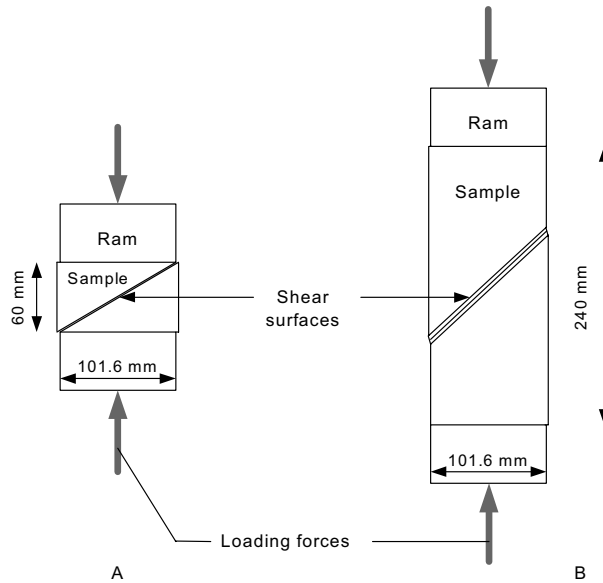


Figure 3.3 The differences in sample dimensions and possible consequence for shear planes of the Hveem Stabilometer sample (A) and the tri-axial sample (B).

Stresses and strains in the Hveem Stabilometer

The origin and interaction of the various stresses and strains in the Hveem Stabilometer sample are listed below;

- Axial deformation and loading;* The axial loading is enforced by use of an external loading device. Using an external displacement transducer monitors the axial deformation.
- Radial confinement stresses and strains;* Due to the nature of the stabilometer a radial confining pressure develops as soon as a radial deformation occurs⁹. How this mechanism causes a strongly increasing progressive and non-linear increase of the radial confining stiffness is illustrated in Figure 3.4. The radial stress on the sample can be deduced by reading the pressure gauge. The radial deformation of the sample cannot be measured directly, but is calculated from the air volume at the relevant pressure. Such a calculation step is a relatively complex activity, which can quickly initiate unreliable results.

⁹ This mechanism occurs because behind the rubber diaphragm an oil-air mixture is locked inside the HSM body. The mechanism obeys the (gas) law of Boyle-Gay Lussac. When the air volume that is locked in is reduced to 50% of the initial volume caused by radial sample deformation, the absolute pressure in the oil is doubled.

Requirements for modifying the HSM

Testing the behaviour of loosely compacted HMA mixtures requires a well-defined and accurate volume control. The disadvantages of the Hveem equipment in its standard form could not be accepted for measuring proper HMA material properties. These disadvantages are; a.) the poor accuracy of the volume control over the sample during a test, and, b.) the non-linear confining stress-strain relationship caused by the air that is locked in. The confining stress-strain relationship applied on the sample is progressive and poorly adjustable.

It is preferable that the confining stress-strain relationship is linear to the radial deformation and better adjustable. Then straight stress paths with different slopes in the $q:p'$ space are possible. In that case a wider set of stress combinations can be applied on the sample.

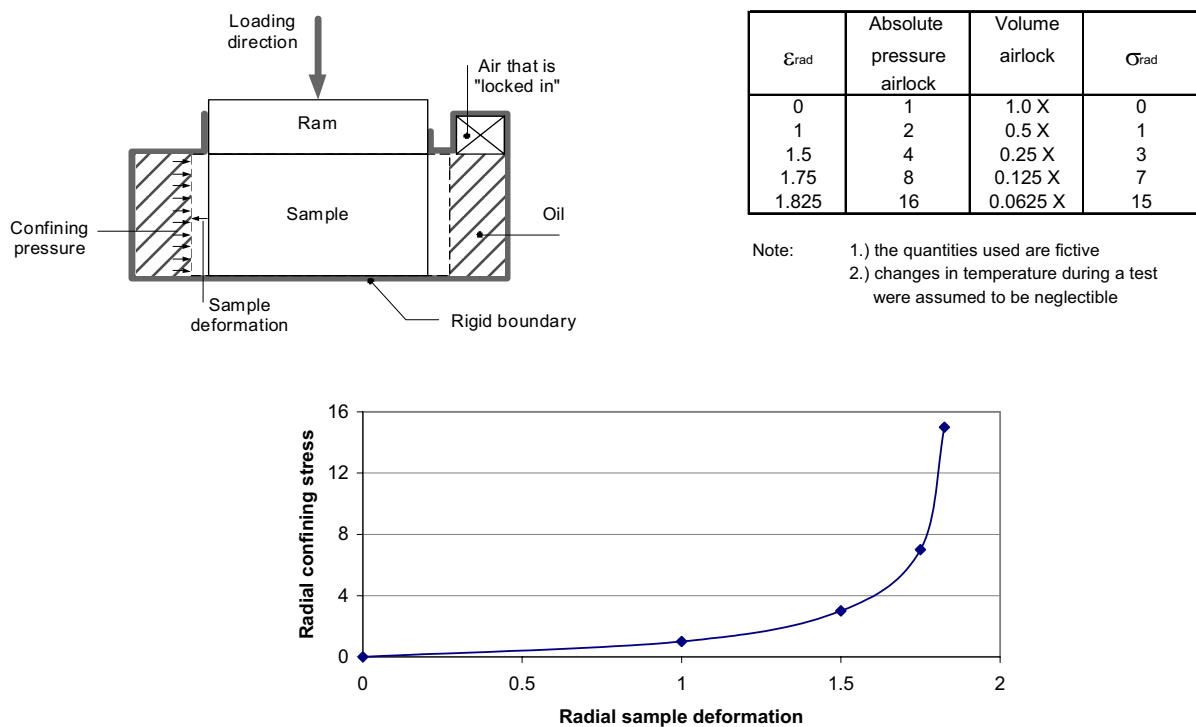


Figure 3.4 An illustration of the mechanism inside the HSM that governs the confining stiffness.

The basic principles of Hveem's equipment are correct; the material is vertically loaded while the magnitude of the confinement stresses is related to the radial deformation. Therefore possibilities were investigated to modify the HSM without disturbing the basic principles and without developing a complete new testing apparatus. The modification should improve the volume control over the sample and it should make the confining stress-strain relationship adjustable.

The modification developed consists of a cylinder with a diameter of 32 mm and a length of 325 mm. Inside that cylinder operates a piston which position is controlled by a mechanical spring. In the modified HSM the oil is the only medium that converts radial sample deformation into piston translation. A measuring gauge that is built in at one end of the cylinder can measure that translation. The principles of this Modified Hveem StabiloMeter (MHSM) are illustrated in Figure 3.5. The modification is developed in such a way that it can be assembled between the two flanges of the manual spindle pump and the Stabilometer body. Assembly of the supplementary cylinder (modification) on the original HSM is shown in Figure 3.6. It is not necessary to dismantle the HSM for assembly of the modification.

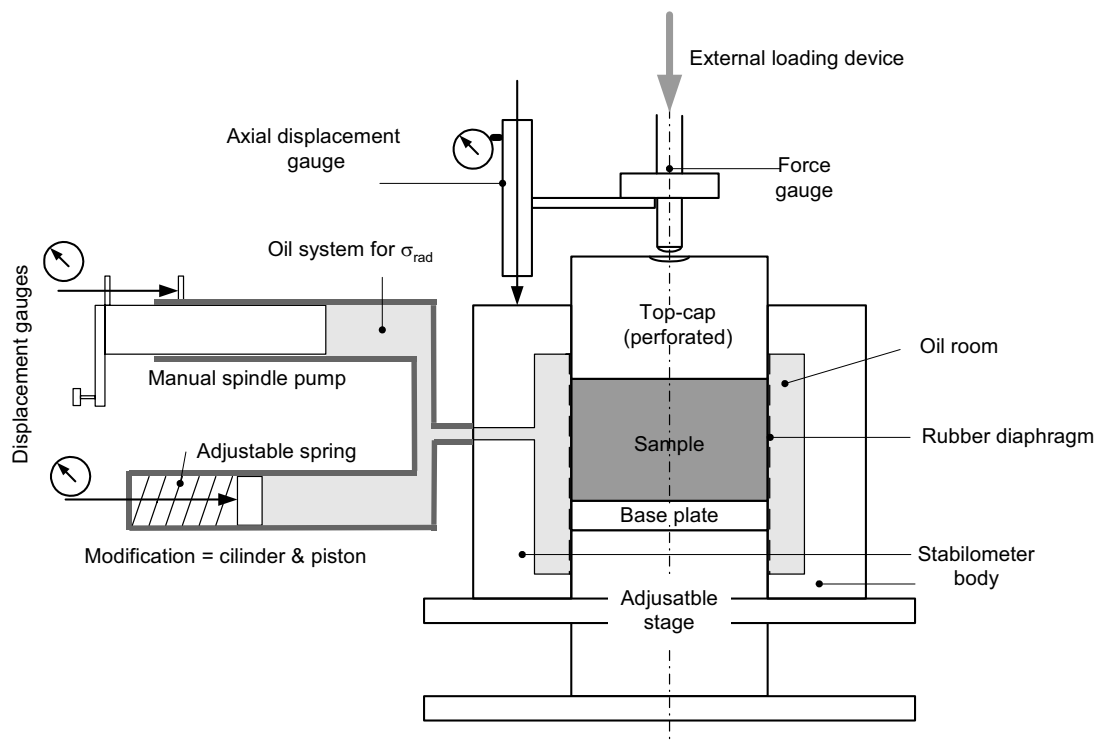


Figure 3.5 The principles of the Modified Hveem StabiloMeter.

The basic principles of the MHSM are the same as the HSM; a vertical loading on the sample generates a radial displacement and this radial deformation generates a radial confining stress on the sample. However, the radial deformation of the sample now generates a displacement of the newly installed piston and alternates the spring length and force. Therefore the piston displacement will alternate the oil pressure and thus the confining pressure on the sample. The radial confinement stress-strain relationship is adjustable by changing the spring stiffness. Due to the modification, the confinement stress strain relationship on the sample is now approximately linear. Additionally, because the oil is now free of air, the radial expansion volume of the sample is equal to the translation volume of the newly involved piston and can be measured accurately. Deduction of the radial expansion of the sample, together with the measured axial deformation, provides volume control over the sample during a test.

A small uncertainty during the test is the way the sample deforms radial. After measuring all the correct quantities the radial deformation of the sample should be homogeneous over the height (i.e. no barrelling). However laboratory experiences indicated that little barrelling did occur. Measurements on tested samples showed that the diameter in the middle was about 2 to 3 mm (i.e. 2 to 3%) larger than the diameter at the top and the bottom of the sample. It proved hard to do these measurements accurately because after testing, the surface of the test sample was very rough. During a test, at maximum load, these measures could not be taken and the extent of barrelling during maximum load stays therefore unknown. For calculating the radial deformation from the piston displacement we assume homogeneous radial deformation of the sample i.e. no barrelling. The consequence of the fact that a little barrelling did occur during the test whereas this was not assumed is that the calculated radial strains will have a small error.



Figure 3.6 The assembled modification (cylinder) in between the standard HSM components.

Quantities measured in a Modified Stabilometer test

A test with the MHSM provides the following measures:

- the axial loading force [kN],
- axial deformation [mm],
- radial stress [MPa],
- piston displacement of the HSM modification [mm].

From these MHSM test signals the axial and radial stresses and strains can be determined.

<i>Axial deformation and loading;</i>	Measurement of axial loading force and deformation is similar to the standard HSM. The axial stress σ_{ax} , and axial strain ε_{ax} , can be calculated from the axial loading and axial deformation.
<i>Radial confinement stresses & strains;</i>	In the MHSM set up the radial confinement stress-strain relationship can be adjusted by changing the spring in the additional cylinder. Due to the nature of the MHSM the magnitude of the confinement stress on the sample is almost linear to its radial deformation. The oil pressure is equal to the radial stress on the sample and depends directly on the deformation of the sample. The electronic oil pressure gauge measures the radial stress, σ_{rad} , accurately during the test. Radial deformations (and strains) cannot be measured directly, they have to be calculated from the piston displacements and other factors.

The required quantities for realising the material relation between p' , q and VMA (or ν), can be calculated at any stage during the test from the primary stresses and strains.

From the radial and axial stresses and strains the parameters p' , q and the strains ε_{vol} and ε_{sh} can be calculated using the relationships given in chapter 2. The VMA value of the sample can be derived at any stage because the total volume of the sample and the amount of aggregate and bitumen is known. From this data the p' - q - VMA relation can be obtained at any point in time during the test.

Translating temperature variables into viscosity variables.

Mixing of HMA in the plant takes place at high temperatures to achieve good wetting of the particles with bitumen. The material is kept hot during storage and transport because the material should stay workable and compactable. When the material is hot the viscosity of the bitumen is low. During compaction the mixture cools while it is rolled. The research aims to model the material behaviour while it is under compaction. It means that a.) the material cools from approximately 140°C to 70°C, and b.) the particle matrix changes from loose to dense.

Measuring material properties is difficult especially when one is dealing with a material with a temperature between 70 and 140°C and when the material does not have coherence. The proposed equipment is not easily made suitable for measurements at such high temperatures. Equipment parts such as the membrane and gauges do not function adequately at those temperatures. Instead of heating the material, a solution was found by adjusting the material in such a way that it behaves as if it was hot; use is made of so-called “fake bitumen”¹⁰.

¹⁰ This material adjustment is made by using bitumen that has a viscosity at room temperature that is equivalent to normal (80/100 Pen) bitumen at compaction temperature.

When the temperature of an HMA mixture changes, it primarily changes the bitumen viscosity and secondly the volumetric ratio bitumen-aggregate. A change in volumetric composition occurs caused by the different temperature expansion coefficients¹¹ of both components. To simulate these effects in a cold condition, the bitumen-content and -viscosity of the tested samples have to be corrected. The experimental measurements are carried out on samples at room temperature (approximately 20°C).

An additional mechanism that can play a role when HMA mixes are compacted is the enclosure of air voids. In the beginning of the compaction process there exists a structure of pores (air filled voids) throughout the material. This structure makes it possible that air can be driven out during compaction. At a certain compaction level this pore structure disappears. The connection between the larger pores ceases to exist and the system turns over in separated air bubbles divided over the material matrix. Nijboer (1948) assumes that this turn over takes place at void percentages of 2 to 4.

Under the assumption that closed air bubbles originate at for instance 100°C and the mixture cools to 20°C the pressure inside the air bubble can be calculated with the ideal gas equation of Boyle-Gay Lussac (Young, 1996). This is the gas equation;

$$P \times V = C \times T$$

in which; P = Pressure MPa
 V = Volume in mm³
 T = Temperature in °C
 C = a fixed value

With this formula one can calculate that when separated air bubbles occur at 100°C and the mixture cools to 20°C, the pressure inside the air bubbles reduces from 100 kPa (1.0 BAR) to 78.6 kPa. It implies that due to the cooling of the material (locally) a change in compression stresses on the particle matrix can occur. In the measuring programme done on the cold mixes with fake bitumen these effects of possible extra stresses are not incorporated. These samples were compressed until isotropic pressures of approximately 1400 kPa. Related to that large pressure of 1400 kPa, the reduction in compressive stress due to cooling of 21.4 kPa can be considered as small. It is believed that neglecting this phenomenon will not introduce large errors and that it is acceptable to ignore it.

Another aspect that plays a role when a cold mixture for tests is used which imitates hot HMA is the volumetric proportionality aggregate-bitumen. When a mixture is cooling the relative volumetric share of the bitumen declines because of the differences in temperature coefficients of the aggregate and binder. In the main testing programme we tested at three different bitumen temperatures. While calculating the bitumen contents for those mixture compositions corrections were made for the above-described phenomenon. The material properties were deduced at three different material temperatures. However, because material properties had to be known for a

¹¹ The temperature expansion coefficients (α) of both involved components do vary enormously. The factor α for bitumen, α_{bit} is 200×10^{-6} , whereas the same factor for aggregate, $\alpha_{agg} = 8 - 14 \times 10^{-6}$.

whole temperature domain, the behaviour between those temperatures was assumed to be linear. On its own this is a plausible assumption, however, it can be that this does not correspond to reality e.g. because of the existence of a solidification temperature inside the relevant temperature domain.

3.3. Conducting an MHSM test

A lot of testing work done by means of the MHSM provided a substantial amount of experience with the equipment. Based on that experience a standard testing method was developed. This section describes how the Modified Hveem Stabilometer (MHSM) can be used for obtaining material properties of HMA. Important elements are:

- checking equipment behaviour,
- test sample preparation,
- running procedures for achieving a test,
- deducing primary stresses and strains,
- deducing accurate initial sample quantities.

Checking equipment behaviour

Before the measurement of material properties can start it is recommended to bleed and test the MHSM. Inside the equipment rubber seals confine the oil in the high-pressure areas. When the MHSM is not frequently used, the rubber seals can harden and possibly leak. Bleeding the MHSM can be achieved by pumping pure oil in the stabilometer body while instead of a sample a metal dummy is placed. If the oil is pressurised for a while the air can be bled at the highest point by opening the “waist gate”. The bleeding should be continued until no further air remains.

A so-called stretch test can be performed to check properly working of the equipment. To do this again a rigid dummy must be placed inside the apparatus. The test should start at an oil pressure of 0.015 +/- 0.001 MPa. That pressure pushes the rubber diaphragm very lightly against the rigid core. Rotation of the Stabilometer body around the dummy, by hand force, indicates that the pressure for our purpose is adequate. The pressure should then be increased until 1.0 MPa by turning the manual spindle pump. While increasing the oil pressure the movement of the piston and the manual spindle pump should be monitored. After a few seconds the pressure can be reduced until the initial value of 0.015 MPa. In an ideal Stabilometer all parts are rigid and the volume generated by the screw pump should correspond to the volume that is released through the piston displacement. However, experience with the apparatus indicated that both volumes did not correspond. The difference between them indicates the magnitude of volume loss that occurs while the oil pressure is raised.

The fact that there is a loss of volume during pressurising the MHSM implies that either the apparatus expands under pressure or a combination of the following points occurs;

- some pockets of air remain in the hydraulic system in spite of being bled,
- oil seals set themselves and consume volume when pressure is increasing.

The differences manifest themselves continuously when pressure increases, and they proved to be relatively constant. Due to this consistent difference the test results were corrected during the analysis. During the test programme, corrections for MHSM tests were always based on stretch tests done at the same day before the testing of HMA samples started.

With the equipment used in this experiment, values for “volume loss” were obtained in-between 1700 and 2200 mm³ for pressures up to 1.0 MPa. These values were obtained by carrying out a large number of “stretch tests”. If the obtained value is above the 2200 this can be an indication that the MHSM is not properly bled. In Figure 3.7 the “volume loss” measured during a particular stretch test is depicted against the oil pressure, P_{oil} . For reliability it is recommended to repeat the test, which is what is done. The volume loss that is deduced by a stretch test will be used for correcting the results measured with the MHSM. The calculated correction line shown in Figure 3.7 is estimated with a polynomial equation.

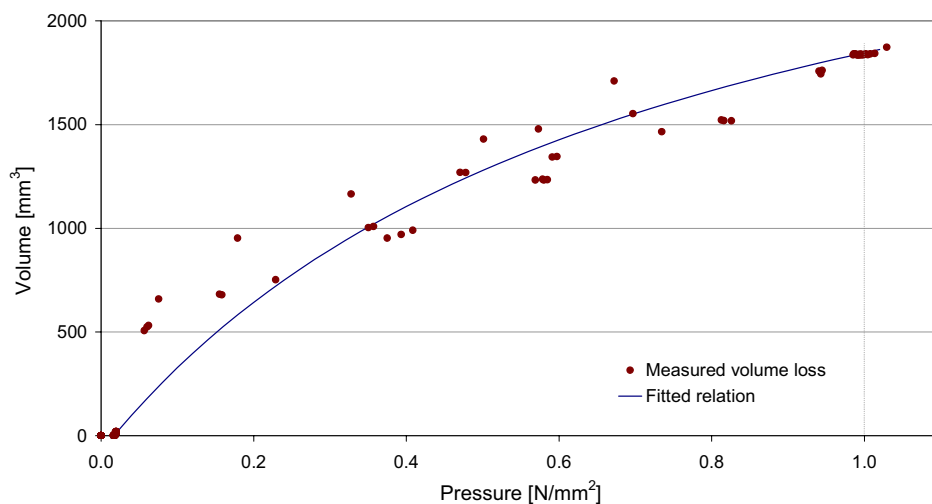


Figure 3.7 Graphical results from a stretch test, lost volume against pressure p' .

Sample preparation

For preparation it is recommended to compose the samples on a separate basis by weighing the correct amount of particles from the right source and size (see gradation of the material, section 3.4). A surplus of 10% of the mixture should be prepared in order to be sure that there is enough material for sample preparation. The samples are individually composed for realising the correct gradation over the different samples.

The aggregate should be mixed with the correct amount of “fake bitumen”. The samples were prepared in such a way that they contain always the same amount of aggregate (i.e. 946.2 +/- 0.1 gram). Therefore all samples start at similar VMA values if they initially have similar heights.

To build the loosely compacted samples two equal shares from the mixed materials were weighted. The two shares should be compacted individually on the correct height for realising a homogeneous compaction state in a split-mould of 101.6 mm in

diameter (i.e. 4"). When the sample is built exactly on the target height of 60 mm the *VMA* value corresponds to 26.3%. Further details about the sample preparation for doing a MHSM test can be found in appendix B.

Deducing initial sample height

Because all material properties are linked to the current material volume, adequate control of the sample volume is crucial. The initial diameter of the sample is relatively certain, but because of the movement of the sample inside the MHSM and also the positioning of the top cap the precise height of the sample can be slightly different from the target value. Additionally, because the deduction of e.g. the radial strain is affected by the sample height, it is of great importance to deduce the initial sample height correctly. Besides making the sample as accurately as possible on height, the sample height was in addition, two times measured.

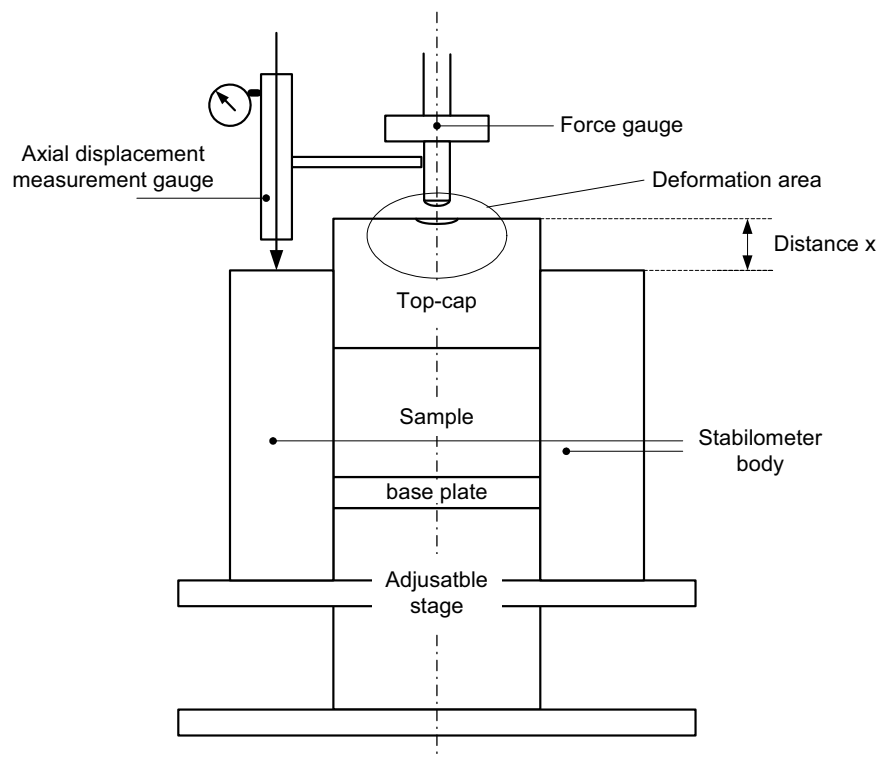


Figure 3.8 The sample height can be deduced when it is inside the MHSM (the exact MHSM dimensions must be known).

The first measurement was done after the MHSM including the sample were positioned inside the external-loading frame but before any axial loading was applied. At that moment the sample height could be obtained by deducing the distance x between the top-cap and the Stabilometer body, see Figure 3.8. Analysis of the repeatability of many tests proved that the best way to do this was by measuring both the height of the Stabilometer and the height of the top-cap measured against the fixed level of the surrounding framework. Use of this method for obtaining sample height

requires full contact between the top-cap and sample. This contact cannot be checked visually. Also, before testing starts, there is no load on the sample and pushing on the sample would affect the compacted state.

The second measurement of the sample height was done when the vertical load was increased until the maximum level (ca 23 kN). The sample height could again be determined by deduction of the x value using the same procedure. Because during the test the axial deformation was accurately monitored, reconstruction of the initial sample height now became possible, see also Figure 3.9.

It was expected that this control mechanism allowed us to check the directly measured sample height. However, the experiments showed a structural and consistent difference between the two obtained measurements. The reconstructed sample heights from the deformed situation were on average about 0.5 mm higher than the directly measured values. Detailed investigation of this phenomenon and tests using a solid metal dummy proved that part of that structural difference could be explained by deformation of the aluminium top-cap mainly in the area where it touches the loading gauge. Precise measurements indicated that this deformation grows until 0.32 mm when vertical load rises to 23 kN (i.e. 0.014 mm/kN). The origin of the remaining part of the error (i.e. $0.5 - 0.32 \approx 0.2$ mm) remained unknown. The knowledge of the magnitude of the deformation of the top-cap was used while reconstructing the initial sample height. For analysis of the results of the MHSM tests the most reliable initial sample height was assumed to be the average between the directly measured and reconstructed initial sample heights. An example of the calculation principle to obtain this initial sample height is given in appendix B.

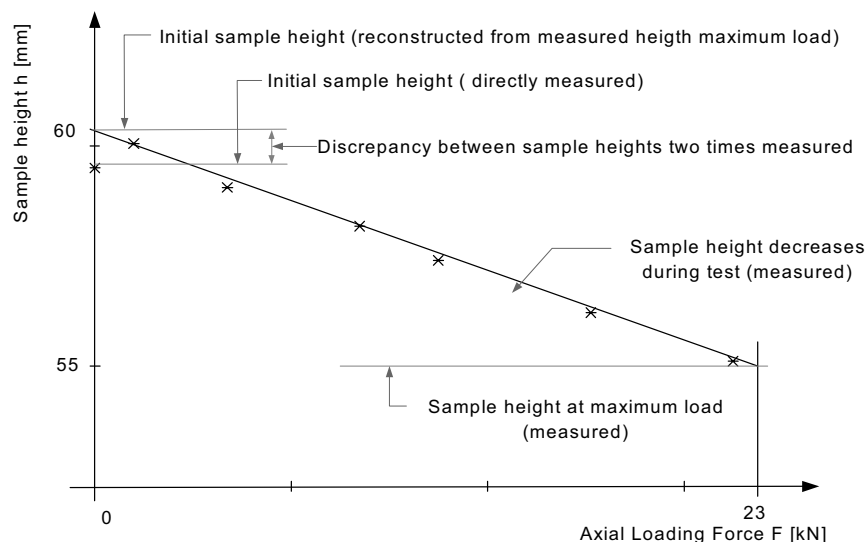


Figure 3.9 Data from directly measured sample heights and from heights determined from deformed situation.

Deduction of primary sample quantities / Operating a MHSM test

In a MHSM test not all the desired sample information is directly measured. A MHSM test obtains; pre-described axial deformation rate, δ_{ax} [mm], required vertical loading force, F_{ax} [kN], derived radial stress, σ_{rad} [MPa] and piston displacements, δ_{pist} [mm]. Deduction of radial strain requires additional analysis.

Deducing the axial stress, the axial strain and radial stress on the sample can be done by using standard techniques. From the measured axial deformation and required loading force the first two quantities, σ_{ax} and ϵ_{ax} , can be calculated by dividing F_{ax} and δ_{ax} by the top-cap area, $A_{top-cap}$, and initial sample height, h_{ini} , respectively.

σ_{rad} can be measured directly but the radial sample strain, ϵ_{rad} , must be obtained by executing the following approximation: The oil inside the Stabilometer body surrounds the sample and enforces the piston movement when the sample expands radial (Figure 3.5). The total radial sample dilation must correspond with the volume that was generated by movement of the piston (apart from the “volume loss” described earlier in this section). This piston movement is a measured quantity during a MHSM test. If it is assumed that the sample deforms homogeneously over the height (no barrelling), the average radial expansion of the sample can be calculated from the piston movement. Figure 3.10 illustrates how from a translated oil volume a radial sample strain can be deduced. Careful use of the MHSM indicates that the assumption related to barrelling is not completely true. A little barrelling does occur. The consequence of this is that the obtained stress and strain quantities are not 100% correct. Nevertheless, a reasonably average radial strain could be calculated. The details about the procedure of doing a MHSM test are discussed in appendix D.

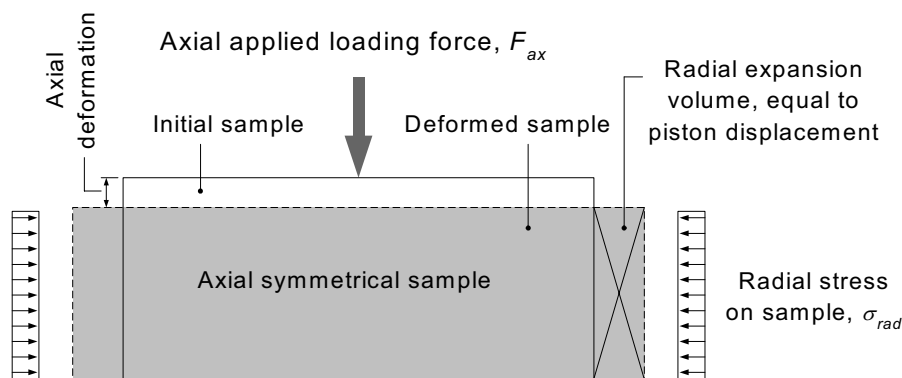


Figure 3.10 Deduction of the radial expansion volume of the sample.

The primary sample stresses and strains can be calculated using the following relations;

$$\begin{aligned}\sigma_{ax} &= F_{ax} / A_{top_cap} \\ \sigma_{rad} &= P_{oil} \\ \varepsilon_{ax} &= \delta_{ax} / h_{ini} \\ \delta_{rad} &= \delta_{pist} \times A_{pist.} / A_{curr_rad} \quad (\text{see Figure 3.11}) \\ \varepsilon_{rad} &= \delta_{rad} / R_{ini}\end{aligned}$$

in which;

$$\begin{aligned}\delta_{ax} &= \text{measured axial sample deformation [mm]} \\ \delta_{rad} &= \text{measured radial sample deformation [mm]} \\ \delta_{pist} &= \text{measured piston movement [mm]} \\ h_{ini_aver} &= \text{deduced average initial sample height [mm]} \\ A_{top_cap} &= \text{contact area top-cap sample [mm}^2\text{]} \\ A_{pist} &= \text{piston area [mm}^2\text{]} \\ A_{curr_rad} &= \text{current calculated radial sample area [mm}^2\text{]} \\ F_{ax} &= \text{measured axial loading force [kN]} \\ P_{oil} &= \text{measured oil pressure [MPa]} \\ R_{ini} &= \text{initial sample radius [mm]}\end{aligned}$$

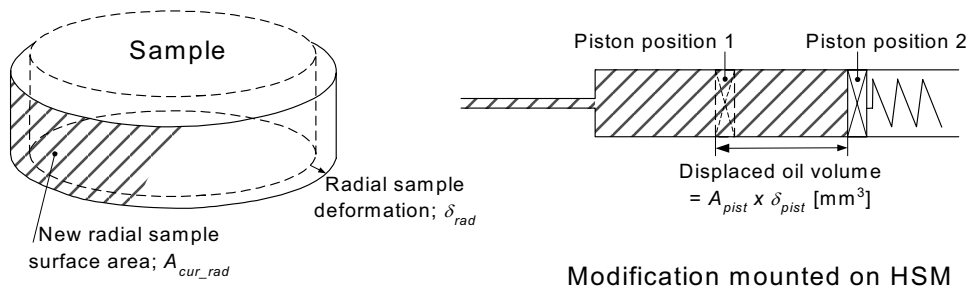


Figure 3.11 The relationship between the radial sample surface area and the oil volume displaced inside the HSM modification.

The current radial sample surface can be calculated because in previous steps the new sample height and radius (respectively h_{curr} and R_{curr}) were deduced.

Type of test

The test is a drained test. Because a.) the top-cap is porous also air can escape¹², b.) the sample is relatively loosely compacted and will therefore have an open pore structure, and c.) the deformation rate is low, it is assumed that during a test no pore

¹² The top-cap is made porous by drilling a structure of vertical and horizontal holes in it. Between sample and top-cap use is made of a plastic perforated plate. Therefore air and bitumen is able to escape during a test. However, the tests showed that no significant volume of bitumen did escape. This implies that the measured volume decrease of the sample is mainly due to air that escapes from the sample.

and or fluid pressure can build up in the sample. Assuming that these assumptions are correct, soil mechanical quantities like p' and q can be calculated by using the standard relations as described in section 2.5.

Conclusions of different sequences while conducting a MHSM test.

The proposed procedure for executing a MHSM test is the result of a continuous development of the initial test procedure. Several tests have been executed on a dry aggregate mixture. Initially it proved a problem that sample heights were different all the time and affected initial sample volume and thus VMA . Selection of the definite test sequence was based on analysis of the repeatability (recurrence) of the specific test sequences (read deducing the most accurate initial sample heights) within one test series. Variations in the sequence were made in an attempt to improve the accuracy of deduction of the initial sample height.

In the proposed procedure the sample height is obtained by measuring the distance between the top-cap and the Stabilometer body. This is done using a Veneer calliper (at two stages, 0 kN and 23.7 kN). From the maximum load situation, the initial sample height was reconstructed as described before. For analysis of the test results the average value of both initial sample heights were used.

3.4. Material measuring programme

Two elements from the research make use of tests done on “real HMA materials”, it concerns; a.) construction of test sections while monitoring compaction progress, and b.) doing laboratory tests in order to obtain material characteristics during compaction. In the final compaction simulations foreseen, information obtained from both elements will be used as input. These elements should therefore be achieved by using mixtures that express comparable behaviour.

Before material measurements are carried out one has to be sure that the equipment used for the material measurements operates adequately. Doing tests on rigid metal dummies and doing measurements on mixture varieties from which the effect is known achieved this.

Two effects known from practice and literature are the effect of the amount of round versus angular material and variation in the amount of bitumen. To test the suitability of the equipment two test-series were carried out before the real programme was started. Series RM with a surplus of Round Material in the sand fraction (below 2 mm), and series LBC with a Lower Bitumen Content.

It was chosen to discuss these, validation mixtures, together with the final tests series achieved for obtaining the required material behaviour. The results of the two validation test series are compared to the results of the Reference (coded REF) series. For a total list the reader is referred to the Section 3.6 “the main test programme”.

Materials Used

The selected material is Dense Asphalt Concrete (DAC) because this is a commonly used material for wearing courses in the Netherlands with more or less general compaction characteristics. Head (1980) recommends a ratio of at least five between the largest particle and the minimum dimension of the sample for tests on granular samples, to ensure homogenous material behaviour. Because the minimum sample dimension of the MHSM sample is around 60 mm this limits the maximum particle size to 12 mm. Therefore the selected material became a DAC 0/11.

Both materials, for test samples and compaction test section, are built from the following raw materials;

Coarse aggregate	Norwegian granite
Sand	Mix of 75% crushed Scottish granite and 25% river sand
Filler	type Vulcom ¹³ 40K
Bitumen	80/100, density 1030 kg/m ³ (only compaction test section)

The gradation of the materials being used can be found in Table 3.2.

GRADATION OF MATERIAL USED	
“on sieve”	Cumulative %
C16	0.0
C11	1.8
C8	15.8
C5.6	37.5
2mm	55.0
63 µm	94.1

Table 3.2 The gradation of the DAC 0/11 material used for the laboratory measuring programme.

Initial MHSM tests showed that measured compactibility material properties are very sensitive to small variations in composition. To increase the homogeneity of the samples, extra sieves (C4, 2.8, 1, 0.5, 0.25 and 0.125 mm) were used to make the variation in gradation between the samples as small as possible.

Normally HMA's are hot during compaction. However materials of about 100-130°C cannot be tested in the equipment because of equipment limitations. For that reason it was decided to do the tests at room temperature. To compensate for this mismatch in material temperature the viscosity of the bitumen used was modified to let the material behave as if it was hot. To arrange this Shell manufactured three types of bitumen that had the same viscosity at room temperature as ordinary 80/100 bitumen at respectively 78, 94 and 141°C. All three bitumen's are composed of a mixture of

¹³ Vulcom 40 K is the brand name of the used filler. The filler is a mixture of; crushed limestone 15-25%, fly ash 50-65%, incinerator fly ash 0-20%, mineral crushed aggregate 5-10% and calcium hydrate 3-6%.

200 Pen bitumen ($\rho = 1020 \text{ kg/m}^3$) and Shell sol A ($\rho = 875 \text{ kg/m}^3$). Some characteristics of the products are shown in Table 3.3.

Also dynamic viscosity measurements were done on the modified bitumen using the Cone and Plate Visco Meter from the DWW (Dutch road administration). The measured viscosity's are also shown in Table 3.3.

Apart from the mixtures with the lower bitumen content (code LBC), all the mixtures were mixed with exactly the same volume of bitumen (64.1 cm^3) on 946.2 gram of aggregate. This corresponds to a bitumen content of 6.35% by weight of a 80/100 pen bitumen of a "normal" DAB 0/11 mixture at 20°C. The temperature-viscosity relationship of the fake bitumen's together with the relation of a normal 100 pen bitumen is illustrated in Figure 3.12.

SPECIFICATION OF FAKE BITUMENS									
Product code	Percent sol A [%]	Measured ¹⁴ dynamic viscosity [Pas]				Density at 20°C [kg/m ³]	Imitated 80/100 temperature [°C]	Estimated viscosity [Pas]	
		70°C	80°C	100°C	130°C			Shell	DWW
052/01	10.0	-	.625	.221	.077	1005.5	78	27	100
053/01	18.5	.343	-	.093	.037	993.2	95	5.6	4
054/01	30.6	.058	-	.024	.012	976.0	141	.34	2

Table 3.3 The specifications of the fake bitumen's used for the laboratory measuring programme.

The materials and stress conditions tested

During the compaction process the HMA cools from approximately 140°C to 70°C¹⁵ and the material is at different compaction stages (different densities) too.

While developing the set up of the test programme the material variations in composition and applied stresses have to be involved. These variations concern:

- tests at different temperatures,
- tests with different confining stress-strain relationships,
- tests at different compaction rates.

The conceptual MHSM is equipped with two springs of a different stiffness. It makes variation of the confining stress-strain relation possible on two levels. Tests at different compaction rates are implicitly achieved while the material is tested, because the compaction of the material increases automatically during the tests. Due to time

¹⁴ The Shell research laboratory provided the dynamic viscosity of the mixed products. Measurements were carried out at an shear rate of 100 1/s and temperatures of 70, 80, 100 and 130°C. From these measurements the viscosity at 20°C was estimated.

¹⁵ This is a guess of the temperature of HMA during rolling based on measurements done during construction of the compaction test section. The specific temperature of every constructed road section can vary widely and is a result of mixing temperature and several other environmental factors.

and material constraints four test series were selected from the range of possibilities. Three test series are conducted at an equal confining stress-strain relation and three different bitumen viscosity's. The other test series is carried out at the reference bitumen viscosity (corresponding to the 78°C temperature) and a higher confining stress-strain relation.

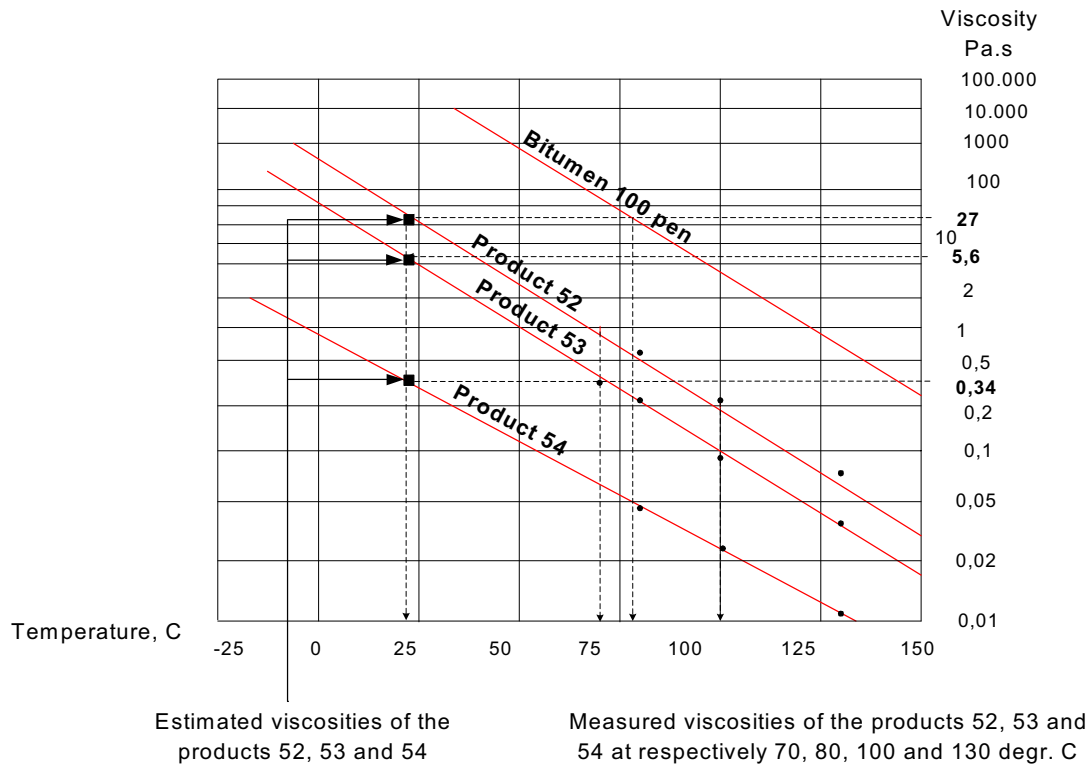


Figure 3.12 Viscosity of fake bitumen at 20°C estimated from measured viscosity's at higher temperatures, depicted in a Bitumen Test Data Chart (BTDC), the characteristics of the fake bitumen are related to the characteristics of a normal 100 PEN bitumen (Shell 1990, penetration area removed).

All test series have code names that capture information on the test materials and conditions. The codes are explained below;

- REF; the reference mixture or material, the standard composition at a “temperature” of 78°C, low confining stiffness. Applying the medium spring stiffness creates this medium confining stiffness, i.e. spring 2 (see also Table 3.4).
- MTM; Medium Temperature Material, the reference mixture composition at a temperature of 94°C, low confining stiffness
- HTM; High Temperature Material, the reference mixture composition at a temperature of 141°C. low confining stiffness
- SP1; a changed confining stress-strain relationship due to a change of the spring with low stiffness (no. 2) to stiffer spring no. 1, imitated material temperature of 78°C.
- RM; a surplus of Round Material in the sand fraction. In such a mixture the crushed sand (i.e. 75% in the reference mixture) below 2 mm is substituted for natural sand, low confining stiffness, imitated material temperature of 78°C.
- LBC; Low Bitumen Content, the bitumen content of the mixture (by weight) was reduced to 5.35%, low confining stiffness, imitated material temperature of 141°C.

The specifications of the samples tested in the laboratory test programme can be found in Table 3.4.

MAIN SPECIFICATIONS OF LABORATORY TEST PROGRAMME						
Mixture code	Imitated temp. [° C]	Viscosity fake bit. [Pa sec]	Bit cont. [% m/m]	Conf. Stiff. (spring no) [N/mm ³]	Perc. Round [% m/m]	Remark
REF	78	27.0	6.35	1.3 (2)	25	reference mix
RM	78	27.0	6.35	1.3 (2)	100	more round sand
LBC	141	0.34	5.35	1.3 (2)	25	less bitumen
MTM	94	5.6	6.35	1.3 (2)	25	medium viscosity
HTM	141	0.34	6.35	1.3 (2)	25	low viscosity
SP1	78	27.0	6.35	1.8 (1)	25	stiffer confining

Table 3.4 The main characterisation of the different test series used in the laboratory test programme.

The reference mixture test series is used as a reference for almost all varieties in composition and loading situations except for the LBC mixture. The reference mixture uses the fake bitumen with the highest viscosity (i.e. the 78°C fake-bitumen). Testing the effects of lower bitumen content is done with the 141°C fake-bitumen. This was done because it was expected that when using this bitumen in a lower content and mixing the whole at 20°C, a reasonable risk of poor wetting of the particles with the bitumen could be introduced. It implies that the HTM mixture became the reference test series to which the results of this particular (LBC) mixture should be related.

3.5. Testing the MHSM suitability

Compactibility results measured with the material-measuring programme as proposed in the previous section are discussed in this section. The section will start by focussing on how the results from MHSM tests can be used in order to achieve critical state parameters. Then the suitability of the equipment for measuring material compaction characteristics was tested, based on the REF, RM and LBC test series. After these tests indicated that the MHSM was indeed suitable, the second part of the measuring programme (additional tests MTM, HTM and SP1 mixtures) was carried out and results were interpreted.

For every test the progress of sample compaction is achieved in p' & VMA values and the calculated p' - VMA path is plotted. The path indicates the ease at which a material can be compacted. It expresses the extent of required stress levels for achieving compaction improvement, given the material conditions (i.e. pre-compaction state and

temperature). Comparing these test-paths can express differences in compactibility between, for example, round and more angular materials.

Deduction of critical state parameters

The material test programme provides the relationship between the volume of the sample (in terms of VMA) and the governing stress conditions in q and p' . Both from the critical state theory and from the material measurement programme, it follows that a particle based material shows a bi-linear loading behaviour when such a material is tested over a sufficient wide loading range and the results are expressed in the $VMA - \log p'$ space. The results of an individual test look as the line depicted in Figure 3.13. Analysing the line is yielding four¹⁶ sections;

Section AB	recoverable material behaviour
Section BC	a transition zone
Section CD	irrecoverable material behaviour
Section DE	unloading

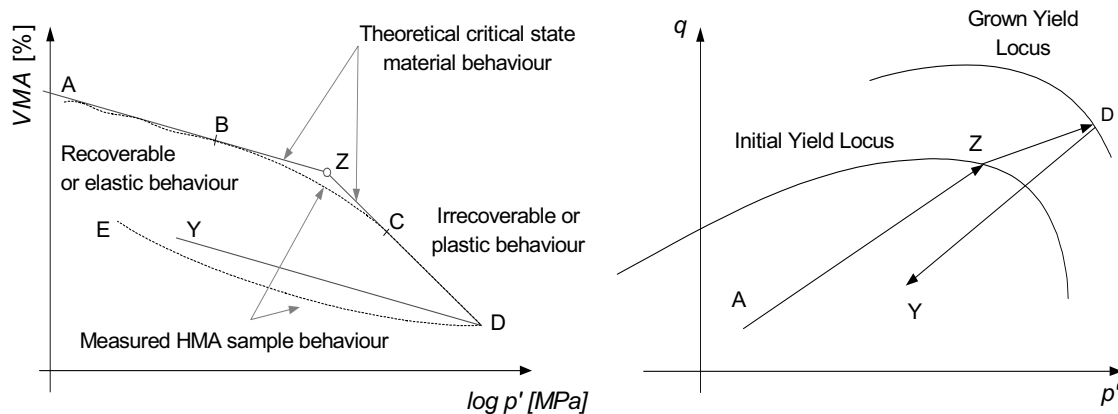


Figure 3.13 The course of a MHSM test in the $VMA;p'$ plane.

At the first part of the loading line, the material shows recoverable behaviour and there should be no particle re-arrangements. When a sample is subjected to a load that corresponds to a point on this line the stress situation is inside the yield locus. In theory in transition point Z but in reality during transition zone BC, material starts to behave irrecoverably. Here, particles start to re-arrange themselves and the stress situation is “on” the yield locus and material start to behave plastically or in terms of HMA it starts to compact. When the material is loaded further the stress situation stays on this yield locus. This can happen because the size of the yield locus is increasing due to hardening. Hardening causes growth of the yield locus. It all corresponds to earlier discussed critical state principles.

¹⁶ The mentioned sections belong to a deformation path of a material or sample tested in practice. When the behaviour is modelled, as in a simulation, the loading path will follow AZDY instead of ABCDE. Now the transition section (BC) is reduced to a transition point (Z).

For each of the test series (one material constitution, temperature or loading condition) six individual tests were done. Each test is yielding to one single loading line. Within such a test series two tangents were deduced by using statistical techniques; one representing the recoverable behaviour¹⁷ and one representing the irrecoverable behaviour. The tangents are deduced by estimating the slopes and intercept for the best straight lines that can model the recoverable and irrecoverable part of material behaviour in the $VMA-\log p'$ plane. In order to be able to do this it must be estimated how much data could be used for calculating those slopes and which data belong to the “transition zones” of the different test data. The results of the loading lines from the Reference test series and the estimated tangents are shown in Figure 3.14.

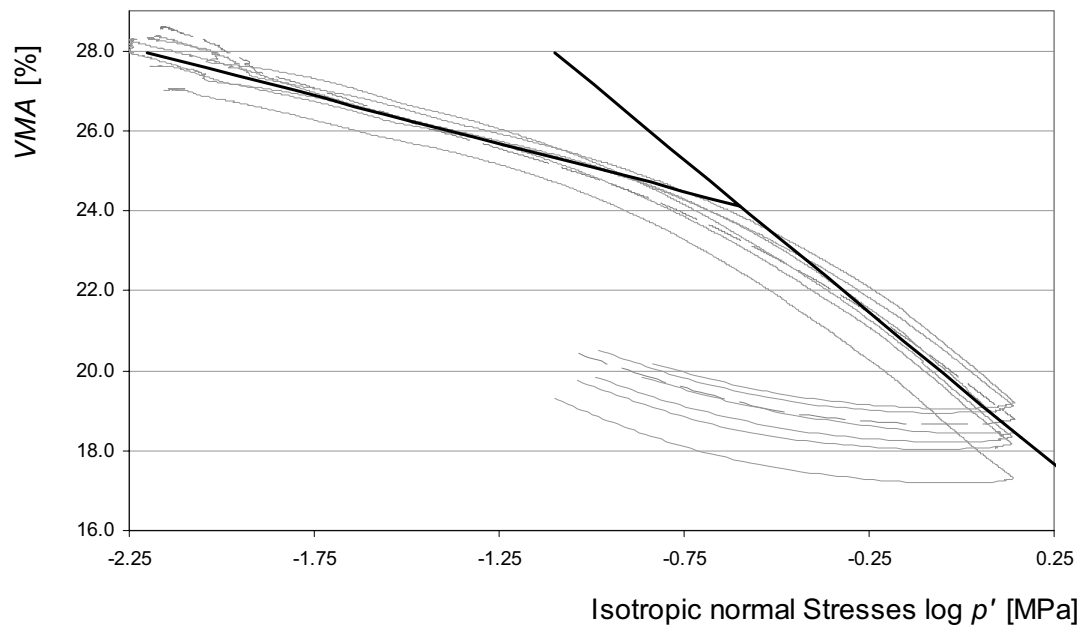


Figure 3.14 The 7 individual test results from the reference (REF) series including the distracted mean curve.

In accordance to critical state principles the two tangents can be represented by the next formulae (Wood, 1990);

$$\text{Recoverable behaviour}^{18}; \quad VMA = VMA_{\kappa} - \kappa \cdot \log(p')$$

$$\text{Irrecoverable behaviour}^{18}; \quad VMA = VMA_{\lambda} - \lambda \cdot \log(p')$$

Besides numerating the two tangents, also the stress ratio q/p' and deformation ration $\varepsilon_{sh}/\varepsilon_{vol}$, have to be extracted from test data. We need this information for modelling the deformation behaviour during plastic flow. Further, the value VMA_I is calculated

¹⁷ Before this was done the specific volumes (i.e. VMA values) of the sample were first of all normalised to the VMA starting value. So when using the calculated slopes and intercepts they have to multiplied by the mean VMA_I values within that specific test series.

¹⁸ In these equations for recoverable and irrecoverable behaviour for expressing the specific volume the parameter VMA is used whereas in the original formulation the soil mechanics parameter v is used.

per test series. This value represents the average of the initial VMA value of the samples within one test series. Also the VMA and p' value of the intersection point (i.e. point Z) of both tangents are calculated.

To test the suitability of the MHSM for providing critical state material parameters, two test series were added, apart from the reference (REF) test series. They involved a mixture with less bitumen (LBC) and one with a surplus of round aggregate (RM). These mixture varieties were introduced because we thought to know how they affect the compactibility of HMA mixtures.

Effects of a rounder aggregate

The bi-linear models deduced from the results of the REF and RM test series are plotted in Figure 3.15. The effect of the RM line is compared to the REF line. The RM line shows a steeper slope for the recoverable part but a more faint slope for the irrecoverable part of the model (related to REF). Also, the RM line lies below the REF line for the VMA domain from 20 up to 27 %. The lower slope of the irrecoverable part and the lower position of the RM line imply that in this VMA domain a lower stress level is sufficient in achieving an equal VMA (i.e. compaction) level. This is in line with indications gathered from road building experience where in general it is known that more round aggregate makes a mixture easier to compact.

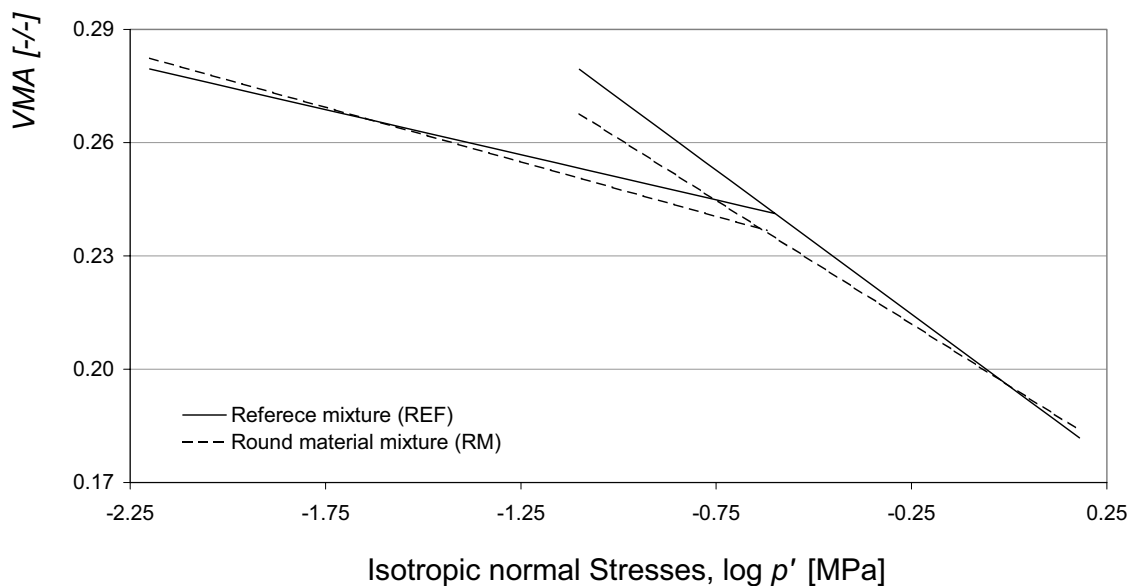


Figure 3.15 The mean p' - VMA curves of the reference mixture and surplus of round material (codes REF and RM).

Relations between roundness of particles and compactibility were studied by Renken (1980) and Gauer(1975). Renken measured C values (see section 2.3) of HMA mixtures as a function of the crushed sand/rounded sand ratio. Mixtures with 100% natural sand (i.e. the RM mixture) show 35% lower C values compared to mixtures with 75% crushed sand (values respectively 14.4 and 22.3). Our material

measurements show that compressing both mixtures to comparable VMA levels (until a VMA level of 0.20) the RM mixture requires a lower stress p' compared to REF the mixture. Gauer studied the compactibility of HMA mixtures with natural and crushed sand. He concluded that compactibility decreases when particles become more angular but found also a difference caused by the origin of the material. Mixtures with crushed Basalt sand are more difficult to compact than mixtures with crushed Granite sand. Gauer used a variant of the complex modulus method for measuring the compactibility. The research of Gauer and Renken and our own material measurements shows that the direction of the relation is point in similar direction although the absolute values cannot be compared.

Variation of the bitumen content

For testing the effect of bitumen content two identical mixtures were tested with different bitumen contents. Because bitumen and aggregate were mixed at room temperature, to arrange good wetting of the particles, these tests were achieved using the bitumen with the lowest bitumen viscosity (i.e. 0.34 Pas to imitate a material temperature of 141°C).

The results of both test series, LBC and HTM, do not differ significantly. These results are different, however, from what would be expected. One would expect that mixtures with a higher bitumen content are easier to compact. On the other hand these results are in line with findings of Powell (1980).

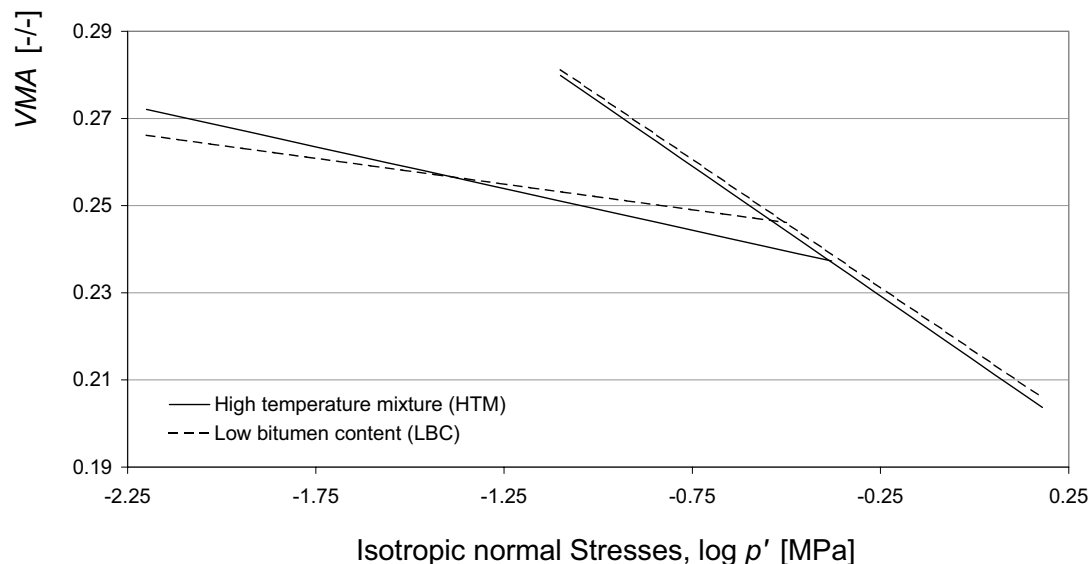


Figure 3.16 The mean p' - VMA curves of the mixture with the lowest bitumen content (i.e. the LBC mixture) and the, for that mixture, reference mixture the mixture with the bitumen of the lowest viscosity (i.e. the HTM mixture).

Powell investigated the compactibility of dense bituminous macadam's and found that a above particular minimum bitumen content (approximately 2 to 2.5%), there is no effect of the amount of bitumen on compactibility expressed in VMA . The relationship

developed by Powell between compactibility and bitumen content is illustrated in Figure 3.17.

This research programme and Powell came independently to identical conclusions; in a certain domain the bitumen content does not affect the compactibility at least when expressed in *VMA*. In this research use is made of the *VMA* parameter to express the stage of compaction because this parameter gives absolute and objective information about the particle proximity. In road-building practice use is often made of the parameters bulk density (ρ_s), voids (*V*) content or voids filled with bitumen (*VFB*) as an indicator for the achieved compaction of the HMA. This is because when an asphalt mixture is well designed, the set of parameters *VMA*, *VFB* and voids content do give a good qualitative indication of the volumetric composition of the material. Individually the parameters cannot indicate material quality.

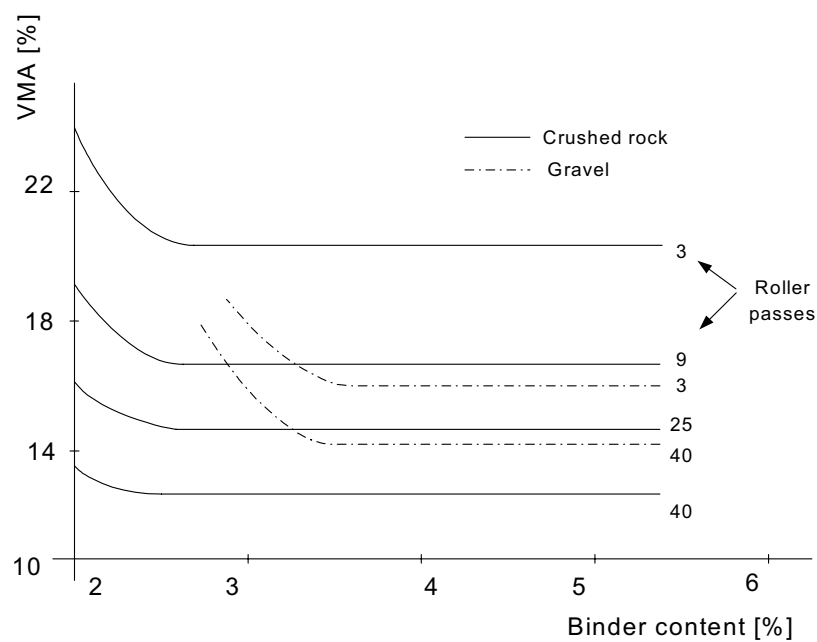


Figure 3.17 Relationship between compactibility and bitumen content, Powell et al (1980).

It is a well-known opinion in the road-building branch that a higher bitumen content does make a mixture better compactable. However, practice commonly uses voids content and bulk density as indicators for the achieved compaction level of the material. This can possibly be the cause for that opinion. These parameters however, as discussed earlier in chapter 2, do not represent absolute and objective information about the bulk particle proximity. The bitumen content affects the volumetric material constitution strongly. Therefore the estimated models for the HTM and LBC test series were additionally plotted in the Voids ratio versus p' (Figure 3.18) and in the *VFB* versus p' space (Figure 3.19). The graphs indicate that when a comparable compaction load level is applied on two similar mixtures with a different bitumen content the mixture with the higher bitumen content does show a much higher *VFB* level and a lower Voids content. If the results are shown in this context one can for example conclude that the LBC mixture (with less bitumen) needs more pressure to “compact” to equal bulk density or equal Voids ratio. This is probably what in common road engineering practice means; “*more bitumen makes a HMA mixture better compactable*”.

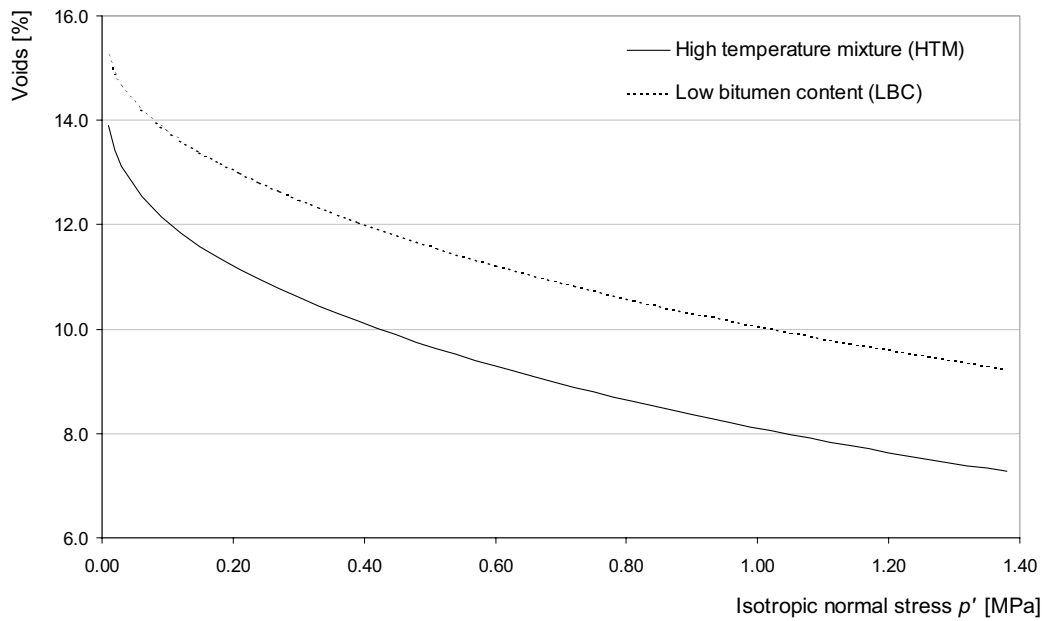


Figure 3.18 The effect of bitumen content on Voids content during compaction as a function of p' for the mixtures HTM and LBC. Viscosity's of bitumen used in both mixtures are equal (i.e. 0.34 Pa sec).

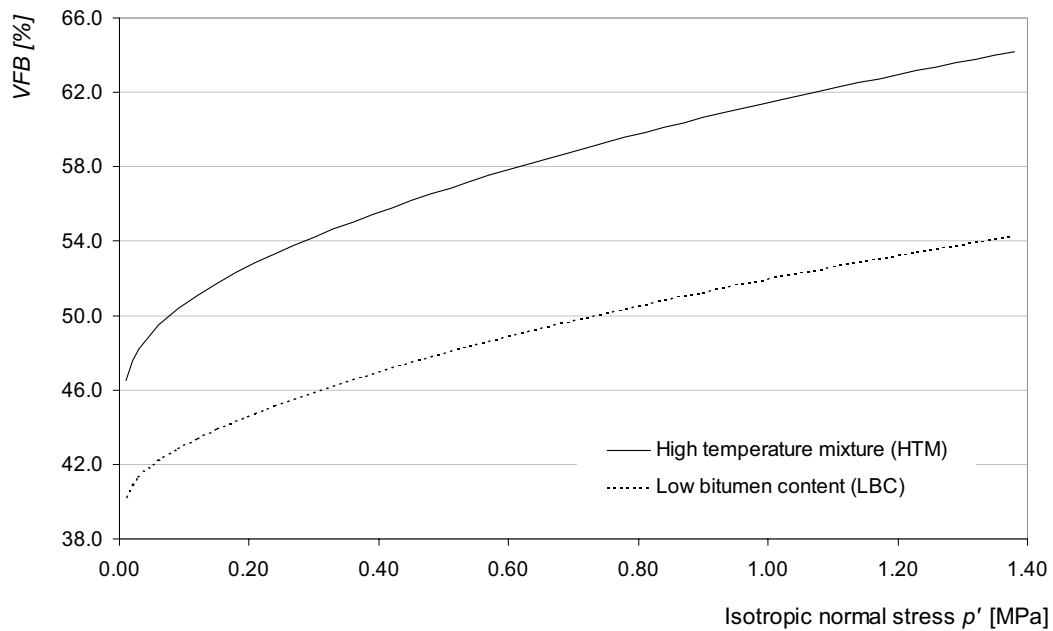


Figure 3.19 The effect of bitumen content on Voids Filled with Bitumen (VFB) during compaction as a function p' for the mixtures HTM and LBC. Viscosity's of bitumen used in both mixtures are equal (i.e. 0.34 Pa sec).

Table 3.5 summarises the critical state parameters as deduced from the REF, RM, HTM and LBC material test series. This information is also used for earlier discussed testing of the suitability of the MHSM and for drawing the models illustrated in the Figures 3.15, 3.16, 3.18, 3.19 and 3.20.

CRITICAL STATE PARAMETERS REF, MTM, HTM AND LBC MIXTURES				
	Mixture codes & Imitated temperatures			
Measured quantities	REF 78°C	RM 78°C	HTM 141°C	LBC 141°C
General	-	-	-	-
VMA_I	.277143	.278513	.268895	.264443
P'_{int}	.259977	.264998	.431536	.313918
VMA_{int}	.240907	.235426	.236759	.246104
Recoverable part	-	-	-	-
Slope, κ	-.086321	-.103744	-.071193	-.0446233
Intercept, VMA_{κ}	.818696	.785746	.855505	.855505
R^2	.997179	.994773	.996904	.996604
Irrecoverable part	-	-	-	-
Slope, λ	-.275165	-.235042	-.221428	-.222372
Intercept, VMA_{λ}	.705540	.702612	.797470	.818922
R^2	.999756	.999857	.999733	.999637
q/p'	1.526452	1.457792	1.652971	1.452629
$\epsilon_{sh}/\epsilon_{vol}$.753572	.747185	.802538	.874939

Table 3.5 Critical state parameters for the REF, MTM, HTM and LBC mixtures.

3.6. The main test programme

The main test programme consisted of testing the REF, MTM, HTM and SP1 mixtures. By using the earlier-mentioned statistical techniques the critical state parameters were deduced for a DAC 0/11 material. Firstly the effects of changes in bitumen viscosity (corresponding to the material temperatures 78, 94 and 141°C) will be discussed here. Secondly the effect of two loading stress combinations (using respectively spring 1 and spring 2) will be discussed.

Effects of bitumen viscosity (or material temperature) on compactibility

The results of the REF, MTM and HTM test series are depicted in Figure 3.20 in the $\log p'$ versus VMA plane. Analysing the lines indicates that for the plastic area the REF mixtures show the steepest slope whereas the HTM mixture shows the faintest slope. The MTM mixture lies in the middle. It can be seen that the lines do act in order, which indicates an unambiguous relationship between the isotropic normal compression stress, p' , and the VMA level. Deforming a granular material plastically is rearranging the particle matrix, which corresponds to changing the compaction state into denser or a more open state (less dense). A fainter slope (HTM versus REF) indicates that a larger stress increase is required for achieving a comparable decrease

of VMA . A higher position of the line (HTM versus REF) indicates that a higher pressure is required to achieve a comparable VMA level. The deduced relationship looks unambiguous; the line with the fainter slope is the upper one, the line with steeper slope is the lower one. It can be concluded unambiguously from the results that use of bitumen with a lower viscosity results in a mixture that is more difficult to compact.

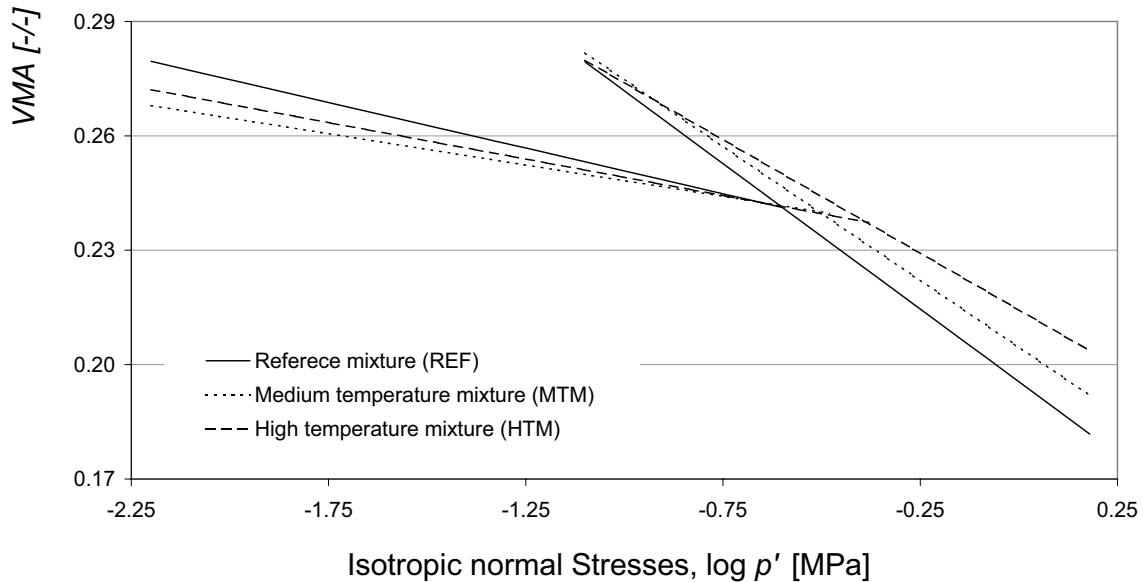


Figure 3.20 Recoverable and irrecoverable tangents drawn from the test series REF, MTM, and HTM.

The behaviour observed during elastic deformation is less unambiguous and more difficult to explain. The REF line is the upper one, the HTM line in the middle, and the MTM line is the lowest one. The HTM line in between the REF and the MTM line for elastic deformation is a result that cannot be explained directly. What can be seen is that the upper line does have the faintest slope and the lowest line the steepest.

The behaviour observed can possibly be compared to known relationships between stiffness of HMA mixtures in general and the type of the bitumen from cold compacted mixtures. It is known that the type of bitumen (i.e. viscosity) has an effect on the stiffness of the total mixture; mixtures with bitumen of a higher viscosity do express stiffer behaviour. This comparison make sense because in the cold compacted state particles in the mixture will not rearrange due to a load, and therefore, the material behaviour can be modelled as elastic. From comparing the results to the known relationships it can be concluded that they correspond so far, that the MTM and HTM lines (highest viscosity's) do run fainter then the REF line. However, the slopes of the MTM and HTM lines, related to each other, contradict to that proposed relationship. Further, related to this, it must also be noted that the steepest line (REF) had initially the lowest VMA level. It is not quite sure what will have the strongest effect; bitumen viscosity or initial VMA level. The critical state theory suggests that it is allowed to shift the elastic lines while keeping the slopes equal. If this is also valid

for HMA¹⁹ this would mean that the comparison as made above (to the stiffness of cold compacted mixtures) is correct because the initial *VMA* level of the samples does then not affect the slope of the line.

The results at least indicate that in the elastic zone (here we cannot speak from compaction because there is no particle reorientation) the mixtures differ in “stiffness”. However, in accordance to theory, particle arrangements in the sense of changing the structure (orientation) of the matrix do not occur, it is plausible that particles are pressed closer against each other while squeezing out (a part of) the bitumen between them. If this squeezing out of bitumen is the cause for the observed phenomenon then the medium bitumen must have the highest resistance against this whereas the less viscous and the high viscosity bitumen provoke less resistance against this squeezing. It is recommended to investigate this phenomenon in more detail during future research after compaction.

Conclusions deduced from the test results indicate that HMA mixes with a lower bitumen viscosity, should be less compactable which contradicts common expectation. In road-building practice it is thought that hotter (the hotter the HMA the lower the bitumen viscosity) HMA mixtures are easier to compact. Research that investigates the direct relationship between current HMA material temperature and its effect on compactibility of that mixture is very sporadic. Only compaction field tests are known that uses a defined temperature window for compaction. It seems logical that the temperature related viscosity of bitumen at a higher temperature causes this but it may also be very plausible that the existence of a solidification temperature inside that temperature window can clarify this phenomenon.

The existence of a solidification temperature

It is conceivable that the commonly presumed relation between material temperature and compactibility has something to do with the solidification behaviour of bitumen.

Nijboer (1948) reports that bitumen has a solidification temperature. If the temperature is inside the domain where compaction is achieved then it is not important at what temperature roller passes are applied but rather how many passes are applied before the material is cooled down to this solidification temperature. In practice, however, this phenomenon can easily lead to erroneous conclusions as is shown in Figure 3.21. In the figure two rolling processes starting at different initial material temperatures are compared. The road section with the highest initial temperature will have the most roller passes before the mixture is cooled down to the solidification temperature and therefore will show the highest compaction. In a superficial analysis it might lead to the conclusion of an apparent correlation between material temperature and compactibility, where the true variable is the number of roller passes before the material meets the solidification temperature.

¹⁹ In relation to this it has to be mentioned that critical state theory is developed for wet soils. In soils however, the fluid is water whereas in HMA the fluid is bitumen which has a much higher viscosity than water.

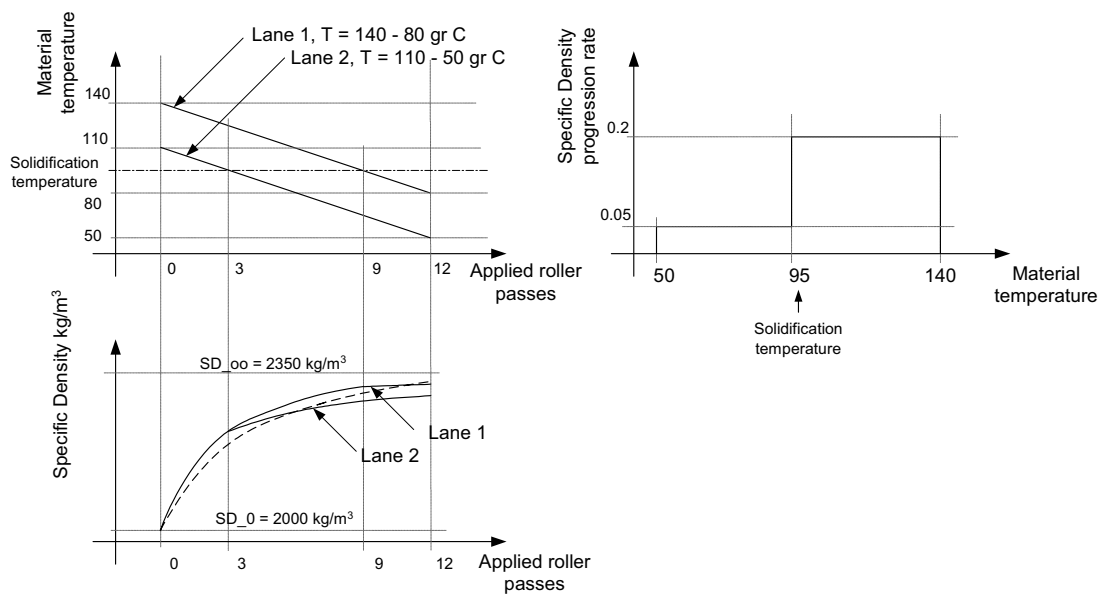


Figure 3.21 Estimated effects of a solidification temperature

The effects of bitumen viscosity

The effects of bitumen “temperature” or viscosity obtained from the test results are difficult to explain. It may be that when bitumen is used with a lower viscosity at smaller stress levels stone to stone particle contact starts to occur. Such a stone to stone contact affects internal friction (no bitumen between the particles). Because compaction is a process of sliding and moving particles along each other this internal friction of course affects the ease of compactibility of the HMA mixture.

The theoretical concept of critical state, including the stress quantities q and p' , proved to be suitable for describing the behaviour of a HMA mixture during compaction. However, it does not explain why and how the viscosity of the involved fluid (i.e. bitumen) causes easier compaction. In order to get more grip on the mechanism that the test results expresses, the results were moreover analysed in the basic stress and strain parameters; σ_{ax} , σ_{rad} , ϵ_{ax} and ϵ_{rad} .

Material test results in σ_{ax} , σ_{rad} , ϵ_{ax} and ϵ_{rad}

It is assumed in road engineering practice that at higher temperatures mixtures are better compactable; the lower viscosity of the binder should be responsible for this. However, the results from the MHSM tests show the opposite. When considering the test results it appears that mixtures with a lower viscous bitumen, require a higher load level p' to achieve the same compaction level (i.e. VMA value). It implicates that a lower bitumen viscosity makes a mixture more difficult to compact.

In an attempt to understand the cause of that measured phenomenon the test results were analysed in terms of axial and radial, stresses and strains. Similar to what really

happens during a MHSM test, the results of a pre-described deformation on the sample were analysed. That pre-described axial deformation should be in the irrecoverable deformation domain, see Figure 3.13 (i.e. between the points C and D). For all test series it became clear that between axial heights of 56.2 and 55.4 mm all samples were in this domain. Two important results, an increase in both the exposed radial strain and the required axial stress as a result of a lower viscosity, are illustrated in Figure 3.22.

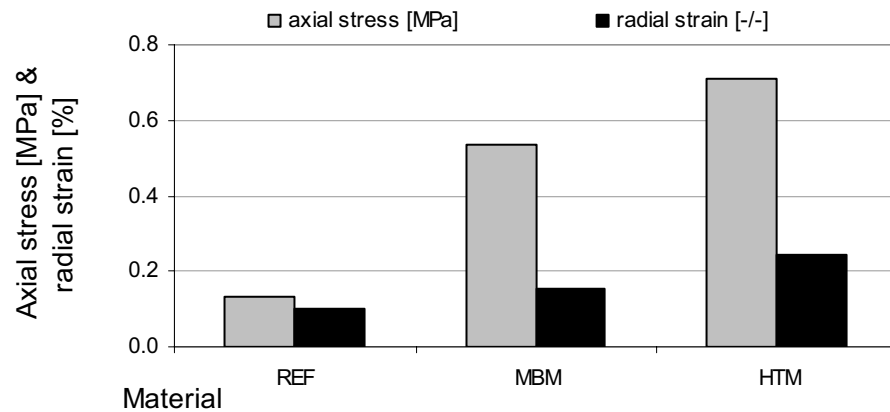


Figure 3.22 The axial stress and radial strain of the samples when they are deformed from 56.2 to 55.4 (plastic deformation regime).

Considering these results it is clear that mixtures with a lower viscosity (i.e. thinner) bitumen (HTM):

1. do require much larger axial stress when they are plastically deformed,
2. show an increased radial deformation. This higher radial strain causes also a higher radial confining pressure on the sample.

In an attempt to explain the results the following causal factors related to bitumen viscosity were thought to be of influence:

- I. inter-particle friction, the assumption is that the viscosity of the bitumen affects the stage (load level) at which stone to stone contact starts to develop and thus friction increases,
- II. particle roughness, the assumption is that the mortar (i.e. bitumen and filler) smoothens the particle's surface and therefore reduces particle interlock.

In order to investigate if these factors can be responsible for the results obtained, two intuitive models are developed. In each model one of the aspects mentioned above is incorporated.

Intuitive model I

Intuitive model I postulates a mechanism that possibly governs a relationship between the magnitude of inter-particle friction and the vertical stress level that is required achieving a defined vertical deformation; this model is shown in Figure 3.23. For vertical deformation, particle 1 has to move downwards. Particles 2 and 3 are supported horizontally. When there is no space in the contact surfaces, such a movement of particle 1 can only occur if particles 2 and 3 move sideways. This motion causes friction. The frictional force will depend on the coefficient of friction. Equilibrium of forces show that due to a vertical deformation the friction force on particle 1 points slant upwards, the friction force is shown in detail A in Figure 3.23. It implies that due to an increased friction the vertical required force for realising deformation rises too.

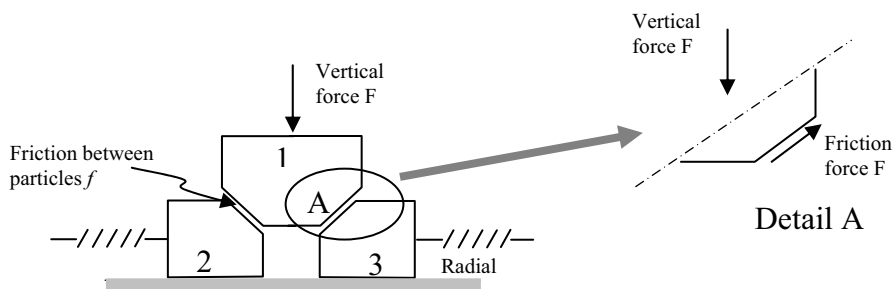


Figure 3.23 Intuitive model I of the vertical force –friction resistance relationship.

The results from the measurement programme indicate that lower viscosity bitumen mixtures require a higher vertical force to achieve a comparable radial/axial deformation ratio. It is possible that due to a lower bitumen viscosity, inter-particle stone to stone contact develops in an earlier stage (read at lower pressures) resulting in increased internal friction. This implies that this intuitive model can explain that higher vertical stresses are required for the mixtures with lower viscosity bitumen.

Another aspect that the model shows is that when the geometry of the particles remains equal the horizontal/vertical deformation also remains equal. This does not agree with the results of the material measurement programme where it was found that in lower viscosity mixtures the radial deformation also increases. It implies that there must be an additional phenomenon involved. In order to investigate that, a second intuitive model was developed.

Intuitive model II

The following postulation suggests that the higher radial/axial deformation ratio is caused by a higher particle roughness (larger particle interlock) due to a different thickness of the bitumen layer around the particle (same type of aggregate).

This postulation does have similarities with model I, however, the shape of the inter-particle sliding surfaces differs. In model I the sliding surface between particles was smooth whereas in this model the surface is rough.

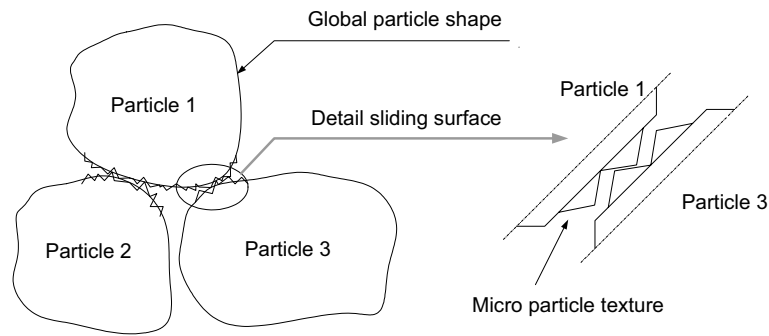


Figure 3.24 Intuitive model II, rough particle sliding surfaces.

The model shows (Figure 3.24) that the horizontal movement of the lower particles depends on the height of the “teeth” on the surfaces that are sliding along each other. When the shear surfaces are rough, particles 2 and 3 first have to move sideways before a vertical translation of particle 1 is possible.

Intuitively model II shows that particles with a higher interlock factor exhibit higher radial/axial strain ratios when loaded axially. But is it possible that bitumen viscosity changes the particle interlock factor? Use is made of Figure 3.25 to investigate that. In Figure 3.25 the surfaces of two identical particles are drawn, each with a different mortar (i.e. bitumen & filler) layer thickness. It is reasonable to assume that a higher bitumen viscosity can cause a thicker mortar layer. This thicker mortar layer will smooth the particle surface. If this is the case then the interlock factor decreases.

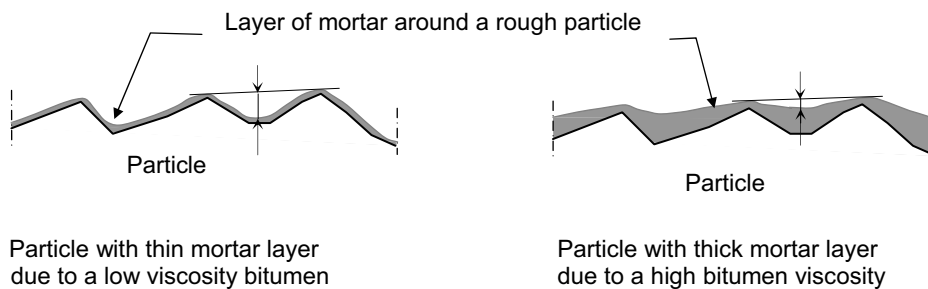


Figure 3.25 The effect of mortar (i.e. bitumen with filler) thickness due to bitumen viscosity on particle interlock capability.

If the illustrated mechanism in the models I and II actually do occur, they provide an explanation for the results of the measurement programme. Basically, model I illustrates that internal friction between the particles affects the vertical stress required for achieving axial deformation. Model II assumes that lower viscosity bitumen can be responsible for a thinner film and a higher particle interlock factor. That higher interlock factor can in turn result in a higher radial/axial strain ratio (see Figure 3.24).

Additionally it has to be mentioned that due to a thinner mortar layer (in the case of the lower viscosity bitumen) less bitumen is absorbed on the particles which means

that somewhere there must be extra free bitumen in the mixture (the same amount of bitumen was added). It was not further investigated where that extra bitumen could be. As a result of the tested samples with the lower viscosity bitumen no extra bitumen was found at the bottom of the sample. The extra bitumen could be dispersed over the sample without changing the compactibility. After all a significant effect of bitumen content on compactibility in terms of VMA was not found.

Evaluation intuitive models

From studying literature it is known that it is possible that mixtures with a lower bitumen viscosity do exhibit inter-particle stone to stone contact at an earlier stage during compaction. This increases the internal friction of the material.

Based on the previous postulates that were presented (page 92, Intuitive model I onwards), it seems reasonable to assume that a thinner bitumen film also results in a less smooth particle surface with a higher interlock capability. Also, a particle matrix with suitable angularity that results in high interlocking has to widen first before re-arrangement (compaction) can occur. This results in a higher radial/axial deformation ratio of the sample when tested in tri-axial or MHSM equipment.

Due to the nature of the MHSM an increase of the radial deformation creates a higher radial stress on the sample. The result of these two effects, higher internal friction and higher radial stress, both contribute to a higher axial stress required to achieve a pre-described axial deformation. If the mechanisms of models I and II do hold, a lower viscosity bitumen can cause two effects a.) an increase of the internal friction of the material and b.) an increase of the interlock of the particles. This could explain the phenomenon that is observed as a result of the material measurement programme (Figure 3.20 and Figure 3.22).

Variation of the axial radial stress combination; the SP1 test series

The test series SP1 and REF were performed in order to obtain critical state parameters for the DAC 0/11. In both series SP1 and REF the tested materials were identical, only the applied loading stress combinations were different. The critical state deformation behaviour as measured during the MHSM tests is illustrated in Figure 3.26. The SP1 test series were done using a stiffer spring in the Modified Stabilometer. The result of that stiffer spring is that the ratio between radial sample deformation and radial sample confining stress decreases; i.e. at an equal sample deformation the radial stress increases (see also section 3.2). Due to this the difference between axial stress, and radial stress, also decreases. The sample becomes more isotropic when loaded and the q/p' ratio on the sample decreases.

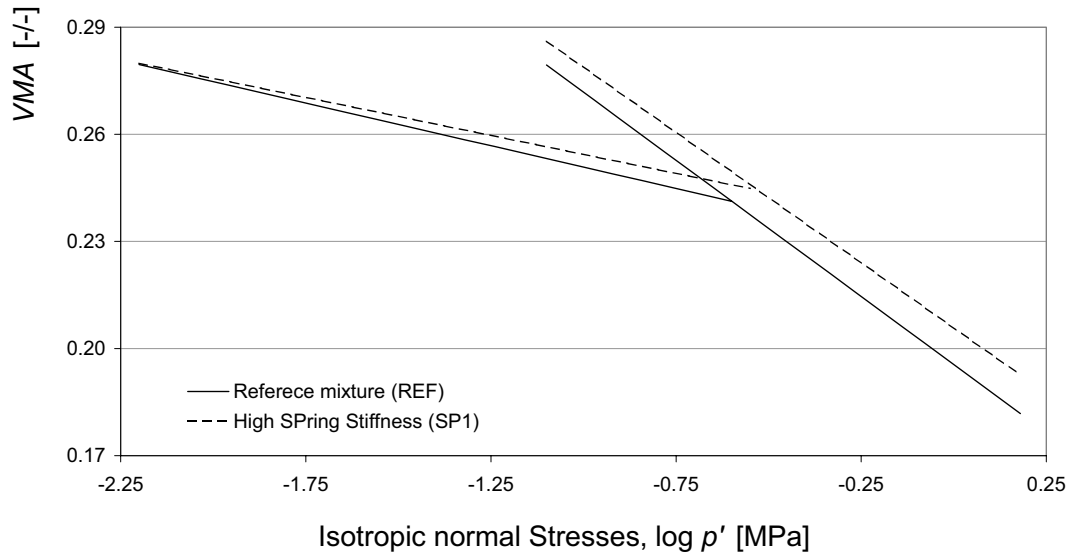


Figure 3.26 The mean p' - VMA curves of the reference mixtures and the changed confining stiffness (coded respectively REF and SP1).

The slopes of both lines for the SP1 test, the recoverable and irrecoverable part of the model, are less steep than the slopes obtained for the REF tests. This indicates that in the SP1 test a larger stress step is required to achieve an equal compaction improvement, expressed in VMA , than in the REF test. This result can be explained as follows; a higher confining stiffness results in changed stress conditions²⁰ on the material (i.e. lower q/p' ratio). The idea that a higher confining stiffness does therefore obstruct easier compactibility of a sample can be illustrated by expounding the following mechanism:

Figure 3.27 shows the effect of the type of stress applied to a loose fictitious particle pattern. In the left part of the figure the particle pattern is subjected to a pure isotropic compression stress (i.e. no deviator stress at all). It can be seen that under these loading conditions the particles do not tend to re-arrange. Theoretically, the applied deformations occur due to deformations of the particles themselves. This has nothing to do with compaction because there are no particle rearrangements.

²⁰ A higher confining stiffness in the MHSM results in higher confining stresses on the sample, this results in less difference between the axial stress and radial stress on the sample and therefore a lower q/p' ratio.

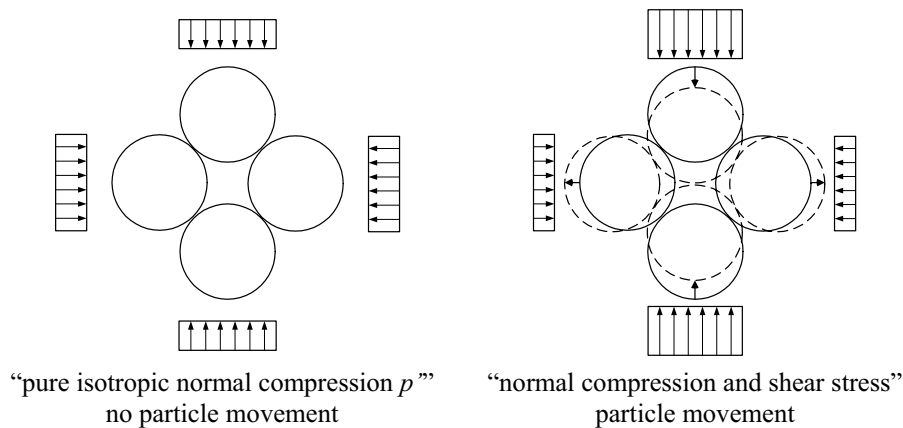


Figure 3.27 The effect of different stress conditions (i.e. q/p' ratio) on particle rearrangements or compaction progression.

In the right part of the figure the particle pattern is subjected to a combination of isotropic compression and deviatoric stress. The figure makes clear that under these loading conditions particles do re-arrange themselves far more easily. This is what happens during compaction. Of course, the visualised particle gradation and pattern are hypothetical and do not occur in reality. Nevertheless, the mechanism helps to explain the effects of different stress combinations (i.e. q/p' ratio in critical state terms) on compactibility. A combination of compression and (a little) shear is better for arranging compaction progress than pure isotropic compression stresses on material.

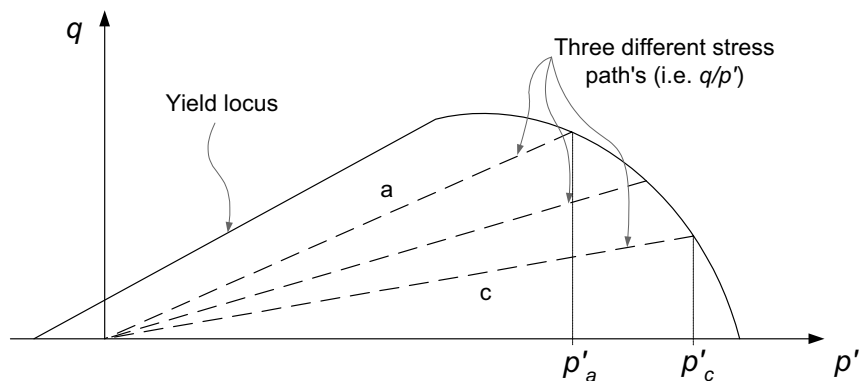


Figure 3.28 Different q/p' ratios touching the yield locus.

The mechanism indicates that while comparing compactibility lines the applied stress combination (i.e. ratio q over p' or shear stress versus normal stress) also has to be taken into account. The REF mixture is identical to the SP1 mixture and therefore the compactibility should also be equal. In Figure 3.26 it can be seen that the SP1 line in the $VMA-p'$ space is positioned above the REF line. It is quite plausible that this difference is caused by a variation in applied loading stresses (i.e. higher q/p' ratio) and not by the material compactibility. Ideally both lines should be plotted into a three dimensional $VMA-p'-q$ space. If cross-sections on the VMA axis perpendicular would be made, different parts of yield loci would be visible. These principles are illustrated

in Figure 3.28. The figure shows that the higher q/p' ratios, (i.e. line a instead of c) touches the yield locus at a lower stress level p' . This implies that the material under that stress condition starts to deform plastically (i.e. compacts) at a lower isotropic normal compression stress, p' .

Conclusions of the mean test programme

Analysis of the results indicate that p' , q parameters are suitable for modelling plastic material behaviour, and enable one to develop better knowledge to what happens with the material during compaction. From the results measured with the modified Hveem Stabilometer, one can compose the yield locus sizes and hardening parameters for different mixes.

The most important critical state information obtained from the measuring programme is summarised in Table 3.6. These figures were also used for the test series model lines as presented in the Figures 3.20 and 3.26.

CRITICAL STATE PARAMETERS FROM TESTS				
	Mixture codes & Imitated temperatures			
Measured quantities	REF 78°C	MTM 94°C	HTM 141°C	SP1 78°C
General	-	-	-	-
VMA_I	.277143	.265325	.268895	.276348
$P'_{int.}$.259977	.318079	.431536	.298218
VMA_{int}	.240907	.240005	.236759	.244309
Recoverable part	-	-	-	-
Slope, κ	-.086321	-.061874	-.071193	-0.076935
Intercept, VMA_{κ}	.818696	.873816	.855505	.843589
R^2	.997179	.997654	.996904	.996050
Irrecoverable part	-	-	-	-
Slope, λ	-.275165	-.264497	-.221428	-.264154
Intercept, VMA_{λ}	.705540	.771154	.797470	.744850
R^2	.999756	.999704	.999733	.999932
q/p'	1.526452	1.584452	1.652971	1.463061
$\varepsilon_{sh}/\varepsilon_{vol}$.753572	.786853	.802538	.729929

Table 3.6 The generalised test results for REF, MBM, HTM and SP1 test series.

Summary

The critical state theory is a well-known theory in soil mechanics. Tri-axial tests are often used for testing granular materials and deducing soil mechanical properties. Hence, they play a crucial role in these tests. In this test the moisture in the granular material controls the volume of the sample during the test. During the test the granular materials have to be saturated because then the material is in a two-phase system. The water that comes out of the sample during the (drained) test is exactly the amount in which the volume decreases (i.e. is compacted). Triaxial tests in the way they are used for soils cannot be used for HMA mixtures during compaction because the HMA mixtures are not “saturated”.

When HMA had to be tested in accordance with “critical state” principles, use can be made of the Hveem Stabilometer (HSM). The HSM loads a sample during a test at a manner that is very similar to the way materials are loaded during compaction in the road. It is recommended to modify the HSM to allow volume control of the sample and a more favourable radial confinement stress course can be applied. Modification of the HSM comprehends an additional cylinder and piston, an adjustable spring and different electronic measurement gauges. Hot samples (e.g. HMA during compaction) can still not be tested with the Modified Hveem Stabilometer (MHSM). They are therefore modified to let them behave, as if they were hot. To achieve this, the viscosity and the amount of the bitumen in the samples were corrected.

Prior to the testing programme different materials with known compactibility characteristics were tested to validate the suitability of the equipment. The material characterisation with the MHSM was achieved with one material (a DAC 0/11) at three “temperatures” (i.e. three bitumen viscosity’s), 78, 94 and 141°C and two stress combinations.

A procedure for conducting the MHSM tests, including control mechanisms for testing the equipment, was developed. An important aspect during testing is the determination of the initial height of the sample. Different methods were considered, tested and judged on their merits.

The sample quantities σ_{ax} , σ_{rad} , ϵ_{ax} , ϵ_{rad} , p' , q , ϵ_{sh} , ϵ_{vol} and VMA were calculated from the readings taken during the test. The radial strain of the sample was calculated from the piston displacement of the additional cylinder. The other stresses and strains were calculated from the directly obtained sample quantities.

The effect of material temperature, or more explicitly bitumen viscosity, on the measured characteristics was partly unexpected. The tests showed that the lower the bitumen viscosity (the hotter the material) the more difficult it became to compact the mixture. This is counter-intuitive. Different intuitive models were developed and analysed for finding a reasonable explanation for the results. The analysis indicated that a higher friction coefficient between the particles and a rougher surface of the particles itself could be the cause for the test results obtained.

4 A FEM analysis of the rolling process

4.1 Introduction

In chapter 2 the critical state theory is discussed. This theory is adopted for describing the Hot Mix Asphalt (HMA) material behaviour. Chapter 3 discusses how critical state properties for a HMA material can be measured using the modified Hveem Stabilometer. The goal of this research project; “*testing the possibilities and further development of a tool that can simulate HMA compaction processes*”, enables us to model the compaction process more accurately, hence, enables better understanding of the mechanisms during compaction.

In this chapter attention will be focused on the Finite Element Model (FEM), an approach that is appropriate for the simulation task. Firstly, in section 4.2, we will look at FEM approaches in general and their applications will be discussed. The two most important reasons that make the use of standard FEM approaches for simulation of HMA compaction inadequate are:

- 1.) the involved material behaves rather complex,
- 2.) during rolling the material suffers large strains.

Both of these aspects have forced us to use a specific FEM, which features are presented in section 4.3.

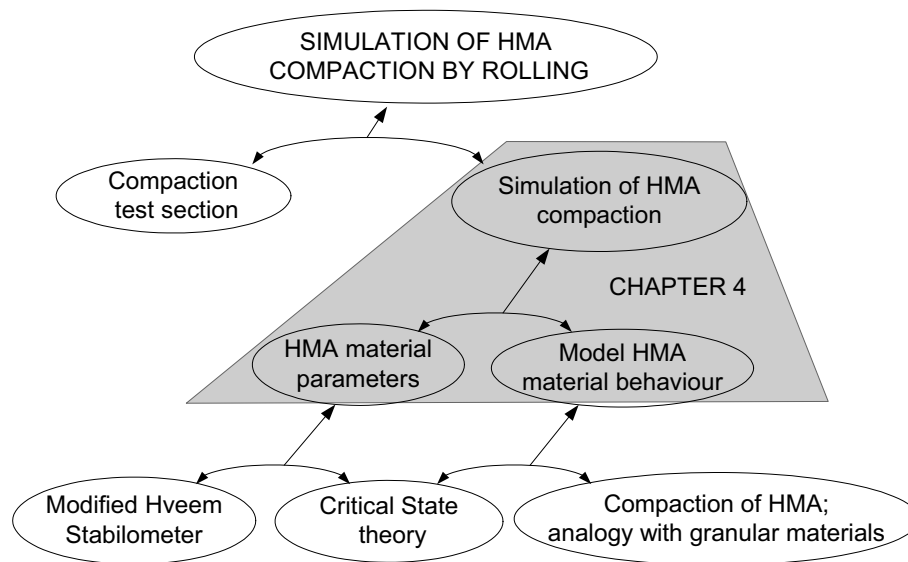


Figure 4.1 The set up of the compaction research project with the grey shaded topics of interest in chapter 4.

Section 4.4 focuses on the set up of the element mesh, nodes and elements. The input variables will also be discussed as well as estimation of material properties for a material model that is implemented in the used FEM code. Figure 4.1 illustrates the goal and set up of the overall compaction research, the topics of special interest in this chapter are marked grey.

4.2 General FEM theory

The Finite Element Method (FEM) is a numerical analysis technique for obtaining approximate solutions for a wide variety of engineering problems. Although originally developed to study stresses in complex airframe structures, it has been extended and applied to the broad field of continuum mechanics (Huebner et al, 1995).

With some problems, for example the process of asphalt compaction, it is difficult to find an analytical solution. It is more attractive to obtain approximate numerical solutions to this type of problem rather than obtaining an exact closed-form solution. The FEM envisions the region of interest as being built up of many small, interconnected sub-regions or elements. A FEM analysis of a problem gives a piecewise approximation of solutions based on the governing equations.

The finite element discretisation procedure reduces the problem to one of a finite number of unknowns by dividing the solution region into elements and by expressing the unknown field variable (i.e. stresses or strains) in terms of assumed approximations within each element. The approximating functions are defined in terms of the values of the field variables at specified points called nodes or nodal points. Nodes usually lie on the element boundaries where adjacent elements are connected. In addition to boundary nodes an element may also have an interior node when this is required for accuracy under specific circumstances.

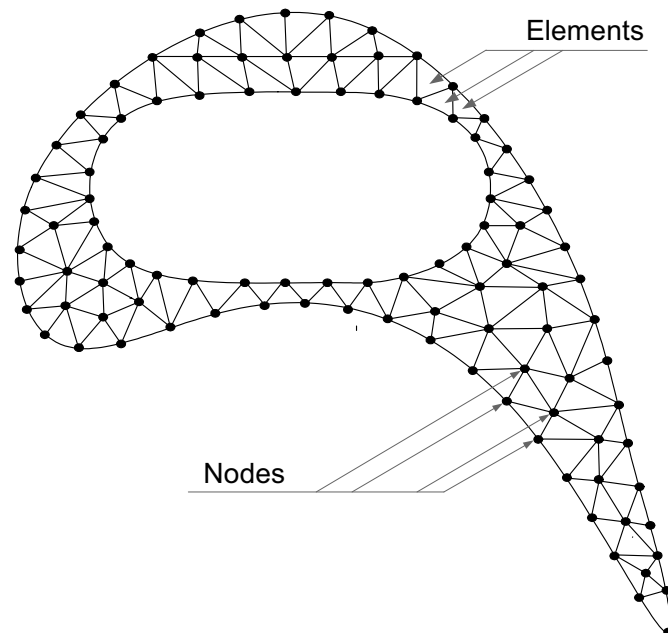


Figure 4.2 A finite element discretisation of a turbine blade profile (Huebner et al, 1995).

The FEM has an important feature that sets it apart from other numerical methods. This feature is the ability to formulate solutions for individual elements before putting them together to represent the entire problem. In essence, by using the FEM a complex problem is reduced to a series of greatly simplified problems. Figure 4.2 illustrates how a structural body (turbine blade profile) is built up by several elements. To give an idea about the availability of elements Figure 4.3 shows some elements that can be implemented in an FEM code.

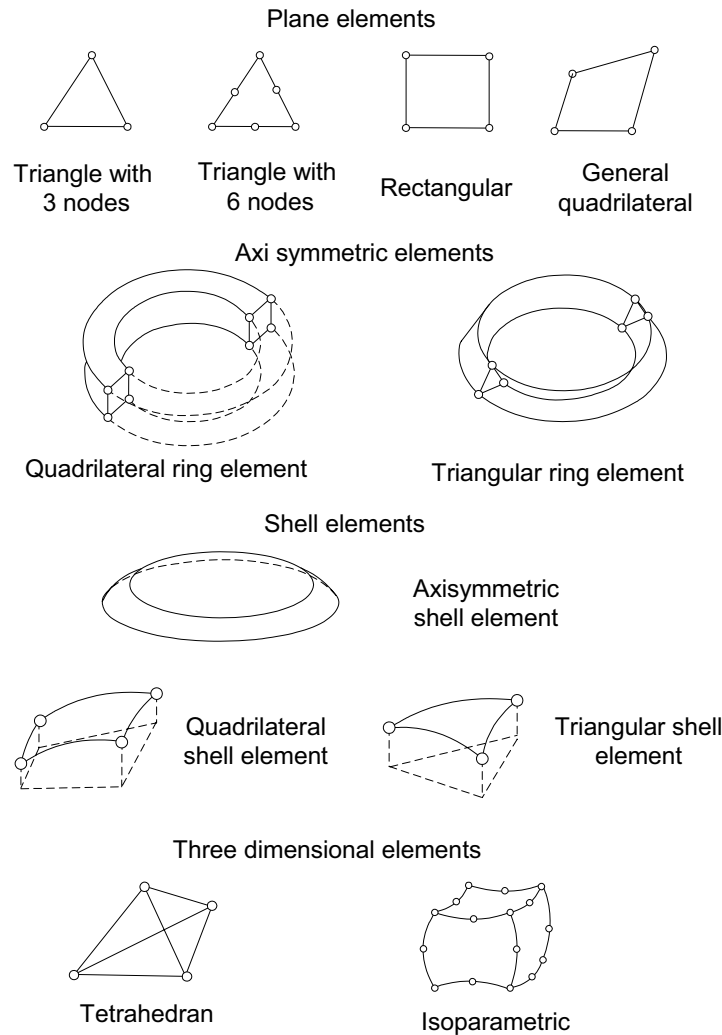


Figure 4.3 Some types of elements as used in FEM codes (Brebbia, 1973).

A FEM approach suitable for compacting HMA

Due to particle movement during compaction the HMA behaves neither as a solid nor as a liquid but exhibits characteristics of both. This results in complex mechanical behaviour. It implies that relatively large deformations (strains) can arise. Schofield (1968) described the continuous deformation of the soil as a stochastic process of random movements of the solid particles until the whole mass behaves as a frictional fluid. This sets specific demands on the chosen approach. It implies that simulating

such a problem with FEM can only be done successfully if appropriate measures are taken.

Such measures are implemented in the Arbitrary Lagrangian Eulerian (ALE) method. A second factor that determines the selection of a particular FEM tool, is the material behaviour. Not each FEM code contains a suitable material model. A suitable model for soil mechanics is one that complies with critical state principles. Such a model would lend itself to an application for modelling HMA compaction.

Within FEM two different approaches can be used, the Eulerian formulation and the Lagrangian formulation. The Lagrangian formulation, which couples the element grid to the material, is often used in structural disciplines. The Eulerian formulation fixes the grid in space and this approach is especially used in fluid mechanics. Both these formulations on its own are not suitable for simulating the compaction behaviour of a particle-based material like HMA. However, a combination of both formulations does exist, it is the Arbitrary Lagrangian Eulerian (ALE) method. The first step of the ALE method consists of an Updated Lagrangian analysis. Since the ALE method will be used for simulating the compaction process and because it uses components of the Lagrangian, the Updated Lagrangian and the Eulerian method, all of the methods will be described briefly with a focus on the ALE-method.

Eulerian formulation.

The Eulerian formulation is a FEM approach that fixes the finite element grid in space. The material and the borders of each element are defined in such a way that material can flow in, out and through the elements. In the Eulerian formulation the fundamental equations at the boundaries concern the material flow in and out of the element. If the formulation is applied on porous media the net flow is related to the pressure (gaseous phases) or to the bulk density of the material inside the element. Using the formulation it is possible to model only a relevant part of the workpiece and let material flow into the mesh at the entrance and out of the mesh at the exit. Its characteristics make the formulation particularly suitable for fluid mechanics problems. Figure 4.4 illustrates a fluid mechanics out-stream problem simulated by using FEM (Eulerian formulation).

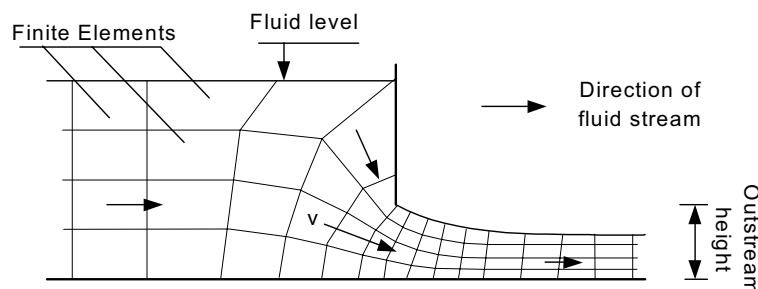


Figure 4.4 An example of a fluid mechanical (out-stream) problem; for simulating such a problem an Eulerian approach can be applied successfully.

Lagrangian formulation

The Lagrangian formulation, which couples the element grid to the material, is often used in structural disciplines. In Figure 4.5 a Lagrangian formulation is used to simulate the behaviour of a bending beam. In a Lagrangian analysis, a material point is followed in time. Deformations experienced by a material point can influence the constitutive behaviour. If the displacements remain small the difference between the non-deformed and the deformed geometry can be ignored and a geometrically linear analysis will be sufficient. If however, the displacements become larger, the notion of stresses and strains depends on the choice of the reference frame. In this case a geometrically non-linear analysis must be performed (Van den Boogaard, 1995).

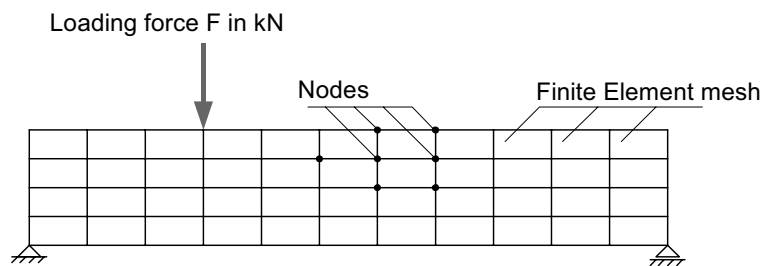


Figure 4.5 The finite element mesh for simulating a structural mechanical example in which a Lagrangian formulation can be applied. It is a bending beam on two supports.

In a finite element analysis the stresses and strains are usually determined only at the integration points. During the Lagrangian analysis an integration point represents the same material point. The Lagrangian formulation is usually adopted for solids. Problems on materials that show a history dependency can adequately be taken into account by using a Lagrangian analysis (Stoker, 1999).

Updated Lagrangian Analysis

An Updated Lagrange description can be used advantageously in case of plastic deformations of solid materials (Van den Boogaard, 1995). In this formulation the material is fixed to the computational grid as it is in the Lagrangian formulation. This method is very useful if the response of the material is path dependent, as in the case of plasticity. In case of large plastic deformations however, the computational grid of a normal Lagrangian analysis can become too distorted to yield accurate results. This can be avoided by remeshing techniques. A new more regular mesh substitutes the distorted mesh. The information that is available in the original mesh must be transferred to the new mesh. These items however, are primarily available in a limited number of discrete points in the continuum. The points of the new mesh will in general not coincide with the points of the old mesh. By defining a smooth function inside the elements and using averaged values in the nodes one can calculate the values of the transferred items by interpolation. This process may yield some

numerical diffusion²¹ of the results. If remeshing is applied only a couple of times during the analysis the numerical diffusion may be acceptable, but if the remeshing is used very often, for example in every step during the simulation of a rolling process, deterioration of results occurs. This makes the updated analysis inadequate for simulation of rolling processes.

Arbitrary Lagrangian Eulerian (ALE) analysis

When considering forming processes, it is advantageous to use the Eulerian approach, fix the grid and let the material flow through it. However two factors complicate this. Firstly the path dependent material behaviour necessitates the integration along streamlines and secondly the boundaries perpendicular to the process flow may not be known in advance. This stimulated several researchers to develop a combination of a Lagrangian and an Eulerian method. In an ALE method the material displacements and the grid displacements are not coupled as in a Lagrangian method and the grid displacement (or velocity) is not equal to zero as in an Eulerian method. The constitutive relations, kinematic relations and the boundary conditions determine the material displacements. The grid displacements are determined in a way to maintain a physically and computationally proper grid, i.e. keeping the information about material boundaries and introducing a less distorted mesh (Van den Boogaard, 1995).

For processes with large strains, like forming processes, the Lagrangian formulation is not suitable due to large mesh distortions. The Eulerian type of analysis is not applicable because the discretisation is then fixed in space and the boundary of the solid cannot change its form. For forming processes it is essential that the free material surface can change its form. In the ALE method, the computational grid is disconnected from the material and can have any displacement. This can be used to keep the mesh more or less regular and let the material flow partly through the mesh and at the same time keep track of the material boundaries. One of the implications of this method is that a material point is not represented by one and the same integration point during the analysis. However, taking special measures that take history dependent material behaviour into account solves this problem.

The associated reference system fixed in space, used in a Eulerian formulation, is called the Spatial Reference System (SRS). Each spatial point of the SRS is unambiguously identified by an invariable set of independent SRS coordinates. The reference system used in a Lagrangian formulation is a material associated reference system and called the Material Reference System (MRS). Each point of the MRS and thus each material point of the body is unambiguously identified by an invariable set of independent MRS coordinates (Schreurs, 1983).

The reference system used in an ALE formulation is a non-associated reference system, called the Computational Reference System or CRS. Every point of the CRS is unambiguously identified by an invariable set of independent CRS coordinates. The

²¹ Numerical diffusion is FEM jargon. It arises when during an update often a new FE mesh must be made and therefore often the material properties must be converted to the new nodal points. Each time when this is done (small) inaccuracies are introduced. When this is done for example 10.000 times (which is a feasible number of calculation steps in a simulated roller process) it can be that output results become inaccurate. This phenomenon is called "numerical diffusion".

position of the CRS points is not given, so this provides much freedom in formulating the mathematical model. In an ALE formulation both the CRS and the MRS are used. The ALE formulation requires that there is an unambiguous connection between these two reference systems in every state. When using the FEM, all sorts of boundary conditions can easily be taken into account but the boundary of the CRS always has to coincide with the boundary of the body that will deform. At the same time the nodal point positions can be prescribed or determined in a CRS determination process, in such a way that the dimension and the geometry of the elements is appropriate (Schreurs, 1983).

Two types of ALE methods exist; coupled and uncoupled ones. The first step of an uncoupled ALE method consists of performing an updated Lagrangian step, then a remeshing step and finally a remapping of state variables. In this method the material velocity per incremental step is calculated first (i.e. a Lagrangian step), then the grid velocity per incremental step is calculated. In the coupled method both steps (calculation of material and grid velocity per incremental step) are done simultaneously. The approach used for the rolling simulations was an uncoupled one. The scheme that is followed during an uncoupled ALE calculation step is illustrated in the flow chart in Figure 4.6.

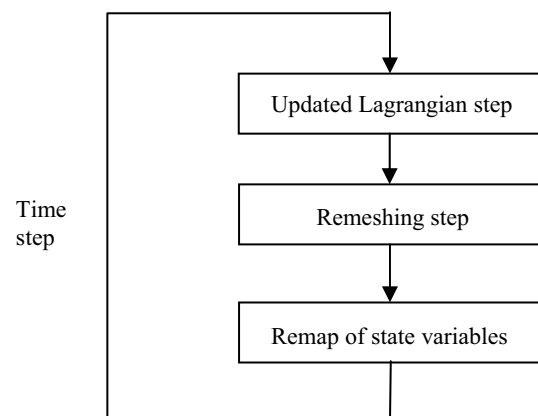


Figure 4.6 A flow chart of the steps followed using an uncoupled ALE method (Stoker, 1999).

Originally the ALE was introduced in the context of the finite difference method, a predecessor of the finite element method. The calculation of the mesh velocity and the remap of the state variables are important aspects of the method (Stoker, 1999). Figure 4.7 illustrates how the ALE method can prevent mesh distortion in the simulation of the setting up process. In (a) the initial set-up can be seen, in (b) the mesh distortion during an Updated Lagrangian calculation is shown and in (c) the corrected mesh during an ALE calculation is shown. Figure 4.7 shows that in simulations where large deformations occur, by means of the ALE method, a much better Finite Element mesh can be ensured. This, of course affects the outcome of the simulation.

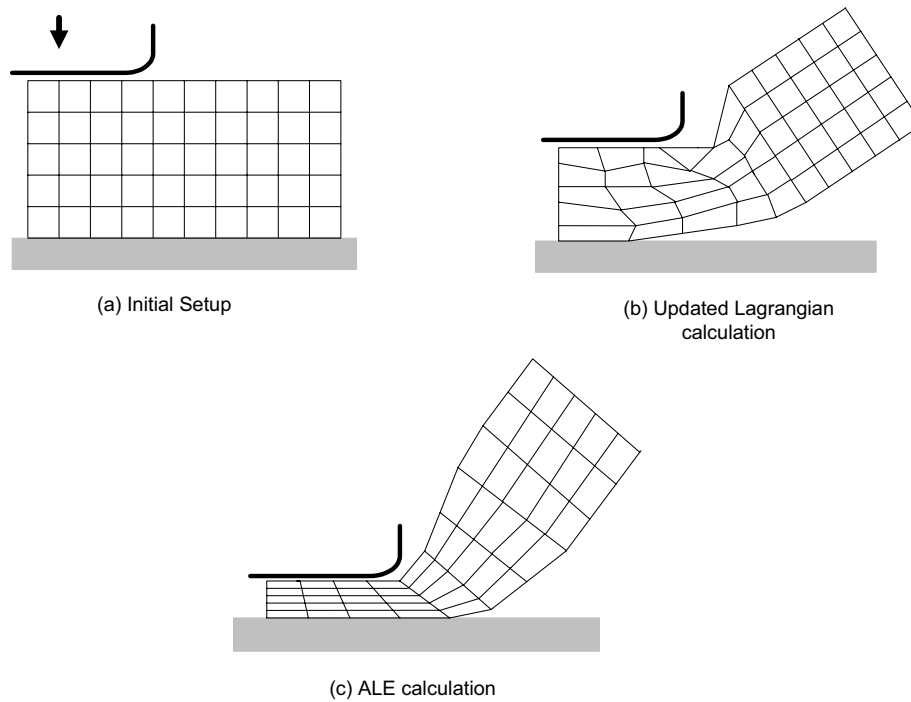


Figure 4.7 Mesh deformation during finite element calculations, (a). initial set-up, (b). Updated Lagrange calculation, (c). ALE calculation (Stoker, 1999).

Numerical simulation of forming processes

It is possible to draw useful analogies between the forming processes in metals (especially rolling) and the compaction process of HMA and granular materials. Forming processes of metals are often simulated using FEM methods and this can be found in several publications, e.g. Van der Lugt (1988). Because a lot of the aspects mentioned are also applicable for the compaction process of asphalt, the simulation of forming processes is briefly discussed in this section.

An example of a forming process is the process of forging metal where often a product is fabricated in several stages. For each stage in the process a different tool is used. It is desirable to limit the number of stages for economical reasons. The simulation of forming processes involves the solution of highly non-linear equations. The material behaviour exhibits plasticity and is temperature and deformation rate dependent. During the forming process the geometry changes significantly, introducing geometrically non-linear behaviour. Besides the non-linearity, large deformations can cause numerical problems because of heavily distorted meshes (Van den Boogaard, 1995).

Stoker (1999) shows (Figure 4.8) the simulation of the extrusion process with a sharp angle at the exit. The comparison with an extrusion process is made here because this process also suffers large deformations. A FEM simulation therefore requires special features, just like what is needed for simulation of a HMA rolling process. The elements at the exit are locally distorted. In order to be able to continue the calculation, remeshing techniques or an Eulerian formulation have to be used. In

contrast with the updated Lagrangian method the Eulerian and ALE methods do not suffer from mesh distortion, because the mesh is spatially fixed during the simulation. However, there are also disadvantages; the fact that the mesh is not connected to the material makes it more difficult to take account of the history of the material.

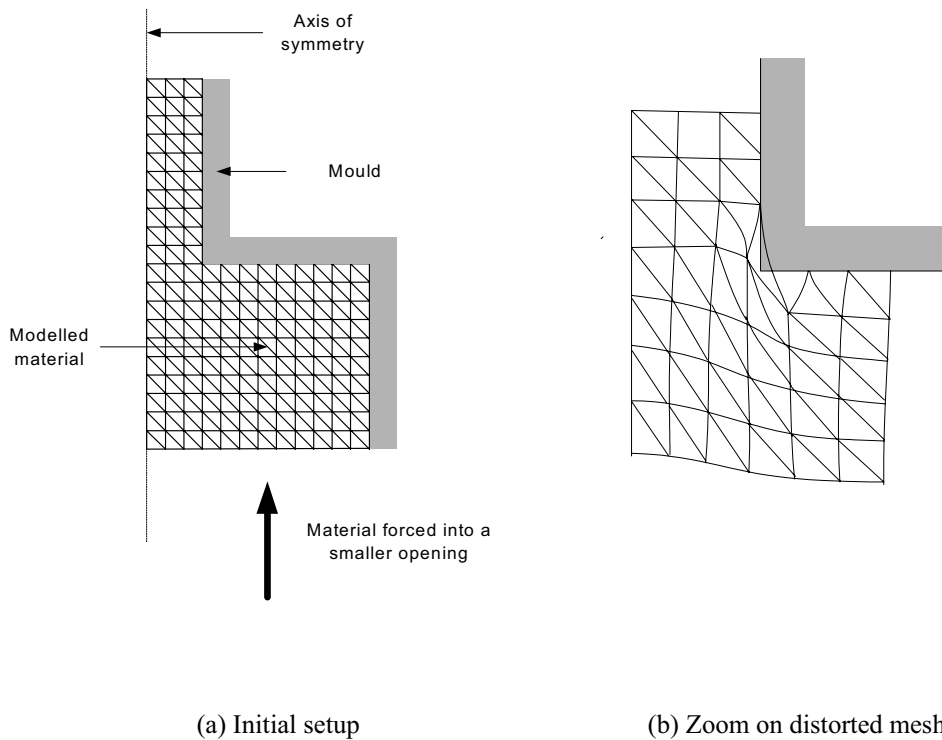


Figure 4.8 Mesh deformation while doing an Updated Lagrangian calculation of an extrusion process. (a). the initial set-up, and (b). Zoom on the distorted mesh, (Stoker, 1999).

Similarities and differences of rolling metal and rolling HMA

Globally seen the process of rolling cold metal is quite different from rolling HMA. Also the visualisation of both processes underlines this assumption, see Figure 4.9. However, the next sub-section will describe that a significant part of the simulation tool for rolling metal, a subject in which there is much experience, can also be used for simulation of HMA rolling. Firstly we will discuss the differences and similarities of both processes.

The similarity during both processes is that during rolling both materials suffer large strains and both materials behave in a plastic manner. Some aspects of the metal rolling process are relevant for the compaction process of HMA for example; a.) the boundaries, b.), the elements used, c.) the geometry of elements and nodes, and, d.) the interaction of the roller drum and the rolled material. The major aspects of a steel rolling process are, together with the major aspects of a HMA rolling process, illustrated in Figure 4.9.

Using steel rolling the rolled steel plate is relatively thin, and stiffness of plate and drum are approximately the same. Therefore the roller drum must also be (partly) modelled to analyse its deformations. With HMA rolling the compacted material is much thicker in comparison with the dimensions of the roller drum. The material is weak relative to the roller drum stiffness. This difference in stiffness between the asphalt and the roller drum makes that the (steel) drum does not significantly deform during rolling. It is therefore sufficient that only the roller drum outline is modelled. Other differences are the position of the involved elements (roller drum and rolled material) in both processes. In the metal rolling process the roller drum(s) are in a fixed position, the metal plate is enforced through both involved roller drums. A result of this is that the opening between both drums is also fixed and therefore reduction of the material thickness is pre-defined. The involved rolling forces to achieve this are variable. In HMA rolling the roller is of a fixed weight, furthermore the material stays in its location whereas the roller itself moves. Because of the nature of this process, the reduction in layer thickness is the variable.

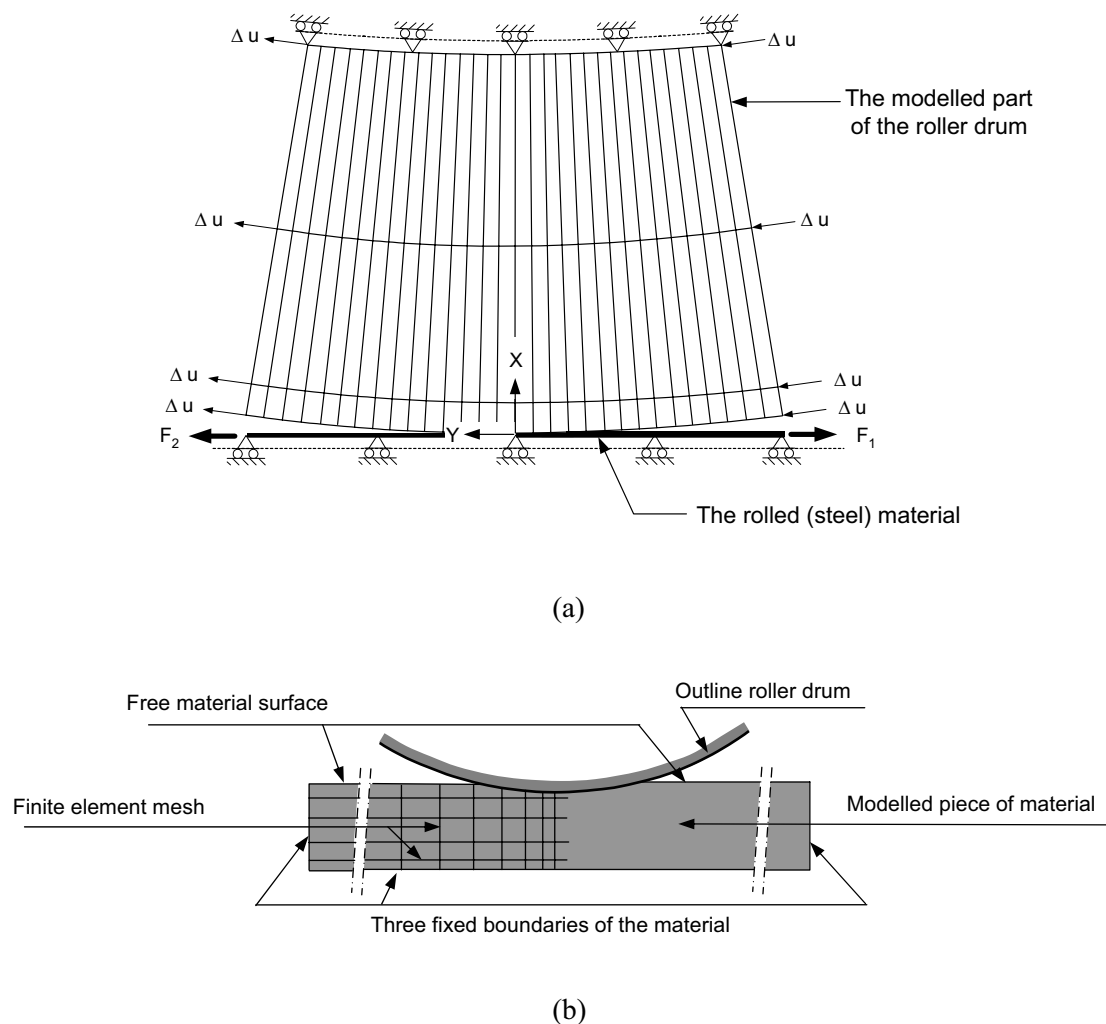


Figure 4.9 The FE set-up for simulation of a cold metal rolling simulation (a), (Van der Lugt, 1988) compared to the FE set-up for a HMA rolling simulation (b).

In simulation of HMA rolling from the complete roller drum and the rolled material just a small part is modelled with finite elements. The relevant part of the material is modelled with plane strain elements. Contact elements are located between roll and rolled material. The element mesh is shown in Figure 4.9. In metal rolling allows symmetry simulation of only half the problem to obtain an understanding of the whole process. For HMA rolling this is not the case, here the whole problem must be modelled. During the simulation of metal rolling the Arbitrary Lagrangian-Eulerian (ALE) method is used. For simulation of both processes (metal and HMA) holds that the end sections of the material were treated in such a way that they remain plane sections. An automatic adjustment procedure was applied to control the exit thickness.

4.3 *Simulating rolling with FEM*

The first section of this chapter was focused on the FEM approaches in general. Here in section 4.2 we will discuss which specific features are required when FEM is used for simulating a rolling process of HMA.

When preparing FEM simulations one of the first tasks is designing a suitable FE mesh for the problem. Designing a FE mesh is always a compromise between computational time, fineness of the mesh and required accuracy. Coarser meshes will give shorter calculation times but may also result in a poor accuracy. The gain in accuracy is heavily paid for in computation time and complexity, hence an optimum has to be determined. Such an optimum is determined based on experience and observation of model behaviour after a few runs.

Dimensionality of the problem

The first decision that must be made when simulating a problem is the dimensionality. For deduction of the required dimensionality of the problem, engineering judgement and minimal insight in the relevant governing problem is required.

When doing FEM simulations, using the ALE approach DiekA, the best suitable material model currently available to approach HMA behaviour is “Rock”. Rock is however a 2D⁺ model; it can handle 3D problems but only if there are no variations in stresses, strains, loads, boundaries etc. in the third direction. The model can therefore only be used on “plane strain” or “axial symmetric” situations. This implies that in the third direction (or tangential direction in the case of axial symmetry) only average stresses (and strains) can be calculated and no changes in load for example, can be introduced.

When we take the HMA static steel rolling process into account, it can be seen that the key stresses and strains are manifested in the vertical and longitudinal (driving) direction. Furthermore, do differences in temperature in the vertical direction of the layer result in different material behaviour at different depths. The consequence is that at least the longitudinal and vertical directions must be incorporated in the model, the width direction can then be modelled as a “plane strain” direction. The choice implies that the edge effects of the roller drum cannot be simulated, so only the effects of roller drums that are relatively wide related to the diameter can be taken into account.

Rolling model “set up”.

A central issue in HMA rolling concerns the relationships between roller drum diameter, roller drum weight, material characteristics and compaction progression. To determine that relationship, the effects of a particular roller (HAMM DV6.42) on a DAB 0/16 were measured during the construction of a test section, see chapter 5. In practice the weight of the roller is fixed during rolling, and progression of compaction (or reduction of layer thickness) is unknown.

It is known from FEM simulations of steel rolling processes that applying a fixed load²² (i.e. fixed roller drum weight) on a material in a FEM simulation results in computational instability. However, prescription of deformation and then computing the force that is required to achieve this deformation can overcome this problem. For obtaining the wanted relation between the roller drum weight and the compaction progression the following iterative procedure can be followed; a.) making one calculation in which the compaction progression is overestimated (line A in Figure 4.10), and, b.) one in which this is underestimated (line B in Figure 4.10). Then, c.) by using interpolation techniques, estimation of a closer approximation of the correct compaction progression related to the roller drum weight can be made (line C). Currently the system works by trial and error. In fact this procedure contradicts to reality and is labour intensive but it ensures numerical stability and yields the same result; i.e. the correlation between down force applied by the roller and compaction progress.

A complete example of an appropriate FE set up as used for the compaction research (5×50 elements, material length 400 mm) is illustrated in Figure 4.11.

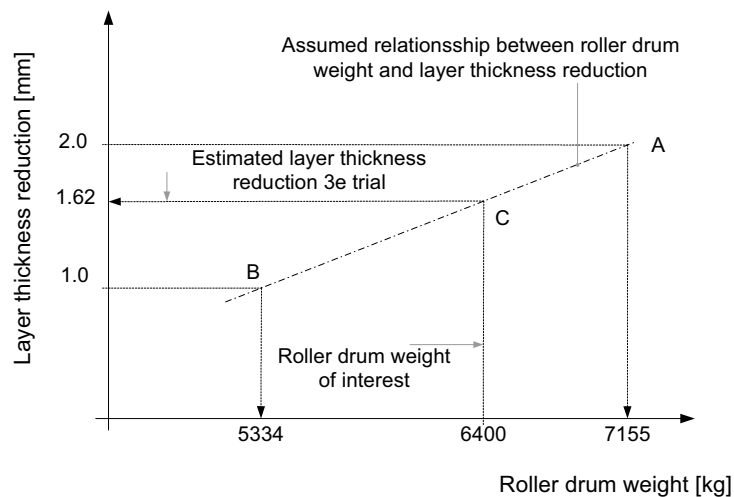


Figure 4.10 Interpolation procedure for getting the right roller drum weight related to measured layer thickness reduction.

²² During our research the effect of a static roller is investigated. However, when in reality use is made of a vibratory roller, the effect of the roller passes can be affected by alternating the vibratory frequency.

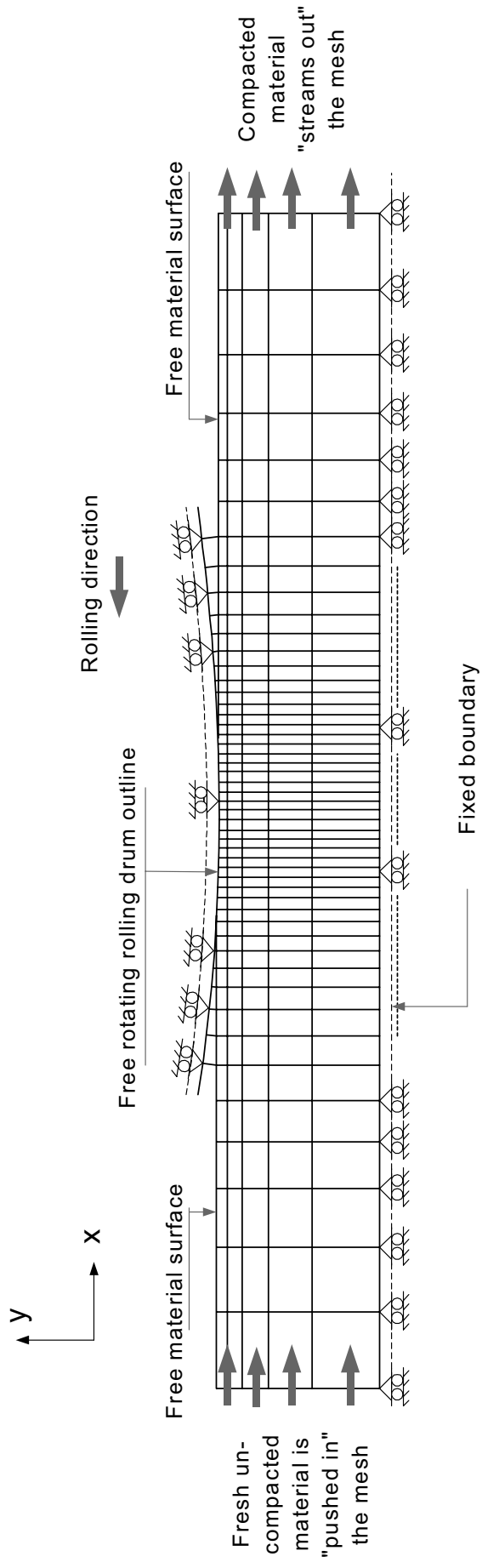


Figure 4.11 An appropriate FEM mesh for the HMA rolling problem.

Length of material that is subjected to compaction forces.

From simulations of steel rolling processes it is known that a certain material length must be “calculated through” (i.e. must be subjected to compaction forces) before the simulated results are homogeneous (in time) and reliable. The process of simulating “rolling” starts when both the material and the roller drum are pushed from left to right. For numerical reasons this horizontal material displacement must be enforced step-wise. It is a rule of thumb that the length that must be subjected to compaction forces should approximate the material length that is modelled (in our simulations about 400 mm).

It must also be considered that the size of the achieved deformation steps is relevant. This size (length) of the material processed (compacted) per iteration step depends on; a.) the complexity of the chosen material, b.) the vertical predescribed layer thickness reduction, and c.) the modelled contact properties. The total number of iterations required can be calculated from the size of material processed per step and the total length of material that should be processed (i.e. compacted).

Modelling the boundary conditions and the roller drum.

Using FEM for structural problems one can model the whole structure but it can also be attractive to model only the area of specific interest in order to reduce the complexity. If the complete structure is modelled the boundary conditions should represent the way the structure is supported in its environment (base, abutment etc). When, as is the case for the rolling problem, only the part of specific interest is modelled, the boundary conditions should represent the way the modelled material is connected to the remaining material part that is not incorporated in the model. Physical boundary conditions are commonly materialised by restriction of the freedom of movement of nodes and/or as loads applied on nodes or edges. However when a (partly) Eulerian approach is applied, at the edges, the material must be able to stream in and out the mesh.

To model the compaction process of HMA, three boundaries were given as a prescribed deformation: a.) the interface between the sub base (old material) and the newly paved layer (bottom of the paved material), and, b.) both the vertical edges of the modelled material. The interface to the sub base is in our model simulated as completely rigid. This does not fully correspond to reality where a HMA sub-base always reacts partly elastically. This procedure may therefore introduce some small errors. However because the major focus was on testing if simulation of compaction of a newly paved HMA layer is possible and to avoid too much complexity in the model it was decided that this simplification of reality was acceptable in this stage of the research.

The upper surface is partly connected to the roller drum, whereas the rest of that material edge is a free surface. This free surface of the material can move freely in the vertical direction. At the interface roller-HMA the situation is more complex. Here,

normal compressive forces, shear forces, slip or even a gap between roller and asphalt mixture can occur. These problems were addressed by using contact elements.

When studying the compaction of the HMA material it is realistic to assume that the stiffness of the steel roller drum is much larger than the stiffness of the compacted HMA. This implies that the drum does not significantly deform and thus all the deformation will be the result of HMA compaction. Therefore, the contour of the drum is modelled as a rigid rotating boundary. The contact elements are four-node elements.

For simulation a roller drum must be modelled that is able to rotate freely. For this the DiekA approach has an interesting feature; the rotated co-ordinate system. The reference point of the system is the centre of the roller drum. An important aspect of the system is that it defines nodes on a segment of a circle. Further, for every node a local co-ordinate system is defined. The rotated co-ordinate system; operates with a local x and y direction. The local x is the radial direction, whereas the local y corresponds to the tangential direction, see Figure 4.12. Imagine that when displacements of these nodes are coupled to each other in the local y direction and all local x deformations are suppressed, a free rotating drum at a fixed position is defined.

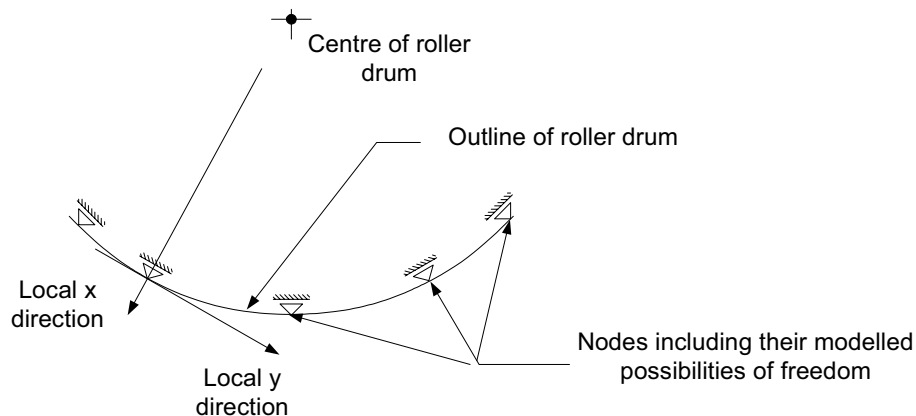


Figure 4.12 The rotated co-ordinate system of the DiekA FE Approach.

An HMA roller contains driven drums and non-driven drums. There must be (slightly) differences between the processes under both drums in terms of stresses applied to the material. The resistance required for movement of the non-driven drum(s) must be generated on the contact surface of the driven role. It is certainly possible to simulate the effects of both situations. However, because of the goal and scope of this research project, we did not focus particularly on these differences. During the simulations, for numerical stability of the calculation process, we chose to drive the roller drum and the material simultaneously with a pre-described deformation. Individual tests were done while driving only the material. Both simulations gave similar results. These results were expected because the effects of gravity are not implemented in the simulation (e.g. starting a movement of the simulated drum does not require energy). It will therefore not lead to different shear stresses in the contact surface when only one of the involved objects (drum or material) is driven instead of both.

Contact elements Roller drum – Bulk material

At places where roller drum (tool) and HMA (workpiece) are in contact, forces can be transmitted from the tool to the workpiece. During such a process the contact area changes considerably in size and orientation. The accurate numerical modelling of that contact is an important prerequisite for the numerical analysis of the process. Interface or contact elements can be placed between continuum elements or between a continuum element and a rigid boundary to regulate this. With such elements, it is possible to model Coulomb friction at element level (Van den Boogaard, 1995).

Contact elements can regulate the behaviour of interfaces between different materials or different material parts. A contact element consists of an upper and a lower plane and is defined (or built) in such a way that these planes can move normal and parallel to each other (Figure 4.13). Highly non-linear springs and dampers bind the upper plane and the lower plane to each other. A relatively small movement of the planes on both sides of a contact element causes stress. The magnitude of these stresses depends on the stiffness of the contact element.

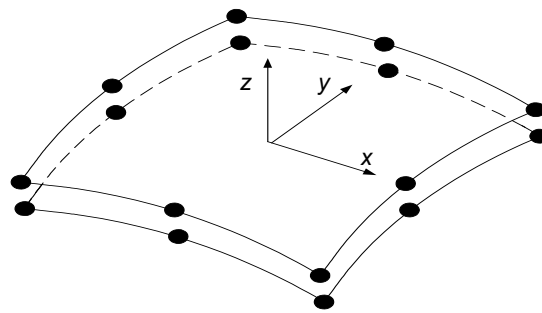


Figure 4.13 Curved interface element (Van den Boogaard 1995).

Different displacement increments of the upper and the lower plane of the contact elements can occur in case of slip between the roller drum and the rolled material. The use of contact elements requires that the nodes on opposite interface planes must be close to each other for simulating the contact behaviour correctly. If this is not the case a correction must be applied. Even if in an initial situation the nodes do coincide, it is common that they move away from each other in the tangential direction during the analysis. The ALE method can prevent this because it regulates the positions of grid points (e.g. nodes). Due to this feature it can be assured that the nodes that are about to make contact are properly aligned.

The example shown in Figure 4.14 may be considered as contact elements between a roller and a plate come in contact. For the ALE algorithm situation a. can be considered as the situation at the start of a pre-described deformation step of the calculation. Situation b. may occur when there is slip between roller and drum. As a result of heavily distorted meshes the contact between drum and plate is not aligned properly anymore. The ALE method can take care of proper mesh outlining and avoids therefore mesh irregularities. The ALE method also keeps further track of stresses, strains and especially parameters that constitute the history dependency (such

as equivalent plastic strains). The values of these quantities must be determined in the new positions, taking the relative grid displacements into account (relative to the material displacements).

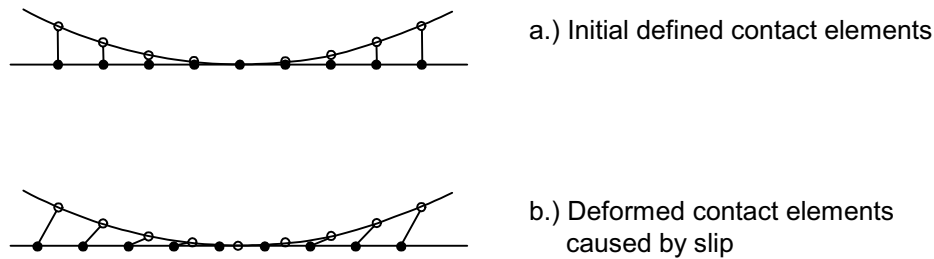


Figure 4.14 Alignment of nodes near interface elements: before (a.) and after (b.) a calculation step (Van den Boogaard, 1995).

The interaction between the roller drum and the rolled material is a very particular and important one. In this interface only normal compressive stresses can be active, tensile stresses cannot occur. If there exists a normal compressive stress, a shear stress could develop in the longitudinal direction. This shear stress may increase when the normal compression stress increases. At a certain point this increase of shear stress stops. When the actual shear stress reaches the maximum, there occurs slip between both elements; when the shear stress is lower than the maximum both elements stick together. This phenomenon is called slip-stick behaviour. This behaviour has to be incorporated into the model for simulating compaction successfully. Within a FEM approach using contact or interface elements can simulate such behaviour.

The contact elements are regulating the normal and shear stress, and the normal and shear strain between the two components (material and workpiece). The size of the contact element in the thickness direction (i.e. perpendicular to the direction of the contact plane) can be zero (the contact element is closed) or can be larger than zero (there is a gap between the two bodies i.e. the contact element is open). The contact behaviour in the normal direction, perpendicular to the contact surface, can be represented by an elastic spring parallel to a damper as shown in Figure 4.15. The damper can be activated or not. The damper is used to smooth the opening and closing of the contact element.

The thickness of the contact element can also become negative, in which case the contact element is turned inside out and one can speak of an overlap (penetration) between the contacted bodies. In reality this penetration cannot occur. In FEM simulation it is a commonly used principle to make the system work. In fact the overlap is limited and can be adjusted with the input parameters.

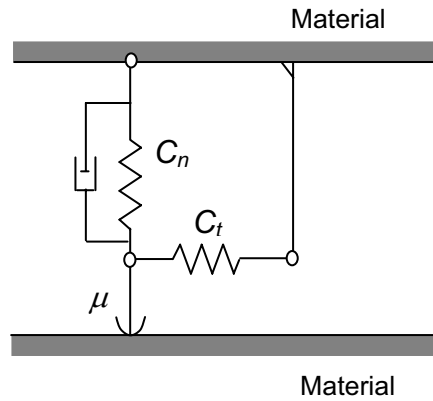


Figure 4.15 Model of behaviour of a contact element (Rietman, 1998).

For the contact between the roller drum and the HMA it is advisable to use the Coulomb friction model. This model uses a cut off above a particular maximum value τ_{max} , as illustrated in Figure 4.16. The maximum friction in the Coulomb model determines friction coefficient μ and the normal compressive forces. In the contact situation, the behaviour is based on a friction layer approach.

The normal stiffness (C_n in Figure 4.15) does not have a physical meaning and it can be chosen rather arbitrarily. By choosing it to low large penetration depths are obtained which can lesson the accuracy of the calculation. By choosing it to high convergence problems can arise. σ_{ref} and g_{ref} are the input parameters for definition of stiffness in normal direction C_n . σ_{ref} is a reference normal stress when the gap g between the roller and rolled material does have the value g_{ref} .

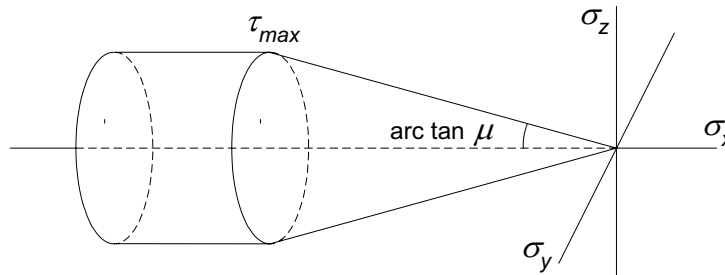


Figure 4.16 Friction surface in the π plane (Van den Boogaard, 1995).

If Coulomb friction is simulated, the maximum shear stress is limited and depends on the normal stress in the element. Depending on both the shear and normal stress, stick or slip occurs in the contact plane. Stick-slip behaviour plays an important role especially in simulating rolling processes. For these reason the parameters representing the phenomenon have to be chosen with care (Rietman, 1998).

The stiffness in tangential direction is represented by the contact parameter C_t . C_t regulates the relation between the shear stress, τ , and the shear deformation, γ . C_t is determined by dividing $\sigma_{ref} \times \mu$ (which value equals the shear stress τ) by the

admissible shear γ_{adm} . γ_{adm} is the admissible shear, it is the shear deformation at which the two involved elements in contact start to slip.

For contact elements, the contact stress in the normal direction only depends on the current positions. If a positive gap is encountered, the shear strength is set to zero and if penetration is encountered an adjusting normal compressive stress is calculated. The shear strength is, however, history dependent. Therefore the information of the previous steps must be transferred to the new locations. The calculation of the new traction follows a two-step procedure.

At places where there is contact between the roller drum and the material, the contact stresses, deformations etc are regulated by the contact elements and their numerated parameters. Here experience and “running enough simulations” also play an important role in selecting values for the variables. The most important adjustable parameters related to this are slip-stick behaviour, vertical stiffness and possible overlap of the tool and the material.

Different contact model parameters may not result in a different relation between the vertical roller force and compaction progress (i.e. reduction of layer thickness). Furthermore, variation of these parameters may also not result in different stress and or strain patterns. The right parameter fine-tuning is crucial for running the FE simulation successfully. The right parameters avoid that a simulation derails before the simulation is completely finished.

4.4 FEM simulation of HMA compaction processes

Part of doing FEM simulations is designing the FE set up. Designing such a set up implies choosing the FEM mesh, the right boundary conditions, contact parameters, doing test runs etc. A lot of engineering judgement is required to create the right set up. The whole procedure is based on trial-and-error, refining the FE mesh, doing test runs and judging results, changing some variables like the contact stiffness, again doing test runs and judging results, etc. until a satisfactory set up is achieved.

A paved layer on which a roller pass is simulated has a compaction level and a temperature profile, which is a function of the depth inside the layer. During the laboratory-measuring programme the material properties for a DAC 0/11 were measured as a function of temperature and *VMA*. First of all the critical state parameters are determined for the right temperature and *VMA* level, and secondly the Rock values are determined from the critical state parameters.

In summary the following steps should be taken before FEM simulations of a HMA rolling process can be done;

- 1.) designing a general set up of a FEM rolling simulation
- 2.) determination of the critical state parameters for the correct temperature and *VMA* level,
- 3.) determination of the Rock model parameters.

Design of the FEM set up for rolling.

Designing a suitable FEM set up is actually making choices about a.) the fineness of the element mesh in longitudinal and depth direction, b.) the material length that should be modelled, c.) the number of elements (2 directions), d.) the characteristics of the contact modelled, and, e.) the size of the pre-described deformation step that can be enforced in an calculation step.

While choosing the above-mentioned items, and thus implicitly designing the set up, the next considerations have to be kept in mind:

- the mesh (and related to this the number of elements) must be fine at positions where this is required but on the other hand coarse at positions where this is allowed. At a rightly chosen fineness a further refinement of the mesh does not result in significant improvement of the results anymore,
- in longitudinal direction the mesh should at least satisfy the requirement that the simulated free material surface can flow gradually,
- the element mesh distribution in vertical direction must be in such a way that the temperature profile in the depth direction can be modelled with enough accuracy,
- the stiffness of the modelled contact must be adjusted to the material stiffness and the predescribed deformation step size.

In the following paragraphs we will discuss the choices related to the statements noted.

Producing the FE mesh means for HMA compaction, deducing an appropriate size and number of elements in longitudinal and depth direction of the material. In order to limit calculation times the total number of elements should be not too large. On the other hand, coarser element meshes result in a limited accuracy. Further, the amount of material (workpiece sizes) that is modelled should not be too small. The final “set up” of the FE mesh, element sizes and number is often a compromise.

Because there exists large changes in stresses and strains in the middle underneath the roller drum (horizontal direction) and in the upper region of the layer (in vertical direction) at these locations a fine mesh is required. Additionally, it is permissible that the mesh is coarse at other locations, e.g. in the area of both vertical edges (horizontally) and in the lower part of the layer (vertically). The translation from coarse to fine should not be abrupt but gradual.

Additional demands concerning the element mesh in vertical direction are caused by the temperature distribution in the layer and the length of contact between the roller drum and the rolled material. The FE mesh distribution in the vertical direction should fit the temperature profile during compaction. The temperature distributions of the material during compaction can be found in chapter 5.

In the area where the roller drum variations of stresses and strains in the material are the highest; a specific fineness of the element mesh is required. These variations reduce significantly when the distance to the roller drum centre increases. It should be checked to see at what position the variations in stresses and strains become so

insignificant that simulations can be ended. Changing the length of the modelled piece of material and judging the relevant stress and strain patterns will indicate when the length is modelled correctly.

In the longitudinal direction the mesh should be fine in the area of contact between the roller drum and the material. Experience in steel rolling simulation has learned that the contact surface should be replicated with a minimum number of elements. Furthermore, to achieve a stable numerical simulation, the contact surface between roller drum and material should be simulated with at least approximately 15 contact elements. This requires a minimum fineness of the FE mesh in longitudinal direction in the region of the contact surface roller drum-HMA material. This is illustrated by means of Figure 4.17, which shows the deviator stress²³, q , in the material. The figure shows that this deviator stress does not change significantly in the region of both vertical edges.

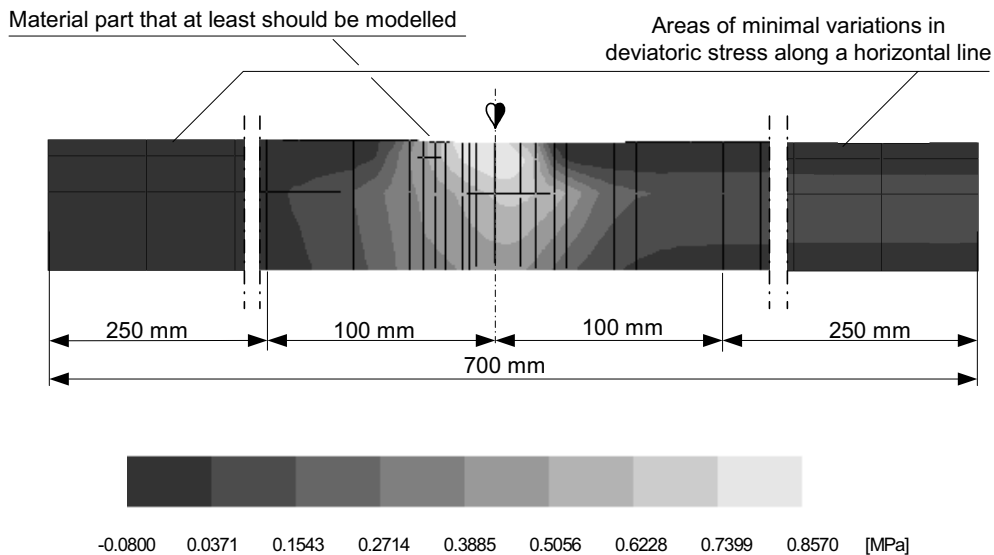


Figure 4.17 The deviator stress pattern, q , in a 3×50 elements and $l=700$ mm test run, dark grey shaded area means stresses around zero, white area stresses until 0.86 N/mm^2 .

The stiffness of the contact between the roller drum and the HMA material is replicated by quantification of the contact model parameters. By changing these variables one also influences the overlap or penetration between roller drum and material. The overlap should not be too large because then the loading pattern of the drum on the material is not realistic anymore. Tuning of this contact stiffness affects the profile of the free material surface. This free material surface must follow a gradual course and should not change in direction per element. During the test runs good results were obtained at a material workpiece overlap of in between 0.3 and 1.0 mm. Managing that overlap reveals that the contact stiffness had to be adjusted to 2 to $3 \text{ N/mm}^2/\text{mm}$ at the start of compaction (first passes) and must be increased until 20 to $25 \text{ N/mm}^2/\text{mm}$ after about 6 roller passes are applied.

²³ The deviator stress, q , is drawn up from the 9 principal stress components (e.g. σ_{xx} , σ_{yy} , σ_{zz} , τ_{xy} , τ_{xz} , and so on) on a 3D element, see chapter 2. q corresponds to the von Mises stress as used in mechanical engineering. For the axial symmetrical samples q corresponds to: $q = \sigma_{axx} - \sigma_{rad}$.

The most important contact parameters that must be quantified for a simulation are the parameters σ_{ref} , μ and g_{ref} . From these parameters it is possible to calculate the parameters C_n and C_t as illustrated in Figure 4.15. In the case of contact, the penetration of the bodies is described elastically with the normal stress σ_n varying with the penetration depth g via the normal stiffness C_n . When $\sigma_t > \mu\sigma_n$ there occurs slip, in accordance to Coulomb's law. By means of the input variables σ_{ref} , and g_{ref} one can vary the stiffness in normal direction. For simulation of rolling for the B sections, see chapter 6, we used the parameters as indicated in Table 4.1. It can be seen that the stiffness in normal direction increases during the simulation of subsequent roller passes whereas the friction stays fixed. As mentioned earlier, this C_n does not have a physical meaning it is only for numerical stability of the calculation. However the quantity should be tuned to the actual material strength for achievement of a smooth calculation process and therefore C_n must increase during simulation of a rolling process.

For our simulations the figures that were used for definition of the C_t were not investigated extensively. From steel rolling processes it is known that friction μ is between 0.1 and 0.2 and further that the parameter τ_{slip} is maximal around the shear strength of the material. For our calculations we defined friction μ on 0.16 and τ_{slip} on 3 N/mm^2 (all roller pass calculations). γ_{adm} is the admissible shear before the two surfaces start to slip. For our calculations we defined γ_{adm} on 1.0 mm.

STIFFNESS AND FRICTION FOR ROLLING SIMULATIONS		
Roller pass	C_n [N/mm/mm]	μ [-/-]
0.5	3.33	0.16
2.0	5.88	0.16
4.0	20.2	0.16
6.0	21.75	0.16

Table 4.1 The stiffness and friction parameters of the contact modelled for roller passes 0.5, 2.0, 4.0 and 6.0 on the B lane.

Test runs for tuning the “set-up”

For the first test runs performed in this study a piece of material was modelled with a length of 300 mm. This piece of material was modelled with 30 elements in the length direction and three elements in the depth direction. The contact area between the roller drum and the rolled material was modelled with 15 elements.

The deformation step-size of the material was initially 0.04 mm whereas the permissible overlap between material and roller-drum was limited to 0.3 mm. This set up was used as a reference to investigate what the effects of different refinements can be.

Further, the following refinements to the FEM set up were tested:

- refining the element mesh in longitudinal direction to 40, 50 and 70 elements,
- refining the element mesh in vertical direction to 5 and 7 elements,
- enlarging the modelled material length to 400 and 700 mm,
- enlarging the prescribed deformation step-size²⁴ to 0.06, 0.08, 0.1, 0.15, 0.2 and 0.5 mm,
- limiting the material-worktool overlap to 0.3, 0.6 and 0.15 mm.

For testing the effect of the set up refinements in combination with the accuracy of the simulation, the calculated test results were compared to each other; the results are given in Table 4.2 and Figure 4.19. The results monitored were:

- the volumetric strain, ϵ_{vol} ,
- the shear stress, σ_{xy} ,
- the vertical stress, σ_{yy} .

The volumetric strain was taken into consideration as the indicator for compaction progress. The shear stress is considered because the amount of shear is important for rate of compaction progress. The vertical stress is considered because the vertical rolling force is calculated from those stresses. All these values noted in the table are the maximum obtained values in the asphalt layer. The global positions inside the layer where these maximum values occur are illustrated in Figure 4.18.

TEST RUNS FOR TUNING THE FEM SET-UP							
Step no.	Calculation	Vol. strain [-/-]	xy stress [N/mm ²]	yy stress [N/mm ²]	Calc. ²⁵ time [sec]	Increm. deform. steps [-]	Length mat. calcul. [mm]
1	Reference, 3x30, l=300	-0.136	0.468	-0.99	257	7525	300
2	3x40, l=300	-0.129	0.434	-0.88	337	7525	300
3	3x50, l=300	-0.111	0.340	-0.61	425	7525	300
4	3x50, l=700	-0.111	0.340	-0.62	449	18525	700
5	5x50, l=400	-0.121	0.372	-0.55	890	10025	400
6	7x50, l=400	-0.122	0.382	-0.53	1221	10025	400
7	7x70, l=400	-0.122	0.372	-0.53	1772	10025	400

Note: 1. the – sign means shrinkage of the volume
2. the – sign means compression stress

Table 4.2 The effect of different variables on the calculation results.

In Figure 4.19 the effects of seven subsequent refinement measures are illustrated with respect to the relevant stresses and strains related to compaction. From this figure

²⁴ The test runs proved that enlarging the deformation step size does not change the output results (i.e. calculated stresses and strains). In our test runs a step size could gradually be increased until about 0.2 mm per step. The extent of this value depends on the resistance of the modelled material and the stiffness of the modelled contact. Particular combinations of step-size contact parameters can be very sensible for the convergence of the calculation process.

²⁵ Net calculation time is defined here as the CPU time the system really needs for the calculation. Because the simulations were done on a multi task machine it could be that when it is busy on the system a calculation with a net calculation time of e.g. 257 sec (i.e. about 4.5 min) needs about 10 to 15 minutes for completing the simulation.

it can be concluded that further refinement than used in trail 5 (5x50 elements, l=400 mm) is not useful. Until trail 5 accuracy improved, from trail 5 up to trail 7 accuracy did not improve further. As a matter of fact this conclusion is underlined by the stress and strain patterns illustrated in the several figures. Figure 4.17 illustrates the deviatoric stress pattern. Similar graphs are made for the isotropic normal compression stress, p' , shear strain, ε_{sh} , and volumetric strain, ε_{vol} . These figures are presented in the appendix G.

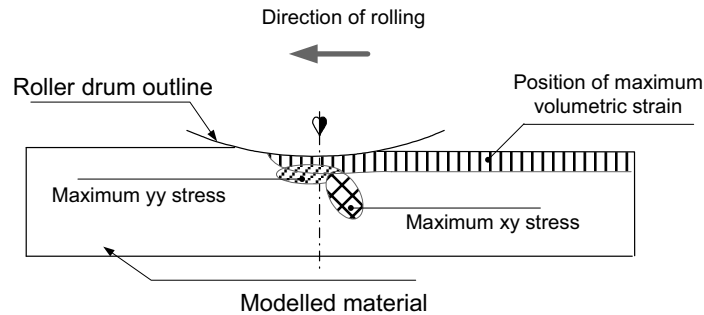
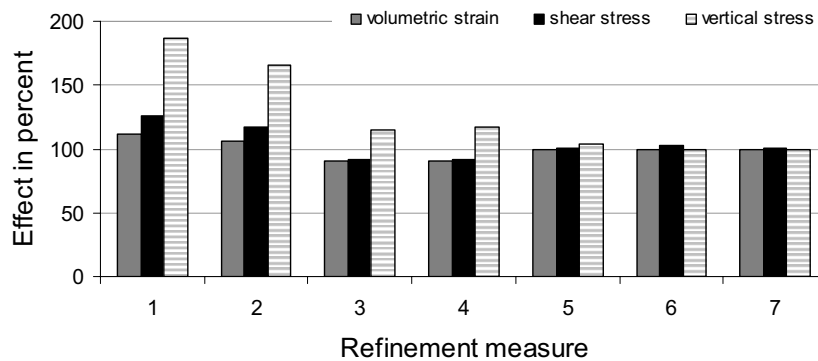


Figure 4.18 Positions of the maximum obtained volumetric strains, and yy and xy stresses.

For simplicity, the material properties, used in all test runs, were modelled homogeneously in the vertical direction, which does not correspond to reality, but for estimating an appropriate FE model set-up this is adequate. From the results obtained by the test runs it can be concluded that a set-up of 5x50 elements, material length of 400 mm and a pre-described step-size up to about 0.2 mm gives good results for compaction calculations of HMA²⁶.



Note: refinement measures;

1. Initial mesh, 3x30 elements, material length 300 mm
2. 3x40 elements, material length 300 mm
3. 3x50 elements, material length 300 mm
4. 3x50 elements, material length 700 mm
5. 5x50 elements, material length 400 mm
6. 7x50 elements, material length 400 mm
7. 7x70 elements, material length 400 mm

Figure 4.19 Results test runs for fine-tuning the FEM set up, results expressed in percent related most refined mesh (measure no. 5).

²⁶ This set up is related to involved material properties, roller drum size and other factors. These quantities were fixed during this research.

Deduction of Temperature and VMA profile from test section data

Since material temperature and compaction level do change during the compaction process the mechanical characteristics of the material to be rolled will also change. To be able to simulate the rolling process the material behaviour should be replicated as closely as possible at every depth, at every moment during the compaction process. To gather these material properties the following information is required (for a specific roller pass):

- VMA level related to depth inside the layer,
- temperature profile in depth direction of the layer,
- the applied roller drum force or the layer thickness reduction.

The information about VMA level and temperature of the material for simulation of real compaction process will be discussed in chapter 5. Therefore we will also discuss in chapter 5, how, based on the measured information from the test section, the VMA and temperature profile, linked to the governing FE mesh distribution, can be obtained. In the same chapter (5) it will be discussed how from the critical state parameters obtained (section 3.6) Rock parameters will be deduced. Here we will discuss how critical state information can be adjusted on the correct VMA and temperature level.

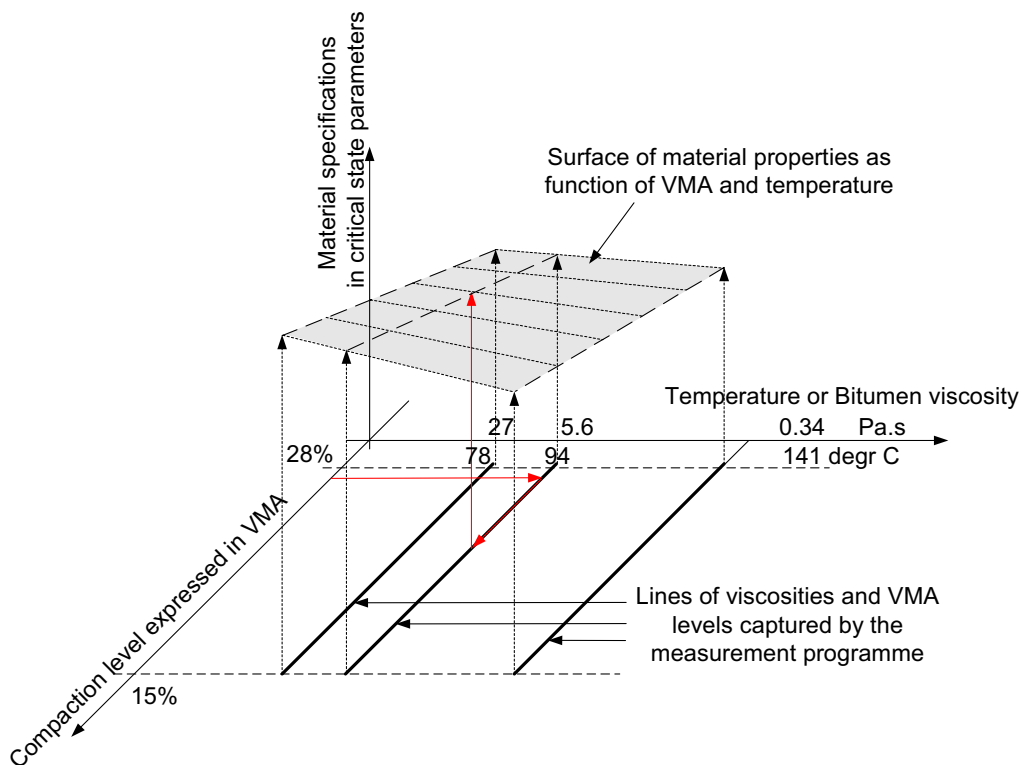


Figure 4.20 Visualisation of the material specifications of the DAC 0/11 measured at three viscosities i.e. three temperatures.

Converting the critical state parameters to material temperature and VMA level

As a result of the material testing programme for a DAC 0/11 mixture, critical state parameters were obtained at three bitumen viscosities equivalent to three material temperatures. The tests were started on samples with a *VMA* level of about 27% to 28% whereas at the end of the test the *VMA* level was reduced to around 15%. During the tests a whole domain of *VMA* levels were also captured, which is logical because we were compacting the sample during the test. Figure 4.20 illustrates a fictively critical state strength value, measured as a function of *VMA* level and material temperature (viscosity). However, when we do roller pass simulations the critical state information must be available for each temperature and pre-compaction level within certain domains.

For the translation of the critical state values to the right temperature and pre-compaction level the following must be done:

- interpolation of recoverable and irrecoverable parameters to the new temperature,
- movement (shift) of the recoverable line to the initial *VMA* level.

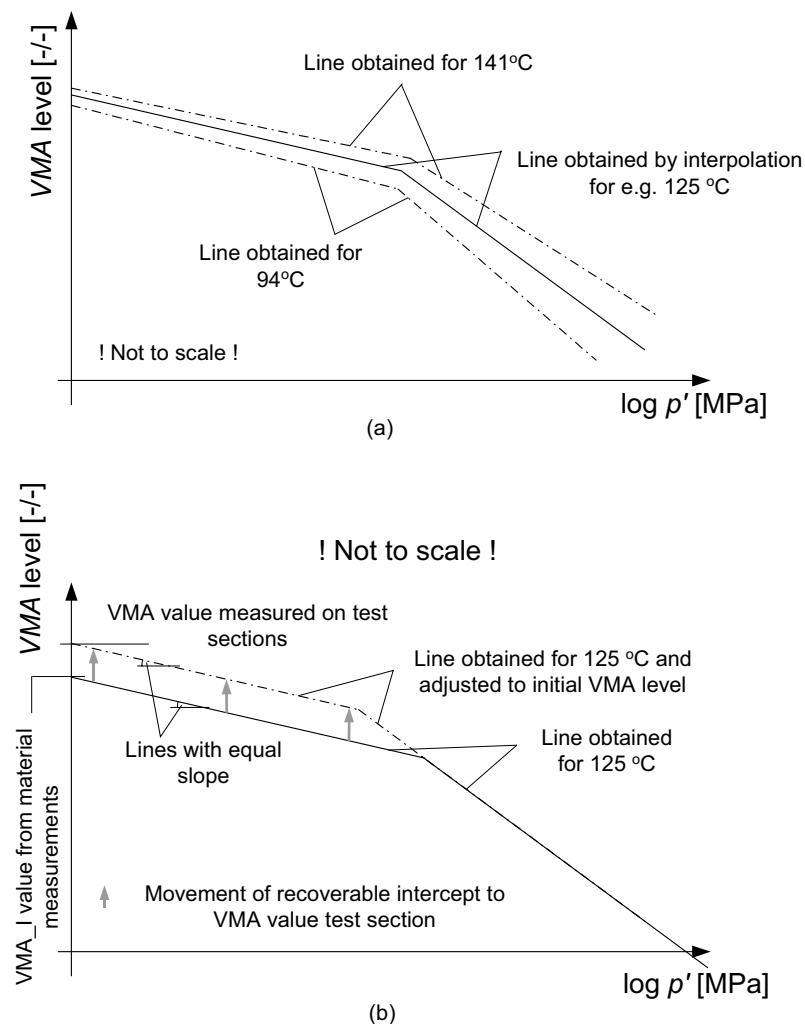


Figure 4.21 Illustration of the details of step 1; translation of the recoverable line and interpolation of irrecoverable parameters.

To obtain critical state parameters for the governing material temperature, interpolation of slope and intercept for both tangents must be achieved between two known lines from the material measurement programme (Figure 4.21 a.). Then adjustment of the obtained model to the current material VMA level must be achieved. It is one of the basic principles of the critical state theory that adjusting such a model to a new pre-compaction state corresponds to adjustment of the intercept (shifting) of the recoverable line (see also chapter 2) while keeping the slope of that line equally in the $VMA \log p'$ plane, see Figure 4.21 b). From the new obtained line, created for the governing material temperature and VMA level, the position of the intersection points (expressed in p' and q) and the size of the yield locus must be obtained.

Deduction of Rock model parameters from critical state information

In the previous paragraph it is discussed how critical state parameters can be determined for the material temperatures and VMA levels, which differ from temperature and VMA levels used in the material-testing programme. Rock is an elastic-plastic material model that is implemented in the FEM approach DiekA. Some basic aspects of the DiekA Rock model were already discussed in chapter 2. Rock models the plastic part of material behaviour in accordance to critical state principles. However, for modelling the recoverable part of the material behaviour, the Rock model uses the modulus of elasticity, E , and poisson's ratio, ν . The critical state theory models the reduction of the volume proportional with the increase of the logarithm of the isotropic compression stress p' . These two methods of approach do not correspond. Nonetheless, the Rock model is currently the best available opportunity within the FEM approach DiekA. So in order to reach the goal of the project ("*testing the possibilities and further development of a tool that can simulate HMA compaction processes*") two tricks were tested:

- soft E modulus in combination with the too strong curved elastic behaviour,
- too stiff E modulus in combination with shifting the whole deformation line.

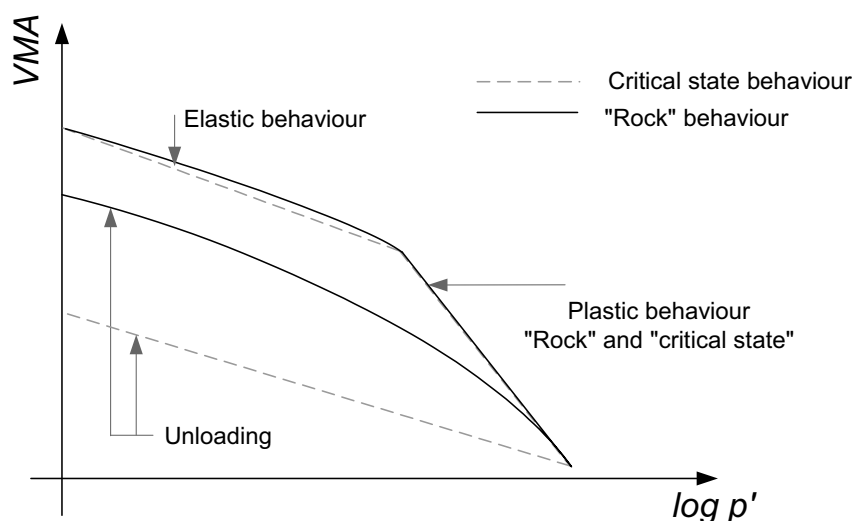


Figure 4.22 The loading and unloading stress path when a soft E modulus is chosen in order to model the elastic-plastic intersection point realistic.

Soft E modulus

To overcome the problems that arise caused by replicating the HMA recoverable behaviour with linear elasticity as a first approach it was aimed to estimate the parameters E and ν to such values that the deformation is modelled correctly at the position where elastic deformation turns over in plastic deformation. This implies that the modelled material stress path runs curved (because stress is expressed in $\log p'$) to the intersection point see (Figure 4.24). Regrettably further analysis indicated that this approach did not work very well. Further inspection of the stress path indicates that mainly during unloading the stress path deviates strongly from behaviour modelled in accordance to critical state principles (see Figure 4.22). It is the linear elasticity part of the model that causes this behaviour. During unloading at high stress levels the behaviour looks very un-realistic.

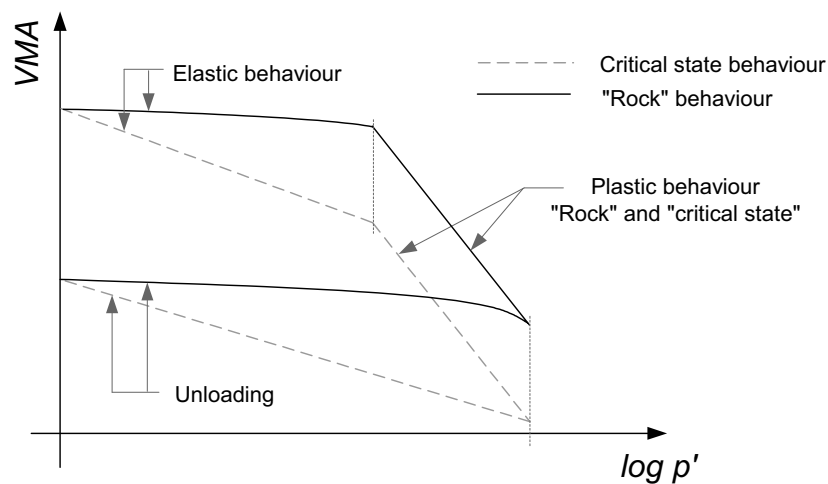


Figure 4.23 The loading and unloading stress path when a much too stiff E modulus is chosen in order to model mainly the elastic-unloading behaviour more realistic.

Too stiff E modulus

A second possibility to tackle this problem was increasing the E modulus to such a level that both elastic-loading and -unloading lines behave as realistic as possible, given the shortcomings of the model. For that purpose the E can be quantified on about 200 MPa whereas in the first attempt discussed, E values were calculated at around 5 MPa. Furthermore, the modelled plastic loading branch does correspond to the critical state plastic loading branch, so plasticity was modelled correctly. The stress path in accordance to the critical state model and the Rock approximation using the overestimated E value are both shown in Figure 4.23. It can be seen that the elastic behaviour is now far too stiff. However, the plastic behaviour seems realistic, it only occurs at a too low strain level. Due to this approximation, in the area where the material is loaded the calculated strains are too small. However, after loading and unloading has taken place the extent of plastic strain that remains is roughly seen

correct as can be seen in Figure 4.23. This is important because the amount of plastic strain is one of the major quantities we are interested in when simulating compaction. Because the rolling simulations are done with a pre-described deformation level the too stiff modelled elastic material behaviour will result in a too high calculated loading stress or force. It was decided that this second approach using Rock (too stiff E modulus), although not perfect, brings enough perspective for achieving the simulations.

In doing FEM calculations with DiekA and the material model Rock the obtained critical state parameters for the material must be converted into Rock model parameters. The intersection of the irrecoverable and the recoverable branch of the bilinear deformation line forms for this purpose a very important mark. By application of the critical state theory, we know that at that specific stress situation the stress path touches the yield locus and elastic behaviour turns over in plastic. Therefore this stress situation forms the initial point for deduction of the shape and size of the yield locus, see Figure 4.24, corresponding to the actual material volume situation expressed in VMA .

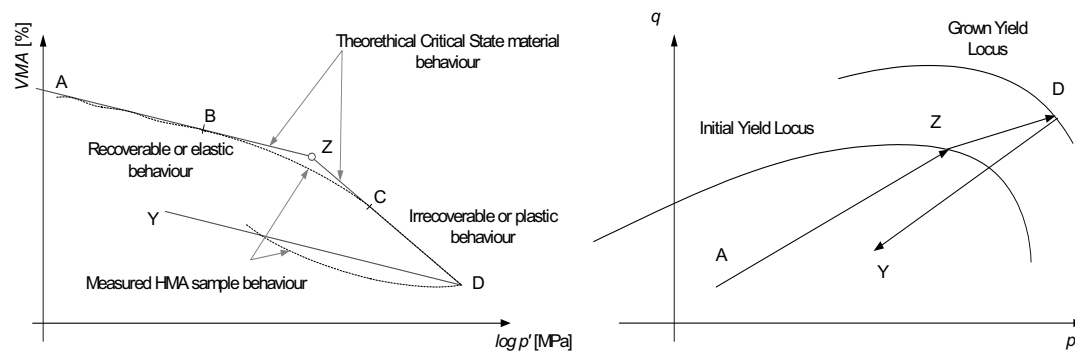


Figure 4.24 Coupling the size of the yield locus to the position of the intersection point of the bilinear critical state material model.

The Rock model makes use of associated flow for the closure cap of the yield locus. This implies that the direction of deformation (i.e. the ratio $\varepsilon_{sh}/\varepsilon_{vol}$) is linked to the yield locus shape. The position of the intersection point expressed in p' and q marks a first point of the yield locus. Further, as a result of the laboratory-testing programme the direction of plastic flow is known, see Tables 3.5 and 3.6 in the sections 3.5 and 3.6. If for a stress point $p':q$ the direction of deformation is known, as is the case, the part of the yield locus around this point can be shaped. The remaining part of the yield locus shape was estimated with help of general information about yield loci shapes for granular materials. It is recommended to study in more detail how the yield loci for HMA materials should run in the future.

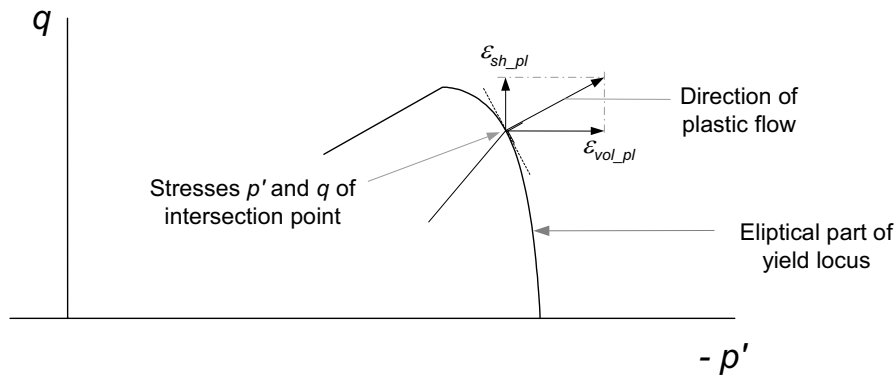


Figure 4.25 Direction of (associated) plastic flow and shaping the yield locus.

The critical state point is by definition the point of maximum deviatoric stress, q . At the right hand side of the critical state point the yield locus is elliptically shaped. Left from the critical state point the yield locus is in this project modelled as a straight line. This latter shear part of the yield locus only got little attention because preliminary calculations indicated that these stresses (high deviatoric stress in combination with low isotropic stress) did not occur during compaction. However, correct modelling of this shear branch is very important for future research because rolling of sensible mixtures or rolling under extreme conditions material stresses can be in such a specific stress situation.

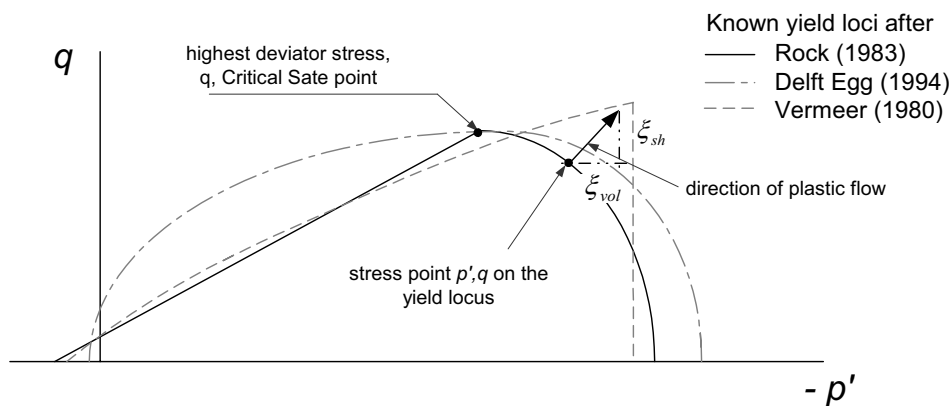


Figure 4.26 Suitable yield locus shapes for granular materials, Teunissen (1983), Van Eekelen (1994) and Vermeer (1980).

The isotropic tension strength is estimated at 0.15 times the isotropic normal compression strength, p' . This value is estimated based on commonly used yield loci shapes for granular materials (Figure 4.26), however, changes in this tension stress will not affect the calculated result; preliminary test runs indicated so. A step-by-step example about how exactly the Rock values should be calculated can be found in the appendix H.

Figure 4.27 illustrates a calculated bilinear deformation line with Rock. When the loading line over a fixed extent of strain is shifted, the fit of the plastic branch obtained by Rock to the critical state behaviour can be seen.

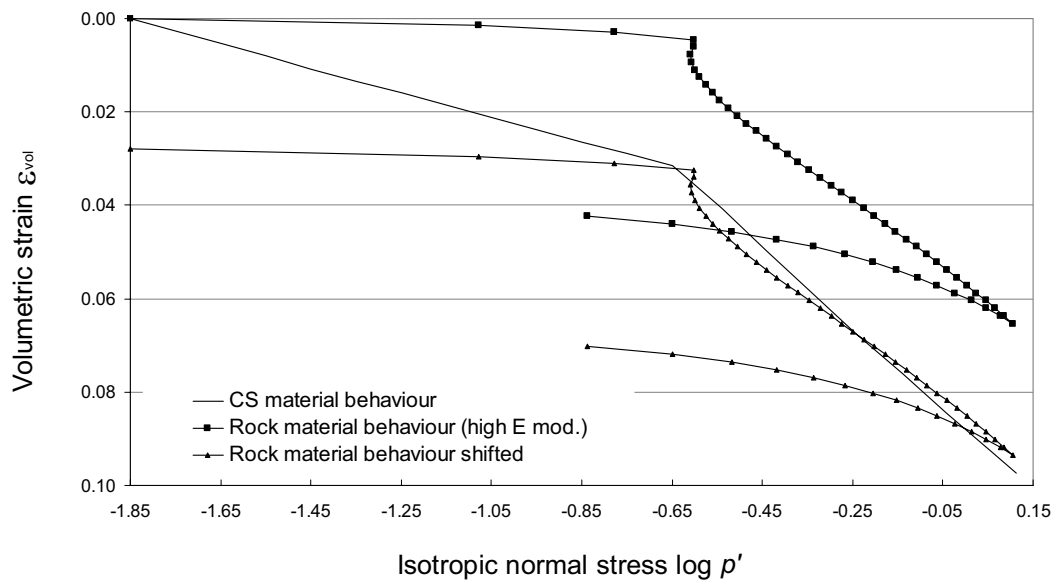


Figure 4.27 The critical state theoretical material behaviour and two calculated material behaviour lines modelled with Rock (one line shifted).

Summary

FEM tools seem very useful in simulating and studying compaction processes of HMA. The material behaviour is complex and the material behaves both, partly as a liquid and partly as a solid. For fluid mechanical problems and for solid structures different common FEM approaches are available. For a material that keeps the middle between a fluid and a solid fortunately a combination approach, the Arbitrary Lagrangian Eulerian (ALE) method, was available. The ALE approach is a complex one, it requires a skilled operator but then it is a very powerful tool. Other pre-requisites for using a FEM tool for simulating rolling are; contact or interface elements and a suitable material model, both features, are available within the approach. Such a material model must run in accordance to critical state principles, however, the available model (Rock) did not fulfil all these demands completely. Furthermore, it is very useful (not per definition a pre-requisite) that the FEM approach can make use of a rotated coordinate system for simulating the roller drum.

Designing the FEM model asks for strong inside knowledge of engineering judgement and a lot of test runs. For limiting calculation times the model FE mesh should not be too fine but on the other hand fine enough to guarantee accuracy. Additionally, a two-dimensional (2D) plane strain approach is suitable for a rolling problem because during rolling only two dimensions (longitudinal and depth) are of more interest than the third dimension. The 2D plane strain approach is also known as a 2.5D one because in the third direction average stresses can be calculated although in that direction no variations in load or other relevant items can be modelled. A 2.5D approach fits also quite nicely with the material measurements because they were

done on axial symmetrical samples, and in such samples the strain situation is also 2D plain strain.

A lot of test runs prove that a mesh of 5x50 elements in combination with a material length of about 400 mm gives accurate results and acceptable calculation times of about 10 to 15 minutes. About 10,000 pre-described deformation steps were applied for pushing the material underneath the compaction rolling drum. The measured critical state material parameters (see chapter 3) must be converted to the right temperature (i.e. bitumen viscosity) and pre-compaction level, information that is measured during compacting the test sections. Then the critical state parameters must be converted into Rock model parameters.

The major design of and the items implemented in the FEM approach for doing the HMA compaction simulations did work well. Involved aspects that can be mentioned are; the modelled contact between roller drum and HMA, use of an ALE method for this purpose (the streaming of the material partly through the FE mesh), fixing the position of the roller drum and enforcing the material underneath the drum, etc. The simulations/calculations are labour intensive and do need a thorough understanding of the process by the operator. For insufficiently skilled operators the calculations become “black box” operations which of course are not advisable and can quickly result in errors.

The Rock model does not represent Critical State material behaviour for the elastic phase (i.e. recoverable material behaviour). As a compromise the elastic material parameter (i.e. E) is enlarged by a factor of 10 to 20 to model the extent of irrecoverable deformation as realistically as possible, see Figure 4.27. Due to this incorrectly modelled recoverable material stiffness the calculated vertical rolling forces were too high.

5 The compaction test section.

5.1 Introduction

In the previous chapters a mathematical tool is described to simulate the compaction of HMA. However, to validate such a tool the simulation results should be compared with the compaction behaviour of asphalt in practice. Therefore, a field experiment had been carried out in which a test section was compacted and the compaction behaviour was carefully monitored. This chapter describes the set up and the results of the field experiment: what were the pros and cons of the experiment, which variables have been measured, what kind of results have been obtained, and which relationships have been derived. Figure 5.1 illustrates the contribution of the content of chapter 5 in the thesis project.

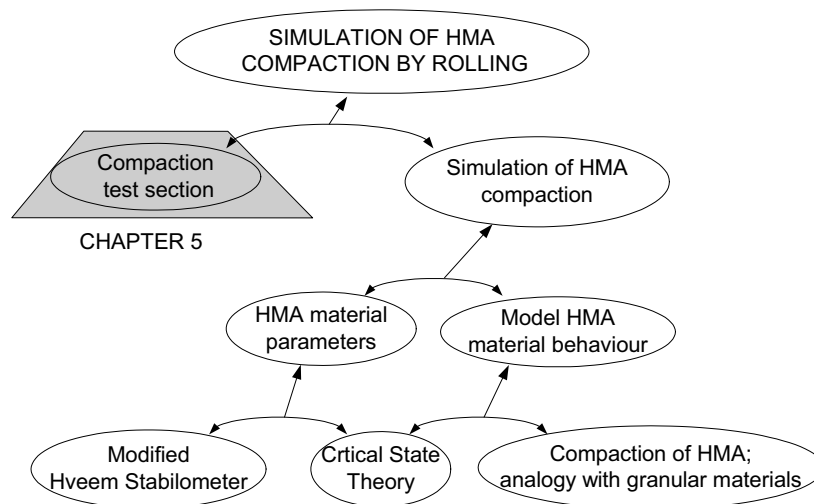


Figure 5.1 The research set up of the overall compaction project, grey shaded area are the topics of interest in chapter 5.

The field experiment had to provide the following crucial information:

- a.) the effect of roller passes on the layer thickness or compaction level,
- b.) the effect of material temperature on the compaction progress,
- c.) the vertical compaction profile of the layer during and at the end of the compaction process.

The laboratory experiments did not yield the results that correspond to prevailing views on the relation between HMA temperature and compactibility (chapter 4). However, there still remain two reasons to monitor material temperature accurately in the field experiment:

- a.) to investigate whether the field experiment provides results comparable to the laboratory experiments with respect to the dependency of the compaction progress on material temperature,
- b.) for accurate estimation of material properties the temperature should be known as a function of time and depth in the layer.

To measure the effect of material temperature during rolling the test section were divided into two lanes: lane A and lane B. Both lanes were compacted with a similar roller but the roller passes were applied at different time intervals, and therefore, at different temperatures. Comparison of the compaction progress of lane A with lane B enabled us to derive effects of temperature on compaction.

Compaction progress was measured by means of three different methods: level and rod measurements, Strato tests measurements and nuclear Troxler measurements. The main considerations for this approach were: i) the field experiment could only be conducted once, ii) compaction progress is the primary object of interest, iii) measurements had to be taken under strict time constraints, and iv) no experience with most of the equipment was available on the scale involved. The extra effort did easily balance the risk of failure of the experiment. An additional advantage of this approach is the opportunity to compare the accuracy of the different measuring methods, mutually and in relation to results obtained on drilled cores.

Finally, the results of the field experiment will be used to derive the relationship between roller drum force and compaction progression (i.e. reduction of layer thickness).

The set-up of the field experiment and the physical layout of the test section will be presented in section 5.2. That section will also provide details of the materials and equipment used. The section closes with a description of the compaction progress parameters and the measuring procedures for respectively; a.) compaction progress, b.) temperature readings, and c.) time readings.

Section 5.3 analyses the main aspects of the field experiment: a.) the timing of roller passes, b.) the trajectory of the HMA material temperature in time, and c.) the compaction progress per roller pass. All these elements have to be linked to get an overall picture of the material temperature at the different applied roller passes. Section 5.3 also addresses the issue of the effect of material temperature on compaction progression and finally, as a spin-off, the empirical evidence of the accuracy of different methods for measuring compaction progression of HMA.

Section 5.4 discusses how from the compaction and temperature information obtained from the test section, VMA and temperature profiles could be deduced for generating the material parameter input for the FEM simulations. The chapter ends with summarising the main results of the field experiment.

5.2 Experiments with a constructed test section

There exist three major aspects related to HMA compaction:

- compaction progress (related to applied no. of roller passes),
- effect of material temperature on compaction progress,
- distribution of material temperature in the depth direction.

Compaction progress.

The most important aspect that should be measured is the compaction progress that is achieved as a result of the applied roller passes. The average compaction progress (averaged over the layer thickness) can be deduced by monitoring the change in layer thickness.

Effect of material temperature on compaction progress.

The second important aspect that has to be deduced is the effect of material temperature on compaction progress. From road building practice it is known that material temperature can have a significant effect on the compaction progression. To determine that temperature effect, the set up of the test section was divided into two parts; lane A and lane B.

The two lanes were compacted with a different number of roller passes (16 for lane A and 8 for lane B) distributed equally over the same time period. This means that roller passes were applied at different times after spreading and therefore also at different temperatures. Lane A is compacted at higher material temperatures than lane B. Assuming that material compactibility is temperature dependent this should become visual by comparing the compaction progression of two equal roller passes applied on the different lanes A and B. Why the set up is chosen in order to determine the material temperature effect is illustrated with the three graphs of Figure 5.2.

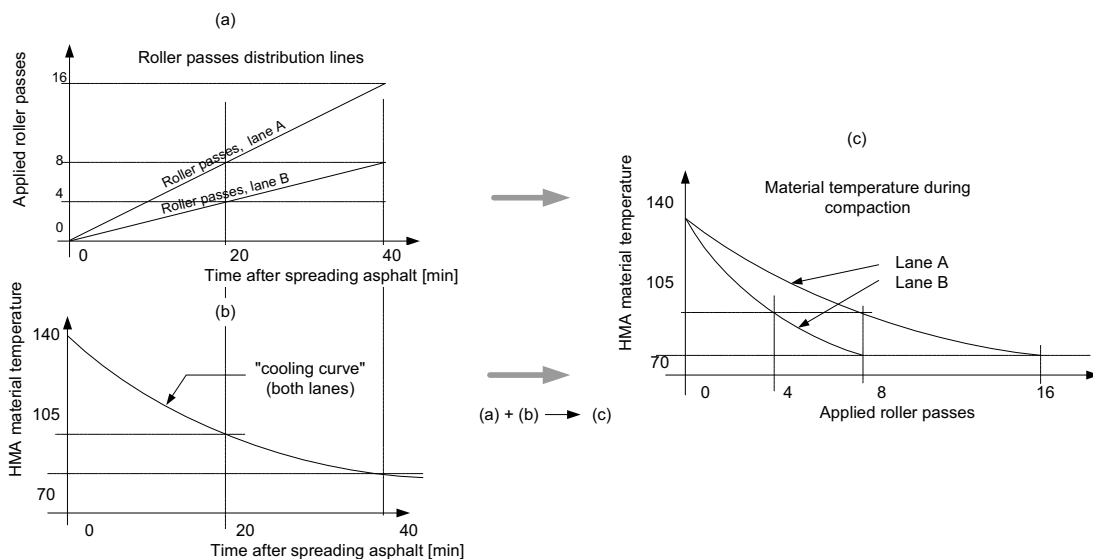


Figure 5.2 Linkage of compaction progress to material temperature, roller pass no. 6, lanes A & B.

The temperature of the material during rolling, part (c) of Figure 5.2, could be achieved by a combination of the information as expressed in parts (a) and (b) of Figure 5.2. The figure also helps to explain what data were measured. The distribution of the number of roller passes (a) in time and measuring the HMA cooling in time (b). Linking both information sources (through the time variable) made it possible to determine the temperature at which the roller passes were applied (c).

The rolling schedule that was followed during compaction to reach this roller pass distribution over the different lanes, is illustrated in Table 5.1. Each X in the table represents a pass of a roller backwards and forwards which therefore corresponds to two roller passes i.e. four roller drum passes.

SCHEME OF ROLLER PASSES APPLIED ON TEST LANES														
Riding scheme roller	1	2	3	4	5	6	7	8	9	10	11	12	Applied roller passes	Applied roller-drum passes
Lane A	X	X		X	X		X	X		X	X		16	32
Lane B			X			X			X			X	8	16

Table 5.1 Scheme of the applied roller passes on the constructed test lanes.

Distribution material temperature

The third important aspect that should be measured concerns the distribution of the material temperature in the depth direction of the layer. This temperature distribution was established by measuring the temperature at three depths in the layer. This temperature distribution is important for simulating the (temperature dependent) material at different depths for creating the FEM simulation.

Physical lay out of the test section

The test section consisted of two asphalt layers on an asphalt foundation. The section was approximately 30m¹ long constructed of two layers of asphalt of respectively 2.70 and 2.50m¹ wide and each 50 mm¹ thick in a compacted state. It was built at the outside test facility of the Road and Railway Research Laboratory of the Delft University of Technology.

Figure 5.3 illustrates the details of the test section. Layer 2 was constructed on a base of ambient temperature whereas, due to time constraints, layer 3 was constructed on layer 2 when this was still warm (the surface temperature of layer 2 was approximately 50 °C).

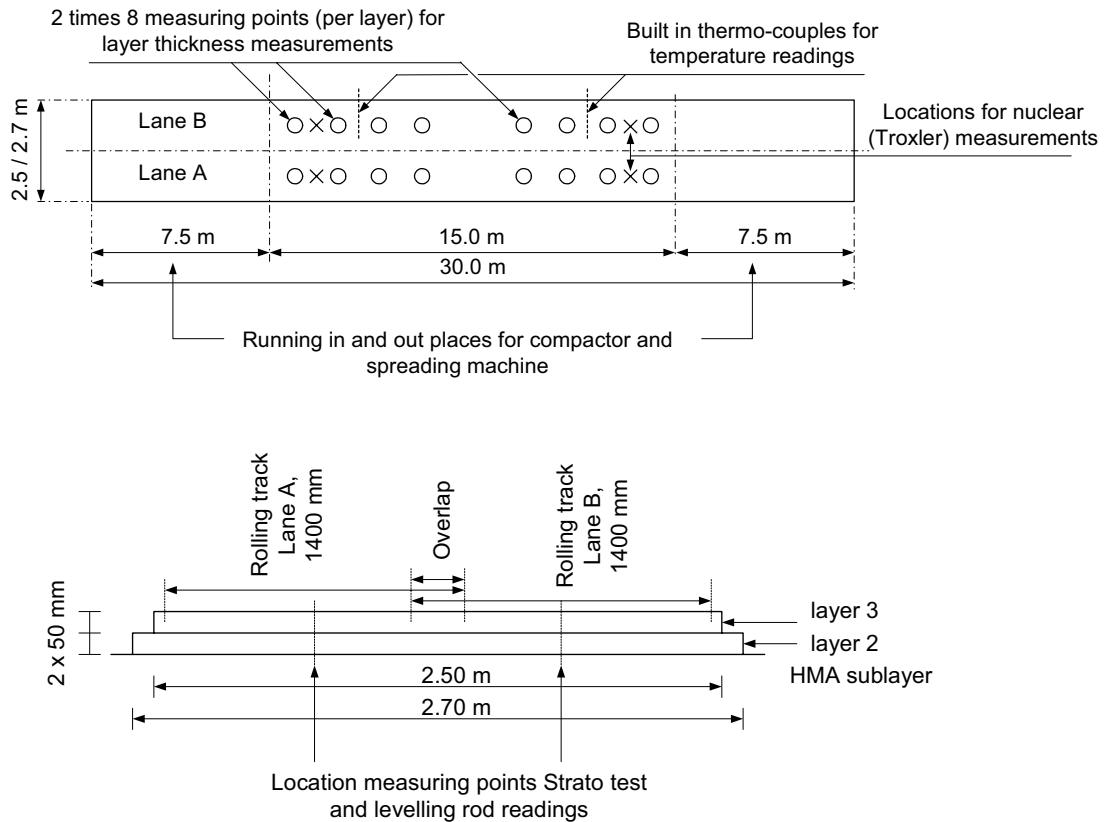


Figure 5.3 The cross section and the plan of the realised compaction test section.

The constructed test layers were divided in two separate lanes, A and B. Lane A is compacted with a total of 16 roller passes whereas lane B is compacted with 8 passes. The motivation for this was discussed earlier. Compaction is enforced using a HAMM DV 6.42 tandem roller in static mode. More details about the roller can be found later in this section.

On top of the test section the 22 measuring points were marked. At those points thickness, bulk density, time and temperature measurements were taken. The set-up of the section was rather unique and this uniqueness made that it was not known how much time remained for taking the readings. It was also not known how adequate the different gauges (the different measuring systems) were for the proposed task. To avoid problems, it was decided to take as many measurements as possible within the time period available. After careful consideration it was decided to monitor the layer thickness with two level and rod teams and one Strato test team. In addition, two nuclear Troxler gauges monitored the density. After compaction was completed cores were drilled from the asphalt layer. At the 16 points marked for the layer thickness measurement (O in Figure 5.3) readings were obtained both with the level and rod and the Strato test equipment. At the remainder four points (X in Figure 5.3) the bulk density was monitored with the two Troxlers.

From the drilled cores, values on the final layer thickness and the bulk density of the material were obtained. By using the bulk density and the composition of the material the VMA value can be calculated. The temperature of the asphalt layer is monitored at two positions using thermo couples inserted at three depths. Figure 5.3 shows the

location of the inserted thermo couples. The times at which the temperature readings were taken was also recorded.

A summary of all the measured items is given in Table 5.2.

MEASUREMENTS PER LAYER				
Goal	What	How	No. of measuring points	When
Compaction level related measurements	Layer thickness	Level and rod	2 x 8	After every roller pass
	Layer thickness	Strato test	2 x 8	After every roller pass
	Bulk density	Troxler / nuclear	4	After every roller pass
	VMA / cores	Volume + weight drilled cores	16	After construction test site
Material temperature related measurements	Material temperature three depths	Thermo couple	3 x 2	After every roller pass
	Sub layer temperature	Thermo couple	3 x 2	After every roller pass
	Material surface temperature	Radiation gauge	ca 25	Continuously (frequency every 2 minutes)
	Material temperature in Hopper	Thermo couple	spot check	During spreading process HMA
Measurements for coupling Temperature to Roller passes	Time spreading process	Chronograph	1	During pass spreading machine
	Time roller passes	Chronograph	12	During pass of compactor

Table 5.2 The measured quantities of the constructed compaction test section.

Equipment and Materials used

The compactor used was a HAMM DV6.42 tandem roller. This type of compactor can be used in the static and in the vibration mode. Because simulation of HMA compaction is complex this research focuses solely on the development of a model to simulate the compaction of a roller in static mode. This roller was equipped with two identical drums of 1400 mm wide and 1100 mm diameter. According to factory specifications, the total weight of the roller was estimated to be 7.9 tons, equally distributed over both drums. During compaction of the test section the drums were running in the same track. Hence, every roller pass counts for 2 roller drum passes. The equipment was weighed to obtain precise information on the operating weight. Because the roller is equipped with a water tank of about 600 litres the roller is weighed both with an empty and a completely filled water tank. The weights of the front and rear roller drum were determined separately. The fact that adding the weight

of the front drum to the weight of the rear drum does not correspond to the total weight of the roller was caused by the inaccuracy of the used weighing bridge. The values obtained are presented in Table 5.3.

SPECIFICATIONS OF THE USED HAMM DV 6.42 OPERATIONAL WEIGHTS AND FORCES						
Roller drum	Front + Rear		Front		Rear	
	Full	Empty	Full	Empty	Full	Empty
Mass [kg]	7.240	6.600	3.620	3.300	3.570	3.260
Force ²⁷ [N]	72.240	66.000	36.200	33.000	35.700	32.600

Table 5.3 The weights of the used roller drum.

Material – Asphalt

The asphalt material used for construction of the test section was a mixture conforming the Dutch Standard (CROW, 1995) for wearing courses; it was a Dense Asphalt Concrete (DAC) 0/16 with a maximum particle size of about 16 mm. A Dutch contractor designed a suitable material composition, produced the mix in a hot mix asphalt plant, paved and compacted the layers and took care of quality control during production. The aggregate of the mixture was composed of;

- 59.8 % coarse aggregate (> 2mm, all crushed)
- 33.6 % sand (3 parts crushed on 1 part natural)
- 6.6 % filler (< 63 μm)
- 6.2 % a 80/100 PEN bitumen (on 100% by mass of aggregate)

The Marshall density (2 times 50 blows) was determined to be 2375 kg/m³. The density of the mixture at 0% voids was determined to be 2416 kg/m³. The detailed results of the sieve analysis (Table 5.4) were obtained from the preliminary and production tests²⁸.

The test section was constructed in combination with the construction of other “Lintrack” accelerated pavement test sections. For the compaction test section, only ca 18500 kg of asphalt²⁹ was needed. For an ordinary asphalt plant this is a rather small amount of asphalt mix. When dealing with small amounts of HMA, the homogeneity of the mixture is an issue due to starting up problems of the asphalt plant. However, especially for test sections, the material should be as homogeneous as possible. Using the same asphalt mixture for both the Lintrack and the compaction test section, the amount of material needed became large enough to overcome the homogeneity problem.

²⁷ For calculating these forces the gravity constant used were $g=10.0 \text{ m/sec}^2$.

²⁸ These investigations were carried out by the organisation; “Kwaliteitsdienst RoHaC v.o.f., Plaatweg 17, Botlek, Rotterdam”. The preliminary investigation was done on 16 July, 1998 in conformity to the Dutch Standards (CROW, 1995).

²⁹ For construction of the two layers in the test sections an amount of asphalt of $0.05 \times 2.60 \times 30.0 \times 2 \times 2375 \text{ kg/m}^3 = 18500 \text{ kg}$ is required.

GRADATION OF THE DAC 0/16 USED IN THE TEST SECTION				
“on sieve”	Weighted in	Preliminary research (extracted)	Production check 1	Production check 2
C31.5	0.0	0.0	0.0	0.0
C22.4	0.0	0.0	0.0	0.0
C16	0.9	0.6	0.0	1.1
C11.2	12.0	10.8	11.6	12.7
C8	23.0	22.0	19.4	21.2
C5.6	35.0	33.6	30.6	33.5
2 mm	60.0	59.8	57.0	58.9
500 μm	78.8	77.9	76.3	78.7
180 μm	90.0	89.0	87.4	89.5
63 μm	94.1	93.4	92.4	93.9
Bitumen ⁽¹⁾	6.2	6.0	6.1	6.2

Note 1. bitumen percentage is on 100% by mass of aggregate

Table 5.4 The gradation of the used DAC 0/16 based on preliminary research and production quality checks.

Required number of roller passes and time available for compaction

To make a rough guess about how many roller passes are needed for compaction of the asphalt materials involved in the test section we will briefly discuss here Nijboer's (1948) theory about compaction. Nijboer developed the P/ID factor and calculated the R_f value to estimate the compaction progress of static steel rollers on asphalt mixtures. The P/ID factor expresses how heavy a roller drum presses on the material whereas the R_f value indicates how far compaction is progressed. A brief description of Nijboer's theory and the R_f formula he developed can be found in section 2.2. In the procedure some material properties that indicate compactibility are also incorporated.

The P/ID factor for the HAMM DV 6.42 can be calculated as $34500 / (1100 \times 1400) = 0.0224 \text{ N/mm}^2$. To characterise the HMA compactibility Nijboer uses information on the composition of the mixture. For the DAC 0/16 these quantities were:

amount of coarse aggregate (> 2mm);	60% m/m ,
filler bitumen ratio;	0.458,
voids content ultimate compacted material;	4%,
equivalent particle size of filler;	20 μm .

From these material data and by using graphs developed by SCW (1971) the τ_{cb} (initial resistance) and η_m (viscosity of the mass) values for the mixture can be deduced.

By using Nijboer's formula the R_f value of the involved material was calculated to be 4.2×10^5 . The Study Centre for Road construction (Studie Centrum Wegenbouw,

SCW, 1978) gathered information about the compaction of thin asphalt layers with help of Nijboer's theory. They concluded that a crushed sand mixture became compacted until 99.4% of Marshall density at an R_f factor of 4.2×10^{-3} . This R_f value will be achieved at 16 roller passes if the average material temperature³⁰ during rolling is at least 110 °C. Applying this early theory on the experimental test section shows that a reasonable compaction rate of at least 98% of Marshall density (2 times 50 blows) should be possible with a number of 8 to 16 roller passes on respectively the B and A lanes.

Time available for compaction

Techniques exist to estimate HMA cooling times based on environmental conditions. SCW research (1967) indicates that at an ambient temperature of around 10°C and wind speed of approximately 5 m/sec³¹; a 6 cm thick HMA layer of initially 160°C cools in approximately 35 to 40 minutes to a temperature of about 70°C.

Vizi (1981) reported that an HMA layer of 40 mm at 160°C cools to 70°C in about 30 minutes when there is no wind and the ambient temperature is about 15°C.

Bossemeyer (1966), one of the researchers who also took sunshine radiation into account, obtained comparable cooling times; cooling from 165°C to 70°C in about 30 minutes for a 40 mm thick layer at an air temperature of 8°C and wind speed of 1.7 m/sec. A second observation by Bossemeyer obtained a drop from 155°C to 70°C within about 28 min of a 52 mm thick layer at an ambient temperature of 0°C and a wind speed of 3.9 m/sec.

The different investigations indicate that approximately 30 minutes must be available before a material of 160°C is cooled down to 70°C when the ambient temperature is around 10°C and wind speed is between 2 to 4 m/sec. This implies that when the aim is to apply 16 roller passes on the A lanes, about 2 minutes are available for every roller pass including the 8 layer thickness measurements and two bulk density measurements. This implies severe constraints on the procedures to measure the layer thickness and bulk density.

Measuring procedures for compaction progress

Deducing the layer thickness and bulk density of the test lanes monitored the progress in compaction. The layer thickness measurements were carried out with both a level and rod and with the so-called Strato tester. The thickness was measured after every roller pass at positions marked in advance as shown in Figure 5.4. Further, the bulk density trajectory was monitored using a nuclear density gauge. After compaction was completed cores were drilled at the positions of the 16 layer thickness measuring points. On these cores density and layer thickness data were obtained.

³⁰ Later on the analysis of the material temperatures during rolling proved that this min average material temperature was not achieved during the compaction process.

³¹ These are typical meteorological conditions for the date of constructing the test sections; early November.

Measurements with a level and rod are rather time consuming. Therefore two teams of two people each were employed to do these measurements on all the 8 locations after each roller pass. That implies that each team measured four locations per pass. Because the teams had to operate within very narrow time constraints it happened that not all points could be measured after every pass. The order in which the different locations were measured alternated so that not two successive readings were skipped at the same location. All measured values were recorded manually.



Figure 5.4 All measurements (temperature, level and rod, Strato test and Troxler) in progress and an illustration of measuring point indicators.

The Strato tester is a radar type of equipment that uses reflection of the radar waves by an aluminium object embedded in the layer. Therefore the Strato tester requires accurate positioning. The Strato test equipment allows very rapid thickness measurements. After the equipment is calibrated to the asphalt temperature it takes less than 5 seconds to obtain a reading. With the Strato test it became possible to measure the layer thickness at all the measuring points in the short period between subsequent roller passes (1 to 2 min.). A team of two people took the measurements. The measured values were recorded manually.

The density of the material was measured at two positions using nuclear (Troxler) equipment (Figure 5.3). Density measurement using the Troxler is a time consuming activity (an accurate reading requires at least one minute). Therefore two teams, each appropriately equipped, were employed. Due to the time constraints each time only one measurement could be taken between two consecutive roller passes.

After compaction of the test section was finished, cores were drilled at all the 16 measuring points. From these cores, the layer thickness was determined using a Vernier callipers. Further, the bulk density of each core was determined by measuring the volume, its weight, and its submerged weight. Because the composition of the core is known, the VMA can be determined using standard techniques.

Measuring procedures for temperature and time readings

The temperature of the HMA under construction was measured at three depths in the layer. The measurements were done at two locations (see Figure 5.3). At each of these two locations three readings were taken at different heights (see Figure 5.5): at the bottom, approximately in the middle and at the top of the HMA layer. For each reading, the time at which the temperature readings were taken was noted. A team of two people did the time and temperature measurements. Thermo couples placed in the layer were used to record temperature, while synchronised chronographs were used to measure the time. The temperature-time relation, could be plotted from the measurement results.

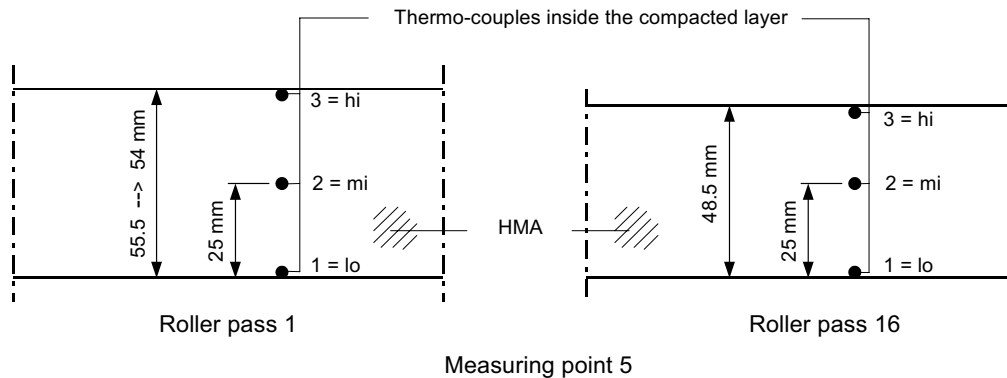


Figure 5.5 Positioning of the thermocouples in the layer under construction.

5.3 Analysis of the test section results

In the previous paragraph the motivation and procedures for obtaining the various measurements were discussed. Here the attention is focussed on how the obtained data was analysed in order to develop useful relationships. The most important aspects concern the progress in compaction of the HMA related to a particular roller pass and the material temperature. To make the link between these variables a technique is used that already is discussed in the previous paragraph and is illustrated in Figure 5.2. Time readings at which the various activities happen are therefore crucial. These time readings enable one to couple the roller passes to the material temperature.

For achieving the wanted relationship between compaction progress per roller pass and material temperature, the following information needs to be analysed:

1. roller passes versus time,
2. temperature of the material versus time,
3. compaction progress versus roller passes.

Measuring the compaction effect of the subsequent roller passes at the current material temperatures is crucial for the aimed relationship. The second mentioned relationship, distribution of roller passes in time, seems unnecessary, but it is not. This particular relationship supports the determination of the actual material temperature at which the different roller passes were applied.

Analysis of the applied roller passes in time.

The roller passes applied on the different lanes (A and B) are distributed as equally as possible in the time domain available for compaction. Temperature and roller pass timing was done simultaneously at different positions. Determination of the temperatures at which the roller passes were applied was based on average temperature information. Therefore the relation of the applied roller passes in time and the cooling in time were estimated based on the data available at two measuring points.

During construction of the test section, the paving of the new asphalt layer and roller passes applied time readings were taken by using a chronograph. Both time and temperature readings were taken simultaneously. Determination of the time a specific roller passed made it possible to calculate the material temperature during that specific roller passes. Separate functions were estimated for the two lanes. The expected slope of the B line should be twice the slope of the A line because on the first one, half the number roller passes were applied in approximately the same time span. The distribution of the applied roller passes over the time available for compaction and the models that represent these are illustrated in Figure 5.6

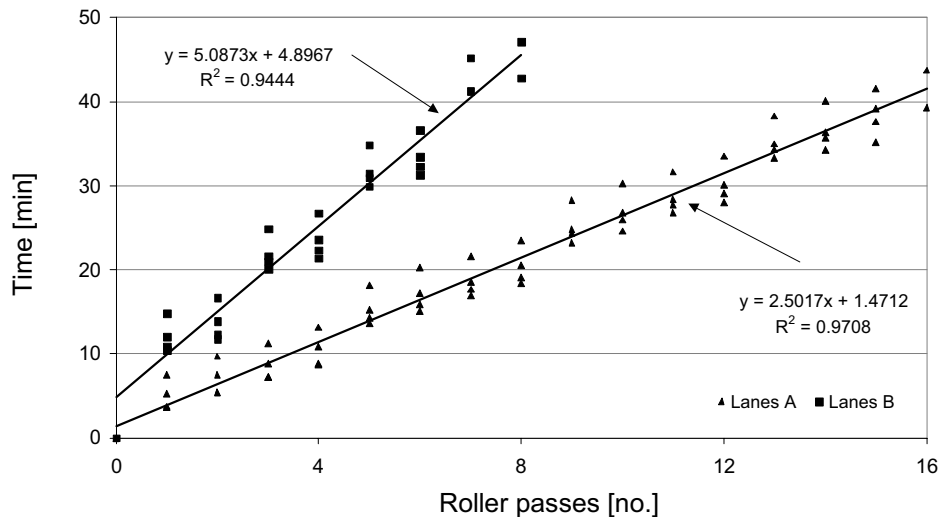


Figure 5.6 The spread of the roller passes versus time after paving the HMA lanes A & B.

Analysis of the HMA material temperature

During construction of the test section, the temperature of the HMA was monitored at two locations at three depths. Apart from the directly measured material temperatures, additional measurements were taken to obtain a better understanding of heat loss in the layers. These additional measurements were; temperature of the sub layer, the temperature of the HMA in the paver, the environmental air temperature, the temperature of the upper surface of the layer by measuring the emitted radiation and the amount of incoming radiation emitted by the sun.

The temperature measurements were started during paving of the lanes and were continued during every roller pass applied. At the moment the roller passed over the thermocouple location, a time and temperature reading was taken. Timing serves two goals; a. registration of the cooling process in time, and b. registration of the moments at which the roller passes were applied. After that, the cooling of the asphalt was modelled in two steps; step 1; estimation of the initial material temperature during paving. In step 2 a curve was fitted after all the obtained results were scaled to the, during step 1 obtained, initial asphalt temperature.

Based on the temperature readings at different depths a polynomial relationship of the temperature in vertical direction could be established. This relationship is required for estimating the (temperature dependent) material properties at different depths for carrying out the FEM simulations.

Modelling cooling of the HMA.

The heat loss of a body depends, on the temperature differences between that body and the environment, the surface properties of that body (roughness, colour etc.) and the distance between the two objects that exchange energy. Mathematically this is represented by the following formula³².

$$q''_x = -\kappa \frac{dT}{dx}$$

in which:

- q''_x = the heat flux (indicator for amount of heat that is lost) [W/m²],
- κ = thermal conductivity coefficient of the material [W/mK],
- dT = temperature difference between the two objects [°C],
- dx = distance between the two objects [m].

From the formula it can be seen that the amount of heat loss depends on the difference in temperature (dT) between (in our case) the asphalt layer and the environment. Because subsequently the new temperature determines the new heat flow (the lower the temperature differences the lower the heat flow) the nature of a cooling curve in time will be logarithmic. This makes it possible to model the cooling behaviour log-linear; the logarithm of temperature versus the time in minutes.

The technique of measuring asphalt material temperatures by thermo-couples usually gives accurate results. However, at the moment the material is spread from bulk stage into a smooth layer such readings are not reliable because at that instant there can be air around the thermo-couple. Nevertheless, accurate information about the material temperature at the start of cooling is required to model the cooling behaviour. Therefore the initial material temperatures at the different locations were estimated by extrapolation of the temperatures measured in the middle of the layer after paving was achieved. Figure 5.7 illustrates this procedure for layer 2 at location 1. The total set of figures for all measuring locations (4 in total) can be found in the appendix I.

³²

One dimensional heat transfer by conduction (Incropera, 1996).

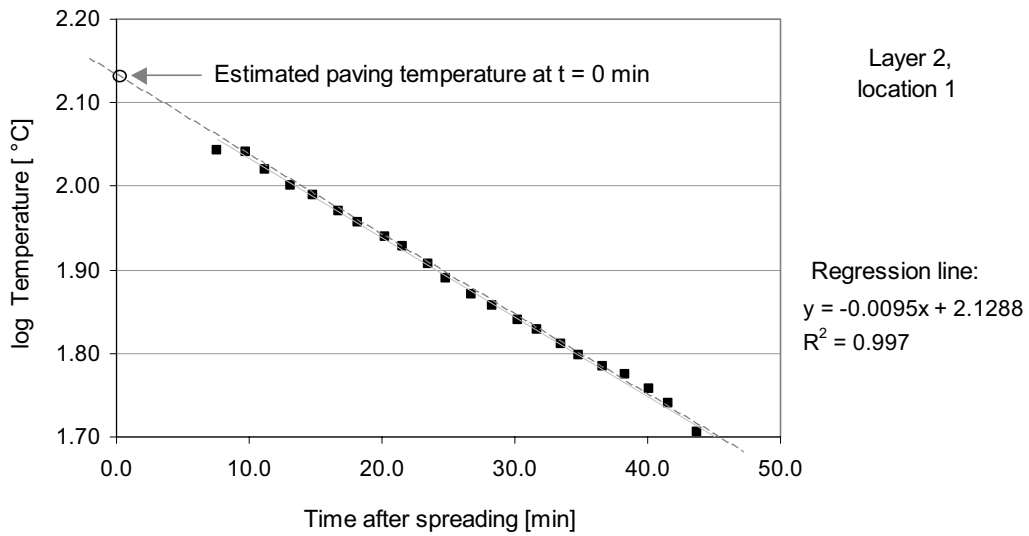


Figure 5.7 The measured HMA cooling data and the estimated model; the logarithm of the temperature difference between air and HMA versus the time after spreading, layer 2 at thermo-couple 1.

Estimating initial material temperatures

By plotting the log of the temperature against the time in minutes of measuring point one of layer 2, a slope of -0.0095 and intercept value of 2.1288 was obtained, see Figure 5.7. The R square of 0.997 indicates a good fit of the model to the data. By means of the model the initial HMA temperature at paving, could be calculated by using;

$$T_{HMA_c} = 10^{(S \times t + I)} + T_{air}$$

In which:

- T_{HMA_c} = current HMA material temperature in °C
- S = estimated slope of the model
- I = estimated intercept of the model
- t = time in minutes after spreading
- T_{air} = current air temperature in °C

For layer 2 using thermo-couple 1 the initial material temperature could be calculated on;

$$T_{HMA_ini} = (10^{2.1288}) + 10 = 144.5^{\circ}\text{C}.$$

The results in Table 5.5 summarise the findings of applying a similar procedure to the data obtained at the remaining temperature measuring points.

ESTIMATED INITIAL HMA TEMPERATURES				
Layer	2	2	3	3
Thermo - couple	1	2	1	2
Curr. air temp. T_{air} [°C]	10	10	9	9
Initial HMA temp. $T_{HMA\ ini}$ [°C]	144.5	142.6	138.6	127.7

Table 5.5 The estimated initial HMA material temperatures during paving.

Generic cooling relation

When the initial material temperatures are known a generic relation for all thermo couples and layers could be estimated by normalising the obtained data to the asphalt paving temperature. Figure 5.8 illustrates the results for the “middle” position for all temperature measuring locations.

A similar procedure could be used to achieve the generic temperature relations at the positions “Hi” for both layers. However, this was not the case for position “Lo”. This was probably because both HMA layers were constructed in a limited time on top of each other (layer 3 on top of layer 2). Layer 2 was constructed on a base of ambient temperature whereas layer three was constructed on a warm layer (layer 2). Due to this construction process the material temperature trajectories of the layers at position “Lo” were different from each other.

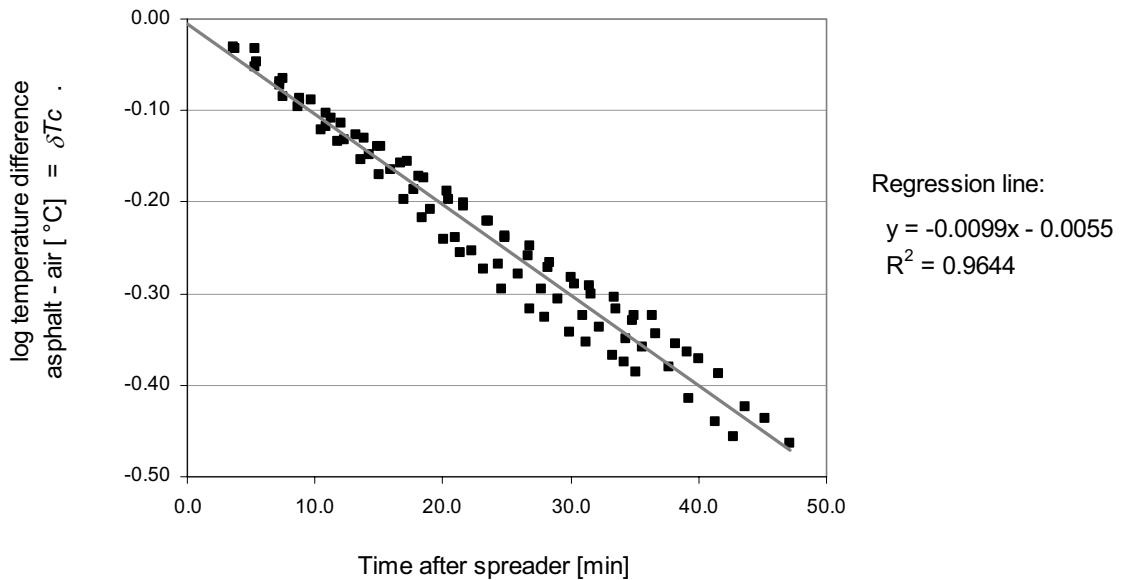


Figure 5.8 The logarithm of the temperature differences HMA-air versus time, modelled and measured values, position “mi” both layers, both thermo couples.

After modelling, the residuals were calculated and plotted against each of the variables; time, measuring point, roller pass and initial material temperature. The residuals obtained were all randomly distributed except for layer 3 position “lo”. However, also no structural pattern as a possibility for improvement of the model could be found.

The above-described procedure is applied on data of all positions. Table 5.6 summarises the obtained results.

ESTIMATED HMA TEMPERATURES DURING COMPACTION				
Position	Lo	Lo	Mi	Hi
Layer	2	3	2 & 3	2 & 3
Slope	-0.0054	-0.0048	-0.0099	-0.0085
Intercept	-0.1844	-0.1322	-0.0055	-0.1806
R^2	0.969	0.804	0.964	0.799

Table 5.6 Slope and Intercept of estimated temperature trajectory during compaction.

The generic temperature relation can now be estimated as;

$$T_{HMA_c} = \delta T_c + T_{air} = \delta T_{ini} \times 10^{(S \times t + I)} + T_{air}$$

where; T_{HMA_c} = the current asphalt material temperature [°C]
 δT_c = current difference between material and air temperature [°C]
 T_{air} = environmental air temperature during construction [°C]
 δT_{ini} = difference between material and air temperature during paving [°C]
 S = slope of the model [/.]
 I = intercept of the estimated model [/.]
 t = time in minutes after paving the involved lane [min]

The obtained temperature readings and the estimated models are illustrated for the thermo-couples at position 1 of layers 2 and 3 in respectively Figure 5.9 and Figure 5.10. The R square values obtained vary from 0.80 until 0.97. This implies that not all estimated curves do have a perfect fit to the measured data. Especially the fit of the curve Lo from layer 3 and Hi for both layers is just moderate. This is visible in both figures. The questionably fit of layer three position Lo can be attributed to the fact that the sub-layer was hot when paving. Because of this hot sub-layer the circumstances for the cooling behaviour at this specific layer/position combination were different from the generic cooling information obtained at the other layer/position combinations. At the positions Hi (top surface of the layer) the questionable fit can be caused by strong fluctuations of the surface temperature. These fluctuations can quickly occur when showers fall on the hot material or an unexpected blast of wind is passing.

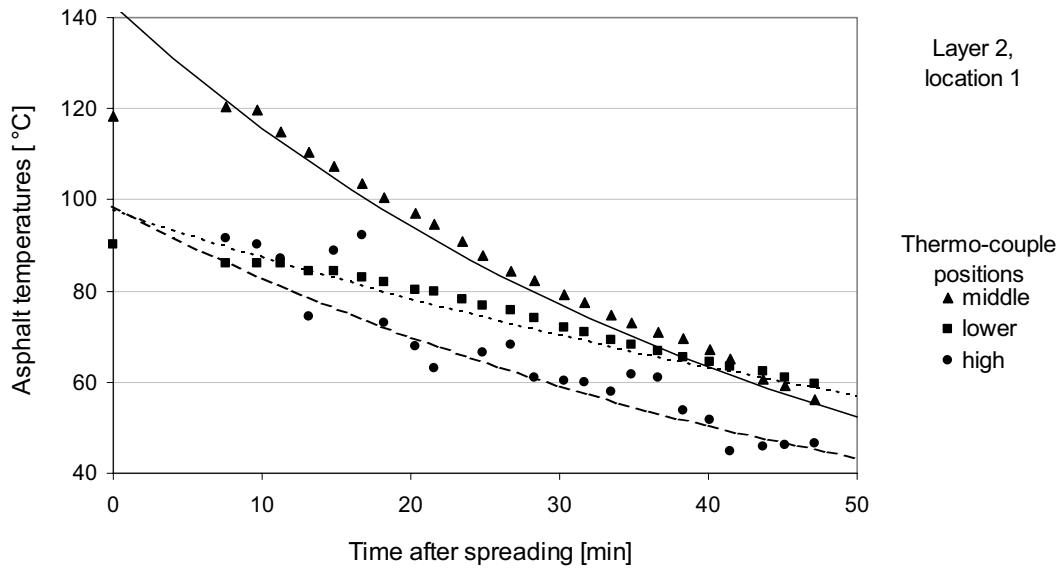


Figure 5.9 The asphalt temperature readings and the estimated models for location 1 during compaction of layer 2.

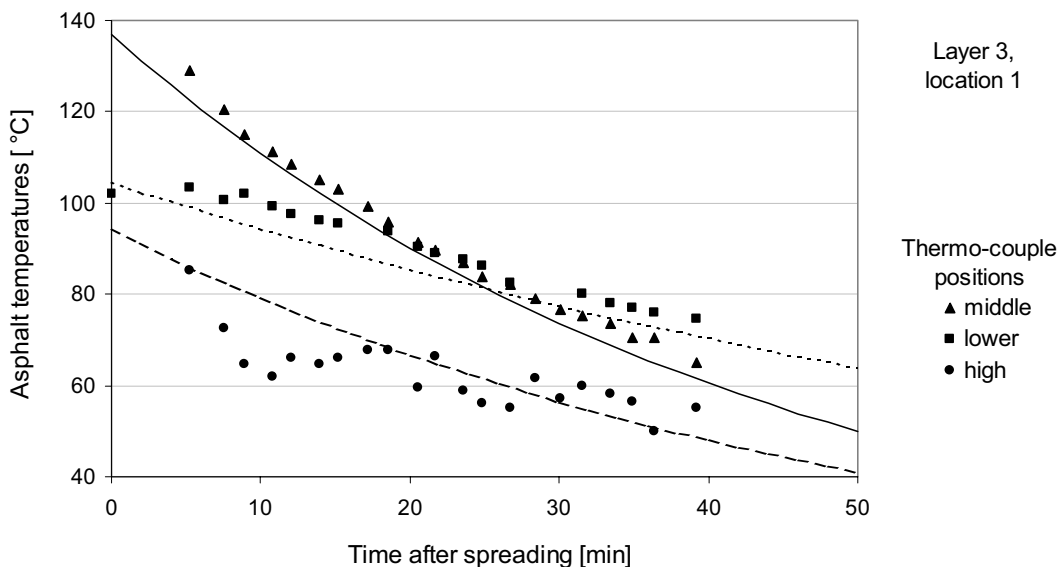


Figure 5.10 The asphalt temperature readings and the estimated models for location 1 during compaction of layer 3.

During the compaction process detailed information was gathered about meteorological conditions that affect the cooling rate of the HMA. It is beyond the scope of this research project to discuss all these details here but we aim to give the reader an impression of the most important circumstances under which the test sections were constructed and information about air temperature and wind speed which are given in Table 5.7. This information was gained from weather reports of the Rotterdam airport “Zestienhoven” which is 6.5 to 7 km from the location where the test sections were built. Paving and compaction of layer 2 occurred between 14.00 and 14.45 hours, whereas paving and compaction of layer 3 occurred between 15.40 and 16.20 hours.

METEOROLOGICAL CIRCUMSTANCES DURING PAVING THE TEST SECTION		
Time [hours MET]	Ambient Temperature [°C]	Wind speed [m/sec]
14.00	10.3	4
15.00	9.8	3
16.00	7.7	1

Table 5.7 The temperature and wind speed conditions during paving and compaction of the test sections at 6 November 1998, measured at Rotterdam Airport “Zestienhoven”.

The temperature of the base just before paving layer two was 10°C around 14.00 hours. The upper surface temperature of layer two was around 50 °C just before layer three was paved on top of it. During the rolling procedure water was sprayed on the steel roller drums (as usual) to avoid sticking of the asphalt to the steel drum. Because it was hard to measure this amount of water accurately the roller operator had to estimate it, he estimated that he used around 50 l of water per layer. Three times a little rain shower did fall during constructing the test sections. During compaction of layer 2 at 14.33 hours (i.e. about 33 minutes after paving started) a light drizzle came down. This happened two times when compacting layer three; at respectively 15.47 and 16.05 hours (i.e. about 7 and 23 minutes after paving started).

Analysis of layer thickness

By measuring the layer thickness and bulk density the progress of compaction during construction of the test section was monitored. The layer thickness was measured by the use of the level and rod, and the Strato test equipment. The bulk density was measured by using a nuclear gauge. Correlation of material density to layer thickness was possible because both quantities were also measured on cores drilled from the test lanes after compaction was completed.

Layer thickness was measured at 32 locations (on 2 layers). Temperature and nuclear density readings were each taken at four locations. The layer thickness readings were therefore the primary source of information. The density measurements were used to confirm the compaction progress trajectory based on the layer thickness readings.

The Strato test equipment is made of a synthetic material that cannot withstand temperatures in excess of 140°C. Therefore, Strato test readings immediately after the asphalt was laid, were omitted.

Modelling the layer thickness trajectory

In Figure 5.11 the results are shown of layer thickness measurements at points 3, 5, 7 and 9 of layer 2 in relation to the number of roller passes. The data suggests a logarithmic relation between the number of roller passes and the layer thickness. In

fact this corresponds with Kezdi (1969) and Renken (1980), see also paragraph 3.2. Furthermore, the measurements show that although it was the intention to construct a layer of uniform thickness, the actual thickness varied between 52 and 58 mm for layer 2, and between the 47 and 53 mm for layer^{33,34} 3.

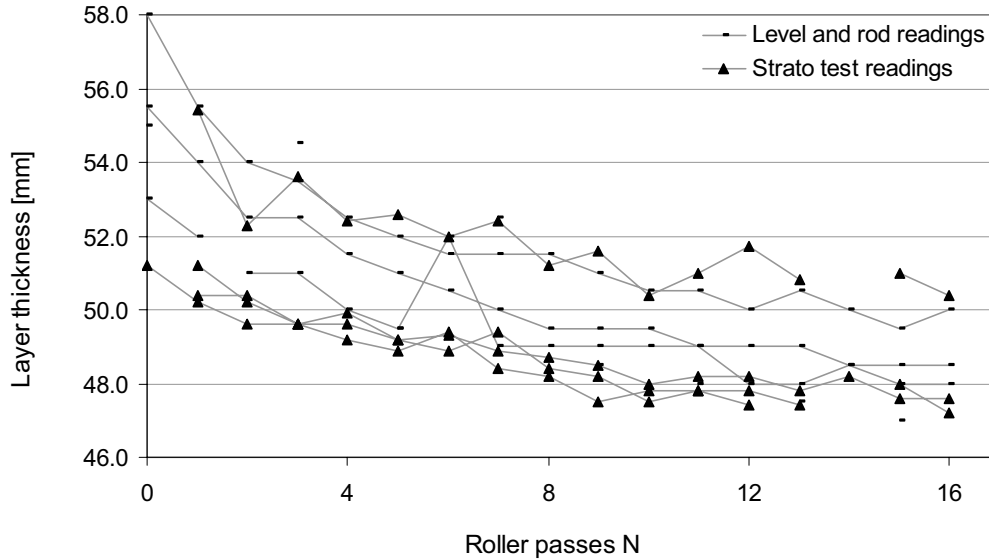


Figure 5.11 Roughly obtained layer thickness readings (Strato test and Level and rod) against roller passes of measuring points 3, 5, 7 & 9, on layer 2.

The layer thickness data shown in Figure 5.11 were transformed into the following relation³⁵;

$$\frac{LT_N - LT_\infty}{LT_\infty} = \frac{LT_0 - LT_\infty}{LT_\infty} * 10^{-\alpha * N}$$

in which:

- LT_N = layer thickness after roller pass N,
- LT_∞ = theoretical layer thickness after an infinite number of roller passes,
- LT_0 = layer thickness before compaction starts (thickness after spreading the HMA),
- N = applied number of roller passes,
- α = factor representing the speed of the compaction progress.

The found relationship is logical and plausible. Logically; the function does have an asymptotical axis. The layer thickness will become LT_∞ after infinite number of roller

³³ At two measuring points initial thicknesses were measured of respectively 57.5 and 58 mm but these values were avoided because they seem to be unusual observations when they become compared to the other data obtained in the same test series.

³⁴ This is beside the measuring points 15 and 16 at the end of layer 2. Here the section became extremely thin; the initial layer thickness was around 40 mm, so it concerns a very strong deviation related to the mean values.

³⁵ Using this formula the data is scaled to LT_∞ , the layer thickness value that should be reached after an infinite number of roller passes. Using this equation makes the layer thickness decline linear dependent from the layer thickness itself. This scaling enables us to compare lines obtained at different measuring points against each other.

passes. It seems logical that after a certain number of roller passes applied, using a roller of specific weight and dimensions, compaction does not increase anymore. Plausible; the progression achieved by a specific roller pass depends on the compaction achieved so far. (i.e. $LT_N - LT_\infty$). Using the same roller, the result of every pass will be smaller than the result of the previous pass. Figure 5.12 helps in understanding the model parameters and the type of model. The LT_N relation can also be written as;

$$LT_N = LT_\infty * (1.0 + \gamma * 10^{(-\alpha * N)})$$

in which;

$$\gamma = \frac{LT_0 - LT_\infty}{LT_\infty}$$

The variable γ represents the pre-compaction state related to the (theoretical) ultimate compaction state possible. If it is assumed that pre-compaction level and material composition was the same over the whole layer this variable can be estimated as a fixed parameter for the whole section (all measuring points). The transformation implies that; a. all obtained data is scaled to the ultimate layer thickness value, LT_∞ , estimated per measuring point, and b. the layer thickness is assumed to be negative exponential related to the number of applied roller passes.

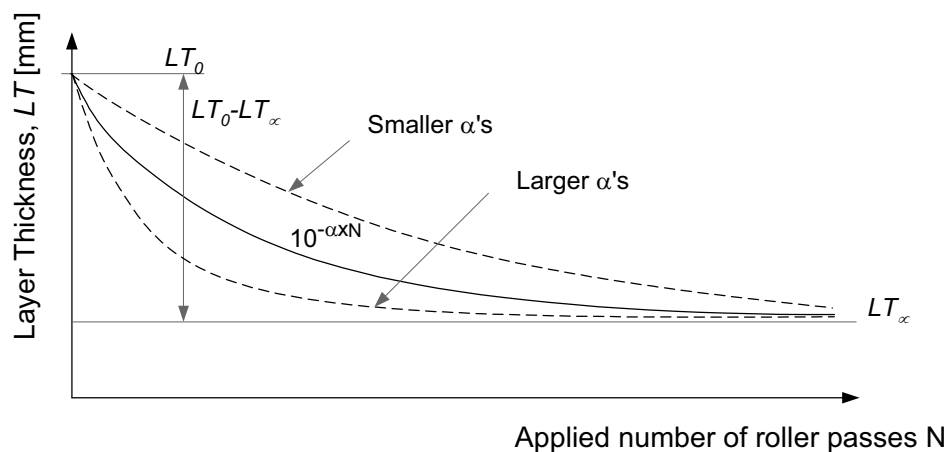


Figure 5.12 The model that is fitted through the layer thickness data.

A relationship is now proposed for modelling the layer thickness as a function of the number of roller passes. The parameters estimated by non-linear regression techniques were; α , γ and LT_∞ . To test the suitability of the model to the test data, the model (i.e. the three parameters) was estimated for every measuring point individually. The obtained R^2 values, an indication of the fit of the model to the data, were mostly above 0.9 as can be seen in Figure 5.13. It implies a reasonable fit, however, there were also measuring points with an insufficient fit (values between 0.5 and 0.8) or even a terrible fit (smaller than 0.5).

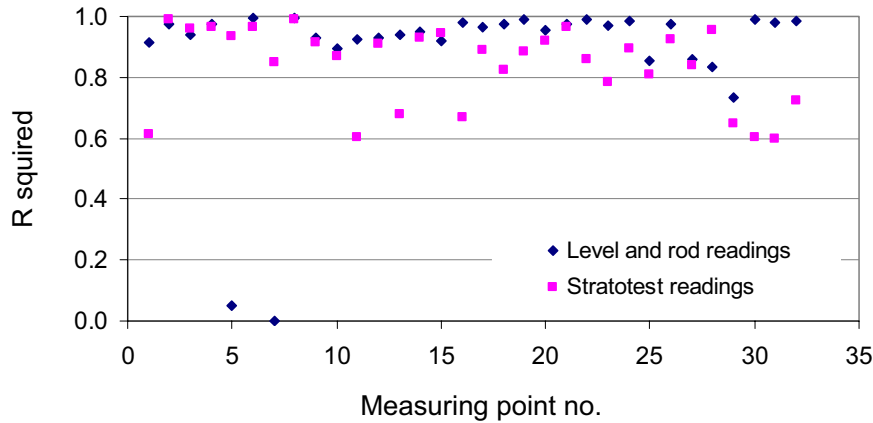


Figure 5.13 The obtained R^2 values as a result of the first step of the layer thickness analyses. For every measuring point the layer thickness relation was estimated using non-linear regression.

For the different measuring methods (level and rod and Strato test) the values proved to be different, the parameter LT_∞ was, of course, estimated for every measuring point separately.

As a next step in the analysis the data was cleaned (removing the unusual observations). An earlier mentioned assumption said that material composition and pre-compaction over the test section was homogeneous. Based on that assumption, the average value for γ was calculated. By means of the average γ , the remaining values for α and LT_∞ were estimated again per measuring point individually. Again cleansing of the database, and estimation of the parameters of the remained data formed the final result of the analysis. More details about how step-by-step the statistical analysis was achieved can be found in the appendix J. Figure 5.14 illustrates the layer thickness data against the number (log) of roller passes as it becomes scaled to LT_∞ .

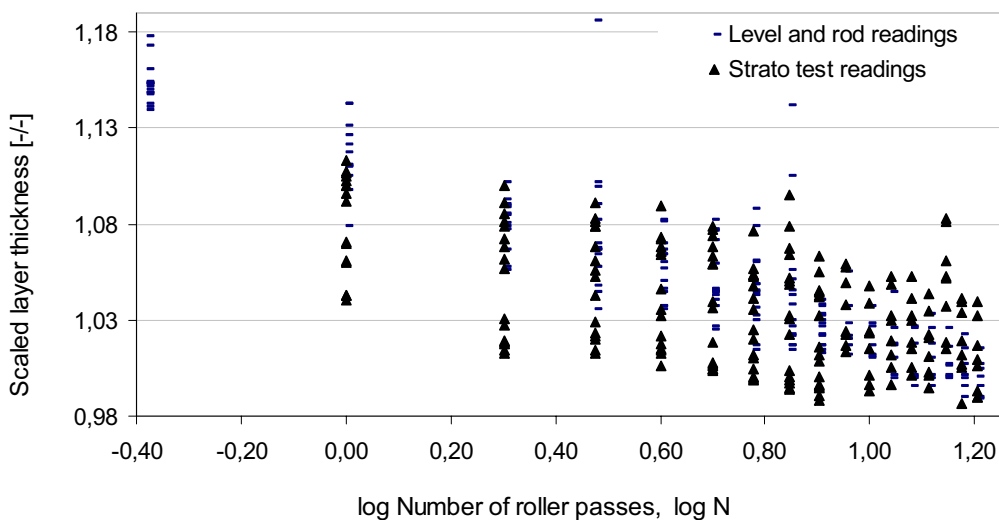


Figure 5.14 The scaled layer thickness of all measuring points versus the logarithm of the amount of roller passes.

By fitting the above-described model to the layer thickness data the model parameters shown in Table 5.8 were obtained.

COMPACTION PROGRESSION OF LANES A & B			
	Lane A	Lane B	Difference Lane A - Lane B
Level and rod			
Slope (α)	-0.094	-0.098	0.004
St. deviation	0.055	0.059	
γ	0.1497	0.1497	
Strato test			
Slope (α)	-.081	-0.192	0.121
St. deviation	0.045	0.128	
γ	0.1087	0.1087	

Table 5.8 The results of the analysis of the slopes of decrease of layer thickness of lanes A (16 passes) and B (8 passes).

Consideration of the material temperature effect

To determine whether the material temperature is a factor influencing the compaction progress one can compare the achieved compaction progress in lane A to the one in lane B.

For example, roller pass 2 in the B section was applied 15 minutes after spreading when the mean temperature³⁶ was 103°C. In lane A roller pass 2 was applied about 6.5 minutes after paving at a temperature of 122°C, see Table 5.9. The variables, α and γ , which represent the compaction progress were calculated separately for the A and B lanes. The obtained difference in α 's for both lanes is so small, see Table 5.8, that statistically they act as two samples coming from the same population. This implies that the compaction progress was approximately equal on both lanes involved (in fact the α value for the B lane was even a bit higher), although the temperature between both lanes differed considerably (19°C for roller pass 2 and 33°C for roller pass 8, see Table 5.9).

The analysis done on the readings of the achieved compaction test sections indicate that the role of temperature during compaction was insignificant. Based on these findings the preliminary mentioned hypothesis that; "*a higher material temperature makes asphalt mixtures better compactable*" is rejected, at least for the material and equipment used here and the actual circumstances surrounding the experiment.

³⁶ The given temperatures are the values estimated in the middle of the layer depth (at 25 mm above bottom) of layer 2, the values for layer three are respectively 95 and 113 C.

MATERIAL TEMPERATURES DURING ROLLER			
Roller pass no.	Lane A [°C]	Lane B [°C]	Difference [°C]
2	122	103	19
4	110	84	26
6	100	69	31
8	91	58	33
10	82	-	-
12	75	-	-
14	68	-	-
16	62	-	-

Table 5.9 Temperature of comparable rolling passes applied on lane A and lane B, measured in the middle of layer no. 2..

Level and rod versus Strato test readings

Because the Strato test equipment was unable to withstand the high temperatures of the freshly laid asphalt layer, the initial layer thickness was not measured using this equipment directly after paving. The Strato test equipment specifies an accuracy of 1 mm added to 2% of the thickness measured. For a 50 mm thick layer this will be about 2 mm. Level and rod equipment specifies the accuracy of a reading of the same ± 2 mm.

Further, the Stratotest equipment gave thickness values that were different from the readings obtained with the level and rod. Especially at the beginning of compaction the Strato test readings gave a thickness that was 1.5 mm thinner than the thickness determined with the level and rod measurements. At the end of the compaction process both measuring systems gave roughly the same thickness. The layer thickness courses of some measuring points both obtained by the level and rod and Stratotest equipment are given in Figure 5.11.

Additional statistical analysis on data obtained with both measuring systems showed that the level and rod measurements had a higher reliability. While estimating the slope of compaction progress (α), it became clear that the standard deviation of the model fitted to the level and rod data was half the standard deviation obtained with the Strato test data. The figures were respectively 0.0561 and 0.011. Further, the R^2 for the complete set of Level and rod data was 0.938 whereas the result of the Strato test was 0.862.

Furthermore the level and rod instrument has proved itself a reliable measuring system for doing height measurements over a long time span. This is not the case for the Strato tester, which is relatively a new apparatus. Therefore it was decided to use the layer thickness information obtained from the level and rod readings as the input for further analyses.

After compaction was completed the layer thickness was obtained by measuring the height of the drilled cores. These layer thickness values were compared to the corresponding quantities obtained by the level and rod and Stratotest readings. The devices involved did not show structural differences. The deficiencies from the level and rod and the Strato test readings compared to the readings on the cores are illustrated in Figure 5.15.

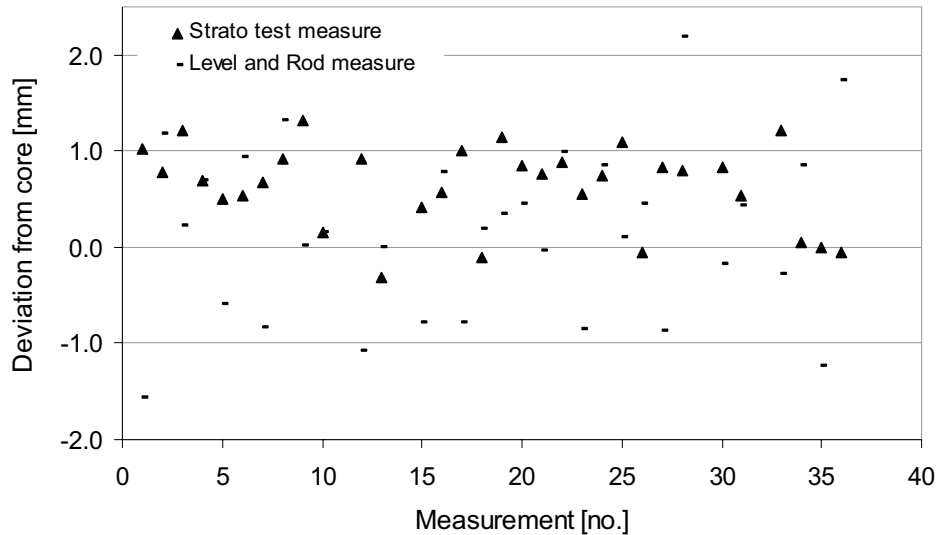


Figure 5.15 Deficiencies of Strato test and level and rod layer thickness readings compared to layer thickness values obtained from cores, after compaction was completed, all measuring points.

Generic model for layer thickness

The data set obtained on both lanes and both layers, is illustrated in Figure 5.14. The generic model is illustrated in Figure 5.16 together with the data of measuring points 1, 3, 5 and 7 of layer 2. Because the data measured on our test lanes show that there is no difference in compaction progress at different temperatures, the same formulae parameters can be used to predict the layer thickness trajectory for all the measuring points. This implies that one single formula, not containing a temperature parameter could model layer thickness trajectory for both test sections.

The parameters α and γ were obtained from the statistical analysis on the level and rod measures. For the compaction test lanes the following values were obtained;

$$\alpha = 0.096$$

$$\gamma = 0.1497$$

The R^2 value for the data from the whole test section became 0.94.

The formula for describing thickness as a function of roller passes now becomes;

$$LT_N = LT_\infty * (1.0 + 0.1497 * 10^{(-0.096*N)}) \text{ [mm]}$$

By using this relationship and the obtained information from drilled cores after finishing the test section, the theoretical LT_∞ could be calculated as 46.72 mm. The

corresponding bulk density could be deduced to 2358.1 kg/m^3 , which corresponds to a voids content of 2.5%. The detailed calculation process can be found in appendix K.

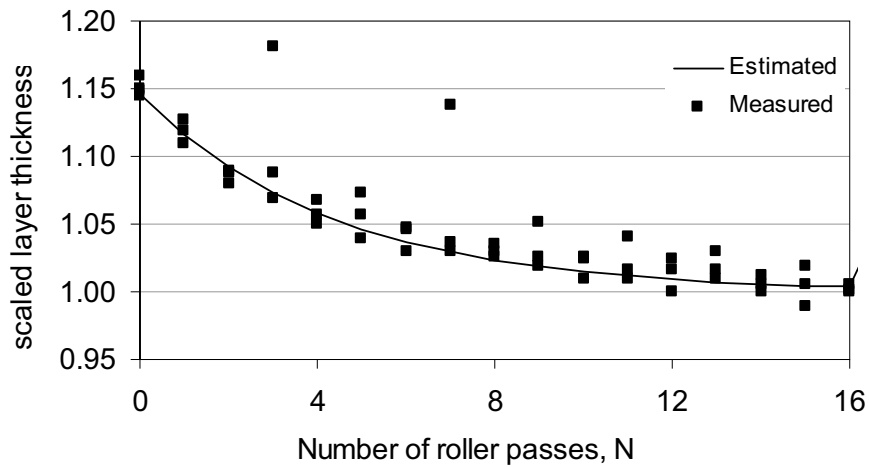


Figure 5.16 Scaled layer thickness data measured at the points 1, 3, 5 and 7 of layer 2 and the estimated model.

Residual analysis

To check if the fit of the model could be improved by introducing other causal variables, the computed residuals (i.e. deviations between estimated and measured values) were plotted against factors that could possibly be influential in the compaction progress. Tested potential causal variables were; the number of roller passes, temperature of the material, measuring point number and final layer thickness. All graphs do show a random pattern. This implies that implementation of one of the variables tested into the model would not result in an improved accuracy of the layer thickness model. The complete set of residuals plots can be found in appendix L. In Figure 5.17 the residuals against temperature are given as an example.

Analysis of the bulk density

The density of the HMA during compaction can be linked to the layer thickness and *VMA* level if for a specific point in time all variables are known. Layer thickness and density measurements do give essentially the same information being the increase in compaction state of the material. When a layer thickness decreases homogeneously with say 5 % its density averaged over the height should increase³⁷ with 5% unless material is “lost” during the rolling process. This information was obtained from measurements on cores drilled from the test lanes after compaction was completed. An additional advantage of drilling these cores was that the layer thickness measured by level and rod and Strato tester could be compared to values measured with Vernier callipers applied directly on the cores. The *VMA* trajectory of the material during compaction can be calculated from the layer thickness trajectory if; a.) the specific

³⁷ An assumption that was made for making this statement is that the material cannot move in horizontal direction. Locally, the HMA material will move in front of the roller but generally the material in the middle of a section cannot go anywhere.

mixture composition is known, and, b.) at least at one stage *VMA* (or density) and layer thickness are known.

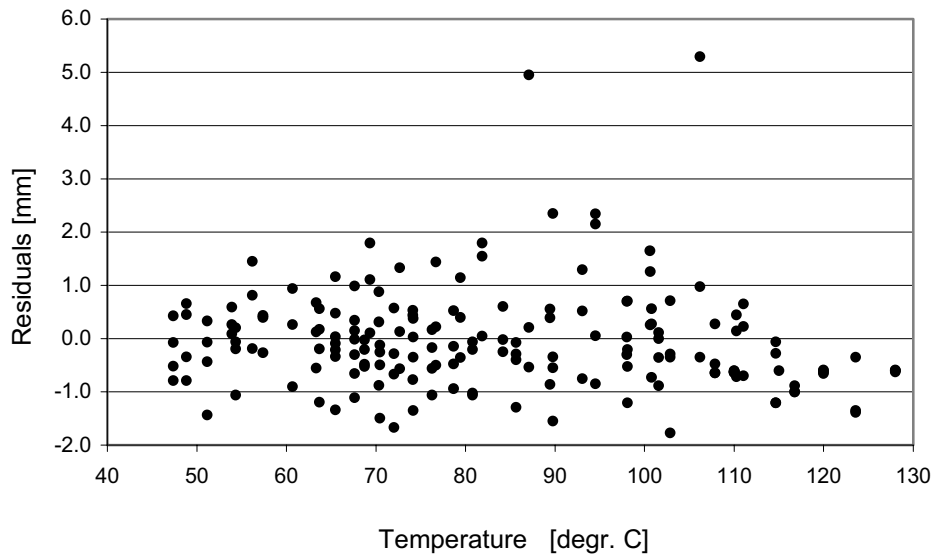


Figure 5.17 The residuals (predicted layer thickness minus measured layer thickness) against temperature during compaction.

Nuclear measured Specific Densities

As mentioned before, the densities of the HMA were also measured during construction by using two nuclear Troxler gauges. Because the number of density readings, in relation to the number of layer thickness measurements is small (about 40 against 350), directly measured density information forms the minority of the information. Nevertheless, the measured bulk density trajectory with the nuclear equipment was used as a check to confirm the obtained compaction progress information from the layer thickness measurements.

The nuclear density readings were taken exactly between two layer thickness measuring locations (see Figure 5.3). From the drilled cores the relation between the layer thickness and bulk density of the compacted layer could be obtained. Figure 5.18 illustrates the compaction progress trajectory; a.) obtained by the two involved Troxlers and b.) obtained from the level and rod measurements.

The compaction progress obtained by the Troxler readings was different from the one obtained by the level and rod measurements. Mainly during the first part of compaction, from zero to approximately 8 roller passes the Troxlers overestimated the achieved density. If the nuclear measurements are used as a guide to achieve a compaction rate of 98% of Marshall density, 3 to 5 passes would be sufficient, whereas level and rod information indicates that at that point only 94% of Marshall density is achieved. Level and rod measurements indicate that at least nine roller passes are required for achieving the 98% of Marshall density. In the latter stage of

the rolling process, approximately from 9 to 16 passes both techniques gave comparable results.

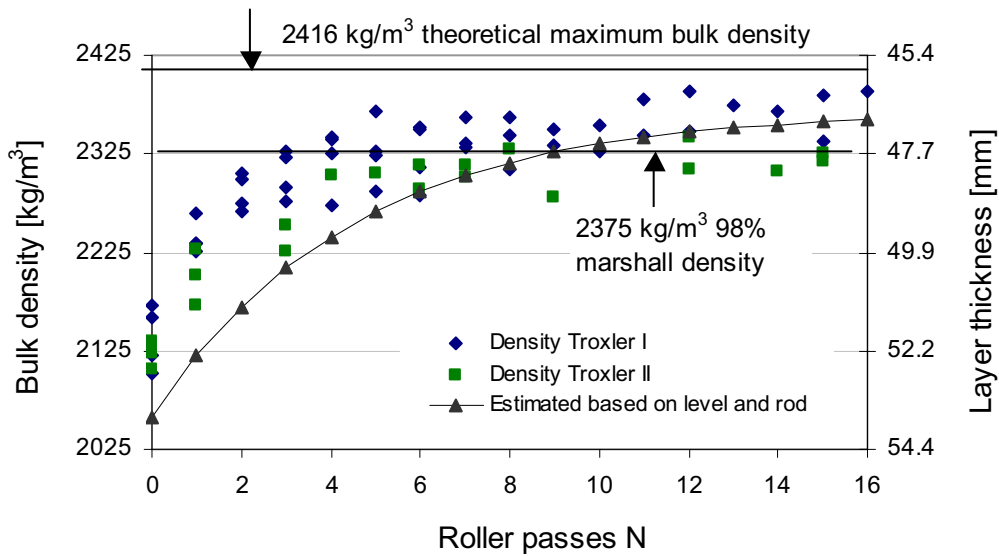


Figure 5.18 The estimated layer thickness trajectory compared to layer thickness values deduced from nuclear density measures.

Based on density information from the two Troxler devices and the information obtained from the cores a comparison was made between the density readings obtained using these procedures. The results show that one Troxler device underestimated³⁸ the bulk density with approximately 13 kg/m³, whereas the other Troxler overestimated the bulk density with approximately 62 kg/m³. Figure 5.19 illustrates the deviation of the Troxler density readings to densities obtained from the cores. Perhaps further work should be done into the accuracy of the nuclear density readings obtained from the partly compacted layers.

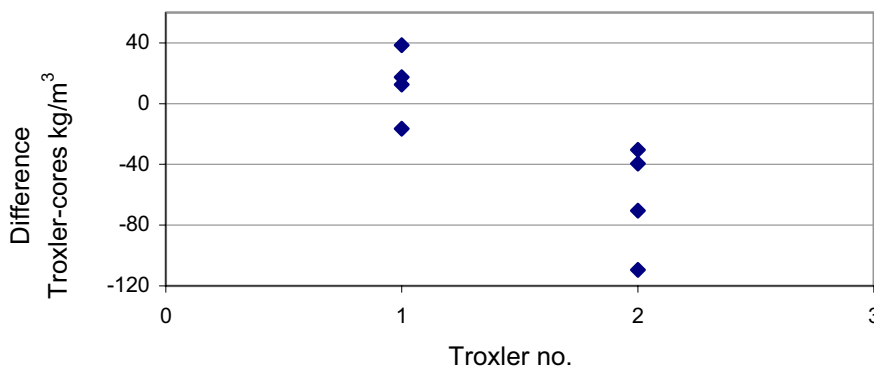


Figure 5.19 The differences in bulk density as measured with the Troxlers (no 1 and 2) related to values directly obtained from cores.

³⁸ An assumption for making this comparison was that the measurement directly from the cores delivers the most reliable values for calculating the specific density.

5.4 Estimation of VMA and temperature profiles of the HMA layer

In chapter 3 it is discussed how from the laboratory measuring programme critical state parameters for a HMA mixture could be obtained. In chapter 4 the fineness of the FEM mesh was discussed. In the previous sections of this chapter it is discussed how by means of the compaction test section information about material temperature and compaction progression was gathered. Therefore it is now possible to link all this information for completion of the material parameters in order to start FEM simulations. Now we can determine what the specific *VMA* level and material temperature for a layer of elements is. This is required for estimation of the temperature and compaction level dependent material behaviour expressed in terms of critical state and/or Rock parameters.

Estimation Temperature profiles HMA

In the compaction test sections thermo-couples were embedded to measure the material temperature. Using these readings generic cooling curves were estimated for three depths as a function of time (in minutes after spreading the asphalt). Examples of some estimated cooling curves and temperature readings are shown in Figure 5.20. From this temperature information the polynomial profiles of the material temperature in depth direction were obtained. The curves obtained for the roller passes 1, 2, 4, 8 and 16 applied in lane A of layer 2 are illustrated in Figure 5.21.

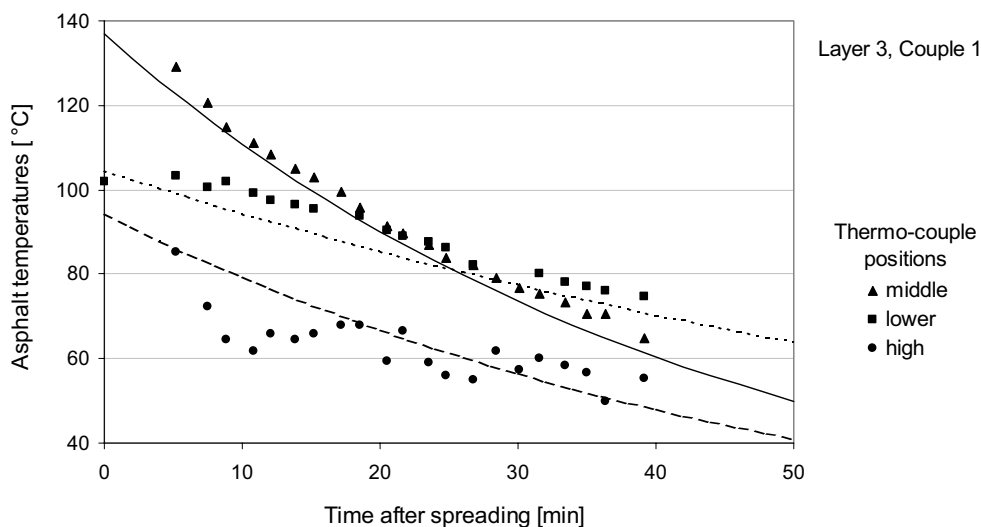


Figure 5.20 Estimated cooling curves at three depths, based on readings made during construction of layer three at position “couple 1” (see Section 5.2).

In the finite element mesh 5 layers are used to which different material properties can be allocated. Per layer of elements just one set of material parameters can be attributed. Therefore for every elements layer a discrete (average) material temperature had to be calculated. This was achieved by estimating the discrete material temperature per layer in such a way that the surface under the curved

temperature line equals the surface under the discrete (step) line. This procedure is illustrated in Figure 5.22.

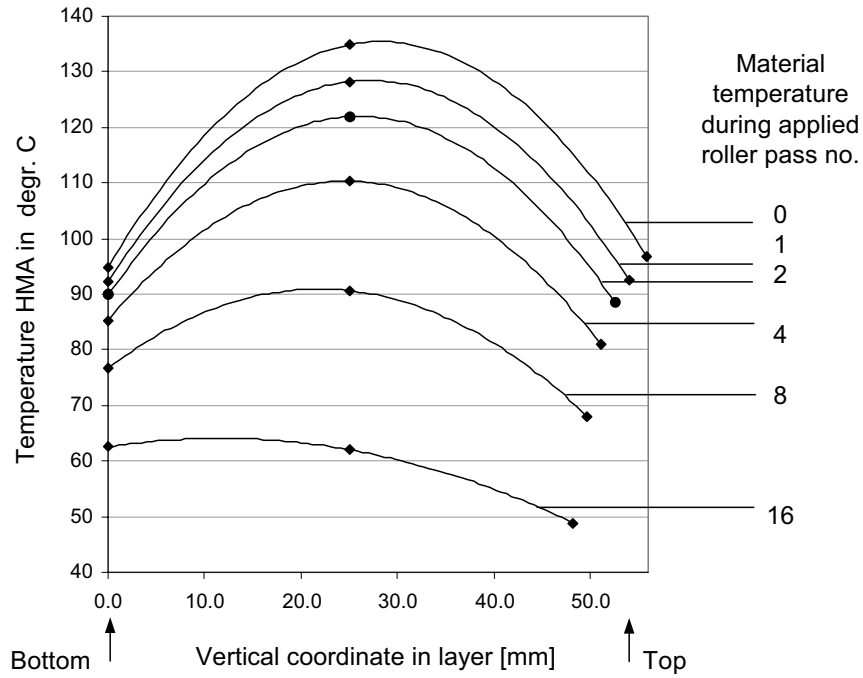


Figure 5.21 The material temperature readings and the polynomial functions estimated through these readings for applied roller passes 1, 2, 4, 8 and 16 at respectively 4.0, 6.5, 11.5, 21.5 and 41.5 minutes after spreading the HMA in the 2nd layer of lane A (Section 5.2)

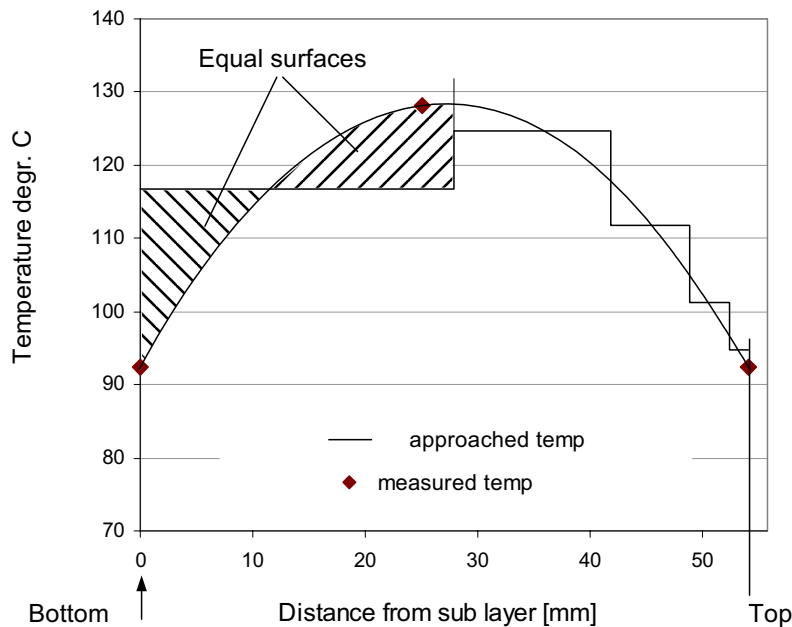


Figure 5.22 The measured temperatures for roller pass no.1 of asphalt layer 2 (dots), the polynomial temperature distribution (full, curved line) and the temperature step function for deducing material properties of the element layers.

Applying the same procedure to the temperature distribution curves of the roller passes 1, 2, 4, 8 and 16 of layer 2 lane A, the discrete temperatures for all the 5 element layers were calculated. The figures are depicted in Table 5.10.

ESTIMATED TEMPERATURES PER ELEMENT LAYER					
	Temperature HMA in Element row no. °C				
Roller pass	1	2	3	4	5
1	116.8	124.6	111.8	101.1	94.8
2	111.7	118.3	106.3	96.4	90.5
4	102.6	106.8	96.2	87.8	82.8
8	86.9	87.4	79.2	73.0	69.4
16	63.5	59.6	54.6	51.4	49.5

Table 5.10 Estimated temperatures for element rows 1 to 5 for estimating material properties for the FEM simulation of roller pass 1, 2, 4, 8 and 16 of layer 2, lane A.

Estimation of a *VMA* profile.

For deduction of the material pre-compaction level, a distinction must be made between the first roller pass ($N=1$) and the subsequent roller passes ($N>1$). It is assumed that the pre-compaction effects of the asphalt-paving machine are equally distributed over the height of the asphalt layer. Based on that assumption the average *VMA* level can be calculated from the height of the layer and the mass of material per layer. The *VMA* profile for the roller passes $N>1$, was calculated from the results of previous roller passes.

Initial VMA level, $N=1$

The layer thickness trajectory during compaction is deduced based on measurements done at the experimental test sections. Using this data a negative exponential function for describing the layer thickness during compaction was estimated. This function was solely dependent on the number of roller passes.

Further, after compaction was finished, cores were drilled at all measuring points. From measurements on these cores, the layer thickness and bulk density were obtained. For layer 2 these quantities are represented in Table 5.11.

MEASURED QUANTITIES ON CORES				
Sections	Roller passes	Layer thickness [mm]	Bulk density [kg/m ³]	Amount of material [kg/m ²]
A	16	47.68	2354.2	112.25
B	8	49.79	2322.6	115.64

Table 5.11 Measured quantities on cores from test section, layer 2 lanes A and B

Linking the layer thickness information to the information obtained from the cores, it enabled us to calculate the averaged bulk density (averaged over the total layer thickness) of any roller pass, and thus also directly after paving.

Further, the *VMA* value can be calculated knowing the following data material:

- material bulk density at 0% voids = 2416.6 kg/m³,
- volume part of the bitumen related to the aggregate = 13.7 % v/v.

The following initial material quantities could be deduced, just after paving;

MEASURED MATERIAL INFORMATION LAYER 2			
Lanes	$LT_{\ 0}$ [mm]	$BD_{\ 0}$ [kg/m ³]	$VMA_{\ 0}$ [%]
A	54.58	2056.5	0.2656
B	55.83	2071.3	0.2610

Note; LT = Layer thickness

BD = Bulk density

$_{\ 0}$ = after zero roller passes

Table 5.12 Initial material information (before the first roller pass) of layer two.

VMA level roller passes $N > 1$.

From compaction simulations on a homogeneous pre-compacted material it is known that deformation as a result of a roller pass will not be equally distributed in the depth direction of a layer. This implies that after the first roller pass the *VMA* is no longer homogeneous. From the roller pass simulations the volumetric deformations of the material are calculated as a function of the depth of the layer. Based on the initial *VMA* value and the calculated plastic volume strain of the achieved roller passes the new pre-compaction (i.e. *VMA*) profile for the next roller pass can be calculated.

The initial *VMA* level of the material (i.e. directly after paving) forms the basis for calculating the input of all the subsequent simulations. The calculated plastic deformation profile of the first roller drum pass can be added to the initial *VMA* value (i.e. *VMA* just after paving) to obtain the *VMA* profile of the simulation of the second roller drum pass. This process should be repeated after every simulated roller drum pass for achieving the *VMA* profile for the next simulation.

Summary

A field experiment was conducted that consisted of constructing a test section under controlled conditions. All the key activities; spreading the material, applying roller passes and material temperature readings, were accurately timed. Compaction progression was measured by using different measuring techniques; a.) level and rod readings, b.) Strato test readings and c.) nuclear density readings. The time readings enabled us to calculate the material temperatures at which roller passes were applied on the test section.

The material that was used for constructing the test section was a Dense Asphalt Concrete 0/16. Our target was to build a layer of 50 mm thickness after compaction

was completed. A HAMM DC 6.42 tandem roller of 7.9 tons operational weight in static mode provided the compaction force. The roller applied 8 passes on lane B and 16 on lane A while the asphalt mat temperatures were between 140 and 58°C (measured in the middle of the layer). The rolling scheme was organised in such a way that the roller passes on the different lanes (A and B) were applied at different material temperatures.

Measuring the changes in density and thickness of the constructed asphalt layer monitored the progress in HMA compaction. Analysis of the results obtained at 22 different locations showed that the compaction progress of the HMA behaved quite regularly and as anticipated. It also indicated that the progress could be expressed very well by using negative exponential formulae.

Based on research literature and field tracing the hypothesis was posed that compactibility of asphalt materials is strongly dependent on material temperature; materials should be better compactable when they are hotter. To test this hypothesis the material temperature variable was incorporated in the experimental set-up. However, the test section results produce evidence that for the material and the circumstances in question the hypothesis had to be rejected. Carefully analysis of the results obtained demonstrated that compaction progression of the test section was independent of the material temperature over a wide range of temperatures whereas temperature differences were registered up to a maximum of 33 °C.

Due to this observed temperature insensitivity of the material compactibility it appeared that the compaction progress could be modelled by a single formula that only depends on the number of roller passes. The field experiment supports the findings of the laboratory experiments in the sense that the prevailing view of the relationship between material temperature and compactibility of the material remains that hotter mixtures are heavier compactable.

Because during building of the test section different devices were used for monitoring the compaction progression, the results of these measurements could be used for comparing them against each other. Compaction progression was obtained by; level and rod and Strato tester (both layer thickness) and by using two Troxler gauges (bulk density). Comparison of the results shows that although the level and rod procedure is a dated measuring method this procedure gives the most reliable results. It was striking that both systems that made use of wave technology (Strato tester and Troxler) demonstrate deviations, especially shortly after paving when HMA is hot and not yet fully compacted. In addition, differences were found between the two Troxlers used.

Because Troxler and Strato test readings appeared to be not reliable enough they were not used for estimating layer thickness trajectories. Therefore, in this thesis project the level and rod readings have been the main source of information.

Based on the fineness of the element mesh (chapter 4), and measured temperatures and compaction progression (chapter 5), the temperature profile and *VMA* profile in depth direction of the asphalt layer could be obtained.

6 Results of the FEM analyses

6.1 Introduction

For simulating rolling of HMA with a FEM, such an approach should contain the following features: a.) the ALE approach, b.) contact elements c.) a rotated co-ordinate system, d.) options for modelling a free material surface, and e.) a suitable material model in accordance with critical state principles. In the DiekA approach all these features are incorporated although the suitability for use on HMA rolling varies between perfect (a, b, c and d) to partly (e). ALE makes it possible that a material behaves partly as a fluid and partly as a solid; it can "stream in" and "stream out" of the finite element mesh. The rotated co-ordinate system assists in modelling a free rotating roller drum. Contact elements make it possible to model the contact area roller-drum-HMA material. The free material surface options make it possible to model a free surface of the material. Nevertheless, there are also two negative aspects that can be mentioned:

- a.) it is not directly possible to enforce a roller drum "weight" on the HMA and calculate the layer thickness reduction, therefore one has to "operate" the other way around; one has to pre-describe the layer thickness reduction and calculate the required rolling force,
- b.) the recoverable part of the material behaviour modelled by Rock is not consistent with the material behaviour modelled by critical state theory.

The results of these two aspects are; a.) by trial and error and a couple of calculations the right relationship between rolling force and layer thickness reduction has to be established, and b.) caused by the faulty elastic phase of the Rock model, a false rolling force is obtained. This error increases when the elastic part of material deformation become more important i.e. when the compaction stage of the material proceeds further. The major differences between a real HMA rolling process and a FEM simulation of it in DiekA are illustrated in Figure 6.1.

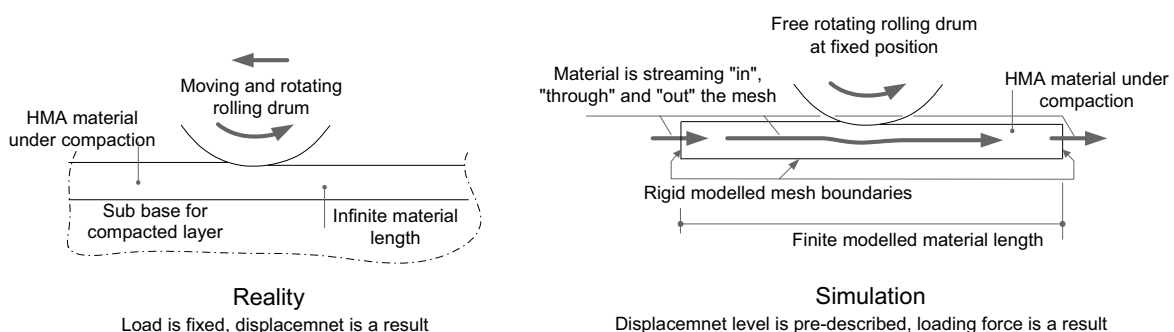


Figure 6.1 The similarities and differences of a real rolling process (left) on a HMA material compared to a simulation of it by using FEM (right).

Irrespective of all this it is still believed that DiekA is currently the best available way to simulate rolling processes of HMA, and so it has been used. In chapters 2, 3 and 4 fundamental theoretical knowledge and refinements of the model for compaction and

how to do material measurements were discussed. Chapter 5 discusses construction of test sections in order to obtain information of real compaction processes, partly to gather input for the FEM simulations. In this chapter the attention will be focussed on a.) the results of an individual simulated roller pass, and b.) the results of six succeeding roller passes in terms of *VMA* and bulk density, elastic and plastic deformation, and contact stiffness and stress. Figure 6.2 is a schematic illustration of the total research project. The area of specific interest of this chapter is marked grey.

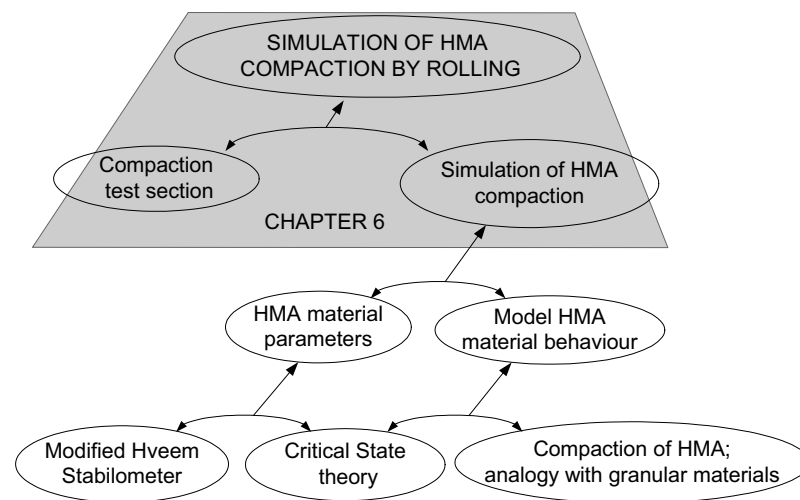


Figure 6.2 The set up of the overall compaction research project with grey shaded the topic of interest of chapter 6.

6.2 Simulation of an individual roller pass

When simulating individual roller passes with FEM, several types of information could be generated. Essential output for an individual roller pass simulation on asphalt is:

- vertical roller force,
- the shape of the curve that represents the top of the asphalt surface during compaction from upstream to downstream of the roller drum,
- deformation pattern (volumetric strain and deviatoric strain) in the vertical direction after rolling, isotropic normal compression stress pattern p' , and the deviatoric stress pattern q ,
- shear stress σ_{xy} ,
- the way the material moves through the mesh (i.e. analysing the particle tracing positions),
- incremental displacements in the x and y planes (i.e. horizontal and vertical directions).

All these items will be discussed separately and illustrated with figures.

For doing HMA rolling simulations by means of a FEM approach an input file must be drawn up that is written in such a way that the FEM tool involved, in this case DiekA, can read it. The input file is divided into blocks of information. The start of a block is marked with a star * on the first position of a new line. As an example a complete input file is given in the appendix M (roller pass 05 on the B lanes). The input is written just below the code words (in brackets) in the input file. The following items are major inputs and must be at least part of the file:

1. co-ordinates of the nodes and nodal numbers, (*NODES),
2. definition of elements and coupling of elements to nodes, (*ELEMENTS),
3. definition of boundary conditions (bottom, vertical borders and roller drum outline) and related to this, it has to be defined which and how different nodes are linked to each other (to connect e.g. a material element to a Coulomb element), (*CONNECT and *SUPPRES),
4. definition of material (asphalt and contact), (*MATERIAL),
5. rotated co-ordinate bases for definition of the roller drum, (*ROTATED BASIS),
6. surface options, for regulating in what extent the element mesh is allowed to deform, (*SURFACE),
7. the output that is wanted, forces, stresses, displacements, etc., (*OUTPUT),
8. pre-described incremental deformation step size (material displacement in x direction), (*PRESCRIBED).

The steps 1 to 3, and 5 to 8 are more or less standard steps in using FEM approaches for fluid mechanical or construction problems. Therefore these steps will not be discussed here. Step 4 however, definition of the material parameters as a function of VMA and temperature, is a major part and also very particular for this compaction research.

Estimation of the Rock parameters based on the material-measuring programme occurs in two stages. The first stage comprises deduction of the right VMA value and material temperature; this step is discussed in chapter 5 because it is based on information obtained from the test section. How critical state parameters are converted to the VMA level and material temperature is discussed in chapter 4. Chapter 4 discusses also how Rock material parameters can be obtained from critical state information is described. Deduction of Rock parameters based on critical state information is step by step illustrated in appendix N.

The free asphalt material surface

As an example the upper free surfaces of the asphalt in combination with the roller drum contour are illustrated in Figure 6.3 for roller pass 05 applied on the B lane of layer 2. The modelled set-up is chosen in such a way that the layer thickness decreases, caused by irrecoverable volumetric strain, from 55.83 mm to 55.06 mm. These layer thickness values do express the compaction increase due to the considered roller pass averaged over the height of the layer. These layer thickness values were obtained by monitoring the layer thickness trajectory of the experimental test section and used as input for the FEM simulation programme.

Using the output from a FEM simulation of a roller pass, the free material surface and the roller drum outline (perimeter) can be obtained; this is illustrated in Figure 6.3.

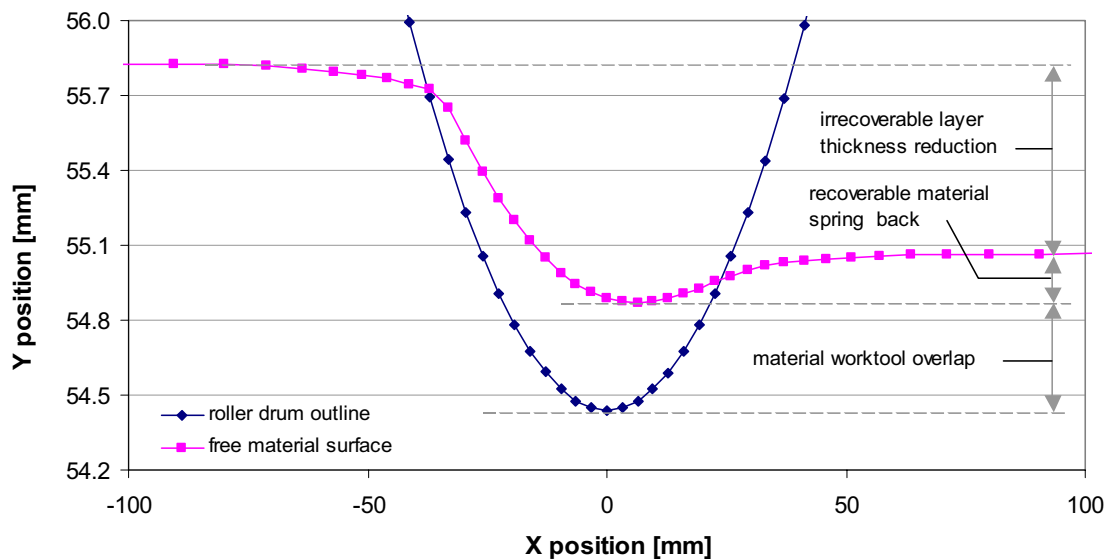


Figure 6.3 The free upper material surface of the HMA and the outline of the roller drum, pass 05, layer 2 lane B.

The figure illustrates that the roller drum penetrates the HMA material. This cannot be true in reality. Penetration (also called overlap) of the two interfaces of a contact element is a well-known phenomenon in FEM simulations. The extent of overlap depends on the contact stiffness in normal direction. If the contact parameters are incorrectly quantified the calculation will not proceed through all the prescribed deformation steps, and will derail during the simulation. If however the simulation set-up is well designed, a minor variation of the contact parameters will not disrupt the integrity of the results.

The way the upper material surface flows (more or less smoothly), forms a check on the tuning of the contact stiffness to the material stiffness being modelled. The material stiffness changes as a result of each subsequent roller pass. The contact stiffness parameters should be adjusted to reflect this increasing material stiffness. A contact stiffness of around 2.0 MPa gave good results in order to get a smooth running simulation of the first roller passes on relatively weak material. Later on, as the material got stronger and stiffer, the contact was modelled stiffer at about 12 MPa after pass 5. The modelled contact stiffness' also determines the extent of overlap. During the simulations presented here, the overlap was kept between 0.2 and 1.0 mm.

Another feature that can be extracted from the figure is the material recovery behind the roller drum. The extent of this recovery depends on the stress level that is obtained by rolling in combination with the recoverable material properties (i.e. variables E and ν used by Rock). The maximum stresses are not known prior to the simulations and thus the extent of recovery must be estimated, after all, the layer thickness reduction was the prescribed variable during the simulation. The vertical position of the roller

drum should therefore be estimated in such a way that with respect to overlap and material recovery the layer thickness reduction should be the observed value. Because overlap and material recovery are not known in advance, this target value is obtained by doing some test runs. The DiekA FEM approach used allows initial adjustment of specific nodes at definite positions. These possibilities can be used to achieve the correct layer thickness reduction for the individual roller pass simulations. However, during the simulations these possibilities were temporarily not available and thus the right roller position had to be determined by trial and error.

Vertical required rolling force

Using the proposed simulation set-up the required rolling force is calculated given the material characteristics and layer thickness reduction. The relation wanted should reflect the calculated rolling force in combination with the layer thickness reduction, the material properties and other rolling variables. Unfortunately the forces calculated are not correct because the E modules of the material are set to values higher than they are in reality. This is done to enable modelling of the unloading of the material more realistically. More details of this procedure are given in chapter 4.

Principal stresses and strains in the material

By means of the FEM DiekA the four strain components are computed for every node³⁹; the elastic shear strain, ε_{sh_el} , the plastic shear strain, ε_{sh_pl} , the elastic volumetric strain, ε_{vol_el} and the plastic volumetric strain, ε_{vol_pl} . The strains in which we are interested most are the plastic ones (ε_{vol_pl} and ε_{sh_pl}). The first one, ε_{vol_pl} , because it represents the irrecoverable volumetric strain, which is actually the compaction progress we are looking for. The second one, ε_{sh_pl} , because it represents the amount of plastic shear strain. The effects of plastic shear strains are not investigated in detail during this project but it is plausible that there is a relationship with shearing of the material and the risk of the occurrence of roller fissures. Irrecoverable strains are caused by the stress situation inside the material related to the yield locus (i.e. the border where elastic (recoverable) is turning over in plastic (irrecoverable)). Figure 6.4 and Figure 6.5 illustrate the deviatoric and isotropic stress patterns inside the material as a result of a simulation of the first roller pass applied on lane B.

³⁹ More in detail the stresses and strains will be calculated in the Gauss point of the element. From the gauss point stresses and strains will be extrapolated to the nodal points of the elements. The output of the calculation will then present an averaged value of the stress and strain over all elements involved.

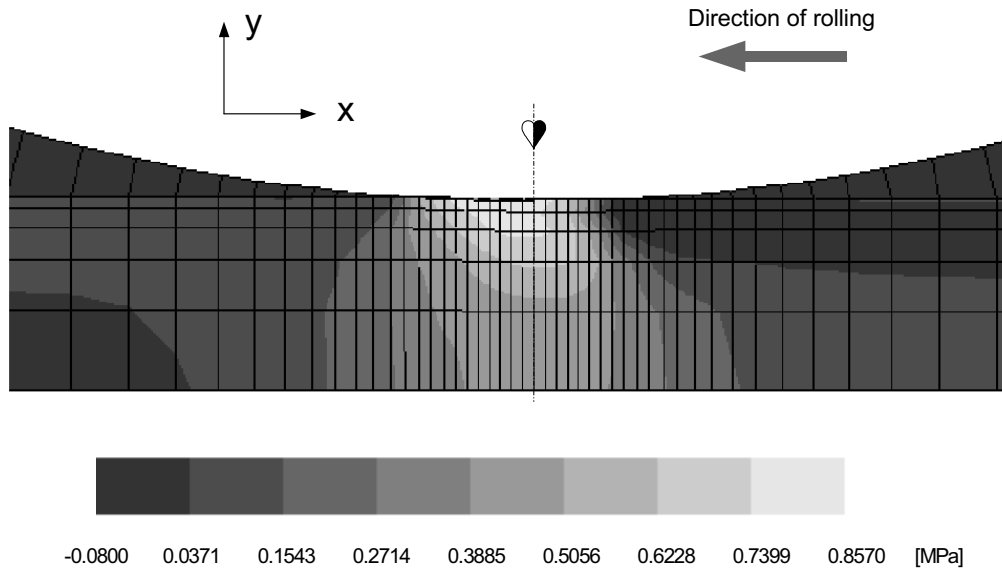


Figure 6.4 Isotropic normal stresses, p' , as a result of the first roller-drum pass 05 on lane B, layer 2.

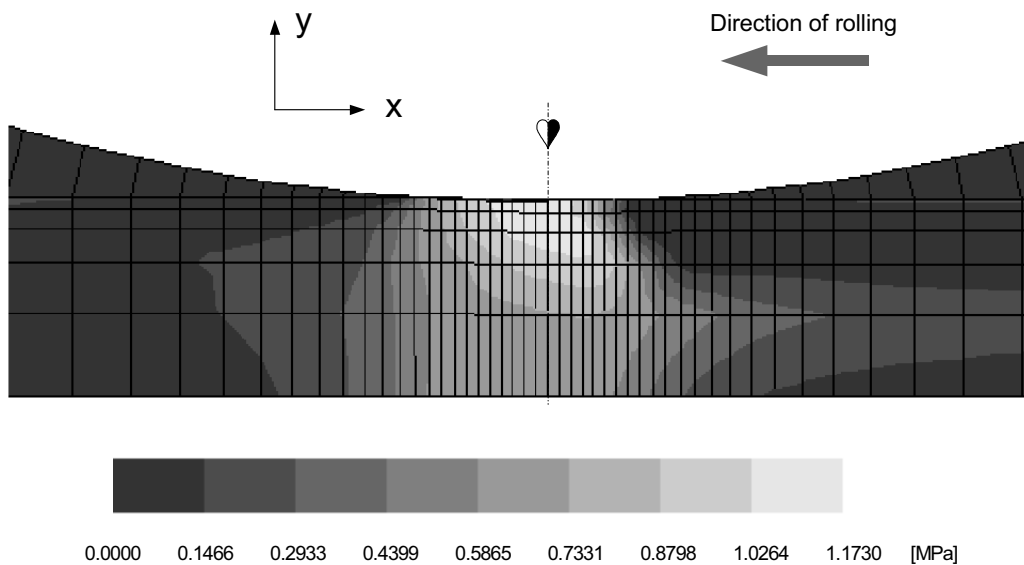


Figure 6.5 Deviator stresses, q , as a result of the first roller-drum pass 05 on lane B, layer 2.

The stress situation in p' and q is also followed along horizontal cross sections through the material. The results of three depths (respectively node row 1, at $y = 0.0$ mm, node row 3 at $y = 37.6$ mm and node row 5 at $y = 52.3$ mm) are illustrated in Figure 6.6. The figure indicates that high in the layer the stresses are large and spread over a shorter length whereas low in the layer the stress levels are small but spread over a much larger length. Furthermore, it can be seen that the isotropic compression stress p' becomes slightly negative (i.e. tension stresses) just after the roller drum loses contact with the material for nodal row 5. The Rock model parameters are quantified with values such that the modelled material has a (small) tensile strength. The value is initially fixed to 15% of the isotropic compressive strength and rises when hardening occurs.

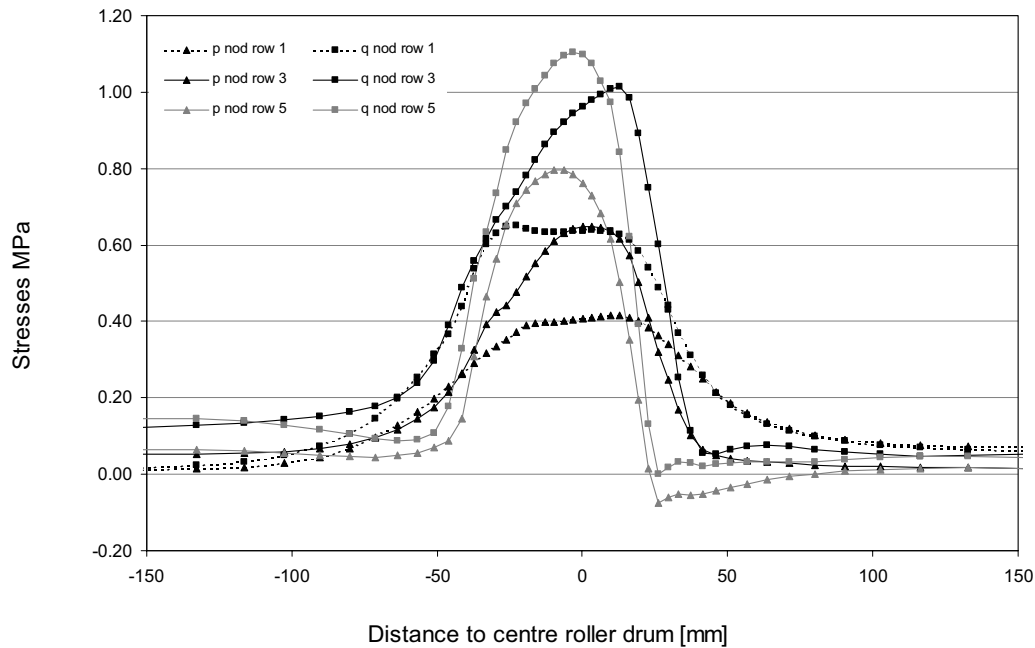


Figure 6.6 Isotropic normal compressive stress, p' , and the deviator stress, q , at three depth levels inside HMA when it is rolled.

Figure 6.7 shows the stress paths that material points inside a rolled material follow at a specific depth. The results at four depths ($y = 0.0, 37.6, 52.3$ and 55.8 mm) are illustrated in the p' and q space. In the figure three (parts of) yield loci are also plotted to indicate where the stress path meets the yield locus. In fact from this figure the stress level at which the material starts to flow plastically can be analysed. The different yield loci plotted in the figure also represent the material strength at different depths after applying that specific roller pass.

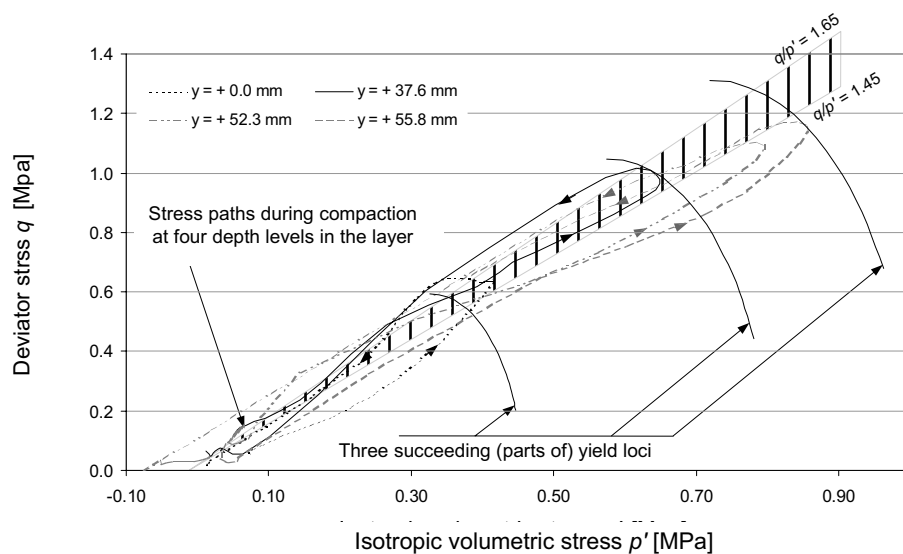


Figure 6.7 Stresses at four depth levels expressed in the $p':q$ plane together with three (partial) yield loci.

Figure 6.8 represents the q/p' ratio at four nodal row's. Because we are particular interested in plastic deformation the q/p' ratio is depicted for the plastic deformation domain. This occurs roughly from 80 mm in front of the centre of the roller drum to 20 mm behind it. The exact horizontal positions where plastic flow starts and ends are different for every individual depth in the layer. The q/p' ratio is relevant because it regulates material behaviour strongly. A high q/p' ratio means the material tends to shear. Relatively low q/p' ratios indicate that there are small shear stresses and high compressive stresses, this stress situation will result in little risk to damage during compaction. A negative aspect of low q/p' ratio can be that because of the absence of shear stresses the material is probably harder to compact (it needs large stress levels for ongoing compaction).

The lines in Figure 6.8 show that there are two “strange” line sections just in front of the roller drum. Analysis of these lines together with Figure 6.6 indicates that the two strange, very stiff parts of the lines for row 5 (in between -42 and -52 mm) and row 6 (in between -37 and -42 mm) are caused by an extreme sharp rise of the deviatoric stress q .

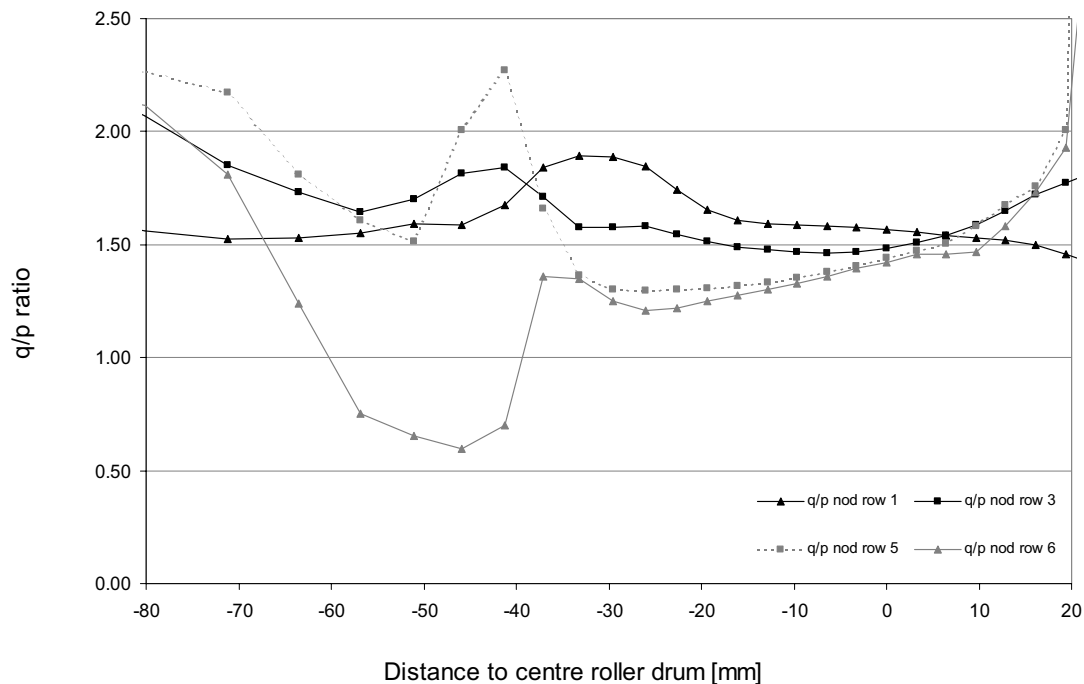


Figure 6.8 q/p' ratio's at four depth levels inside the material during plastic flow.

Relationship between plastic strain and stress

Deviator stress q and isotropic normal stress p' presents the current stress situation in the material. A strong relationship between the current stress situation and the strain exhibited by the material does exist. This relationship is enclosed in the modelled

yield locus. The position at which the stress situation meets the compression cap⁴⁰, the q over p' ratio, determines the direction of plastic flow. At high q/p' ratios, when the stress path meets the yield locus very high in the closure cap, the irrecoverable shear strain dominates over volumetric strain. At low q/p' ratio nevertheless, shear strain is almost zero and the major part of the irrecoverable strain will be volumetric. The situation is illustrated by Figure 6.9.

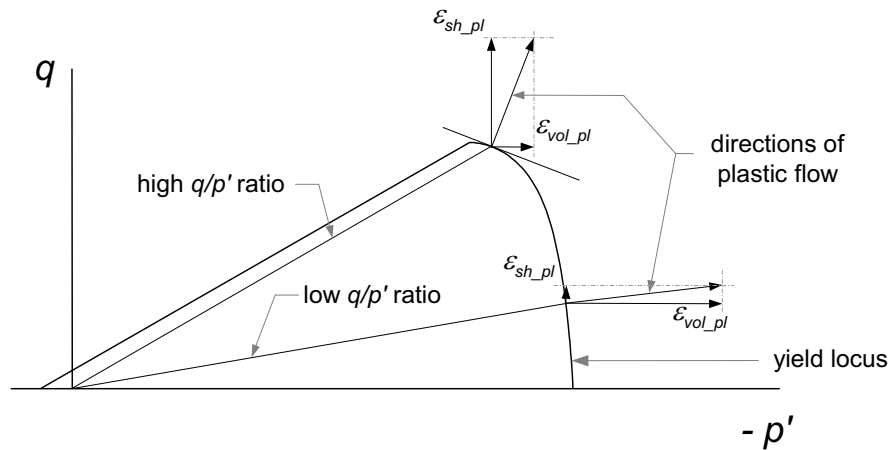


Figure 6.9 Effect of the position where the stress meets the yield locus on the distribution of the irrecoverable deviator strain and the irrecoverable volumetric strain.

Changing the shape of the yield locus closure cap can regulate the nature of the linkage between stress situation and the direction of irrecoverable flow. Using the Rock material model, the flow is modelled “associated”, which means that direction of irrecoverable deformation is directly linked to the yield locus shape. Material models that de-couple this link do exist, and such behaviour is known as non-associated flow. The principles of associated and non-associated flow are explained in more detail in chapter 3. Using non-associated flow generally increases the possibilities to model a material. Currently a fully non-associated model with suitable yield locus is not implemented in the DiekA approach. Additionally, using such a model asks for more accurate description of material behaviour based on advanced material tests.

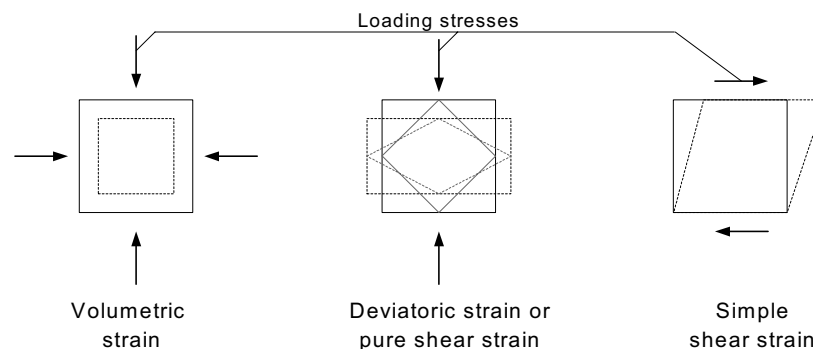


Figure 6.10 The effect of volumetric strain, deviatoric strain and shear strain on an initially square material element.

⁴⁰ Adequate compaction processes of granular materials like HMA, as it is the case in our simulations, do not serve too high shear strain levels.

For the sake of completeness the different types of strains expressed are illustrated in Figure 6.10. In the plot “deviatoric strain or pure shear strain” two patterns are illustrated for the same strain condition. Note that only the orientation differs. Figure 6.11 and Figure 6.12 illustrate the simulated patterns of the irrecoverable volumetric and deviatoric strain in the material for the first roller-drum passes lane B of layer 2 (numbered as 0.5B). The graphs clearly indicate that behind the centre of the roller drum (right from the drum as the roller moves from the right hand side of the graph to the left hand side) the irrecoverable strain mainly develops in the upper part of the layer. This counts for both the volumetric and the deviatoric strain. In our simulations the positions of highest volumetric strain and deviatoric strain were approximately the same in all situations.

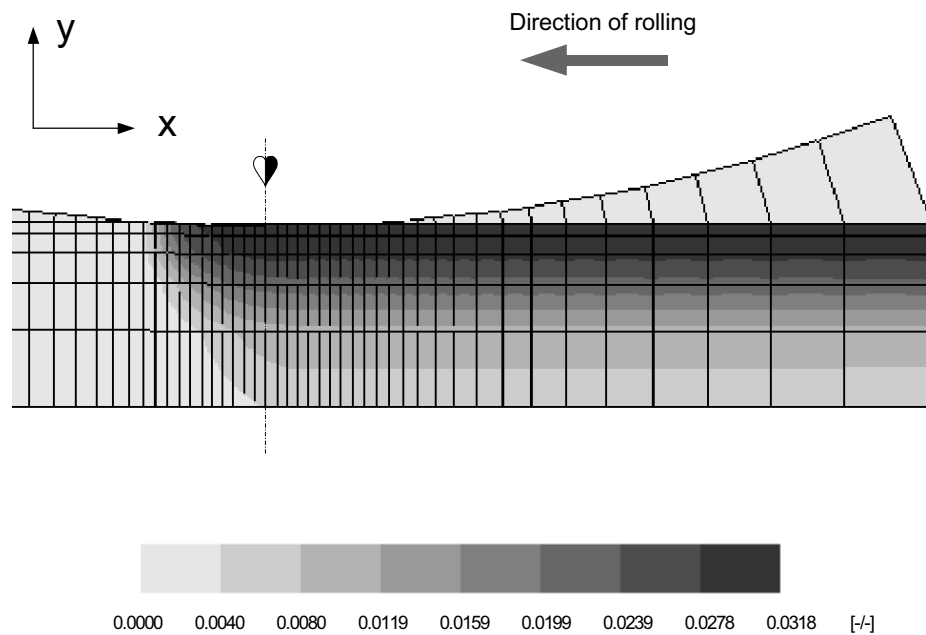


Figure 6.11 Irrecoverable volumetric strain as a result of roller pass 0.5 on lane B, layer 2.

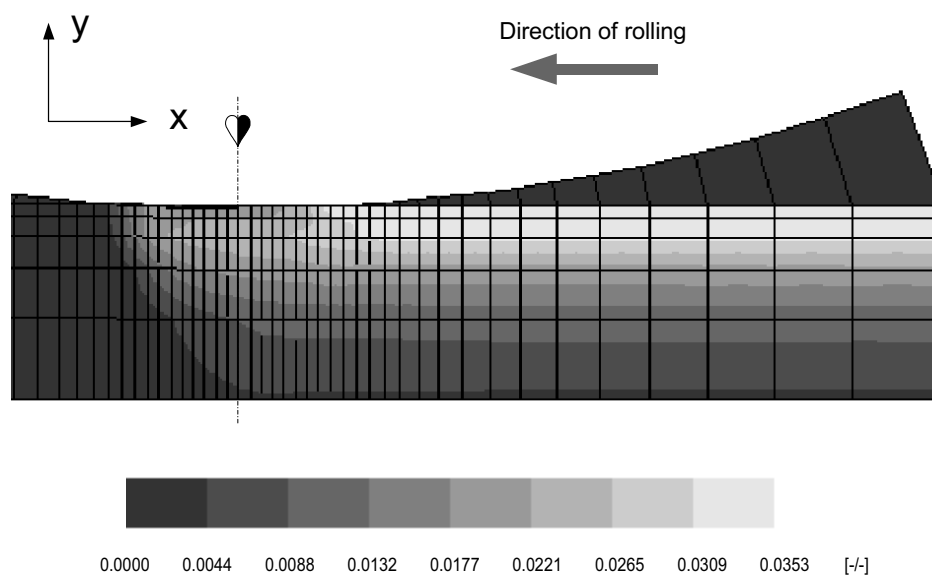


Figure 6.12 Irrecoverable deviatoric strain as a result of roller pass 0.5 on lane B, layer 2.

The strain figures further illustrate that at locations at the right hand side of the roller drum centre, where the drum has lost contact with the material, the strains do not change anymore along a horizontal line. This is plausible because behind the roller drum the primary stresses p' and q became zero again, which implies that the driving forces (or stresses) for changing strains are absent. When the plots do show changes of plastic strain along a horizontal line after the contact between roller drum and HMA had been lost, the simulation should be carefully checked because of the suspicious results.

Plotting the irrecoverable strain patterns does make sense because it indicates the position and amount of material deformation. Attention must also be paid to the plastic volumetric strain because it represents the progress in compaction. Further should one pay attention to the irrecoverable shear strain because this indicates that the material is shearing. This could result in initial cracks in the material.

Shear stresses

Shear stresses are responsible for shearing of the material. In Figure 6.13 the shear stress pattern of roller pass 05 is illustrated. These shear stress patterns do give intuitively the best view on what really occurs inside the material when a roller is compacting it. The shear stress parameter does give approximately the same information as the deviator stress parameter, q . A small distinction is that the variable “shear stress” can go from negative to positive and expresses the direction of shear whereas the deviatoric stress q runs from zero to a maximum, this parameter only expresses how far the stress condition is away from pure normal compression. The sign of the shear stress does not affect the material behaviour; it merely indicates the direction in which the material is sheared. What, on the other hand, can be important is a change in the shear direction, from positive into negative or vice versa, see Figure 6.13. This can affect compaction.

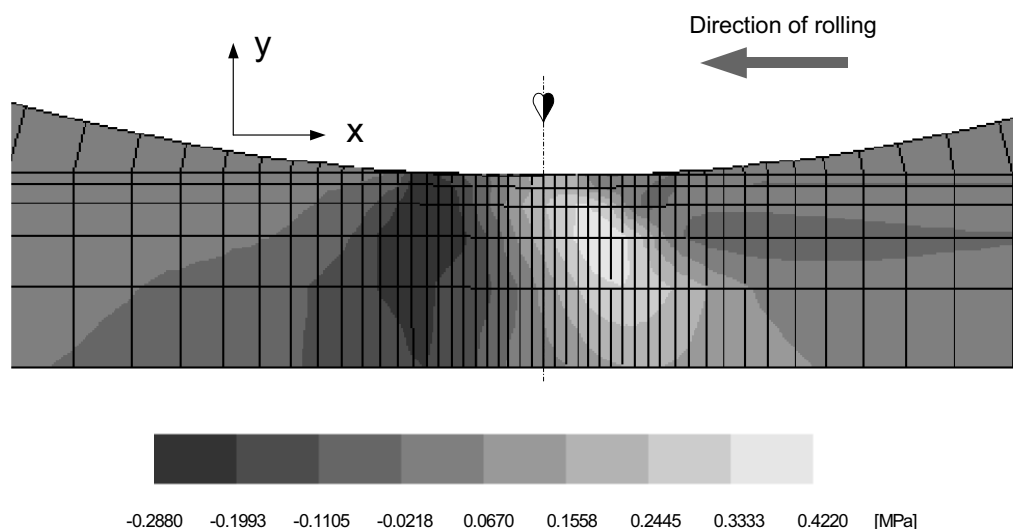


Figure 6.13 Shear stresses as a result of roller pass 05 on lane B, layer 2.

The shear strain pattern presented in Figure 6.13 illustrates the reverse of the shear stresses beneath the roller drum. Just in front of the roller drum the material is pushed up (initially square material elements would become high and small). Under and behind the roller drum centre the material becomes squeezed horizontally (initially square material elements would become wide and thin). The largest rate (change) in shear stress occurs under the roller drum just in front of its centre. This is also the position where the deviator stress q is the highest. In this context it is also very informative to consider the rotation of the principal stresses inside the material because it indicates how the material is exactly loaded as a result of rolling. The principal stresses and their orientations are illustrated in Figure 6.14. The length of the vectors represents the local stress levels.

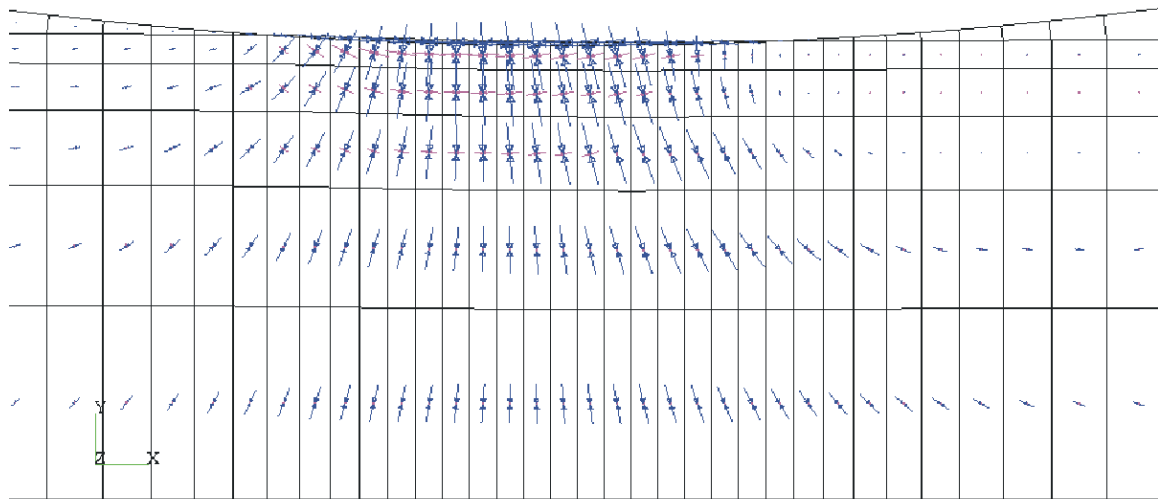


Figure 6.14 The principal stresses in the HMA material while rolling it.

Incremental displacements x and y .

Figure 6.15 illustrates the incremental displacements (i.e. displacement per pre-described deformation step) of the material under compaction in the horizontal direction. The direct output of the DiekA calculation shows material movements of around 0.2 mm per step size as a pre-described movement of the material as it is forced through the mesh in a horizontal direction. However, because it is known that the material in reality stays where it is (i.e. no movement in horizontal direction) it was better to reduce all the material movement output obtained with that pre-described step size of 0.2 mm. Now the figure expresses material movement, as it would be in reality “in” or “opposite to” the rolling direction. Areas with a negative sign express movement in the rolling direction, areas with positive sign movement reverse to the rolling direction. The pre-described incremental displacement is movement of the material related to the roller drum (or v.v. movement of the roller drum related to the material). When a roller drum drives at a certain speed it rides a particular distance in a unit of time. Every deformation step of the material can also be seen as a fixed time

unit. Therefore the movement of the material per step size can be seen as a speed of the roller drum. This argument does not only hold for the horizontal movements and speed, but also holds for the material movements in the vertical direction. When the roller speed is known, it is possible to calculate via the horizontal deformation per step size the vertical material speeds from the vertical incremental displacements (Figure 6.17).

In Figure 6.15 a dark area can be seen directly beneath the contact surface roller drum-rolled material and deeper inside the layer a lighter one. In this dark area the material movement is up to -0.002 mm per step, which means 0.002 mm in the direction of rolling. The material is enforced underneath the roller drum with 0.2 mm per step so the local horizontal material speed in the dark area is up to 1% of the roller speed. The lighter areas indicate a material movement of $+0.0007$, which is a movement of 0.0007 mm in reverse direction of rolling per step. This is about 0.35% of the roller speed (in the reverse direction). Also at the top of the layer just in front of and just behind the roller drum light areas exist, which indicates here that the material movement is reverse to the rolling direction. Apparently the material seems to be restrained (or obstructed) by the roller drum.

Globally it can be seen that the bulk of the material has a speed around zero, whereas locally small areas do exist where the speed is reverse to the direction of rolling. Intuitively such a pattern is plausible. When at certain locations the speed is below the average then it must be higher at other areas because at the borders the speed of the “inflow” and “outflow” is prescribed on the average level of 0.2 mm/step.

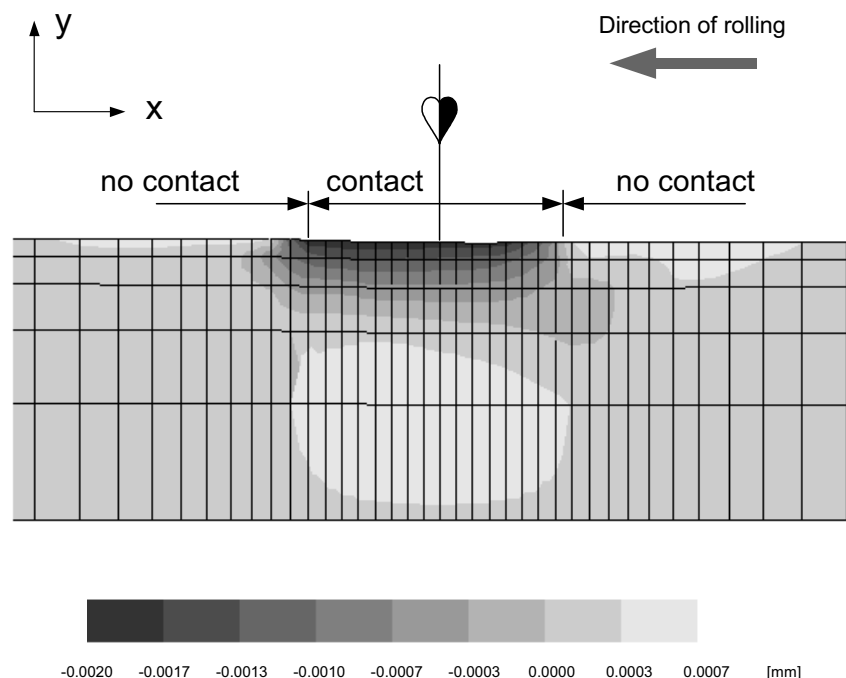


Figure 6.15 Incremental material displacements in the x direction (i.e. horizontal material movement). A negative sign means movement in the rolling direction, a positive sign means movement reverse to the rolling direction.

Figure 6.16 and Figure 6.17 illustrate the incremental vertical material movement. Figure 6.17 focuses in more detail on the contact area just beneath the roller drum. Both graphs indicate that the average movement is downward oriented (negative signs in the material means the material moves downward), which, of course, must be the case because the layer thickness decreases during rolling and the material movement is related to the bottom of the layer. The material movement expressed in the plots (i.e. material speed at which the material moves) is related to the roller speed. For instance, just in front of the roller drum the material moves vertically with 0.006 mm/step downward (i.e. 3% of the roller speed). The vertical speed of the material will be analysed in two steps a.) generic; the whole material piece, and, b.) detailed; just around the roller drum-material contact.

a.) Global, whole material piece:

- far upstream; material movement is 0.3% of incremental step-size, upwards,
- just upstream; material movement is 0.3% of incremental step-size, downwards,
- just downstream; material movement is 0.3% of incremental step-size, upwards,
- far downstream; material movement is 0.3% of incremental step-size, downwards.

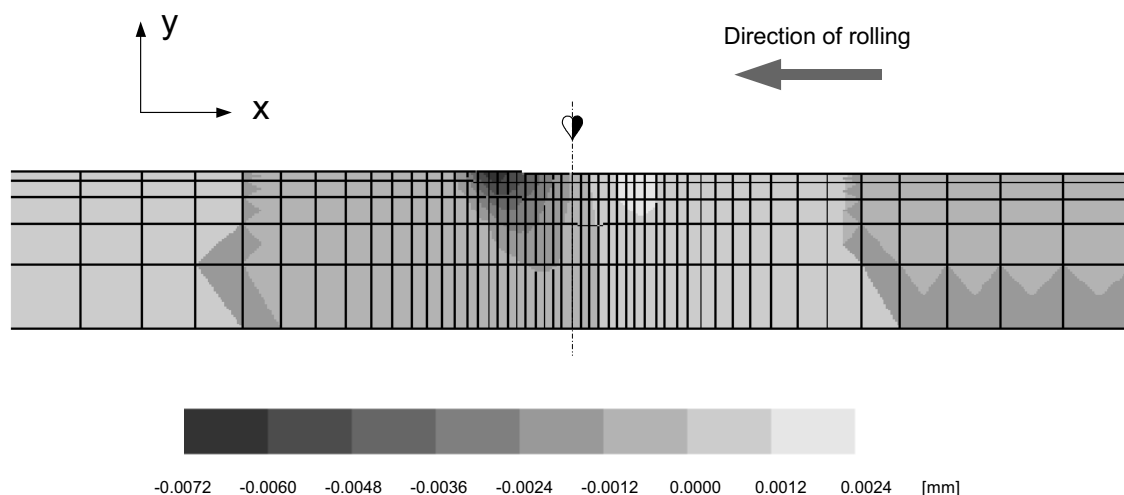


Figure 6.16 Incremental material displacements in the y direction, (i.e. vertical material movement).

b.) More detailed, around the roller drum-material contact, high in the layer:

- around the point contact/no contact, upstream; material movement is 3.2% of incremental step-size, downwards,
- around the point contact/no contact, downstream; material movement is 0.7% of incremental step-size, upwards.

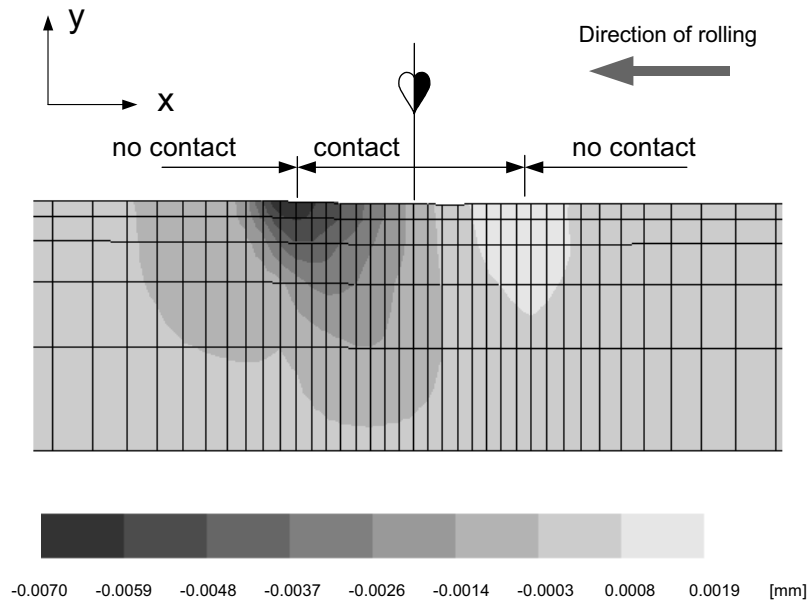


Figure 6.17 Incremental material displacements in the y direction (i.e. vertical material movement). A positive sign means movement upwards, a negative sign means movement downwards.

It looks quite plausible that the strongest movements are downwards and just beneath the front part of the drum. It is intuitively also correct that just beneath the backside of the roller drum movements are upwards, because elastic recovery is taking place here. The upstream and downstream movements further away from the drum centre behave like a wave motion. One can imagine that such a phenomenon happens just in front of a drum since it compacts a softer medium. An analysis of the free material surface, mainly in front of the roller drum, may indicate such an event. Material that is pushed forward by the roller drum is sometimes also seen during rolling in practice.

Particle tracing

One of the output possibilities of an ALE calculation done with the DiekA approach is known as “particle tracing”. This application follows the material while it is streaming through the finite element mesh during the simulation. For a rolling problem one expects that material initially at the top of the layer also stay at the top of that layer. The same counts for material at the bottom of the layer. It would not be plausible if, due to rolling, the material at the bottom was mixed with material at the top. Furthermore, it would not be expected that there are large differences in horizontal movements of the material in the horizontal direction at different depth levels in the layer.

In Figure 6.18 and Figure 6.19 the particle tracing of the material is illustrated in respectively the X and Y direction. Both graphs do show a neat stratification, which indicates correctness of the material movements during the simulation. Figure 6.18 shows almost perfect vertical contours. It implies that the material is pushed gradually forward. The graphs indicate that the material from the left-hand side (at position $x = -200$ mm) comes from initial position $X = -605.6$ mm related to the co-ordinate axis (i.e. $X = 0$ equals the centre of the roller drum). The material at this location has thus moved 405.6 mm. The material currently on the right hand side of the figure (at

position $x=+200$ mm) comes initially from the position $X= -205.6$ mm, and has also moved 405.6 mm. So from these results it could be established that the whole piece of material (400 mm long) is pushed from left to the right over exactly⁴¹ 405.6 mm and did not shrink or enlarge. This must also be the case because of the way the simulation is set up.

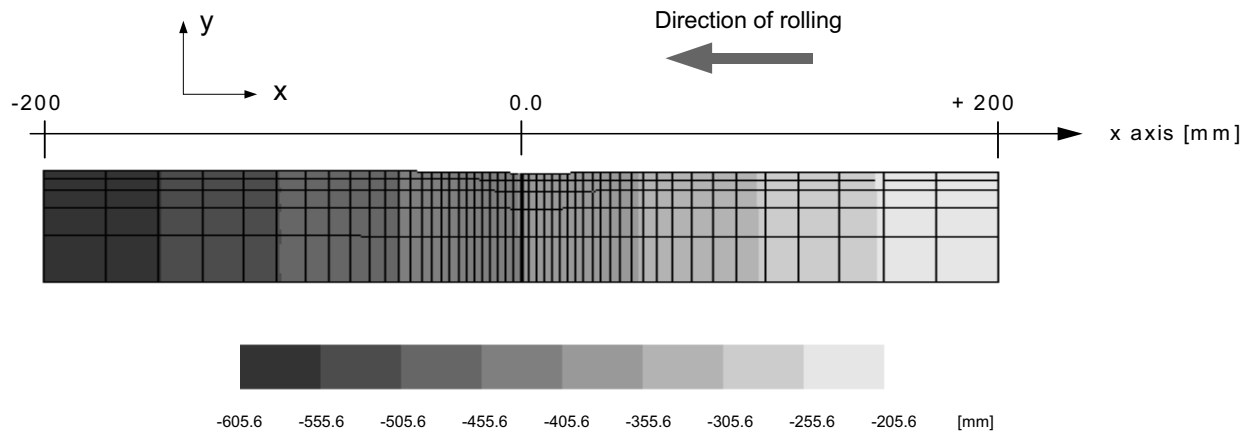


Figure 6.18 Particle tracing positions in the X direction.

Figure 6.19 illustrates that the borders of the vertical movement neatly follow the lines in between the free material surface and the bottom of the rolled layer. It indicates that material that initially was at the upper part of the structure stays at that upper part of the structure during rolling. This is as expected. The figure shows a “streamline” along the upper surface of the material. It explains that material that was initially (at position $x = -200$) at the upper surface (light grey area, $y = 48.85 - 55.83$ mm) stays at the highest location inside the layer under the roller drum (position $x = 0.0$) and after compaction (position $x = +200$). The different stream lines are neatly parallel, it indicates that no strange things did occur.

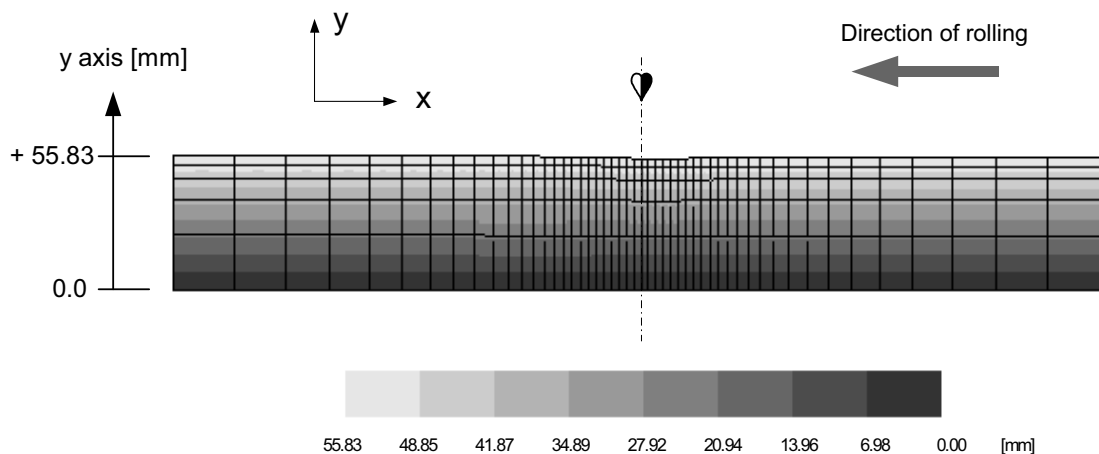


Figure 6.19 Particle tracing positions in the Y direction.

⁴¹ The material that initially was on the position -205.6 mm is currently on the position $+200.0$ mm. So the movement is from -205.6 to $+200.0$ is 405.6 mm.

6.3 Subsequent roller passes

It has been shown so far that an analysis of the results of an individual roller pass yields a lot of information. Nevertheless, a typical roller pass forms part of an overall rolling process, which requires 10 to 15 passes. Mostly the first passes are of major importance and also the most critical in realising good compaction without generating damage. Furthermore, the results from previous roller passes, in terms of material compaction state, must be taken into account when simulating a subsequent roller pass.

From the simulated rolling process two items are of major interest and have been calculated:

- development of the compaction progress in the vertical direction of the layer expressed by bulk density,
- development of the compaction progress in vertical direction of the layer expressed by VMA .

Figure 6.20 and Figure 6.21 show the progress in compaction as calculated by means of DiekA (expressed in bulk density and VMA) during 6 simulated roller passes applied on the B lanes of layer 2. The figures show that the progress (increase) of the bulk density is quite similar (except the sign) to the progress (decrease) of the Voids in the Mineral Aggregate (VMA). This should of course be the case.

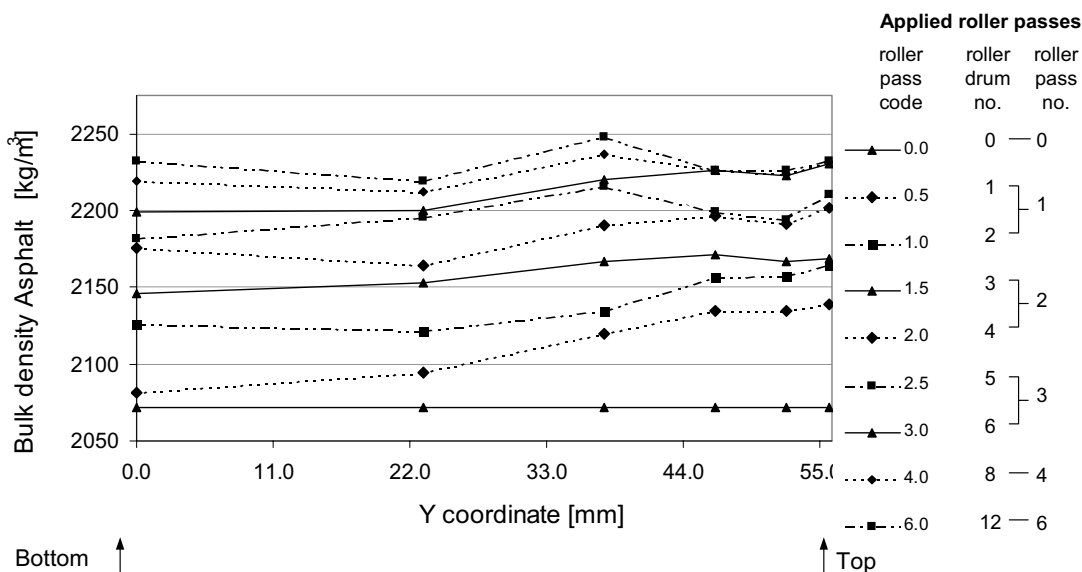


Figure 6.20 Development of the bulk density of the material achieved by subsequent roller passes, layer 2 lanes B (calculated results).

Analysis of the progress in compaction, with respect to the height of the material in the layer, shows that the first 6 roller drum passes (first three roller passes) are the most important. During these passes the bulk density increased from about 2070 to 2220 kg/m³. The VMA level decreased from almost 0.26 to 0.20. From the figure it can be seen that the first roller drum pass (code 0.5) achieves the largest compaction progress in the top region of the layer. In the second roller drum pass the largest compaction progress occurred low in the layer whereas also medium compaction

progress is achieved high in the layer. During the third roller drum pass (code 1.5) the majority of the compaction increase is achieved in the middle of the layer. This seems to be a process of levelling. Large compaction increase is achieved at positions where the stresses are high (first pass high in the layer) and the current material is “soft” (because of compaction already achieved, e.g. pass 2 “low”), or a combination of these two (pass 3 “middle”).

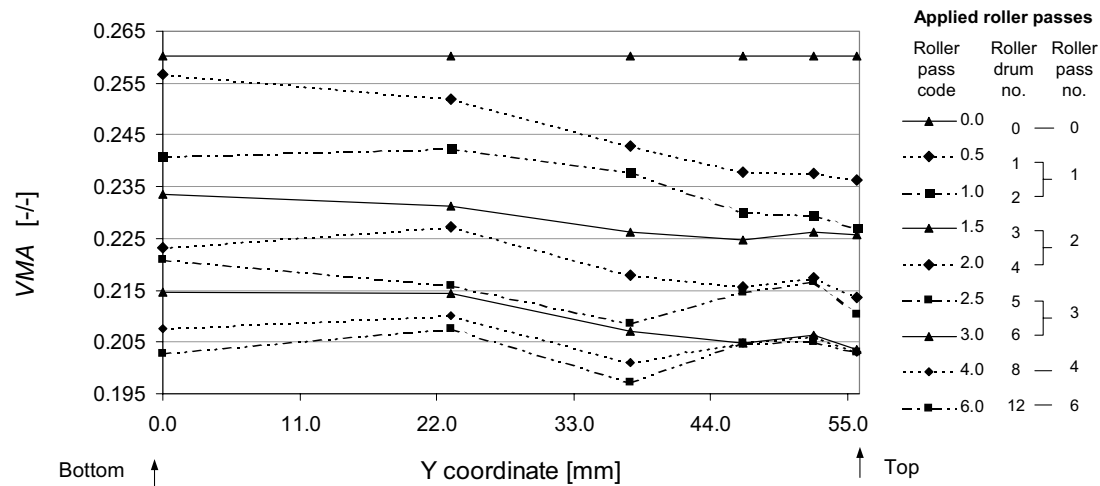


Figure 6.21 Development of the Voids in the Mineral Aggregate (*VMA*) of the material achieved by subsequent roller passes (calculated results).

Analysis of the compaction progress shows that, a more homogeneously compacted layer was achieved later on (after about 6 passes) probably because of the nature of this levelling process. Further, the compaction progress per roller step decreases as the rolling process proceeds. This was measured during monitoring the compaction test section. In fact, the compaction progress that is calculated by doing the simulations is a re-distribution of pre-described plastic deformation.

Contact stiffness, overlap and contact stress

Analyses of the variables contact stiffness, overlap achieved and contact stress between drum and material does give control over the calculation. There is a direct correlation between these variables. The contact stiffness value can be selected. In a selected FEM set-up the roller drum is “inserted” at a specific position “in” the material. Given specific material properties and a contact stiffness this results in a particular contact pressure between material and roller drum. This contact pressure together with the contact stiffness modelled determines the magnitude of overlap between roller drum and material. The magnitude of this overlap together with the resulting stress level and the material properties determines the extent to what the material surface recovers.

By changing the contact stiffness as well, the contact pressure, the material-roller drum overlap and thus the resulting irrecoverable material deformation change. A stiffer modelled contact increases the contact pressure, decreases the overlap and therefore increases irrecoverable deformation. The interaction between these

variables/parameters and how they change at subsequent roller passes is shown in Figure 6.22.

Typically, as a result of ongoing compaction the material stiffness increases too. This increasing material stiffness results also in an increasing contact stress when plastic deformation of the material for further compaction is enforced.

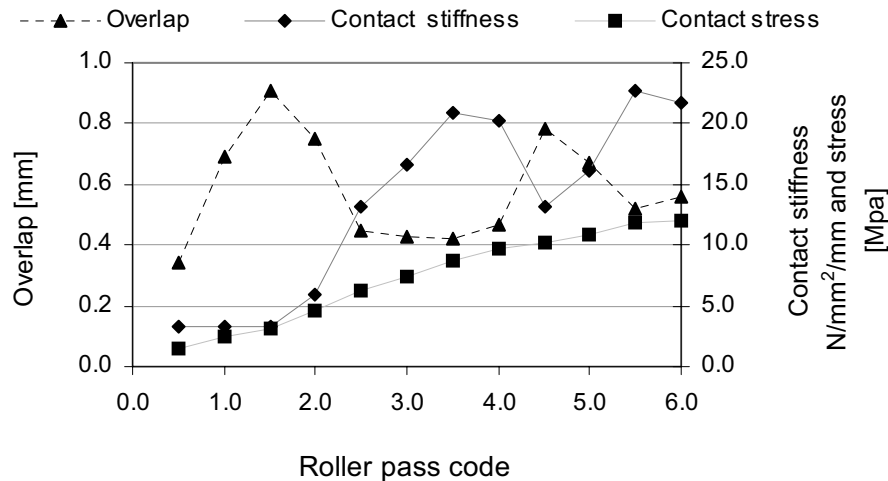


Figure 6.22 Progress of contact information (i.e. overlap, contact stiffness and contact pressure) as a result of the subsequent simulated roller passes no. 1 till 6 on the B lanes.

For running numerically stable calculations the contact stiffness should be in balance with the material stiffness. This implies that the contact stiffness must increase when due to applied roller passes the compaction level increased too. The overlap and the contact stiffness are, within certain limits, arbitrary chosen values. Contact stiffness, contact stress and overlap for the simulated roller passes coded 0.5 to 6.0 on the B lanes of layer 2 are shown in Figure 6.22. Normally one would adjust contact stiffness during the simulation process in such a way that it increases proportionally with the contact stress. The overlap should then stay more or less on constant extent. Because of the pilot character of our simulations this was not the case here⁴². Figure 6.22 indicates that the contact stiffness of roller passes coded; 1.0, 1.5, 2.0, 4.5 and 5.0 was relatively low, which made the overlap a little too large⁴³, however, these deficiencies from the ideal situation were not that large that they would harm the results significantly. During our calculations the overlap was limited to a maximum 1.0 mm whereas contact stiffness was in between 3 to 23 N/mm²/mm. From the information obtained during the calculations it is concluded that it was possible to limit the overlap for our calculations to about 0.5 mm. This can be achieved by an improved fine tuning of the contact stiffness to the actual material stiffness.

⁴² When the series of calculations had to be done a second time one could adjust the overlap within a more narrow range.

⁴³ That the contact stiffness of these roller passes were too low, and caused by that, the overlap too large, became known when the total series of simulations where completed and the results analysed. The criterion is that the overlap should be as small as possible but on the other hand so large that the simulation does run numerically stable. Details of this can be found in chapter 4

It is possible to adjust the magnitude of overlap by changing the normal stiffness of the contact elements. The overlap should be not too large because overlap causes a somewhat flattened contour. Such a deviance from the real rolling drum contour affects the stress distribution enforced by the drum on the material. On the other hand the overlap should not be too little. The modelling of contact is so sensitive because contact is a strongly non-linear phenomenon. A contact that is modelled stiff, limits the overlap, but because of that high stiffness, just small variations in the distance of the roller drum to the rolled material already results in strong variations in the contact pressure. It implies that a contact stiffness chosen too high may easily result in a calculation process that runs in an unstable fashion.

Plastic material deformation and elastic material recovery.

For the first roller drum pass (code 05) of the B lanes, the plastic material deformation and the recovery of the free material surface, were already shown in Figure 6.3. The plastic deformation is the extent the layer thickness has decreased due to a specific roller pass. It is the magnitude to which the calculation is driven (i.e. controlled).

During the subsequent roller passes the ratio between elastic material recovery and plastic deformation changes significantly, as was expected. This happens because rolling compacts the material and thus makes it stronger⁴⁴. The implication of this is that the material continues to behave elastically until higher stress levels. While the simulation of the rolling process proceeds, the magnitude of the elastic part of material deformation increases and the magnitude of plastic deformation decreases. It implies that the ratio between recoverable and irrecoverable deformation changes considerably. The development of the plastic material deformation and elastic material recovery is depicted for the subsequent roller passes applied on layer 2 of the B lanes in Figure 6.23. The plastic deformation line is the extent that the layer became thinner and corresponds therefore with the measured line as expressed in Figure 5.16 of chapter 5 (i.e. it was input).

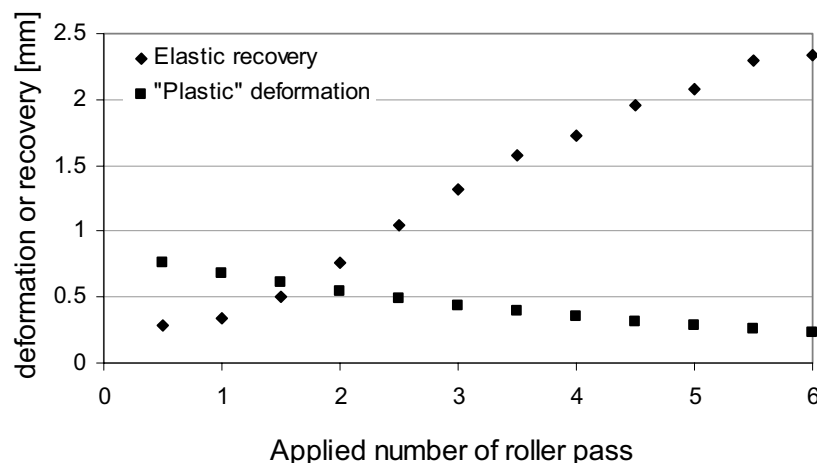


Figure 6.23 Progress of recoverable and irrecoverable material deformation as a result of the subsequent simulated roller passes no. 1 till 6 on the B lanes.

⁴⁴ In terms of critical state the yield locus size increases. When the specific volume- $\log p'$ path is considered the transition point where elastic strains go over in plastic moves to higher p' values.

Obtained vertical compaction forces

In chapter 4 it was already noted that Rock did not model the HMA behaviour perfectly. It is mainly the elastic part of Rock that expresses shortcomings. It is also discussed how, by modelling the E modulus too stiff, an approximation is made in such a way that the magnitude of plastic deformation in the material corresponds to how it should be in reality, in combination with a reasonable unloading behaviour. However, the results that are found using such an approach, while simulating different roller passes, indicate that the required rolling forces are (much) too high and become even higher when the compaction process proceeded, see Figure 6.24. It is thought that the reason for these too large obtained rolling forces can be explained by the too stiff modelled E modulus.

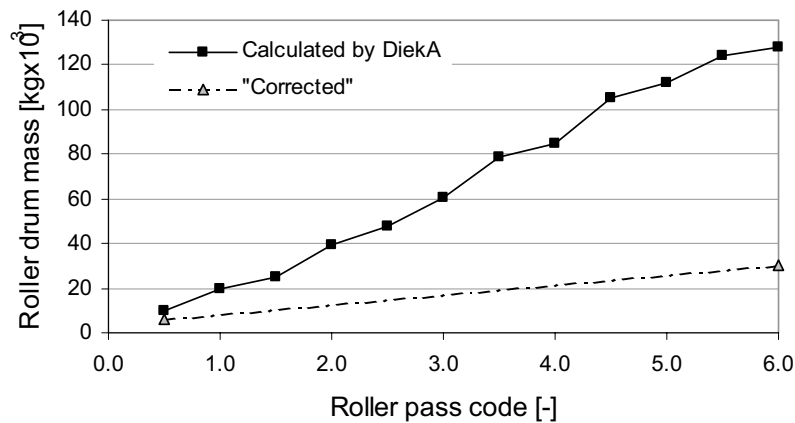


Figure 6.24 The calculated forces that are required to deform the HMA material as measured from the B lane of layer 2.

As a first step in analysing this reasoning a view is created of the material in which locations of elastic and plastic deformation are marked, see Figure 6.25. It indicates that a reasonable area is loaded to plastic stress levels but an even larger area is subjected to stress levels that fall inside the elastic domain.

To check how far this too stiff modelled E modules could be responsible for the too high obtained (calculated) roller drum forces, a rough estimation for the roller drum forces of the passes 0.5 and 6.0 was made. During this analysis the force required for plastic deformation is separated from the force required for elastic deformation. The elastic part is “corrected” and subsequently a new total force calculated. The obtained “corrected total forces” are also depicted in Figure 6.24.

If this corrected procedure is applied the calculated forces for passes 0.5 and 6.0 become respectively 6.06 tonne and 30.4 tonne which is a factor of 1.73 and 8.7 wrong related to the roller drum weight applied in reality by the HAMM DV 6.42 (i.e 3.5 tonne). Because the rolling forces could not be calculated correctly, the ultimate validations (comparing the simulation results to results obtained from the test section) could not be done.

To investigate what the cause could be for this remaining error in rolling force, it is analysed if the difference between real material behaviour and modelled material behaviour in the $VMA:\log p'$ plane could be responsible (see also Figure 4.25). This procedure is more in detail discussed in appendix O, although it could not be quantified because material measurements for the actual VMA values later on in the rolling process were not involved in the laboratory measuring programme.

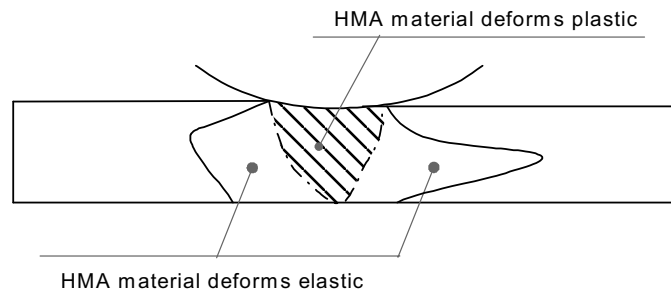


Figure 6.25 Locations inside the modelled material where material is plastic and elastic.

Summary

In conclusion it can be said that the results of the simulations have been reasonably successful. They have provided a good insight in the behaviour of the material during compaction and how the material “flows” through the finite element mesh. It is however clear a skilled operator is needed to perform such an analysis. It is certainly not a tool that can be applied on an everyday basis e.g. by consultants. The simulations have been influenced by the fact that it was not yet possible to apply a load and determine then the deformation. Unfortunately the process had to be; apply a deformation and calculate the load. Furthermore, the simulations have been influenced by the fact that the Rock model, and especially the elastic part of it, did not model the behaviour of the HMA as measured in the laboratory correctly. It has been shown that this had a large influence on the back calculated roller forces. Therefore the ultimately validation of comparing the compaction results to results obtained from the test section could not be done.

7 Conclusions and recommendations

In this chapter conclusions and recommendations are drawn from the work done in this HMA compaction project. In the first section the issues raised in chapter 1 will be addressed. Based on those answers the final conclusions are drawn. In the second part of this section potential applications of the simulation tool developed are discussed.

In section 7.2 improvements to the tool based on experience gained during the course of the project are proposed. Finally possible improvements that can be applied to road building technology will be discussed.

7.1 Conclusions

The main objectives of this thesis project was to “*assess the suitability of various options to simulate the compaction process of HMA, to identify and select the most promising option and refine the selected option into a working model capable of accurately simulating the compaction process of HMA*”. All these objectives have been met, although there is still scope for refinement of the model developed. Some of these issues are identified as recommendations of further work later in this chapter.

In the set up of the project, covered in chapter 1, a set of four research questions was identified. Following are brief answers to the four research questions based on theoretical investigations, material testing and simulations done.

Answers to the research questions

Question 1

“What happens precisely during compaction of HMA? Are there models available that describe adequately the behaviour of asphalt mixes during compaction? Which materials behave similarly and are there suitable material models available? What does a suitable model look like?”

Detailed investigation of the constitution, the behaviour of soils and HMA, illustrate that although there are a lot of differences between both materials, there are also a lot of similarities. One of these similarities is the mechanical behaviour that is based on particle reorientation. A theoretical framework that describes such behaviour is the *critical state* theory.

The idea to apply soil mechanics principles was borne from the analogy between the internal structure of sandy soils and asphalt. Both soil and asphalt are mixtures of particles, fluid and air filled voids. It has been shown that this analogy appears to reason. A material-measuring programme demonstrates that critical state principles are applicable to model the HMA material behaviour. In conclusion it can be stated that these is a suitable model that describes the behaviour of asphalt mixtures during compaction. The critical state model, well known from soil mechanics, can be perfectly used for this purpose.

Question 2

“Is there equipment available that (after modification) is suitable to measure the material parameters of HMA mixtures when being compacted? What are the requirements of suitable equipment? How can material parameters be measured?”

Standard equipment for doing tests on hot HMA samples to obtain critical state parameters were not available. The Stabilometer was a good starting point in spite of not having sufficient volume control over the sample. Furthermore, the equipment cannot withstand typical temperatures encountered in time during compaction. Therefore, as a part of the project, the Hveem Stabilometer, was modified to make it suitable for the necessary measurements. With the Modified Hveem Stabilometer (MHSM) two measurement programmes have been carried out: the first one to test the response of the equipment, and the second to test whether the critical state theory describes HMA behaviour adequately. By performing the tests we proved that the response of the equipment was adequate. The newly developed MHSM performed well, however, the equipment was still not suitable for hot materials. In order to gather information of how hot material behaves the mixtures were also modified, using lower viscosity bitumen, to simulate the behaviour of hot asphalt without increasing the temperature. In conclusion it can be stated that the modified Hveem Stabilometer as developed in this project, together with the use of bitumen that has the same viscosity at room temperature as ordinary bitumen at compaction temperature, proved to be an excellent tool to determine material parameters of HMA when compacted.

Question 3

“Given a suitable material model and given a set of material parameters, is simulation of a HMA compaction process by rolling possible? Which tool can be used for simulating such a process? What are the requirements for such a simulation tool?”

With use of FEM it is possible to simulate and study the progress of HMA compaction in detail. FEM simulations offer a profound insight in what actually happens during compaction within the material. However, the FEM tool used must be suitable for the task. In the case of rolling HMA the selected approach should be of the ALE type, it must be able to model contact and the approach must contain a material code that describes behaviour in accordance with the critical state principles.

For this thesis project the FEM code DiekA was selected. DiekA can do ALE calculations and can model contact phenomena. However, a drawback of that code was that the material code implemented, “Rock”, could not completely fulfil the demands with respect to critical state principles. However, with some adaptations it is possible to run good simulations of HMA mixtures being compacted using a static steel roller. Good insight in stress, strain and deformation patterns could be obtained although an appropriate roller drum weight could not be calculated. ALE is a prerequisite for simulation of processes of rolling; it lets material flow through the mesh, and it is required for outlining contact elements. A rolling process cannot be simulated without contact. The ALE method handled the outlining of nodes perfectly on both sides of contact elements.

In conclusion it can be stated that FEM approaches in general are perfectly suited to simulate compaction processes of asphalt on condition that the selected FEM comprises the right features. The simulations did improve the insight in stresses, strains and material movements caused by rolling extremely well, however, for being able to achieve the simulations a skilled operator is required. For calculation of the correct rolling forces implementation of a real critical state model must be achieved.

Question 4

“What information is needed as input for simulation of a HMA compaction process? What information can be used to validate a developed simulation tool for HMA compaction? How can such a simulation tool be validated?”

As part of the project a test section was built to acquire data on the actual compaction process -as happens in the real world- for the purpose of validation of the simulation and for gathering information for the rolling simulations. The test section consisted of two layers Dense Asphalt Concrete (DAC) 0/16, that were compacted by a static steel roller.

Two test lanes were compacted at different material temperatures to test, among other things, the hypothesis that a higher material temperature has a positive impact on the compaction progress. Analyses of the results indicate that there is no evidence to support this hypothesis. A relationship was developed between the decrease in layer thickness (i.e. compaction progress) and the number of roller passes applied.

Analysis of the data obtained indicated that the relation between compaction progress and number of roller passes is best modelled using a negative exponential relation based on the initial layer thickness (LT_0) or the ultimate layer thickness after an infinite number of roller passes (LT_∞). The temperature of the material was monitored during each roller pass. These three sources of information (temperature and compaction progression) together with the weight of the roller used, were the main source of information for the simulations. The calculated force that is required to achieve a specific (measured) layer thickness reduction (i.e. compaction progression) must correspond to the roller drum weight. Further validation is based on assessment of the plausibility of the results obtained e.g. stress patterns, strain patterns, material movements and particle tracing plots.

7.2 Recommendations

This section will propose and discuss possible improvements to;

- a.) the FEM material model “Rock”,
- b.) the FEM approach,
- c.) the theoretical effects of material temperature and refinement of yield locus shapes,
- d.) the apparatus MHSM, new pistons and springs.

It will be discussed which extensions are possible using the improved features developed.

Improvements

Improvements of the FEM material model. The Rock material model currently implemented in the DiekA approach describes linear elastic behaviour in combination with plastic model behaviour in accordance to critical state theory. Critical state models recoverable material behaviour in such a way that the specific volume of the material changes proportionally to a change of the logarithm of the isotropic compression pressure, p' . Comparing Rock model behaviour to critical state indicates that both systems for modelling recoverable behaviour are different. Although the Rock model forms a proper base for modelling plastic behaviour, including softening and hardening, it is strongly recommended to build a new (FEM) material model that operates correctly in accordance with critical state theory.

Load controlled simulations. In the DiekA approach it is currently not possible to pre-describe the loading force in the simulation (i.e. the roller drum weight) and calculate the corresponding layer thickness reduction. Estimating the layer thickness reduction beforehand and then calculating the required rolling force is thus a trial and error process to determine the correct rolling force-layer thickness reduction correlation. However, making calculations with a target layer thickness reduction must, again, be done by trial and error because, the elastic material recovery is not known in advance. This makes the whole simulation process very labour intensive. It is recommended to implement in DiekA a couple of features that accommodate simulations by prescription of a layer thickness reduction or, a pre-described roller drum load. The latter is even better.

Improving the specification of the Yield Locus. The Rock material model uses a closed yield locus in exactly the way as it is postulated by the critical state theory. The material parameters are estimated based on the laboratory-measuring programme carried out with the MHSM. However, because all tests were done at approximately equal q/p' ratio the parameters have been calibrated for a limited variation in the q/p' ratios. As a consequence only a limited part of the yield locus could be calibrated. On the remaining part of the yield locus (shape and size) assumptions have been made based on literature (Vermeer, 1980). To obtain more accurate information about the entire shape and size of the yield locus a more extensive test programme is recommended.

Associated versus non-associated flow. The Rock model uses an associated flow⁴⁵ rule for modelling the closure cap of the yield locus. Associated flow couples the deformation of plastic flow to the current stress state. It is recommended to investigate whether the implementation of non-associated flow can introduce further improvements. Perhaps the results of such an investigation might indicate that non-associated flow better fits to the modelling of plastic flow of HMA. Because non-associated flow has more degrees of freedom, the measuring method and/or equipment and the material model should then be adapted.

⁴⁵ Associated flow means that the yield locus shape equals the plastic deformation contour, for more details see chapter 3.

Effects of material temperature on compactibility. For a successful and widespread application of FEM simulations of HMA compaction it is of major importance that the effects of material temperature on the progress of compaction becomes clear. To understand the effect of material temperature on material behaviour, a theoretical investigation in combination with material experiments may be required. In this respect one can think of additional testing of the shear rates of bitumen and bitumen-filler mixtures at different temperatures, or performing Gyrator compactibility tests on asphalt mixtures

The Modified Hveem StabiloMeter (MHSM). The MHSM is equipped with three different springs with the objective of being able to vary the (radial) confining stiffness of the sample to different levels. We aimed to test the compactibility of the materials at three different stress combinations (expressed q/p' ratio). Experience with the testing equipment reveals that the interaction (i.e. stick-slip and friction) between the piston and cylinder in combination with the stiffness of the spring is crucial for achieving a smooth confining pressure increase linear to the radial sample deformation. When the resistance of the piston in the cylinder is high, related to soft spring stiffness, the piston moves in fits and starts (not smoothly). It is important to avoid this to maintain a fixed q/p' ratio during a MHSM test. Two of the three springs performed well in the current design of the piston inside the MHSM cylinder. It is recommended to develop at least one extra piston design, which should have less resistance to use in combination with the weakest spring. During the research we studied the stress path in the layer at several points and from that it became clear that the q/p' ratio obtained from simulations fits quite well the q/p' ratio in the samples as they were tested during execution of the laboratory measuring programme.

Extensions

Use of critical state theory. The research project shows that it is appealing to apply a theory based on critical state to model the behaviour of a HMA mixture during compaction. This was possible because both materials, soils and HMA, exhibit behaviour governed by movement of particles inside the particle matrix. These particle movements create irreversible material behaviour that can be characterised as elastic-plastic. Elastic, the material behaviour is recoverable until the stress reaches a level where the particles start moving, that is the plastic domain. Critical state does model this and enables one to deduce the volumetric changes based on combinations of stresses applied. By this ability to model elastic plastic behaviour, critical state lends itself to use in other situations such as; understand rutting behaviour, corrugations at intersections, etc.

Use of the MHSM. As a result of the research project a piece of laboratory equipment is further developed for measuring material parameters that can characterise material behaviour during compaction (i.e. that can indicate compactibility). The apparatus is the Modified Hveem StabiloMeter (MHSM). The forte of the equipment is that it applies on the material a stress load combination similar to that encountered during compaction. In other equipment for measuring compactibility of mixtures (Marshall hammer or Gyratory compactor) this is not the case. It may be useful to do further tests using the apparatus in determining compactibility parameters for different

materials. However, serious consideration has to be given to developing this equipment to test samples at high temperature.

7.3 Final conclusions and reflections

A material model, that is able to simulate a HMA material during compaction, did not exist at the beginning of this research and therefore one had to be developed or adopted from other disciplines. The model was found in soil mechanics and is known under the name “critical state theory”.

The final conclusion for using FEM for simulation of HMA rolling processes is that they are very suitable and do deliver a lot of information about the process. In the context of this study it was not possible to develop a fully applicable material model with respect to the critical state principles but the way ahead has been described.

Additional results obtained

An insight in stresses and strains that occur when asphalt is rolled by a roller drum was developed. By means of FEM simulation processes it is possible to determine the magnitude of stresses and strains, material movement, and other variables inside the material. It is observed that the effects of material temperature (or bitumen viscosity) are different as initially thought related to the material behaviour during compaction.

Relevance to the asphalt industry

As a result of the project it is proved that the principle of “using FEM for simulating HMA compaction processes” does work. Furthermore, a prototype of a simulation tool is not even far away anymore. However, additional work must be done before the tool really works adequately and the full record of possibilities can be seen. There is also scope for examining which elements function reasonably well (more detailed; the MHSM, critical state, ALE, FEM and DiekA, here only some fine tuning is necessary), what parts must be redeveloped (e.g. the material model in accordance to critical state that can be implemented a FEM approach) and what parts need further investigation (e.g. the effect of material temperature on compactibility).

A FEM tool is a powerful tool to simulate stresses, strains, deformations, etc. Using FEM for simulation of HMA compaction creates the possibilities to “look inside” the material and analyse what happens in terms of stresses and strains in the vicinity of the roller drum during compaction. It has become clear that the tool must be improved further. However, it is demonstrated that it is an initial starting point for simulation of HMA compaction. Possible applications of the tool are:

- a.) Definition of the circumstances that are suitable for compaction and determination of the borders of these areas or circumstances for suitable compaction. Further, definition of circumstances under which no good compaction can be expected anymore and estimation of the loss of quality that can be expected if compaction is carried out under unsuitable conditions.

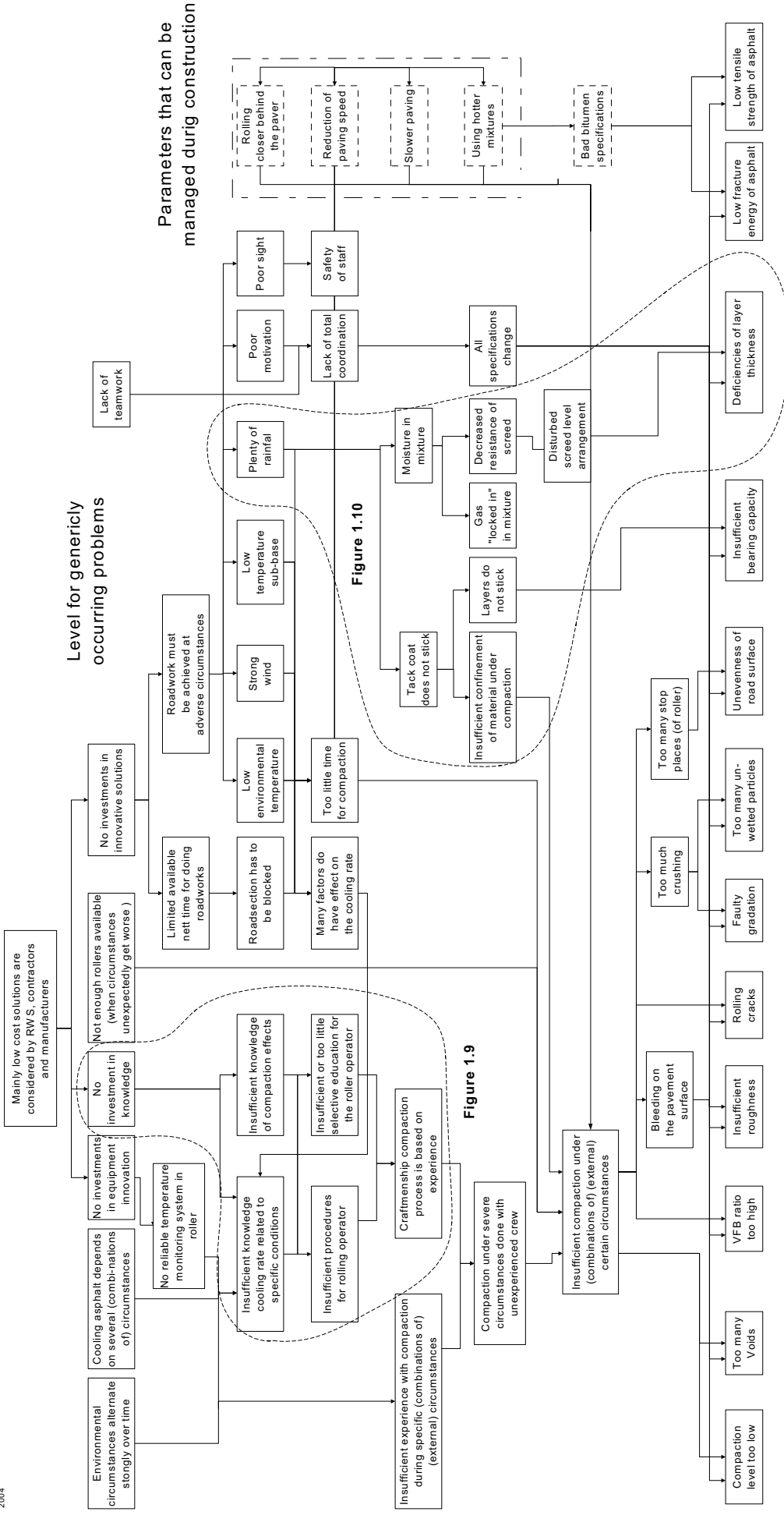
- b.) One can think of development of new procedures or testing the available procedures for roller operators. A theoretical basis can be developed to explain existing procedures. One can for example determine whether it would be better to apply rolling passes directly behind the paver with a high frequency or if it would be better to distribute the passes over a longer time span using a lower frequency. Another aspect that is useful to investigate is deduction of the minimum temperature until it is possible to achieve ongoing compaction.
- c.) We can look into investigation and definition of suitable and unsuitable combinations of mixtures, rollers and circumstances. On some mixtures for example compaction can be perfectly done using a heavy three-wheeled roller whereas on other mixtures such a roller is a guarantee for damage. In this context it is also useful to study situations of which it is known that they can easily cause rolling problems. The tool can be used to study where something is going wrong and why. When this is known, measures could be taken to avoid such situations.

The tool is still too complicated to use by an average consultant. Simulations are labour intensive and require skilled FEM operators. To simulate the effect of different types of rollers the tool must be adapted.

Appendix A

Doing roadwork under severe weather conditions (workshop model)

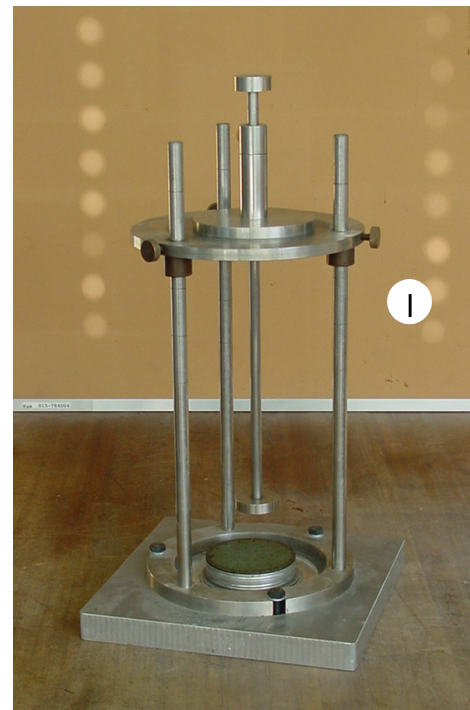
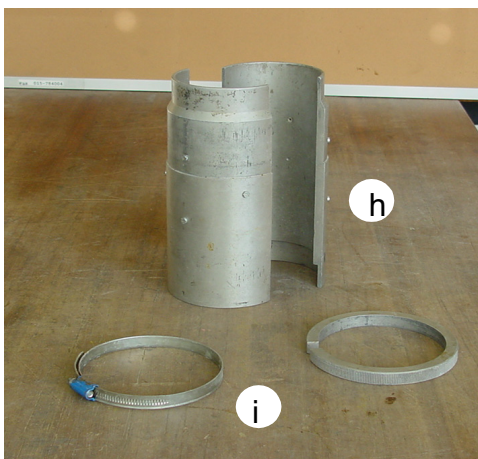
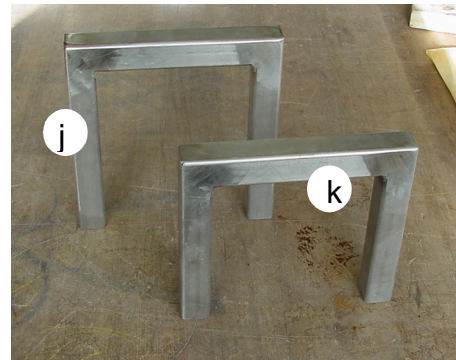
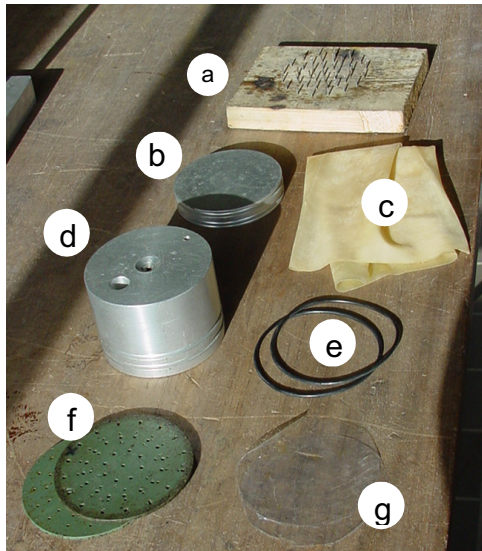
CAUSAL SCHEME_APP_1_1_VSD
 Wednesday 11 February
 2004



Appendix B

Procedure for building a Stabilometer test sample

(how the mixture is composed from the base materials is not included)



The different components required for building a Modified Hveem Stabilometer (MHSM) test sample.

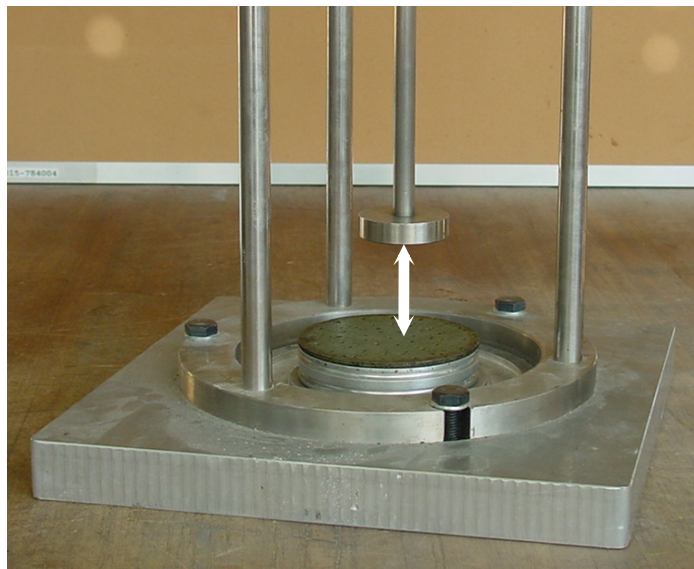
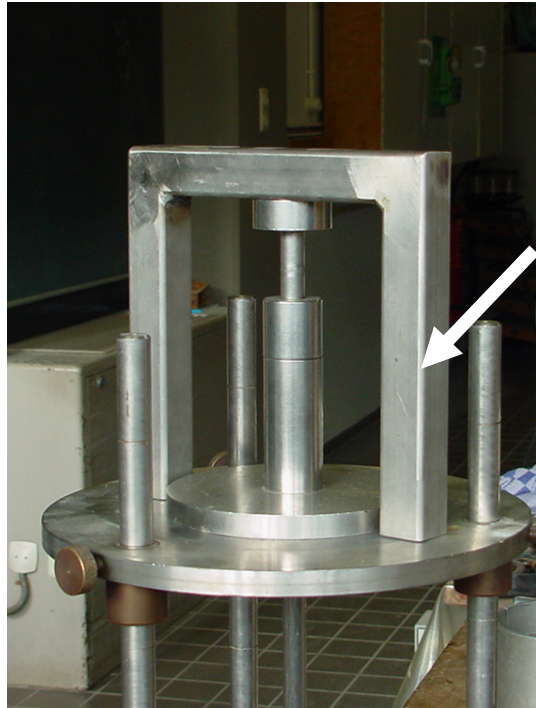
Left, above:

Assisting tool for perforating foil (a),
Base-cap, aluminium, 19 mm thick (b),
Latex Membrane, 25 μm (c),
Perforated Top-cap, aluminium, 70
mm thick, (d),
2 rubber o-rings (e),
2 perforated plastic plates, 2 mm thick,
(f),
Plastic foil, thick 0.03 (g),
Left, below;

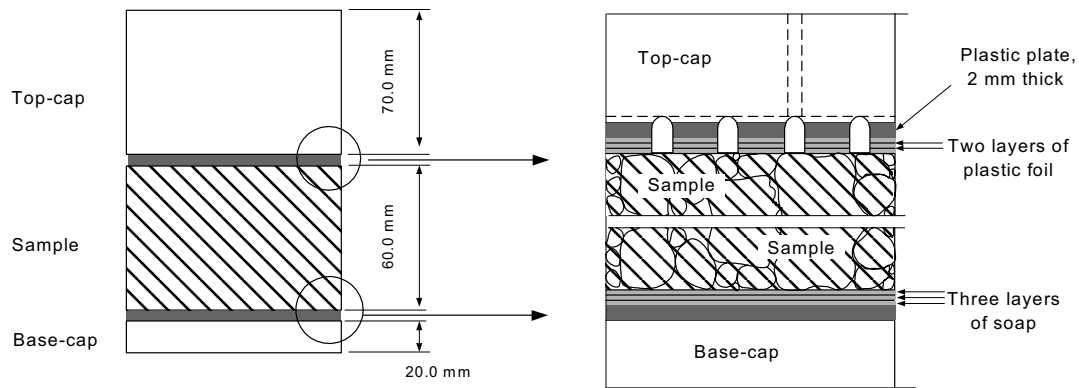
Tools for adjusting the hammering tool
(l) to create the correct sample height (j
& k).

Right above;
Split-mould (h) 101.6 mm (4'') inner
diameter, with two clamps, (i),

Right, below:
Hammering tool (l).



1. Adjustment of “hammering tool”. The hammering tool is used for preparation of the sample to the correct height. The base-cap with plastic plate is positioned on the stage of the hammering tool. The metal sub frame that is marked in the upper picture is an “assist tool” for adjusting the hammer in such a way that the sample will be built to the right height. The sample is built in two layers of 30 mm height each. For preparation of the first charge of the sample the hammering tool should be adjusted in such a way, with help of the marked assist tool, that the distance between “base-cap” and “hammering plate” is 30 mm.



2. Preparation of the base-cap and top-cap using one plastic plate (f), 2 layers of foil (g), 3 layers of grease per cap.

Base-cap

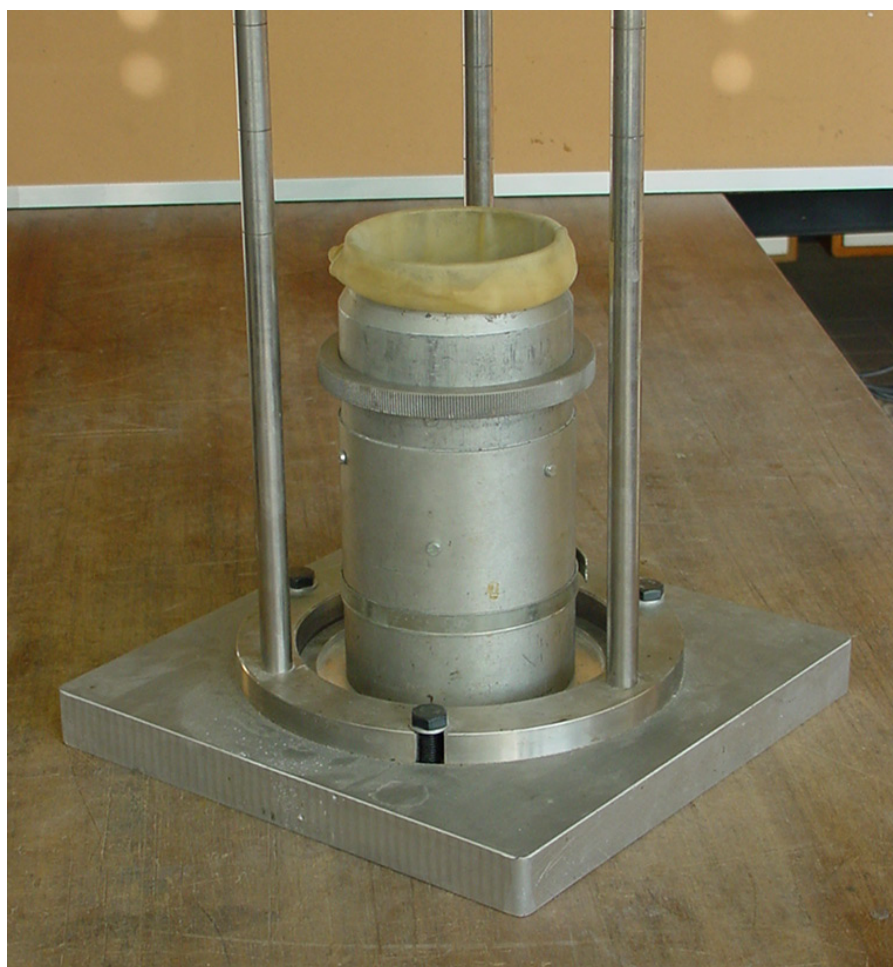
- Cut 4 pieces of foil in a circle of about 101.6 mm (4")
- Grease one of the plastic plates with 2 to 3 grams grease.
- Put one piece of foil on top of the plastic plate.
- Grease the foil with 2 to 3 grams of grease
- Put the second piece of foil on top of the grease.
- Grease the second layer of foil with again 2 to 3 grams of grease.
- Put the whole package (plastic plate, three layers of grease and two layers of foil) on top of the aluminium base-cap.

Top-cap

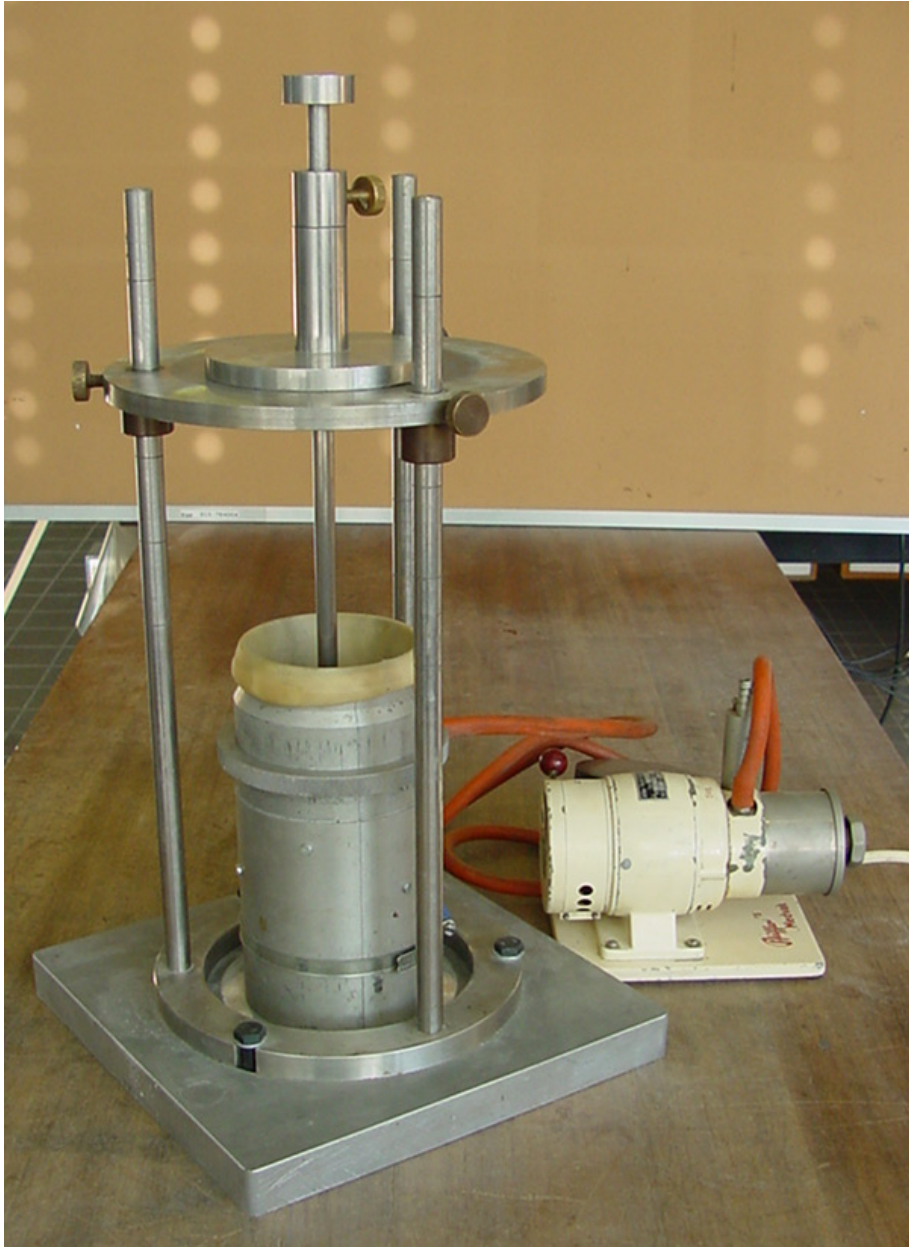
- Prepare the plastic plate, which goes on top of the sample just as is described for the base-cap with two layers of foil and three layers of grease.
- Then perforate the two layers of foil using the "perforation assisting tool" (a). Take care of the alignment of perforation of the foil on the perforation of the plastic plate. The perforation must enable air to escape from the sample during the test.



3. Assemble the latex membrane (25 μm) on the aluminium base-cap (19 mm thick) using the rubber O-rings. The plastic plate, grease and foil must already be on the base-cap before the membrane is assembled.



4. Position the combination of base-cap, latex membrane and o-rings on the stage of the hammering tool.
5. Combine the split mould parts, assemble the two clamps and position the mould over the base-cap on the hammering tool stage.
6. Stretch the latex membrane and pull it over the top of the split-mould in such a way that the membrane does not wrinkle.



7. Lower the pressure between the latex membrane and the split-mould using a vacuum pump (the membrane is sucked against the split-mould wall).

The tools are (set up is) now lined up for preparation of a test sample.



1. The correct amount of the HMA mixture for building one sample is divided into two equal parts. (composition of the mixture is not discussed here).



2. Fill the split mould with the first charge of the mixture (avoid segregation).



3. “Compact” the first charge until the right height/VMA level is achieved by using the hammering tool.
4. Roughen the upper surface of this first “compacted” half of the sample by using a screwdriver.
5. Re-adjust the hammering tool now on the target sample height of 60 mm. Use the largest adjustment tool (j) for this purpose.
6. Fill the split-mould further with the second charge of the mixture (avoid segregation).
7. “Compact” the total sample to the right height/VMA level by using the hammering tool.

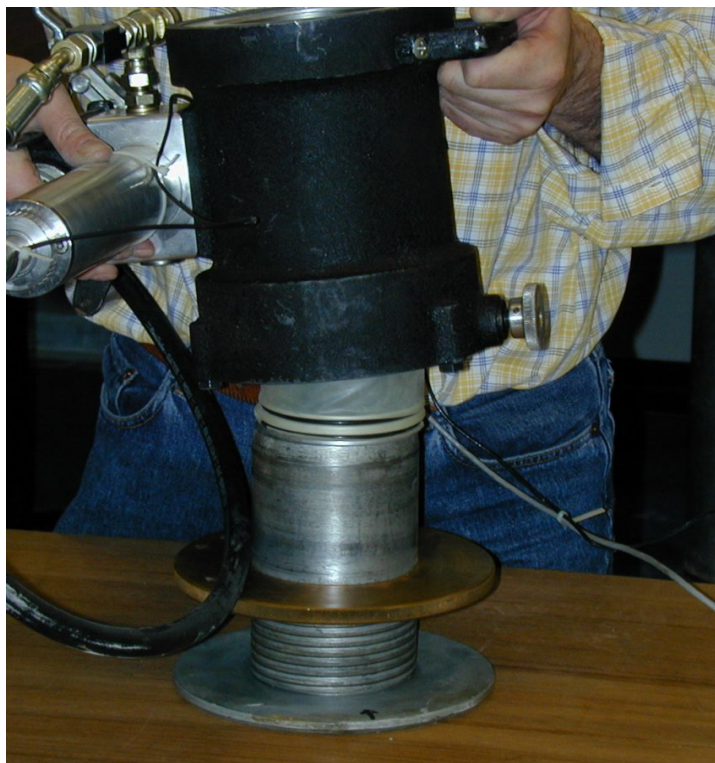


8. Loosen the clamps for dismantling the split mould. The sample is now ready but very vulnerable (weak). Handle the sample with care. Pushing too hard against it will easily disturb the only slightly compacted sample configuration. The second perforated plastic plate, together with 2 layers foil and three layers grease, should now be carefully placed on top of the prepared sample.

Preparation of the sample is now completed. The sample can be transported to position it on the MHSM stage.



9. Centre the pre-compacted sample, together with the base-cap and the inside membrane, on top of the adjustable stage of the MHSM.



10. The stabilometer body can now be placed carefully over the top of the sample on the stabilometer stage.



11. The top-cap can be positioned on top of the sample inside the membrane. The remaining part of the membrane can be coiled up (wound up).



The MHSM including the prepared sample is now ready for positioning inside the framework of the external loading device.

Appendix C

Deduction of an accurate initial sample height.

For accurate analysis of the Modified Hveem Stabilometer results (i.e. calculated strains etc.) it is necessary to know the correct starting height of the sample. Because initially the sample is only slightly compacted it is difficult to measure this value with enough accuracy. However, because the sample deformation during a test is accurately monitored, it is also possible to reconstruct the initial sample height from the deformed situation. In this appendix we discuss how an average value for the initial sample height can be obtained from these two sources of readings.

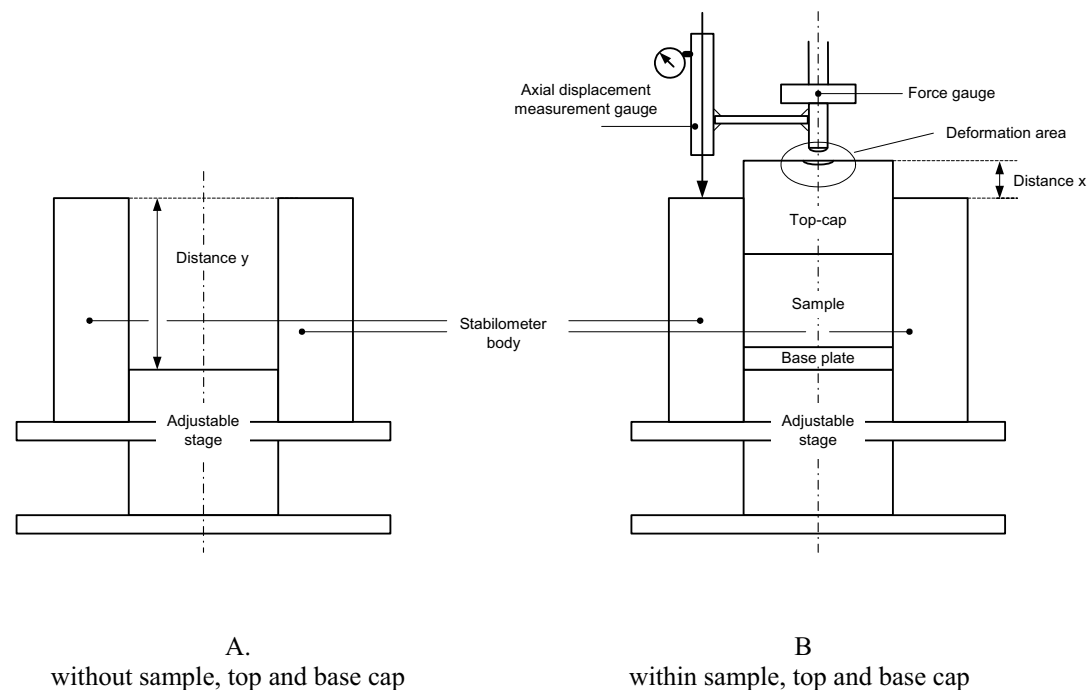


Figure 0.1 Two illustrations of the Hveem Stabilometer body, without (A) and with (B) sample, top-cap and base-cap.

Figure 0.1 shows two illustrations of the MHSM body:

- A. without sample, top- and base-cap, and,
- B. with the sample (inside), top- and base-cap.

The height of the sample inside the MHSM can be deduced when the distances y (illustration A) and x (illustration B) are known, and the height of the top- and base-cap and used plastic plates, folio and grease layers are known. Adequate measurements on top and base cap, plastic plates ($2x$), folio ($4x$) and grease ($6x$), have proved that the thickness of the overall set of used elements was 94.9 mm. Further accurate readings proved that distance y in our set-up was 131.1 mm. This implies that current sample heights (at any load) could be calculated using;

$$h_{ini} = x + 131.1 - 94.9 = x + 36.2 \text{ [mm]}$$

in which; x is the height the top-cap towers above the stabilometer body (see illustration B).

Use of the accurate measured axial sample deformation during loading, enables us to reconstruct the initial sample height from any situation between “start test” and “fully loaded”. Note, that when the top-cap deforms, caused by the force applied on it (see situation b), the axial measured sample deformation must be corrected for this top-cap deformation, see also note¹.

The procedure for obtaining the average initial sample height will be illustrated by using readings of test 4 of the REF test series (reference mixture).

CALCULATION OF AVERAGE INITIAL SAMPLE HEIGHT			
		F = 0 kN	Full load, F = 23 kN
Distance ¹ x	(a)	25.10 mm	17.38 mm
	(b)	36.20 mm	36.20 mm
Current sample height	(a+b)	61.30 mm	53.58 mm
Measured axial deformation (LVDT)	(c)	0.0 mm	8.15 mm
Correction for top cap deformation ²	(d)	0.0 mm	-0.32 mm
Calculated initial sample height, h_{ini} ;	(a+b+c+d)	61.30 mm	61.41 mm
Average initial sample height			
Situation F = 0;	(e)	61.30 mm	
Situation F = 23 kN;	(f)	61.41 mm	
Average initial sample height;	(e+f)/2	61.35 mm	

¹ Obtained by Vernier callipers.

² When the force gauge meets the aluminium top-cap the latter one deforms as a result of loading. Because the axial displacement measuring gauge is positioned over the top-cap, see Figure 0.1, the gauge measures the top-cap deformation as it would a sample deformation. By means of tests using an in-deformable, rigid dummy, it is shown that the deformation of the top-cap increases linear with the load to a value of 0.32 mm at a load of 23 kN. This value of 0.32 mm is used as a correction value while deducing the back-calculated initial sample height, and for completing the analysis of the MHSM results.

Appendix D

Test procedure for doing a MHSM test.

In this appendix a procedure for doing an MHSM test is described.

Required equipment;

- External loading device

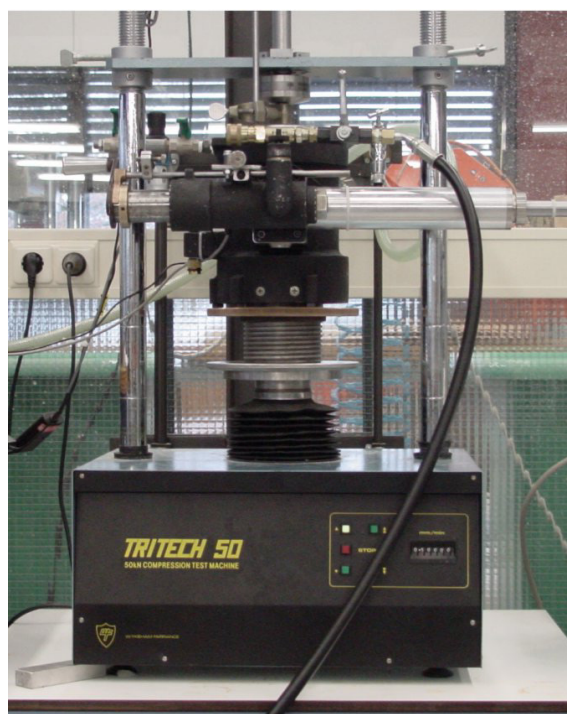
- Modified Hveem Stabilometer (MHSM)

- Prepared test sample

- Pc and software or other equipment for storage and reading of data

- Force gauge for measuring the actual load on the sample (until ca 25 kN)

- Gauge for measuring axial deformation of the sample (until ca 20 mm)



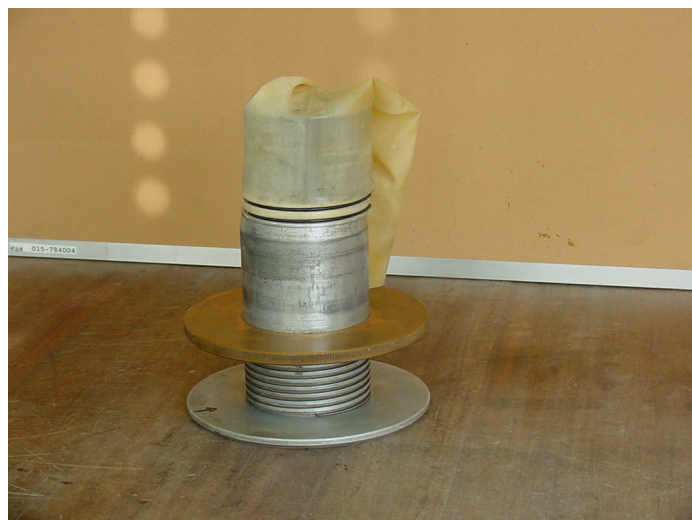
The Modified Hveem Stabilometer installed inside the external loading device.



The Modified Hveem Stabilometer body, a sample on the adjustable stage and the top-cap.

Inside the stabilometer-body the oil functions as a non-compressible medium, a role for measuring the radial deformation of the sample. The oil is enclosed inside the stabilometer with the use of a rubber diaphragm and other rubber seals. If, the equipment has not been used for an extended time period, for example, and air is leaking inside the MHSM; the air then functions as an extra spring and the oil is not an incompressible medium anymore. The radial displacement of the sample cannot be obtained anymore with sufficient accuracy.

To avoid such problems it is recommended to check that the equipment is working properly before a MHSM test is started. Checking the MHSM asks for a specific procedure; the so-called “stretch test”. This test is discussed separately in appendix E.



1. Transfer the prepared sample, base-cap and membrane from the split mould onto the MHSM stage.



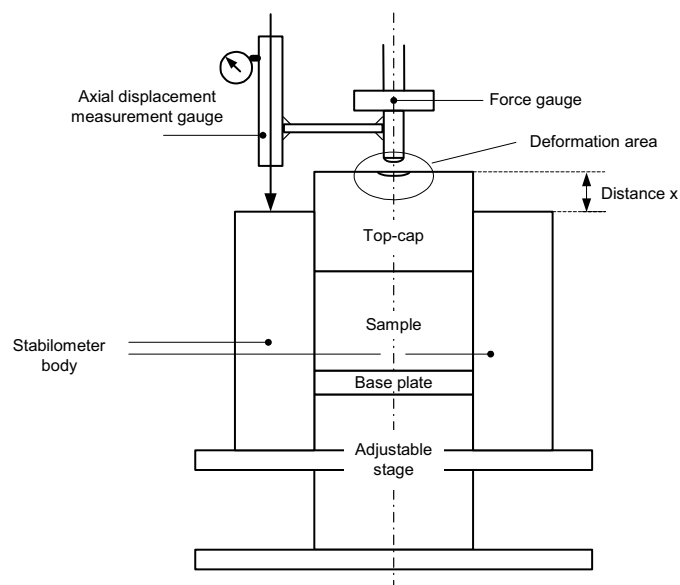
2. Place the MHSM body over and around the sample and the base-stage.



3. Install the top-cap (70 mm high) with caution; this activity requires precision and practice. The cap has to touch the sample lightly, the carefully achieved pre-compacted sample situation may not be disrupted.



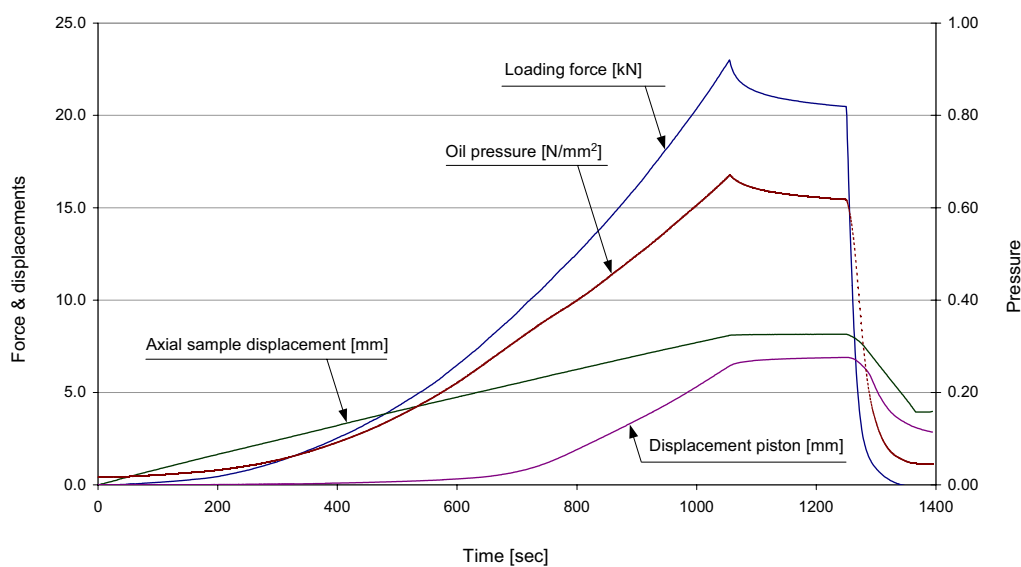
4. Transport the MHSM including the sample onto the external loading device.



5. Deduce the initial sample height by measuring the distance from the top-cap to the Stabilometer body.
6. Adjust the oil pressure by turning the manual spindle pump until the correct starting value is achieved (i.e. 0.015 ± 0.002 MPa).

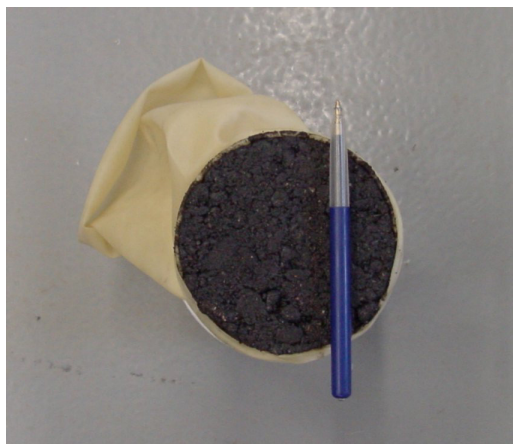


7. Start loading the sample with a fixed axial displacement rate of 0.5 mm/min (displacement controlled).



8. Stop loading when the axial force has reached the value of 23.5³ kN or the radial pressure has reached 1.0 MPa.
9. Determine the sample height at maximum load (for reconstruction of the initial sample height, see also appendix 3.2).
10. Reduce the load on the sample to 0 kN.

3 23.7 kN is the limit for the used force (loading) gauge. When a force gauge with a higher limit is used a higher axial loading stress can be achieved. The confining stress of 1.0 MPa is the limit of the MHSM body. This value has always been respected. It may be the case that a test must be stopped before the maximum load of 23.7 kN is reached.



11. Remove the MHSM from the external loading device and remove the sample from the MHSM

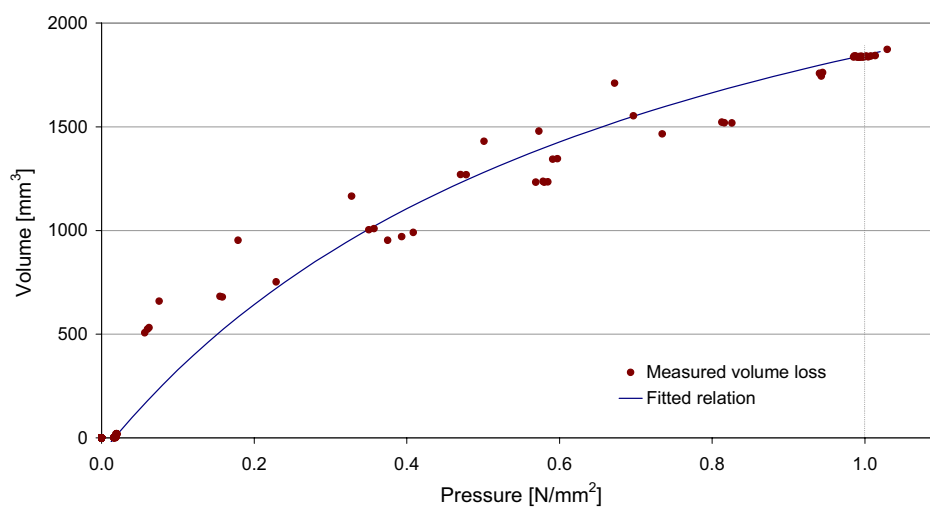
Appendix E

Doing a MHSM stretch test

Inside the stabilometer-body oil functions as a non-compressible medium, a role for measuring the radial deformation of the sample. The oil is enclosed inside the stabilometer by the use of a rubber diaphragm and other rubber seals. If, for example, because of not using the equipment for an extended time period, air is leaking inside the MHSM the air functions as an extra spring and the oil is not an incompressible medium anymore. The radial displacement of the sample cannot be obtained anymore with sufficient accuracy.

The following is a procedure for doing a MHSM stretch test;

1. Install a displacement gauge on the stabilometer in such a way that the displacement of the piston in the modification of the MHSM can be measured.
2. Position a rigid dummy sample (e.g. of steel, without plastic plates, foils and grease) inside the MHSM.
3. Position the MHSM inside an external loading device and put a loading force of around 10 kN on the dummy sample.
4. Adjust the oil pressure to the start value of 0.015 kPa by turning the manual spindle pump.
5. Increase the oil pressure inside the stabilometer in around 30 sec to just above 1.0 kPa by turning the manual spindle pump. During this process the piston displacement, manual spindle displacement and the oil pressure should be accurately monitored.
6. Increase the oil pressure after a few seconds, by turning the manual spindle pump, until the start value (i.e. 0.015 kPa) is reached.
7. Repeat steps 4 till 6 a few times.
8. Analyse the results.



Graphical results from a stretch test, lost volume against pressure p' .

In the stretch test the amount of lost volume is measured by increasing the oil pressure inside the stabilometer from around zero to 1.0 kPa. Theoretically there should be no air inside the stabilometer. However the stabilometer has rubber seals inside and a rubber diaphragm between the (dummy) sample and the oil. Experience with the MHSM learned that a properly bled stabilometer should show a volume loss of around 1700 till 2200 mm³. When the measured volume loss is larger than 2500 mm³ one should bleed the stabilometer again. The rubber diaphragm is around 1.5 mm thick. A thickness reduction of 0.04 mm of that membrane can already explain a volume loss of approximately 2000 mm³.

Appendix F

Deduction of critical state parameters from material test programme

To obtain critical state parameters for the asphalt materials as tested in the laboratory a specific procedure is followed. For each of the test series (material composition, imitated temperature or loading condition) six individual tests were done. Each test yields an individual loading line. From 6 of those loading lines (6 tests within one test series) two average tangents were estimated. The four steps that were taken to do so will be discussed in this appendix. The procedure is assisted with help of Figure 0.1.

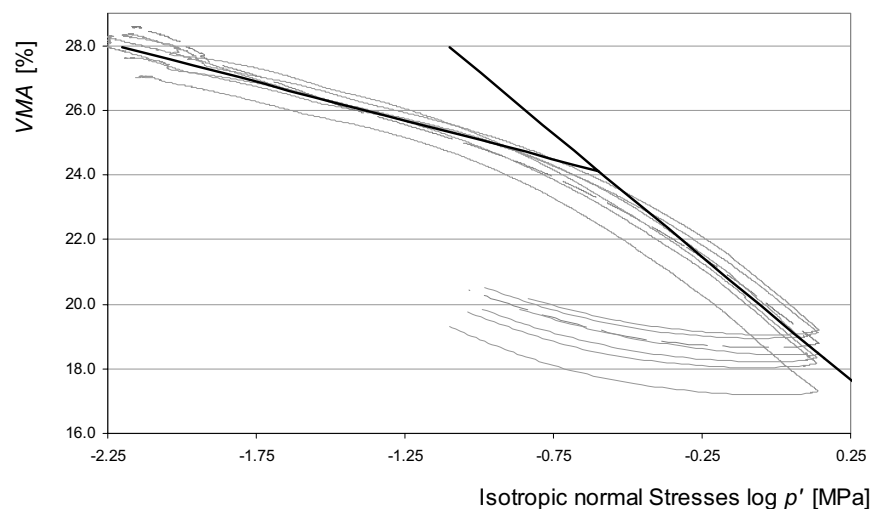


Figure 0.1 The 7 individual test results from the reference (REF) series including the distracted mean curve.

- Step 1. Calculation of the average VMA value at which the (7) individual tests started. This value was used for normalisation⁴ (i.e. scaling) of the individual lines. This normalisation made it possible that the different lines could be compared to each other.
- Step 2. Plotting of the VMA values against the logarithm of the isotropic normal compression stress p' , see Figure 0.1.
- Step 3. Selection of the data that should be taken into account for deduction of respectively the recoverable and the irrecoverable part of the bilinear critical state model (fat line in Figure 0.1). Note: Start for the recoverable part of the branch at the lowest $\log p'$ values and take successively more and more data into account while analysing the fit of the model to the data. The procedure should be stopped before the fit significantly drops. For estimation of the figures corresponding to the irrecoverable branch a similar procedure should be followed, however, now it should be started with the largest p' values

⁴ The loading lines were scaled to the average initial VMA value within the complete test series, because then the different lines could be compared to each other.

instead of the lowest p' values (i.e. the involved data set is now increased by adding lower stress values).

Step 4. Calculation of the slope and intercept values for both the recoverable and the irrecoverable average lines per test series (REF series, MTM series, HTM series, etc.) using the data domain as selected in step 3.

Appendix G

A test run on a material model of 700 mm length.

Before the definite model set up for doing the simulations was developed test runs were carried using different material lengths to investigate what a proper material length would be. In this appendix p' , q , τ_{xy} , ε_{vol} en ε_{shear} are shown in relation to the distance from the load. At places where the parameters do not change anymore, it is assumed that the load has no influence anymore.

Stresses and strains from a test run on a configuration with 3 x 50 elements, modeled material length 700 mm. The runs are done to determine the minimum material length to be modeled.

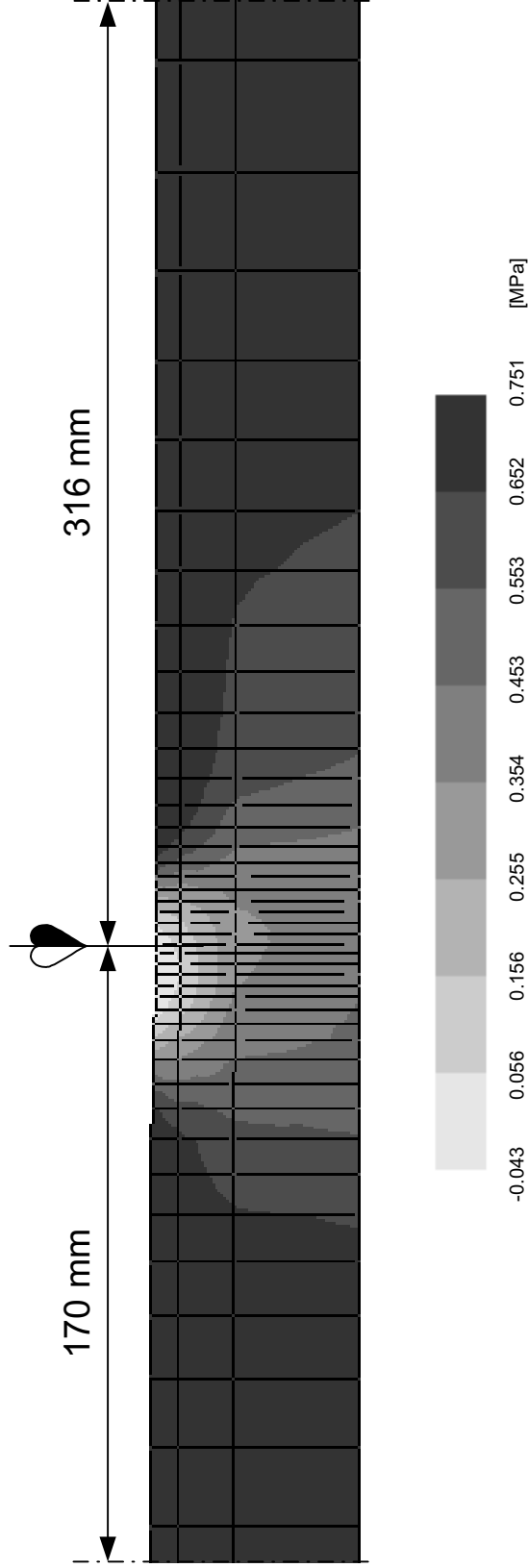


Figure 0.1 Isotropic normal compressive stresses in the material, p' [Mpa].

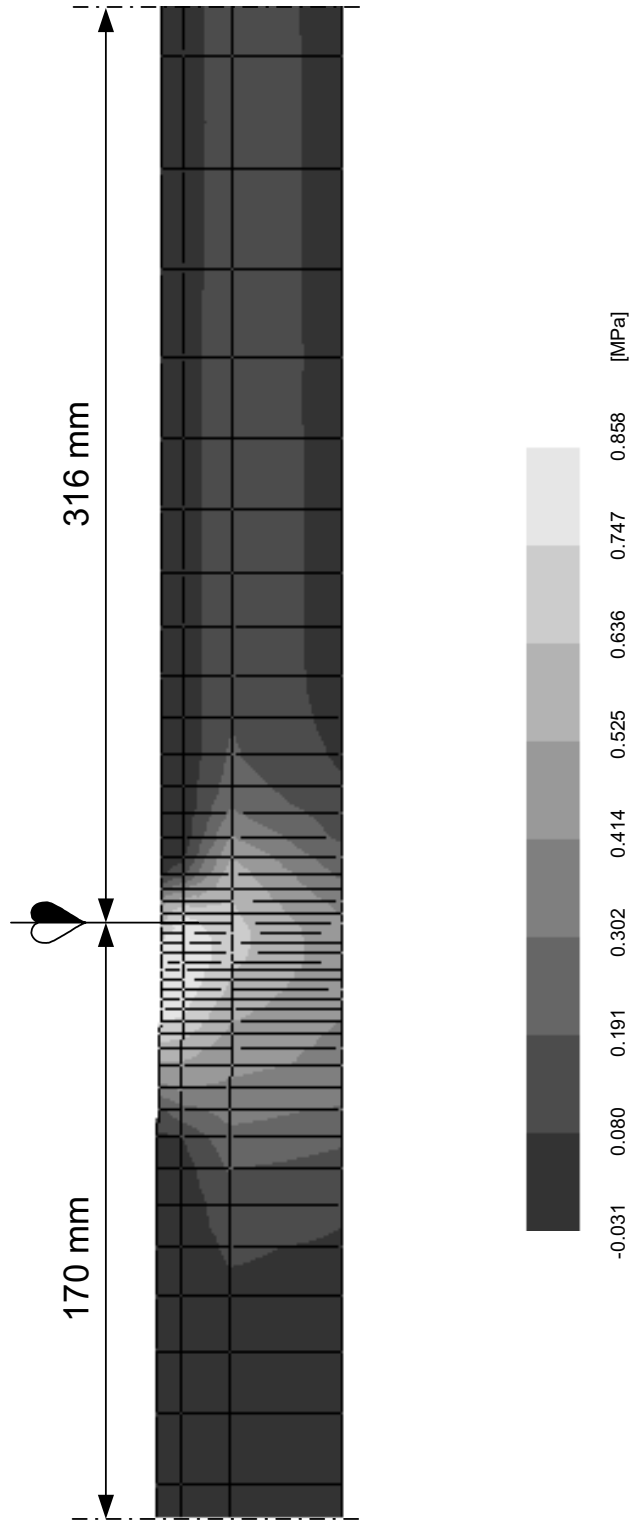


Figure 0.2 Deviatoric stresses in the material, q [Mpa].

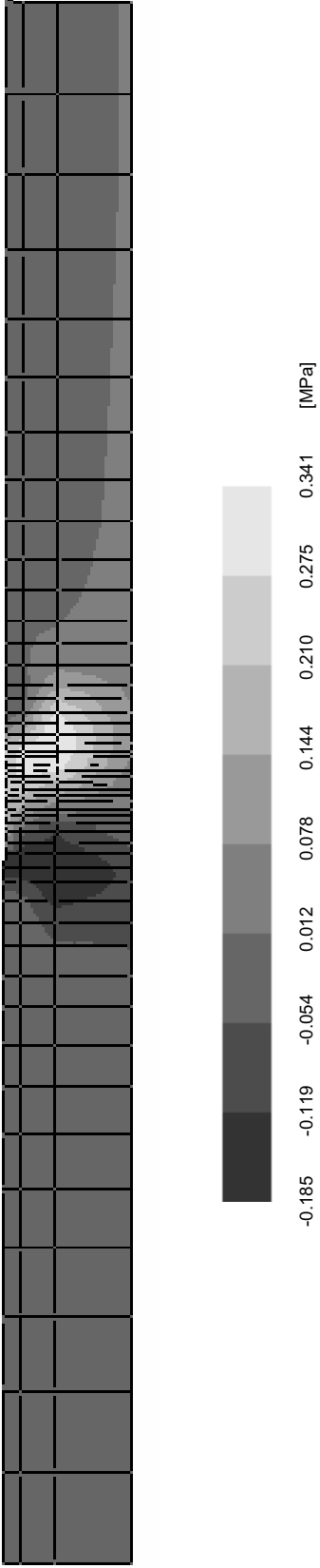


Figure 0.3 Shear stresses in the material, σ_{xy} [Mpa].

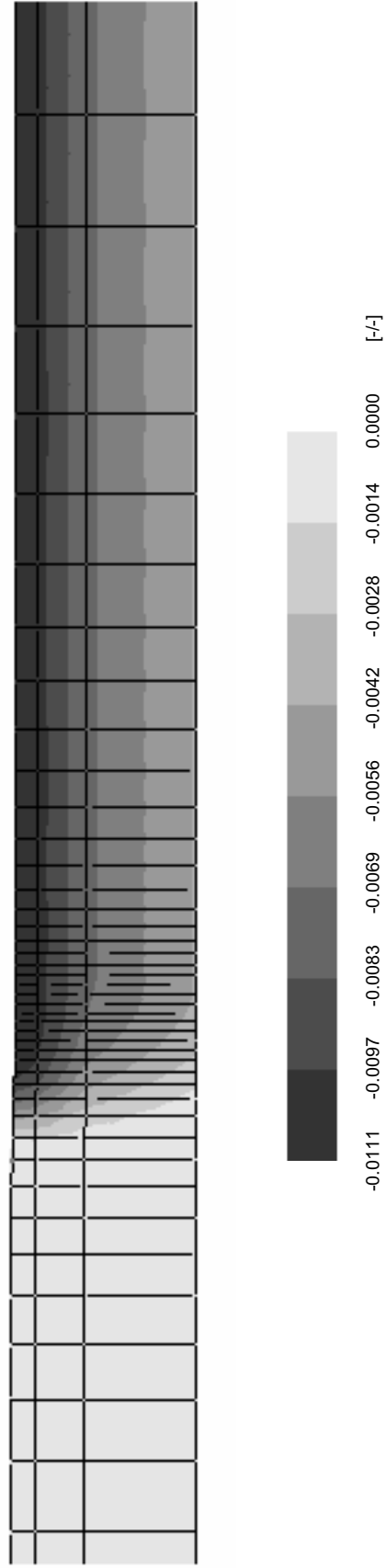


Figure 0.4 Volumetric plastic strain in the material, ϵ_{vol} [-/-],

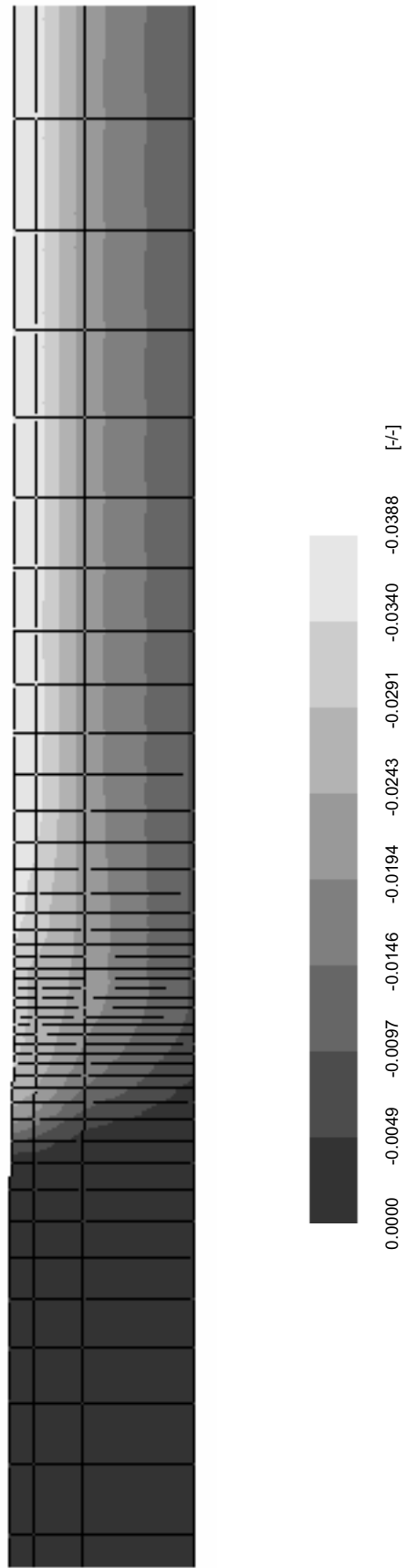


Figure 0.5 Plastic shear strain in the material, ϵ_{sh} [-/-],

Appendix H

Quantification of Rock model parameters for asphalt mix

In DiekA a material model called “Rock” is implemented for simulation of the behaviour of soft stone materials. However, this material model is designed in such a way that it operates reasonably well in accordance with critical state principles for the plastic part of the material behaviour. The model comprises twelve quantitative parameters. Two for modelling elastic behaviour, two for regulating the hardening and softening and the remaining (8) parameters are for regulating the shape and size of the initial yield locus. The Rock model is used in FEM simulations of the HMA rolling process as discussed in the chapters 4 and 6. In this appendix the determination of Rock parameters from critical state material information will be discussed.

The Rock model uses four different areas to shape the yield locus:

- Area I: Tension area; shape of yield locus can be straight or curved, direction of deformation during plastic strain is characterised as associated flow.
- Area II: Brittle plastic area; shape of yield locus for this part of the yield locus can be modelled curved or straight depending on parameters HP and HB , direction of deformation during plastic strain is characterised as non-associated flow, during the asphalt compaction research this yield locus part is kept straight,
- Area III: Closure cap area; shape of yield locus is an elliptical or circle as special form of an ellipse, direction of deformation during plastic strain is characterised as associated flow.
- Area IV: Ductile shear area; shape of yield locus can be part of a curved or straight line depending on parameters HP and HB . Direction of deformation during plastic strain is characterised as non-associated flow.

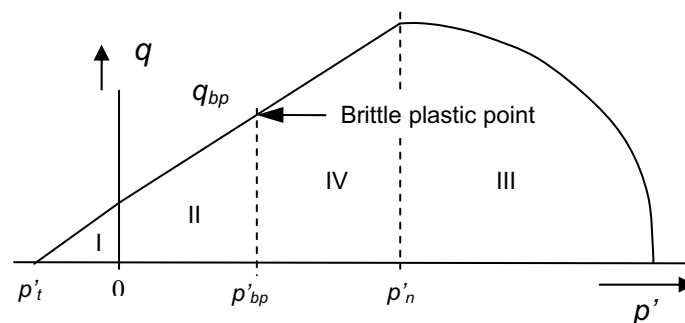


Figure 0.1 The four areas of the Rock model yield locus as is implemented in the FEM approach DiekA.

The eight parameters that shape the Rock model yield locus are:

AA	deduces the slope of the yield locus in the area's II and IV
EX	deduces the eccentricity of the ellipse in area III,
HP	regulates the curvature of the yield locus in area's II and IV, when $HP=HB=1.0$ this part of the yield locus is a straight line,
HB	regulates the curvature of the yield locus in area's II and IV, when $HP=HB=1.0$ this part of the yield locus is a straight line,
p'_{bp}	establishes the border of the area's II and IV,
q_{bp}	deduces the height of the yield locus for area II,
p'_t	deduces the tension strength of the material,
p'_n	establishes the centre of the compression cap.

Critical state parameters were deduced for a DAC 0/11 mixture at three material temperatures respectively 78, 94 and 141°C. As an example, the Rock material parameters for the REF material, which are given should correspond to behaviour of the DAC at 78°C. The critical state information of the REF mixture to start with is given in Table 0.1. The information can also be found in table 3.5 of chapter 3.

CRITICAL STATE PARAMETERS REF MIXTURE	
	Mixture code & Imitated temperature
Measured quantities	REF 78°C
General	-
VMA_I	.277143
P'_{int}	.259977
VMA_{int}	.240907
Recoverable part	-
Slope, κ	-.086321
Intercept, VMA_{κ}	.818696
R^2	.997179
Irrecoverable part	-
Slope, λ	-.275165
Intercept, VMA_{λ}	.705540
R^2	.999756
q/p'	1.526452
$\varepsilon_{sh}/\varepsilon_{vol}$.753572

Table 0.1 Critical state parameters for only the REF mix.

From the critical state information of the REF mixture the following information can be obtained by shifting the elastic branch of the model to the actual VMA_0 value and the deduction of the new intersection point between the elastic and plastic branch (procedure discussed in section 4.3 see Figure 3.

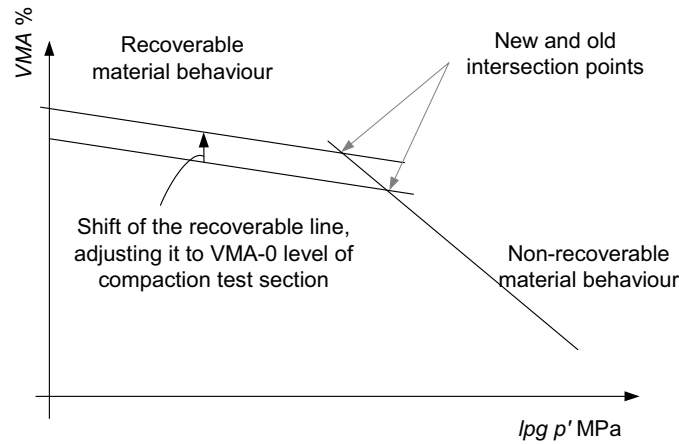


Figure 0.2 Parallel shift of the recoverable branch that describes the material behaviour, for tuning the material parameters to the actual compaction (i.e. VMA) level.

The information that we further need for deduction of the Rock model yield locus parameters is;

CRITICAL STATE PROPERTIES ADJUSTED TO VMA_0				
Material	VMA_0	p'_{int}	q_{int}	$\varepsilon_{sh}/\varepsilon_{vol}$
REF 78°C	.260	.259977	.396842	.753572

Table 0.2 Critical state parameters adjusted to the correct VMA_0 level.

The E modulus and Poisson's ratio for the material to be modelled can be calculated in such a way that the material deformation at the turn from elastic to plastic corresponds exactly to the one modelled by critical state. This procedure results in an E modulus of about 3 to 5 MPa. However, such a soft modulus gives very unrealistic unloading behaviour, therefore the elastic behaviour is modelled with an E modulus of 200 MPa and Poisson's ratio of 0.2.

The shape and size of the yield locus are deduced by using information from the test programme.

It is one of the key principles of the critical state theory that the intersection point of the elastic and plastic branch of loading line, exactly corresponds to the position where the stress path hits the yield locus, see Figure 0.1.

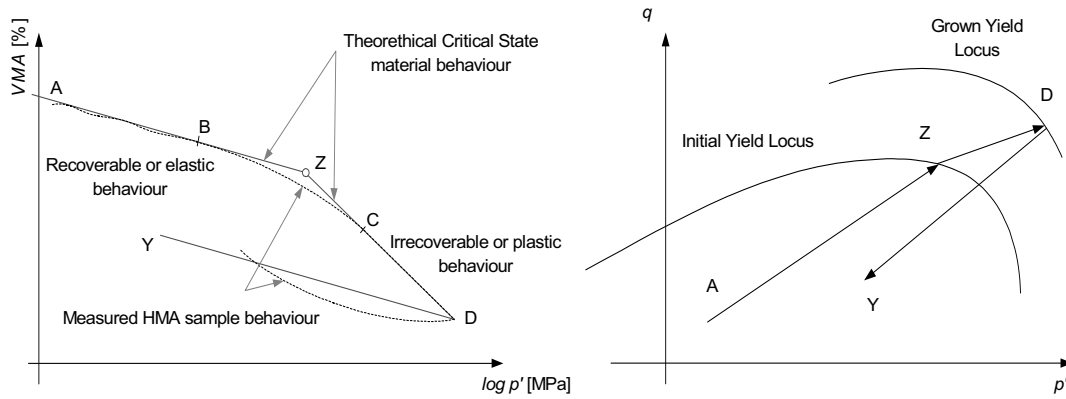


Figure 0.3 The correlation between the position of the intersection point of the elastic and plastic branch of the loading line related to the stress path and yield locus.

It implies that the stresses p' and q of that intersection point must be positioned on the yield locus matching the specific volume of the sample (fig 2, right hand side of the figure). Because during compaction the material is in a stress state that corresponds to the “wet side of critical” the ellipse of the Rock model (area IV), must run over that specific stress point (expressed in p' and q). It is further possible to estimate the direction of the yield locus ellipse at that specific stress point from the direction of deformation (expressed in $\varepsilon_{sh}/\varepsilon_{vol}$) measured in the laboratory tests.

Quantitatively the Rock model parameters can be deduced using the following equations;

Using one quarter of an ellipse shapes the compression cap of the “Rock” model yield locus. In general the shape of an ellipse can be described as,

$$A \times x^2 + B \times y^2 = 1$$

In which the parameters A and B determine the size of the ellipse.

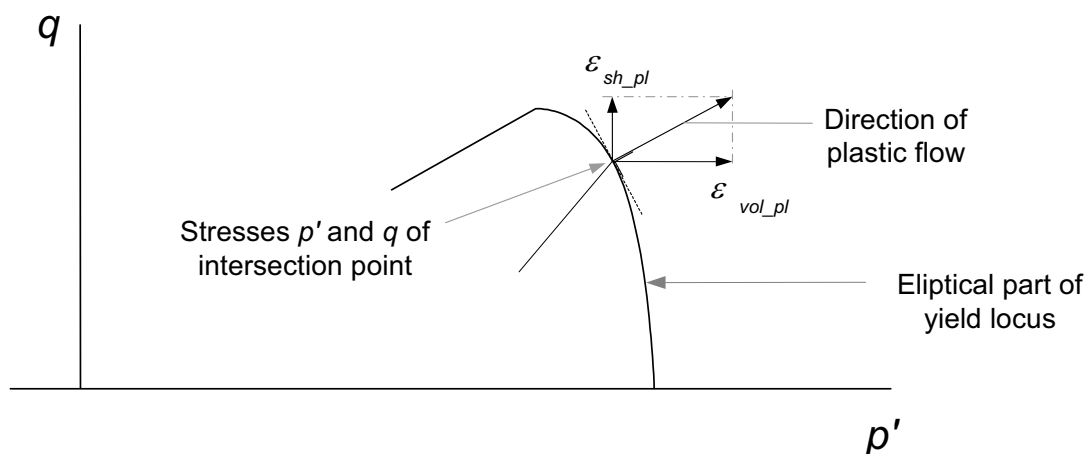


Figure 0.4 Shaping the elliptical closure cap based on measured quantities.

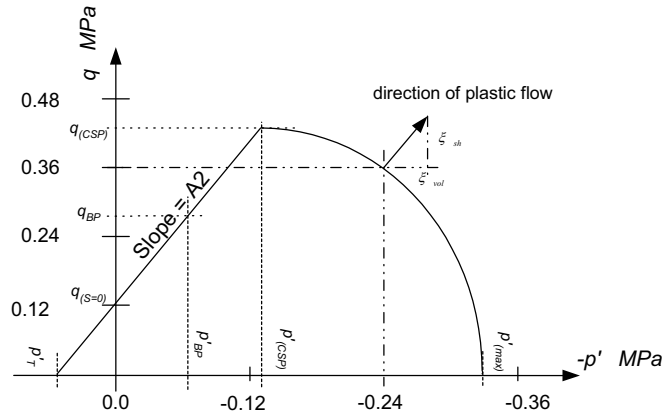


Figure 0.5 The complete rock model yield locus

In the Figure 0.4 above a suitable ellipse is plotted that meets the following conditions; crossing the $p';q$ stress point and the direction of the ellipse at $p';q$ is perpendicular to the ξ_{sh}/ξ_{vol} direction (i.e. associated flow). For shaping such a suitable ellipse for the “Rock” model, the constants A and B from the equation must be quantified. The constant B determines the height of the ellipse. This factor must not be chosen too small, because the ellipse must at least be able to encounter the stress point $p';q$. The maximum value for B , called B_{max} , can be calculated using;

$$B_{max} = 1/(q \times q) \quad [-]$$

Further, while deducing the Rock parameters, the actual B value was taken as a fixed part (i.e. 0.93) of the maximum B value. Globally? this corresponds to, for example, fixing the eccentricity of the ellipse. By doing so the A value can be determined using;

$$A = \frac{-((B \times q)/-RC)^2}{((q^2 \times B)-1)} \quad [-]$$

in which RC is the direction of plastic flow (i.e. ξ_{sh}/ξ_{vol})

After determination of A and B the Rock parameters can be estimated. The EX value; the eccentricity of the ellipse is computed by;

$$EX = \sqrt{((3 \times B)/A)} \quad [-]$$

The centre⁵ of the ellipse (i.e. the centre is the p' value of p'_n in MPa) is computed by;

$$p'_n = p' - \frac{((q^2 \times B)-1)}{((B \times q)/RC)} \quad [\text{MPa}]$$

Although not a Rock parameter, the maximum isotropic compression strength p'_{max} can be deduced using;

⁵ Mathematically seen an ellipse does not have a centre. Here, it is the middle of the chord between the two focal points.

$$p'_{max} = p'_n + \sqrt{(1/A)} \quad [\text{MPa}]$$

And, also not a Rock parameter, the maximum deviatoric stress (i.e. critical state point), q_{max} ;

$$q_{max} = \sqrt{(1/B)} \quad [\text{MPa}]$$

In the next step the shear branch of the yield locus can be deduced. Early simulations of roller passes on HMA indicated that this shear branch for rolling calculations is not very relevant (unless shear occurs during rolling). The shear branch is therefore estimated running straight from the point of critical state (highest point of the ellipse) to the isotropic tension strength. The latter one was estimated at 0.15 times the maximum value for isotropic compression, based on yield loci shapes as obtained for soils by Vermeer and Delft Egg (after Vermeer, 1980 and Van Eekelen 1994).

Quantitatively the next Rock parameters can be deduced;

The maximum isotropic tensile strength, p'_t ;

$$p'_t = 0.15 \times p'_{max} \quad [\text{MPa}]$$

For further shaping the yield locus we need to define the “brittle plastic” point of the yield locus because the point plays a role during the determination of the size of the closure cap. However, the meaning of “brittle plastic” is not so relevant for this HMA compaction research and will therefore not be discussed here. The brittle plastic point is expressed in p' and q , and for this research, arbitrarily shaped half way the shear branch (in between $p'_n = 0$ and the critical state point itself);

$$p'_{bp} = 0.5 \times p'_n \quad [\text{MPa}]$$

$$q_{bp} = q_0 \times \frac{(-p'_{bp} + p'_t)}{\sqrt{3} \times (-p'_n + p'_t)} \quad [\text{MPa}]$$

For further shaping of the yield locus the parameter AA must be calculated. The parameter AA is an input parameter for Rock and deduces the slope of the yield locus. For calculation of AA first parameter $A2$ (not a Rock input parameter) it must be calculated. $A2$ is the real slope of the shear branch.

$$A2 = \frac{(q_{max} / (q_{bp} - 1))}{(p'_n / (p'_{bp} - 1))}$$

$$AA = \frac{(A2 - 1) \times (q_{bp} - p'_t)}{p'_t}$$

The hardening parameter, $w3$, regulates the rate the material strength increases related to the changes in volume (i.e compaction). This $w3$ parameter does also tune the slope of the irrecoverable line in the $VMA: \log p'$ plane, see Figure 0.6. Doing one-element, axial symmetrical compression simulations and comparing them to results obtained by

the laboratory measuring programme deduced this parameter. The larger w_3 , the stiffer the plastic material behaviour. For the three material temperatures (78, 94 and 141°C) the hardening factors were deduced as shown in Table 0.3. The Table indicates that W_3 increases with material temperature. This corresponds to the material measurements done in the laboratory see e.g. Figure 3.21 in Section 3.6. The hotter mixtures do have a fainter slope of the irrecoverable part of the deformation line which corresponds to “weaker” plastic behaviour.

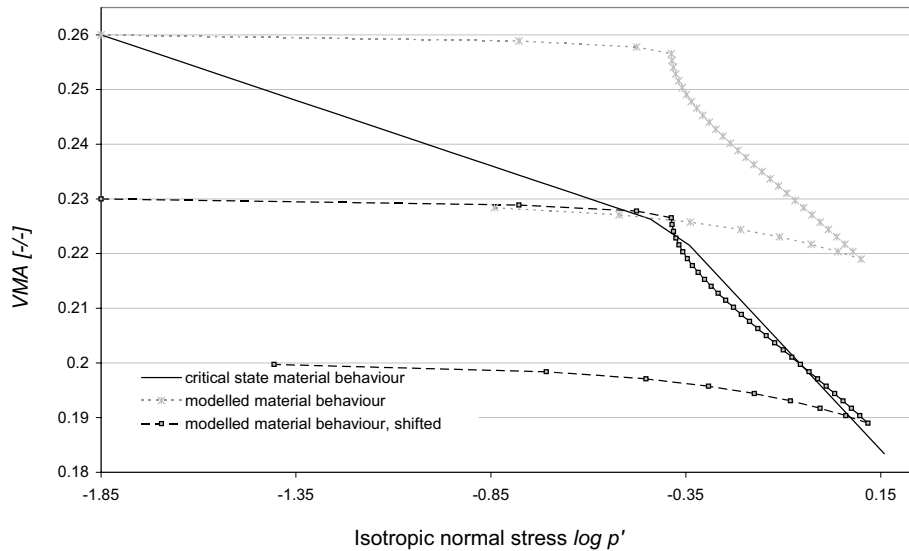


Figure 0.6 The critical state theoretical material behaviour and the calculated material behaviour modelled with Rock.

ESTIMATED W_3 VALUES FOR DAC 0/11 MIXTURE			
Imitated material temperature	78°C	94°C	141°C
W_3 [-]	10000	10900	13540

Table 0.3 The estimated W_3 values for a DAC 0/11 mixture at three material temperatures (i.e. 78, 94 and 141°C)

Example of obtained material Rock parameters

The following (table 0.3) is a summary of all the Rock material parameters for a DAC 0/11 material of 78 °C and an initial VMA level of 0.260;

ROCK MATERIAL PARAMETERS	
<i>Current temperature</i> [°C]	78
<i>Initial VMA level</i> [-/-]	0.260
<i>E</i> [MPa]	200
<i>ν</i> [-]	0.2
<i>W1</i> [-]	0.05
<i>AA</i> [-]	1.0
<i>EX</i> [-]	0.3755
<i>HP</i> [-]	1.0
<i>HB</i> [-]	1.0
<i>p'bp</i> [MPa]	-0.1878
<i>qbp</i> [MPa]	0.4056
<i>p'ten</i> [MPa]	0.0765
<i>p'n</i> [MPa]	-0.3727
<i>W3</i> [-]	10,000

Table 0.4 The estimated Rock material parameters for a material of 78 °C and an initial VMA value of 0.260.

Appendix I

Estimation of the initial HMA material temperatures

In order to simulate compaction of asphalt layers it is important to know what the temperature of the material is during compaction. Therefore the cooling of the layer was modeled. An important quantity during (modeling) such a cooling process is the initial material temperature during paving. This appendix shows the figures that are used to estimate the initial HMA material temperature of the two test layers of the test sections at two locations. The complete procedure is described in Section 5.2.

The following relation is used for estimating the initial material temperatures:

$$T_{HMA_c} = 10^{(S \times t + I)} + T_{air}$$

In which:

- T_{HMA_c} = current HMA material temperature in °C
- S = estimated slope of the model
- I = estimated intercept of the model
- t = time in minutes after spreading
- T_{air} = current air temperature in °C

Log-linear regression through obtained temperature data in order to obtain the initial HMA material temperature, paved layers 2 and 3, thermo couples 1 and 2, position; middle. Estimating the initial material asphalt temperatures from extrapolation of the temperature readings in the middle of the layer (i.e. $h = 25$ mm).

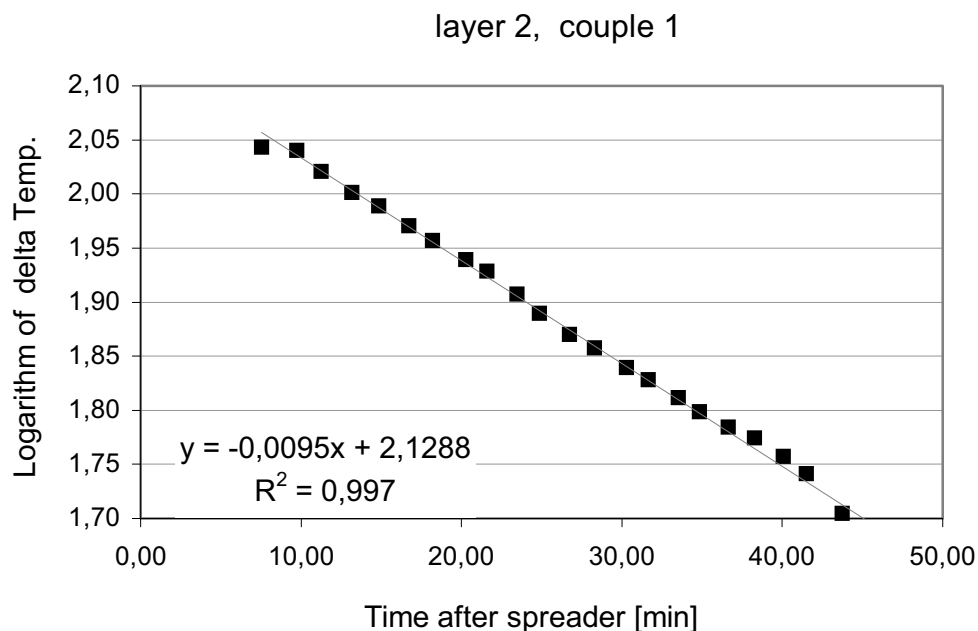


Figure 0.1 Temperatures measured in layer 2, thermocouple location 1.

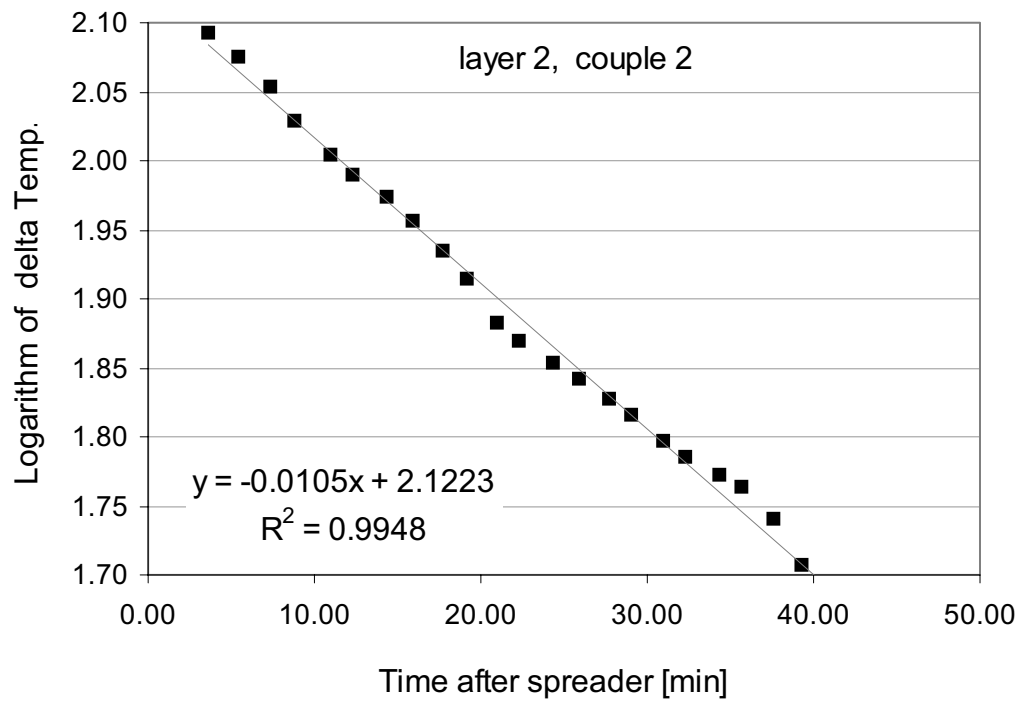


Figure 0.2 Temperatures measured in layer 2, thermocouple location 2.

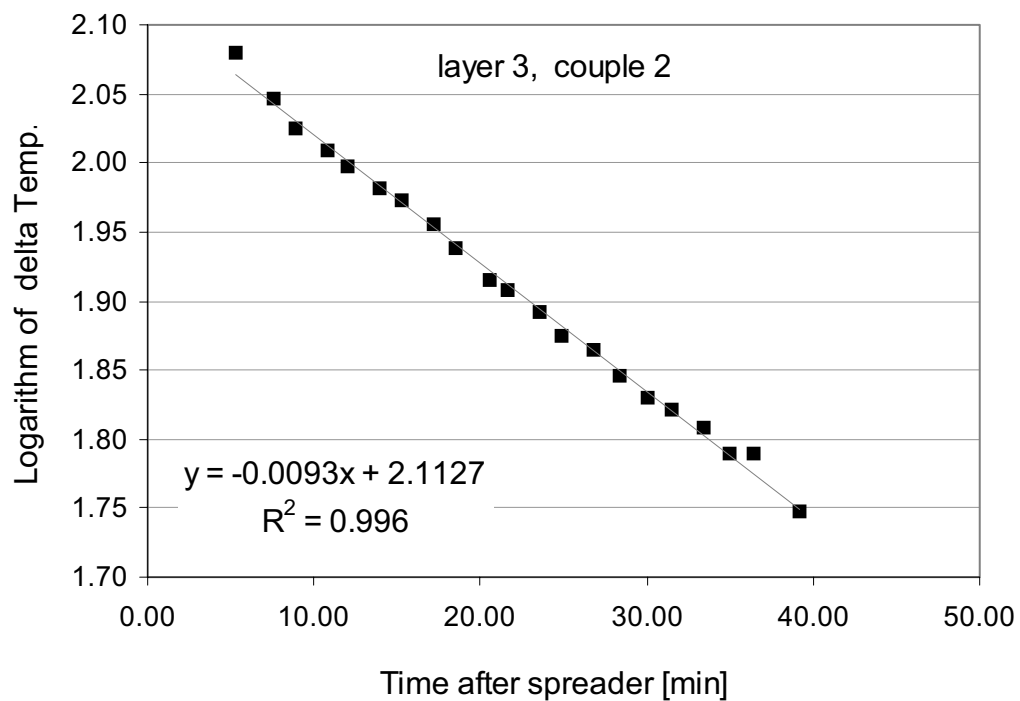


Figure 0.3 Temperatures measured in layer 3, thermocouple location 1.

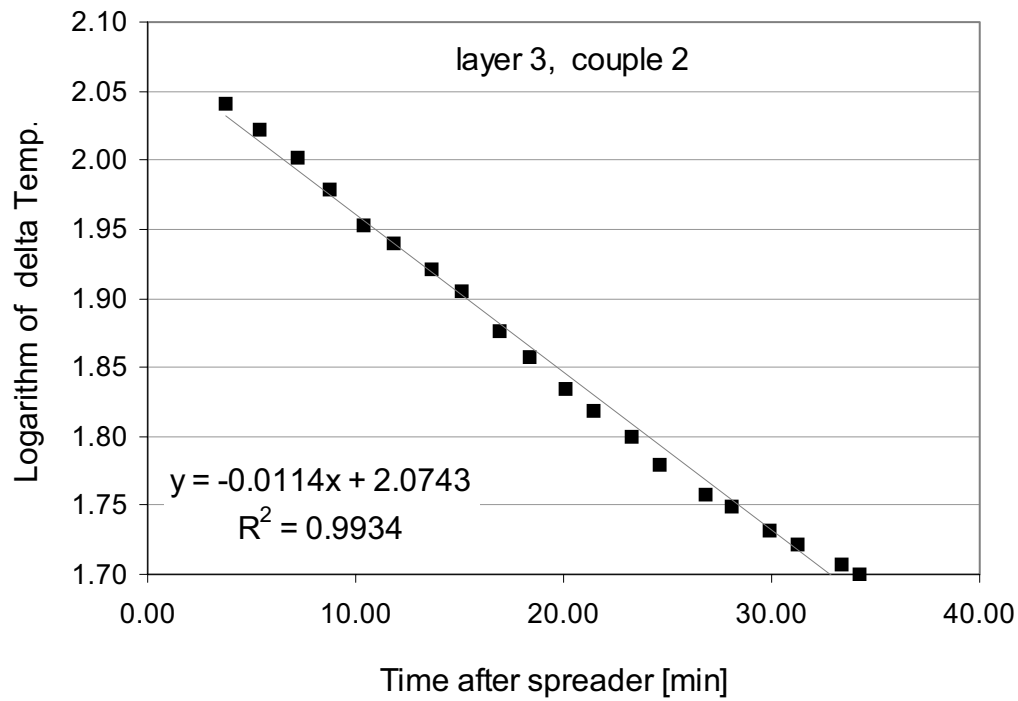


Figure 0.4 Temperatures measured in layer 3, thermocouple location 2.

Appendix J

Statistical analysis of layer thickness measurements

To obtain information on compaction progression of asphalt material during construction processes of roads, the compaction process of a test section was accurately monitored (see also chapter 5). The compaction progress was based on measuring the layer thickness after each roller pass using different measuring techniques. Layer thickness data was obtained by doing level and rod and Stratotest readings. This appendix discusses how from the layer thickness readings obtained during construction (compaction) of the test section a link can be established. Because of the complexity of the procedure it is illustrated in the flow chart below

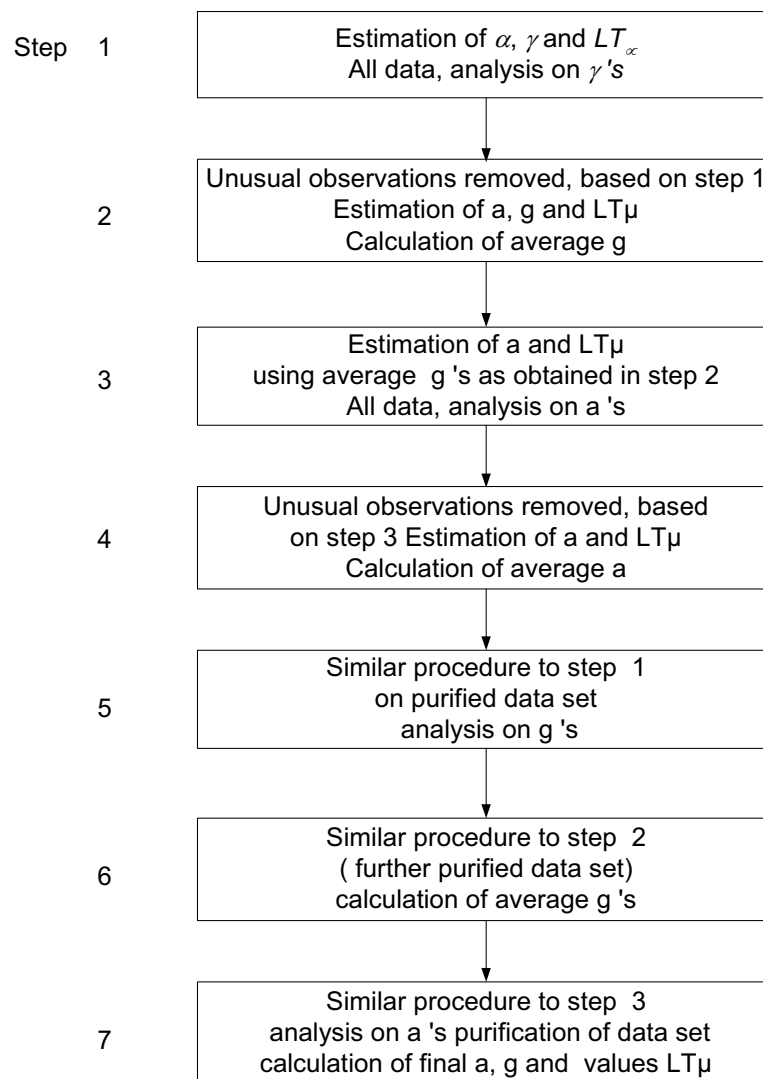


Figure 0.5 A flowchart of the procedure followed during the statistical analysis to obtain the layer thickness to number of roller passes relation.

Achieved steps for layer thickness analyses; General.

When the layer thickness readings are depicted in a graph (Figure 0.6) the data suggests a negative exponential relationship. Therefore the following equation is proposed;

$$\frac{LT_N - LT_\infty}{LT_\infty} = \frac{LT_0 - LT_\infty}{LT_\infty} * 10^{-\alpha * N}$$

in which:

- LT_N = layer thickness after roller pass N,
- LT_∞ = theoretical layer thickness after an infinite number of roller passes,
- LT_0 = layer thickness before compaction starts (thickness after spreading the HMA),
- N = applied number of roller passes,
- α = factor representing the speed of the compaction progress.

This relation can also be written as;

$$LT_N = LT_\infty * (1.0 + \gamma * 10^{(-\alpha * N)})$$

in which;

$$\gamma = \frac{LT_0 - LT_\infty}{LT_\infty}$$

Or into the form that together with Figure 0.6 indicates the transformation that will be used during the analyses.

$$\equiv \frac{(LT_n - LT_\infty)}{(LT_0 - LT_\infty)} = 10^{(\alpha N)}$$

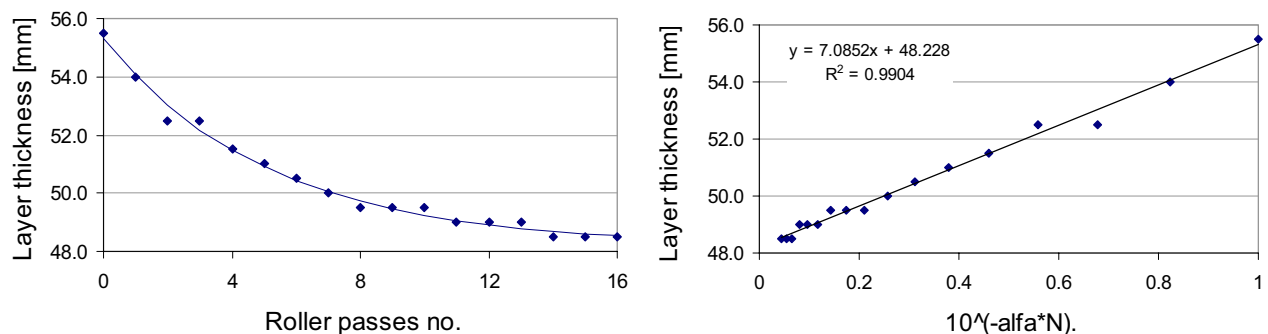


Figure 0.6 The layer thickness data obtained for an individual measuring point; plotted linear-linear (left hand side) and log-linear (right hand side).

The figure on the right hand side illustrates the linearity when a transformation is applied. The figure can be explained with the formula. Note that for all the readings obtained at a specific measuring point, the parameters LT_∞ and LT_0 are fixed values. This makes the quotient at the left hand side of the equation equal to a factor times LT_n .

The statistical analysis was done using the statistical programme SPSS for Windows (Release 9.0, 18 Dec. 1998). The method used was non-linear regression. Apart from the data, the model (formula) and start values for the used parameters were given. For all individual measuring points, a regression analysis was achieved; subsequently, the analysis was done according to estimated parameters, α , γ and LT_{∞} (discussed in this appendix).

During the analysis use is made of the code for definition of series of layer thickness data.

Example: LR3B16 means;

LR; data obtained by Level and Rod readings

3; layer no. 3

B; the B lane

The layer thickness measured after 16 roller passes

General procedure

For the estimation of the model parameters describing the layer thickness during compaction an iterative procedure is applied to obtain the best accuracy. The procedure is discussed in detail in 7 steps. It may be the case that in between some steps outliers were deleted from the database. Outliers are defined as completely unusual observations, Figure 0.7 illustrates at least one of them (Strato test readings, N=14).

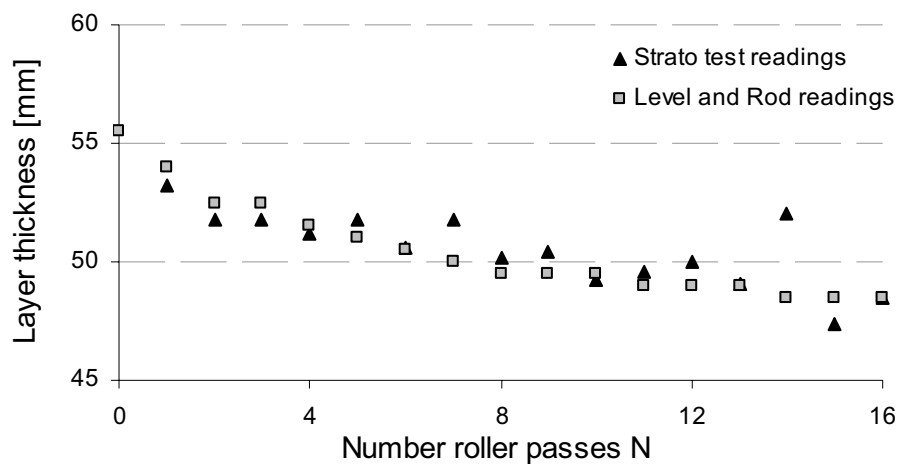


Figure 0.7 The rough layer thickness data of layer 2, measuring point 5.

Step 1: deduction of γ

As a first step for all measuring points a non-linear regression is applied by using the LT_n formula as a model. For each measuring point the factors α , γ , and LT_{∞} were estimated. The target of the steps 1 and 2 is to obtain an average γ value, based on the assumption that γ represents the ratio between pre-compaction level and ultimate compaction possible. This γ value would be equal for all measuring points if; the

material composition and pre-compaction level is constant at the involved road section. Figure 0.8 shows a histogram of the different γ values obtained. The plot indicates that the γ value of 4 to 6 measuring points differs quite a lot from the remaining ones, one can see them as outliers. 95% of the observations fall in the class $0.06 \leq \gamma \leq 0.54$

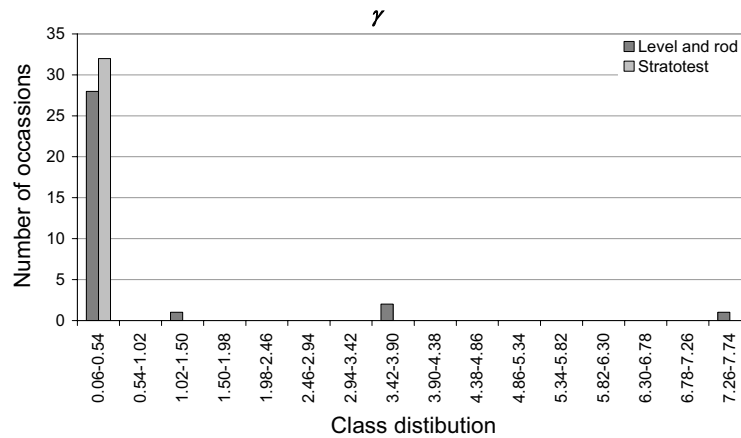


Figure 0.8 A histogram of the parameter values γ obtained during step 1, for all measuring points, level and rod and Stratotest readings.

Step 2; improvement of γ

In step 2 the outliers as determined in step 1 are removed from the dataset. The data series coded: LR3B16, LR3B4, LR3B8, LR2A7 were removed. These data series were all level and rod readings. Again analysis of γ gave the results as illustrated in Figure 0.9. Average γ values and the standard deviation σ_{n-1} obtained per measuring device (Level and rod versus Stratotest) were determined. One can see quite a difference between γ obtained by level and rod and Stratotest measuring systems.

Figure 0.9 Histogram of the parameter values γ obtained during step 2, level and rod and Stratotest readings, for all measuring points except LR3B16, LR3B4, LR3B8 and LR2A7.

The calculated variables were:

level and rod	stratotest
$\bar{\gamma} = 0.1567$	$\bar{\gamma} = 0.1209$
$\sigma_{n-1} = 0.0583$	$\sigma_{n-1} = 0.0629$

Step 3: deduction of α values

However, estimating the α values per measuring point by means of non-linear regression, the average γ values as obtained in step 2 (0.1567 for the level and rod test series, and 0.1209 for the Stratotest test series) were used in the LT_n model. Analysis was done on all data. Analysis of the α values gave results as illustrated in Figure 0.10.

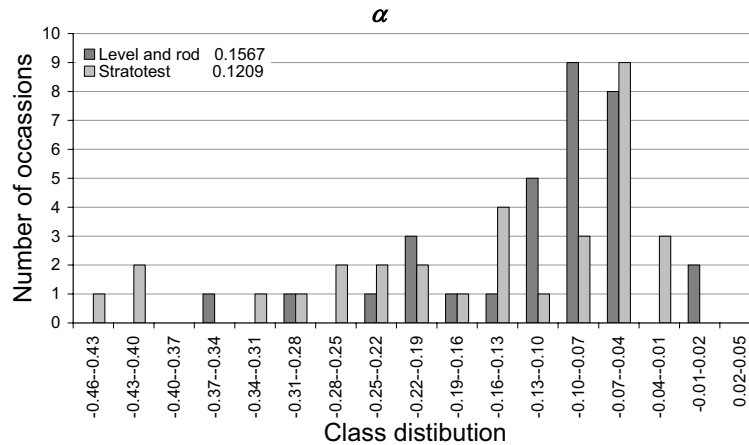


Figure 0.10 The parameter values α obtained during step 3, for all measuring points, level and rod and Stratotest readings.

Again four observations points were identified as unusual. In general we defined observations as unusual when they fell outside the reliability domain. A domain that can be obtained by the average value ± 2 times the standard deviation.

Step 4: improvement α

The α values obtained during step 3 showed again outliers. The calculated R^2 values for that data series also gave large differences.

A couple of data series gave unusual results. The notes of the day the readings were taken were consulted and they indicated a cause for unreliable readings for some measuring points.

The following data points were removed:

LR2A11: Reading N=6

LR2A07: Reading N=3,7

LR2A09: Reading N=6

LR3B04, LR3A11, LR3A13, LR3A03, LR3A07: Reading N=1

LR3B08: removed completely (too few plausible readings)

S2A01, S2A03, S2A05, S2A07: Reading N=14

S2A15: Reading N=7

S3A01: Reading N=6

S3A11: Reading N=5

The unreliable marked data (readings) were removed and again all α values were estimated. The result is given in Figure 0.11. The plot shows that the distribution of α is slightly improved, although still some outliers can be observed.

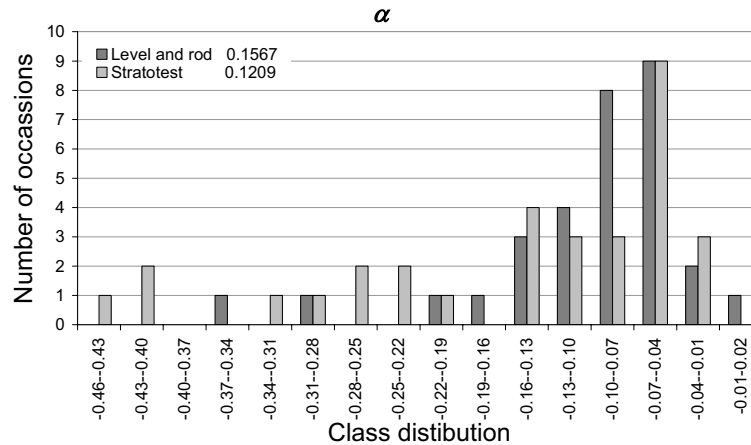


Figure 0.11 The parameter values α obtained during step 4, level and rod and Stratotest readings for all measuring points except LR3B08. From some data series one reading was skipped.

Level and rod ($\bar{\gamma} = 0.1567$)	Stratotest ($\bar{\gamma} = 0.1209$)
$\bar{\alpha} = -0.1001$	$\bar{\alpha} = -0.1526$
$\sigma_{n-1} = 0.0738$	$\sigma_{n-1} = 0.1245$

Step 5: deduction of γ using a purified data set

In step 5 the same procedure is applied as in step 1, regarding the analysis of the γ parameter and deducing an average γ value. However, this time the analysis was done based on a purified data set. By purifying we mean here that all unusual observations (as indicated in step 4) were removed. The distribution of γ as plotted in Figure 0.12 is better than the one obtained during step 1.

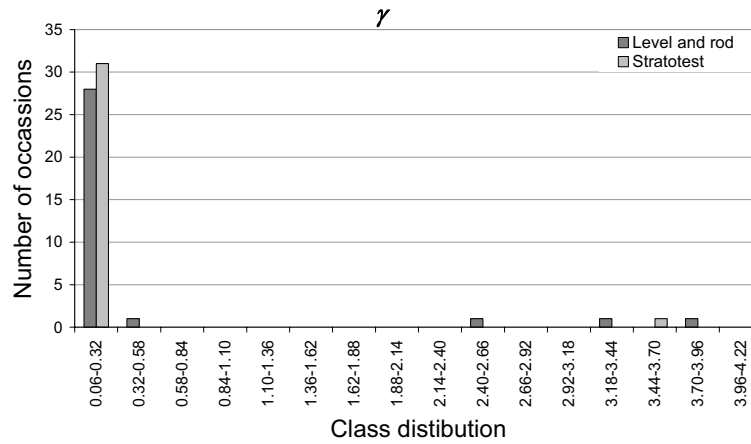


Figure 0.12 The parameter values γ obtained during step 5, level and rod and Stratotest readings for all measuring points, some individual data readings were removed.

Step 6: as 2 again deduction of γ using the purified data set

The same procedure as during step 2; improved analysis of γ value. Removed data series (based on information from step 5): LR3B16, LR3B08, LR3B04, S2A05. The results can be seen in Figure 0.13.

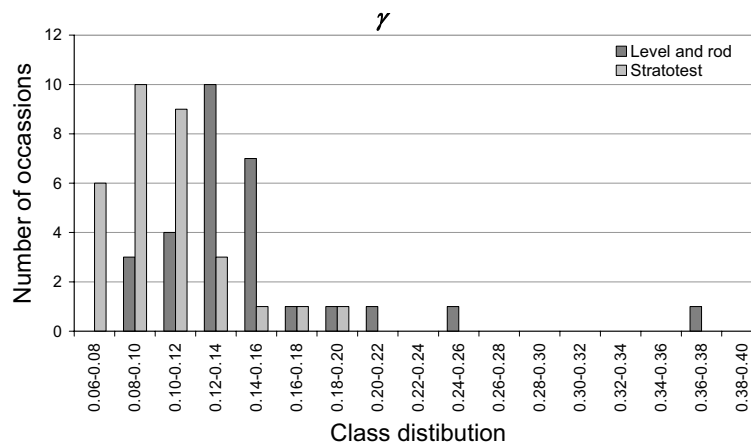


Figure 0.13 The parameter values γ obtained during step 6, level and rod and Stratotest readings for all measuring points except: LR3B16, LR3B08, LR3B04, S2A05.

Results:

Level and rod

Stratotest

$$\bar{\gamma} = 0.1497$$

$$\bar{\gamma} = 0.1087$$

$$\sigma_{n-1} = 0.0530$$

$$\sigma_{n-1} = 0.0305$$

Step 7: deduction of α similar to step 3 using the purified data set

Again, using the γ values as obtained in step 6 for deduction of new α values (similar procedure as during step 3 now on cleansed data set). The results can be seen in the Figure 0.14. Analysis of the level and rod data indicate a reasonable consistency of the obtained information, however, the constituency for the Stratotest information is worse. The standard deviation obtained for the Stratotest data is twice the one obtained for the Level and rod data.

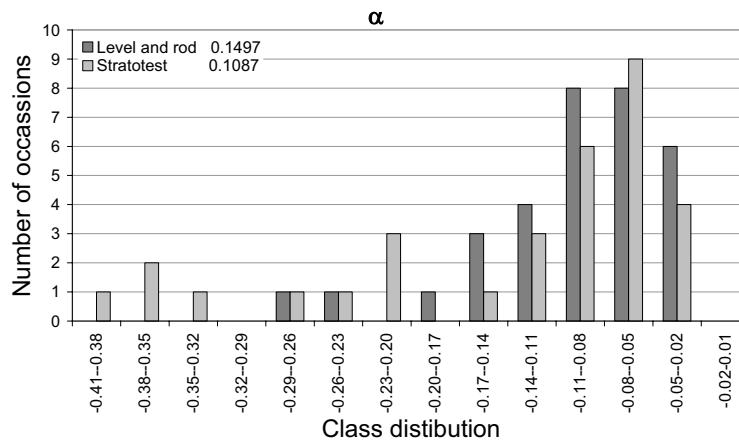


Figure 0.14 The parameter values γ obtained during step 7, level and rod and Stratotest readings for all measuring points, some individual data readings removed (see step 4).

Result:

Level and rod ($\bar{\gamma} = 0.1497$)

Stratotest ($\bar{\gamma} = 0.1087$)

$\bar{\alpha} = -0.0964$

$\bar{\alpha} = -0.1367$

$\sigma_{n-1} = 0.0561$

$\sigma_{n-1} = 0.1100$

Discussion of the results;

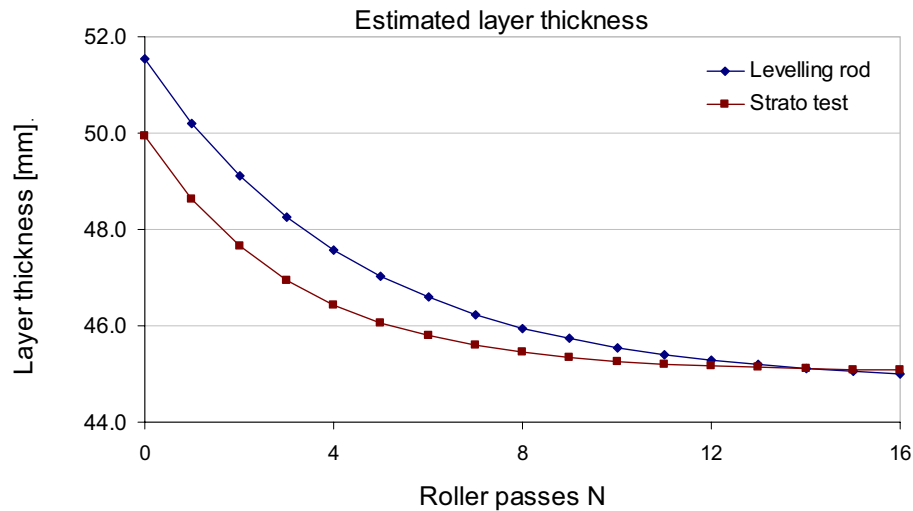


Figure 0.15 The layer thickness modelled using the average obtained parameters α , γ and LT_{∞} as a result of the different applied roller passes until no. 16.

Comparing the obtained model from the level and rod information to the one obtained from Stratotest information in Figure 0.15, indicates that during the start of the compaction process the level and rod model indicates an approximately 1.5 mm thicker layer. However, the obtained layer thickness values at the end of compaction are similar. This indicates that one of the systems must obtain faulty results. Because the level and rod is a system that has proved its reliability over a long time period whereas the Stratotester is relatively new, level and rod measurements are used for the research simulations. An additional consideration is that the faulty results mainly were obtained from the Stratotest on hot mixtures. The Stratotest equipment uses radar wave technology, and it is therefore plausible that this type of system is affected more by temperature than the level and rod system.

Appendix K

Calculation of bulk density and VMA during compaction

Based on the layer thickness trajectory during rolling (obtained from the test section), the specific densities and VMA values during compaction can be calculated. The following example illustrates the procedure used;

Example:

The layer thickness relationship is given with the formula;

$$LT_N = LT_\infty \times (1.0 + \gamma 10^{(-\alpha N)})$$

Where, the parameters $\gamma = 0.1467$ and $\alpha = 0.0964$

From measurements on the cores the following results are obtained;

$$LT_{16} = 48.0 \text{ mm}$$

$$\rho_m_{16} = 2270 \text{ kg/m}^3$$

and, from mix design (material composition) reports;

$$\text{and } \rho_m (0\% \text{ HR}) = 2416.6 \text{ kg/m}^3$$

$$\text{VMA at } 0\% \text{ HR} = 0.137 \text{ [-/-]}$$

Given that at a specific point the layer thickness is 48.0 mm after 16 roller passes, the infinite layer thickness LT_{∞} can be estimated, for given values, LT_{16} , α and γ ;

$$LT_{16} = LT_{\infty} \times (1.0 + \gamma 10^{(-\alpha \times 16)}) = 48.0 \text{ mm}$$

$$\rightarrow LT_{\infty} = 47.79 \text{ m}$$

Using the same relationship it can be calculated that after the 4th roller pass the Layer Thickness value should have been;

$$LT_4 = 47.79 \times (1.0 + 0.1467 \times 10^{(-0.0964 \times 4)}) = 50.74 \text{ mm}$$

Combining the layer thickness, LT_4 , and layer thickness and bulk density in the infinite state, the density after four passes is;

$$\rho_m = 2270 \times 48.0 / 50.74 = 2147 \text{ kg/m}^3$$

The VMA value associated with this layer thickness and material density can also be calculated as the sum of a [-/-] voids + b [-/-] bitumen, Where a and b are calculated as,

$$a \% \text{ voids} = (2416.6 - 2147) / 2416.6 = .111 \text{ [-/-]}$$

$$b \% \text{ bit} = 0.1370 \times (1 - 0.111) = .122 \text{ [-/-]}$$

The VMA value can now been calculated on;

$$\rightarrow \text{VMA} = 0.111 + 0.122 = 0.233 \text{ [-/-]}$$

Appendix L

Residual analysis of the HMA cooling

For modeling the cooling rate of the asphalt layer as it was constructed during the test section a statistical analysis of the temperature readings was achieved. After obtaining the model (see Section 5.2) doing a residual analysis as discussed here can indicate if there is an extra causal variable that can be incorporated to improve the predictive force of the model.

Residual analysis of the HMA cooling model for the temperature reading positions “middle”.

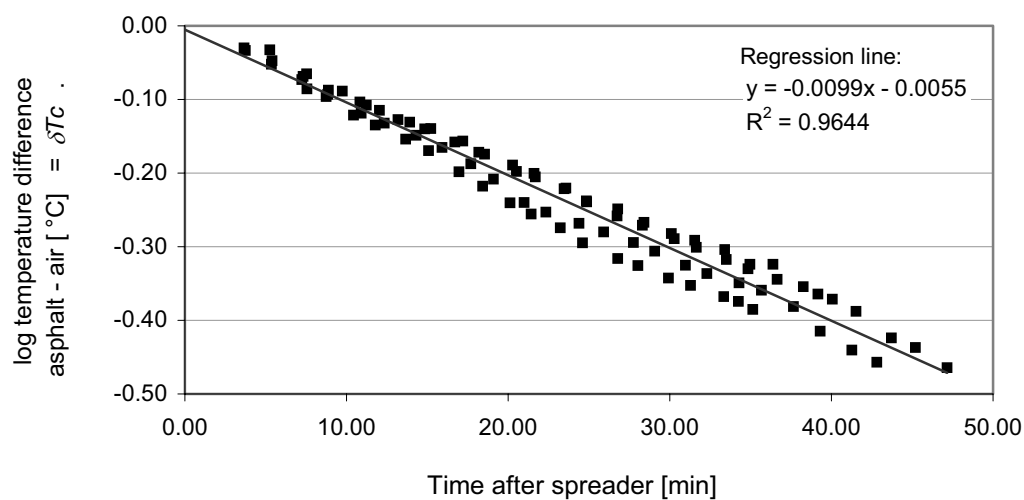


Figure 0.1 Estimated model for all locations, position middle (h = 25 mm).

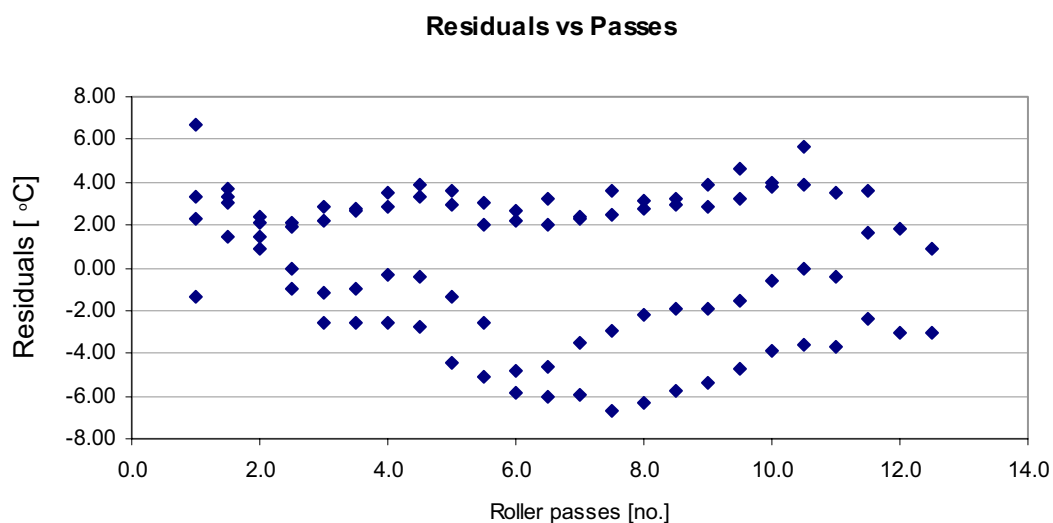


Figure 0.2 Residuals versus number of roller passes.

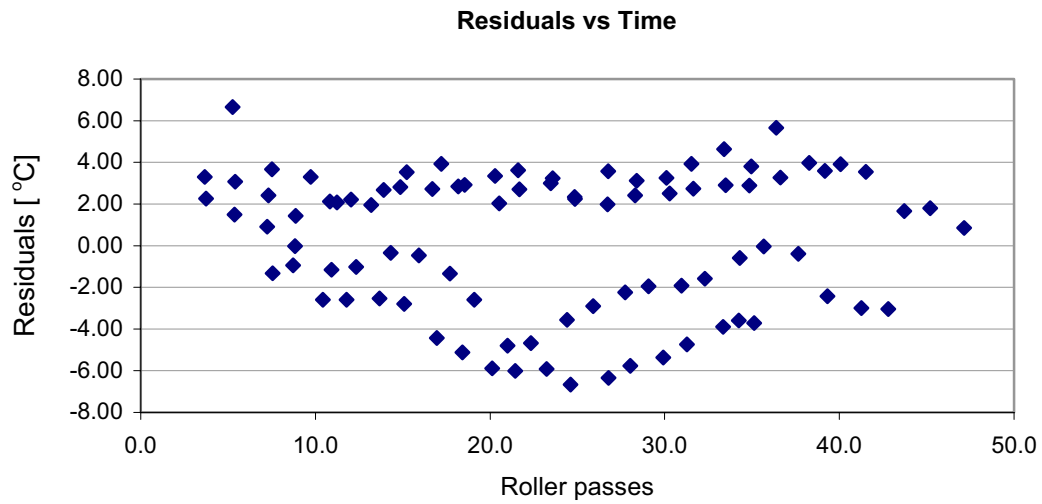


Figure 0.3 Residuals versus time in minutes after paving.

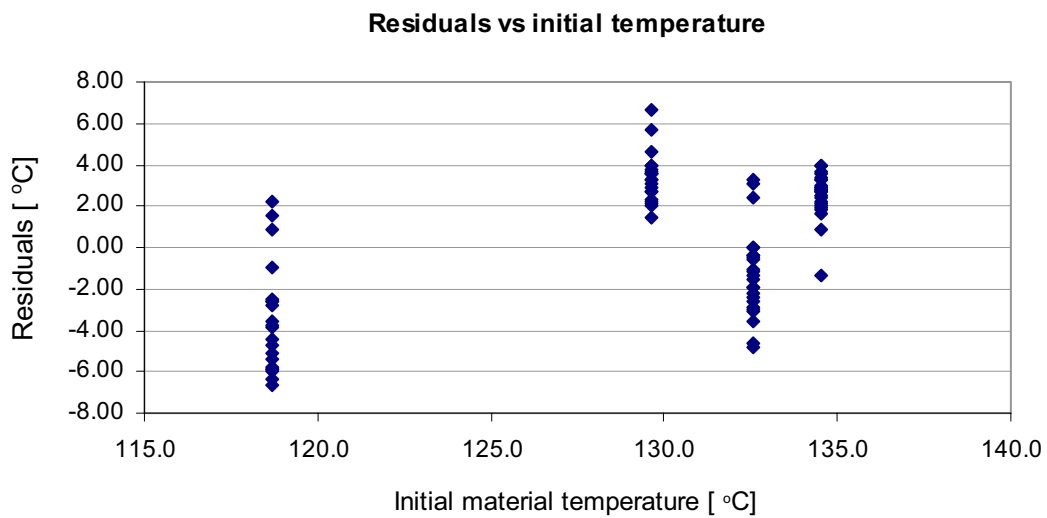


Figure 0.4 Residuals versus initial material temperature.

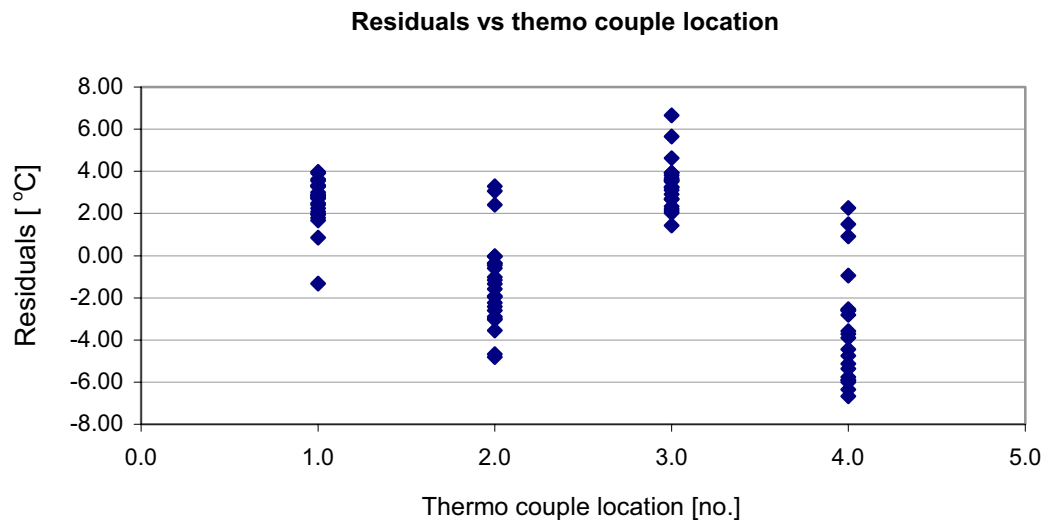


Figure 0.5 Residuals versus thermo couple location.

Analysis of the residual plots;

The plots do show a sort of a pattern; residuals are not random distributed. This may indicate that some structural factor is missed in the model. However, a specific factor for improvement of the model could not be identified.

Appendix M

An input file for a FEM simulation of a roller pass on asphalt

Input file for a DiekA simulation of a roller drum pass on HMA. The roller pass is coded 0.5 applied on B lane of the test section (chapter 4). All main input information blocks start with a code word with a star * on the first position of a new line. All lines that start with at least five – symbols are “comment”. The comment is in Dutch.

```
-----Invoer file voor walsberekening, uitgaande van vijf lagen met
-----verschillende materialen 50 elementen in langsrichting,
materialen met
-----verschillende elastische en plastische eigenschappen
-----Preprocessor Walsen -creëert een invoerfile voor DIEKA- versie
2.30
```

```
*START
*IMAGE
*NODES
  1   -2.0000000E+02   0.0000000E+00
  2   -2.0000000E+02   2.3141301E+01
  3   -2.0000000E+02   3.7604615E+01
  4   -2.0000000E+02   4.6644186E+01
  5   -2.0000000E+02   5.2293918E+01
  6   -2.0000000E+02   5.5825000E+01
401  -2.0000000E+02   5.5825000E+01
402  -1.8837759E+02   8.7706139E+01
  7   -1.7427537E+02   0.0000000E+00
  8   -1.7427537E+02   2.3141301E+01
  9   -1.7427537E+02   3.7604615E+01
 10  -1.7427537E+02   4.6644186E+01
 11  -1.7427537E+02   5.2293918E+01
 12  -1.7427537E+02   5.5825000E+01
403  -1.7427537E+02   5.5825000E+01
404  -1.6651563E+02   8.0252491E+01
 13  -1.5207423E+02   0.0000000E+00
 14  -1.5207423E+02   2.3141301E+01
 15  -1.5207423E+02   3.7604615E+01
 16  -1.5207423E+02   4.6644186E+01
 17  -1.5207423E+02   5.2293918E+01
 18  -1.5207423E+02   5.5825000E+01
405  -1.5207423E+02   5.5825000E+01
406  -1.4691815E+02   7.4425795E+01
 19  -1.3296576E+02   0.0000000E+00
 20  -1.3296576E+02   2.3141301E+01
 21  -1.3296576E+02   3.7604615E+01
 22  -1.3296576E+02   4.6644186E+01
 23  -1.3296576E+02   5.2293918E+01
 24  -1.3296576E+02   5.5825000E+01
407  -1.3296576E+02   5.5825000E+01
408  -1.2955073E+02   6.9915344E+01
 25  -1.1655579E+02   0.0000000E+00
 26  -1.1655579E+02   2.3141301E+01
```

```
-----
```



```

PSC4
      6      1
GENEL
      50     251     403     404     402     401     2
EOT
EOG
EOD

```

-----de volgende knooppunten worden gekoppeld:
-----de punten boven de plaat aan de aanliggende contactpunten
-----alleen in x-richting: de punten van de intree, de onderrand en
de uittree
----- van de plaat aan het daar bovenliggende contactpunt.
-----de walsrolpunten in geroteerde 1 richting

```

*CONNECT
DOF
      306      2      501      2      0
      501      1      401      1      0
EOG
GENODE
      50      6      6      401      2      0
EOG
GEDOF
      5      1      1      1      401      0      1      2
EOG
GEDOF
      6      301      1      1      401      0      1      2
EOG
GEDOF
      49      7      6      1      401      0      1      2
EOG
GEDOF
      50      7      6      2      1      0      2      2
EOG
GEDOF
      50      404      2      1      402      0      1      2
EOG
EOD

```

-----van de volgende punten wordt de verplaatsing in y-richting
onderdrukt:
-----de contactpunten aan de rand van de rol

```

*SUPPRESS
      1      2
EOG
GENOD
      51      402      2      2
EOG
EOD

```

-----de volgende materiaalgroepen worden gegenereerd:
-----de eigenschappen van de plaat
-----de eigenschappen van de contactelementen

-----vijf verschillende materialen (per laag een materiaal)
gedefinieerd

-----Laagnummer	1	2	3	4	5		
-----Mat. No.	209	261	183	92	27		
-----Temperatuur	104.0	112.0	100.0	86.0	76.0		
-----VMA_O	0.260	0.260	0.260	0.260	0.260		

*MATERIAL

ROCK

200.0	0.2						
0.005	1.0	0.37448	1.0	1.0	-0.18000	0.22290	
0.07535		-0.36001	11187.6				

EOG

ROCK

200.0	0.2						
0.005	1.0	0.37597	1.0	1.0	-0.19136	0.23918	
0.08039		-0.38272	11707.0				

EOG

ROCK

200.0	0.2						
0.005	1.0	0.37374	1.0	1.0	-0.17492	0.21559	
0.07309		-0.34984	10927.9				

EOG

ROCK

200.0	0.2						
0.005	1.0	0.36536	1.0	1.0	-0.17807	0.21308	
0.07337		-0.35613	10019.0				

EOG

ROCK

200.0	0.2						
0.005	1.0	0.35627	1.0	1.0	-0.19007	0.22108	
0.07724		-0.38014	9369.7				

EOG

LINEAR

COUL

10.0	0.16	3.0	3.0	1.0	0.8	1.0	0
------	------	-----	-----	-----	-----	-----	---

EOG

EOD

*LNSR

0.8	0.1	1.5	5
-----	-----	-----	---

*ALE

ORTHO

DEFAULT

EOD

*ROTATED BASIS

ANGLE

402	-3.4964903E-01
404	-3.0764322E-01
406	-2.7046122E-01
408	-2.3782914E-01
410	-2.0938458E-01
412	-1.8471630E-01

```

414    -1.6339449E-01
416    -1.4499260E-01
418    -1.2910197E-01
420    -1.1534116E-01
422    -1.0336140E-01
424    -9.2849146E-02
426    -8.3526881E-02
428    -7.5152531E-02
430    -6.7487689E-02
432    -6.0393141E-02
434    -5.3726454E-02
436    -4.7366560E-02
438    -4.1217843E-02
440    -3.5207074E-02
442    -2.9280383E-02
444    -2.3400250E-02
446    -1.7542516E-02
448    -1.1693403E-02
450    -5.8465398E-03
452     0.0000000E+00
454     5.8464399E-03
456     1.1692603E-02
458     1.7539818E-02
460     2.3393846E-02
462     2.9267839E-02
464     3.5185274E-02
466     4.1182875E-02
468     4.7313514E-02
470     5.3649080E-02
472     6.0283304E-02
474     6.7334523E-02
476     7.4948337E-02
478     8.3300134E-02
480     9.2597368E-02
482     1.0308150E-01
484     1.1502937E-01
486     1.2875376E-01
488     1.4460267E-01
490     1.6295673E-01
492     1.8422386E-01
494     2.0883002E-01
496     2.3720461E-01
498     2.6975891E-01
500     3.0685594E-01
502     3.4877100E-01

```

EOD

*EULER

*SURFACE

AUTOPRIOR

OPT4

0 0 0

GENOPT

```

4 2 1 1 0 401 0 1 0 1 0
4 8 1 7 0 403 0 1 0 1 0
4 14 1 13 0 405 0 1 0 1 0
4 20 1 19 0 407 0 1 0 1 0
4 26 1 25 0 409 0 1 0 1 0
4 32 1 31 0 411 0 1 0 1 0
4 38 1 37 0 413 0 1 0 1 0

```

4	44	1	43	0	415	0	1	0	1	0
4	50	1	49	0	417	0	1	0	1	0
4	56	1	55	0	419	0	1	0	1	0
4	62	1	61	0	421	0	1	0	1	0
4	68	1	67	0	423	0	1	0	1	0
4	74	1	73	0	425	0	1	0	1	0
4	80	1	79	0	427	0	1	0	1	0
4	86	1	85	0	429	0	1	0	1	0
4	92	1	91	0	431	0	1	0	1	0
4	98	1	97	0	433	0	1	0	1	0
4	104	1	103	0	435	0	1	0	1	0
4	110	1	109	0	437	0	1	0	1	0
4	116	1	115	0	439	0	1	0	1	0
4	122	1	121	0	441	0	1	0	1	0
4	128	1	127	0	443	0	1	0	1	0
4	134	1	133	0	445	0	1	0	1	0
4	140	1	139	0	447	0	1	0	1	0
4	146	1	145	0	449	0	1	0	1	0
4	152	1	151	0	451	0	1	0	1	0
4	158	1	157	0	453	0	1	0	1	0
4	164	1	163	0	455	0	1	0	1	0
4	170	1	169	0	457	0	1	0	1	0
4	176	1	175	0	459	0	1	0	1	0
4	182	1	181	0	461	0	1	0	1	0
4	188	1	187	0	463	0	1	0	1	0
4	194	1	193	0	465	0	1	0	1	0
4	200	1	199	0	467	0	1	0	1	0
4	206	1	205	0	469	0	1	0	1	0
4	212	1	211	0	471	0	1	0	1	0
4	218	1	217	0	473	0	1	0	1	0
4	224	1	223	0	475	0	1	0	1	0
4	230	1	229	0	477	0	1	0	1	0
4	236	1	235	0	479	0	1	0	1	0
4	242	1	241	0	481	0	1	0	1	0
4	248	1	247	0	483	0	1	0	1	0
4	254	1	253	0	485	0	1	0	1	0
4	260	1	259	0	487	0	1	0	1	0
4	266	1	265	0	489	0	1	0	1	0
4	272	1	271	0	491	0	1	0	1	0
4	278	1	277	0	493	0	1	0	1	0
4	284	1	283	0	495	0	1	0	1	0
4	290	1	289	0	497	0	1	0	1	0
4	296	1	295	0	499	0	1	0	1	0
4	302	1	301	0	501	0	1	0	1	0
EOT										
EOG										
OPT3										
0	0	0								
GENOPT										
49	403	2	401	2	405	2	1	0	6	0
EOT										
501	499	640	1	6						
EOT										
306	499	640	1	6						
EOT										
EOG										
EOD										

-----er worden verplaatsingen voorgeschreven voor:
-----de hartlijn punten van de plaat (met waarde 0 in de y-richting)

-----de contact punten op de rand van de rol.

```
*MAXITER
40
  2.0000000000E-02      0.0000000000E-03
```

```
*BATCH
0.9
```

```
*OUTPUT
DISPLACEMENT
INCRDIS
UNBALANCE
FORCES
ELGROUP
  1  2  3  4  5  6
NODAL
  1  5  6  7  21
PRESSURE
PARTTR
EOD
```

```
*POST
*STEP
```

```
*PRESCRIBED
401  1  0.02
EOG
402  1  0.02
EOG
EOD
```

```
*STEP
```

```
*NOPOST
*STEP 98
*POST
*STEP
```

-----100 steps, materiaal verplaatsing 2 mm

```
*PRESCRIBED
401  1  0.04
EOG
402  1  0.04
EOG
EOD
```

```
*NOPOST
*STEP 99
*POST
*STEP
```

-----om de 100 stappen uitvoer

-----200 steps materiaal verplaatsing 6 mm

*PRESCRIBED

201 1 0.06

EOG

202 1 0.06

EOG

EOD

*NOPOST

*STEP 99

*POST

*STEP

-----om de 100 stappen uitvoer

-----300 steps materiaal verplaatsing 12 mm

*PRESCRIBED

201 1 0.08

EOG

202 1 0.08

EOG

EOD

*NOPOST

*STEP 99

*POST

*STEP

-----om de 100 stappen uitvoer

-----400 steps materiaal verplaatsing 20 mm

*PRESCRIBED

201 1 0.10

EOG

202 1 0.10

EOG

EOD

*NOPOST

*STEP 99

*POST

*STEP

-----om de 100 stappen uitvoer

-----500 steps materiaal verplaatsing 30 mm

*PRESCRIBED

201 1 0.15

EOG

202 1 0.15

EOG

EOD


```
*NOPOST
*STEP 99
*POST
*STEP
```

```
-----materiaal verplaatsing ca 45 mm
-----600 stappen genomen, uitvoer 1 maal om de 300 daarna om de 500
stappen,
```

```
*PRESCRIBED
201    1    0.20
EOG
202    1    0.20
EOG
EOD
```

```
*NOPOST
*STEP 299
*POST
*STEP
```

```
-----900 stappen, materiaal verplaatsing 105 mm
```

```
*NOPOST
*STEP 499
*POST
*STEP
```

```
-----1400 stappen, materiaal verplaatsing 205 mm
```

```
*NOPOST
*STEP 499
*POST
*STEP
```

```
-----1900 stappen, materiaal verplaatsing 305 mm
```

```
*NOPOST
*STEP 499
*POST
*STEP
```

```
-----2400 stappen, materiaal verplaatsing 405 mm
```

```
*STOP
```


Appendix N

An FEM simulation of HMA rolling

This appendix discusses from start to finish how FEM can be used to simulate a roller pass applied on a HMA layer. Before a simulation can be started the following information must be available:

- a.) the material behaviour is known in terms of critical state parameters for every temperature and every initial *VMA* level,
- b.) a running set up for the rolling problem has already been designed including suitable contact model parameters.

Necessary Input information for a FEM simulation;

- a. rolling drum weight (kg) and rolling drum dimensions (width and diameter in m)
- b. material information in critical state parameters,
- c. from the layer that should be compacted; the actual temperature and the compaction (i.e. *VMA*) state distribution over the depth of the layer,
- d. composition of the mixture.

The procedure for doing a simulation is discussed in the following 9 steps:

1. calculation of actual *VMA* and temperature profile in depth direction of the layer
2. calculation of Rock material parameters based on *VMA* and material temperature
3. deduction of the position of the roller drum related to the material layer
4. first test run; overestimation layer thickness reduction
5. second test run; overestimation layer thickness reduction
6. pointed run based on info obtained from steps 4 and 5
7. judgement of correctness force-compaction progress relation, eventually next trial
8. judgement of output, stress and strain patterns, flow of free material surface, particle tracing, and material movement,
9. calculation of new bulk density and *VMA* profile in depth direction.

The steps will be discussed here individually in the correct order. Where possible and/or useful the steps are illustrated with a figure or a quantified example.

Step 1.

Given the Finite Element mesh distribution in the depth direction of the layer, per row of elements the actual temperature and *VMA* state for the material should be deduced. From the temperature readings at three depths (dots, Figure 0.1) a polynomial function in depth direction can be estimated. From this polynomial temperature distribution a step function of the temperature is calculated. The borders of that step function must be adjusted to the element distribution of the FEM mesh. The measured temperature at three depths, the polynomial function and the step function representing material temperature of layer 2 on the A lane during roller pass 05 are illustrated in Figure 0.1.

Calculation of the *VMA* level for simulation of the first roller drum pass is based on the material composition, the amount of material at the location of interest and the current layer thickness.

Example:

Information about Layer Thickness and material composition

Information about thickness of layers 2 and 3, A and B lanes;

$$\gamma = 0.1497 \text{ [-/-]}$$

$$\alpha = 0.0964 \text{ [-/-]}$$

General relation estimated for layer thickness;

$$LT_N = LT_\infty \times (1.0 + \gamma \times 10^{(-\alpha \times N)})$$

Specific information layer 2, lane B, obtained from measurements on cores

$$\text{layer thickness after 8 passes} = LT_{-8} = 49.8 \text{ mm}$$

$$\text{density after 8 passes} = \rho_{m_{-8}} = 2322.6 \text{ kg/m}^3$$

From this information the calculated amount material per square meter is

$$2322.6 \times 0.0498 = 115.6 \text{ kg/m}^2.$$

Material information (DAC 0/16) used for the test section (i.e. from mixture composition reports);

$$\text{density at 0\% voids} = \rho_m (0\% \text{ HR}) = 2416.6 \text{ kg/m}^3$$

$$\text{Volumetric bitumen content at 0\% voids} = 0.137 \text{ [v/v]}$$

Calculation of LT_∞

For the B lane of layer 2 now, LT_∞ can be calculated using the following equation;

$$LT_{-8} = LT_\infty \times (1.0 + 0.1497 \times 10^{(-0.0964 \times 8)}) = 49.8 \text{ mm}$$

$$\text{Solving the equation leads to; } LT_\infty = 48.6 \text{ mm}$$

Initial situation zero roller passes; VMA distribution

Using the same relation it can be calculated that, the initial layer thickness (i.e. directly after paving, 0 passes) have been;

$$LT_{-INI} = 48.6 \times (1.0 + 0.1497 \times 10^{(-0.0964 \times 0)}) = 55.9 \text{ mm}$$

The Density just after paving can now be obtained on;

$$\rho_m = 115.6 \times 1000 / 55.9 = 2068 \text{ kg/m}^3$$

The Voids content can now be calculated as;

$$HR_{INI} = (1 - (2068/2416.6)) = 0.144 \text{ -/-}$$

Bitumen content volumetric:

$$BIT_{INI} = (1 - HR) \times \text{bit cont} = (1 - 0.144) \times 0.137 = 0.117 \text{ -/-}$$

The initial VMA of the material (0 passes);

$$VMA_{INI} = HR + \text{Bit} = 0.144 + 0.117 = 0.261 \text{ -/-}$$

Initial situation zero roller passes; Temperature distribution

During constructing the test section the temperature was monitored at three depths inside the layer (dots in Figure 0.1). During the first roller pass the temperature in layer 2 of the B lane was;

MATERIAL TEMPERATURE INSIDE LAYER	
Y co-ordinate [mm]	Measured temperature [°C]
0	92.33
25	128.24
54.07	92.48

Table 0.1 Measured material temperature in layer, first roller pass, lane B (code pass 0.5B),

Through this data a polynomial function of the form; $y = ax^2 + bx + c$ can be drawn. Using the temperature readings (Table 0.1) and solving the equation enables deduction of the parameters a, b and c. For this specific situation the values proved to be; $a = -0.0493$, $b = 2.6693$ and $c = 92.33$.

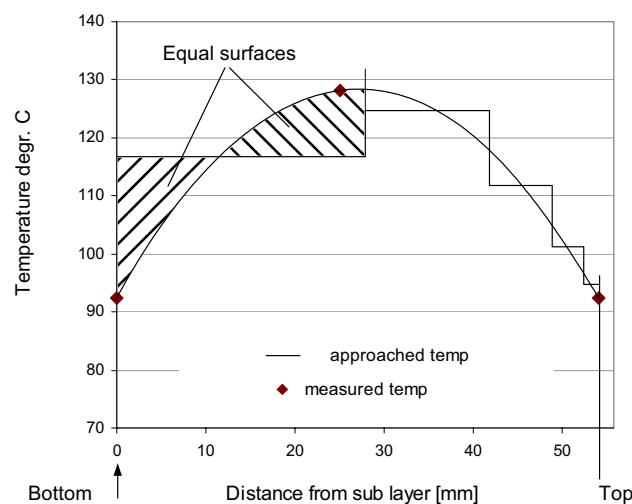


Figure 0.1 Material temperature distribution based on temperature measurements and the modelled temperature step function for deduction of the Rock material parameters.

From calculating the surface underneath the polynomial function (by integral calculus) from one border of the finite element to the second border and equivalent element temperature can be deduced using the following equation. The vertical lines in Figure 0.1 form the borders of the FE mesh. The figure is rotated 90 degr. clockwise.

$$\left(\int_{x=0.0}^{x=23.1} A \times x^2 + B \times x + C \right) / 23.1$$

The result of applying this procedure on all five element layers yield the following result:

TEMPERATURE AND VMA IN LAYER 2 LANE A					
Elements row	1	2	3	4	5
Y co-ordinate, depth [mm]	0.0 – 23.1	23.1 – 37.6	37.6 – 46.6	46.6 – 52.3	52.3 – 55.8
VMA level [/-]	0.260	0.260	0.260	0.260	0.260
Temperature [°C]	115.1	125.9	112.2	95.7	82.3

Table 0.2 pass 1 lane A layer 2(coded 05A)

Step 2.

Based on the local material temperature and compaction situation (i.e. per row of elements) the Rock material parameters could be established. The critical state information expresses the stresses p' and q and the VMA value of the intersection point. Additional information about the ratio $\varepsilon_{sh}/\varepsilon_{vol}$ during plastic flow assists in shaping the yield locus around the initial stress point $p':q$. Further estimation of the yield locus shape was based on known shapes of yield loci for soils. Estimation of hardenings-parameter $W3$ based on the material stiffness during compaction (i.e. plastic deformation compared to critical state behaviour). $W1$ was arbitrarily quantified on 0.005 because this proved to be a reasonable value. Precise quantification of that parameter was for this stage of the compaction research not so relevant because earlier rolling simulations indicated that shearing the material “on the dry side of critical” did not occur.

Example:

The example concerns element row 1, roller pass 1 (code 05A), lane A, The Current VMA level is 0.261, the material temperature 115.1, the Y co-ordinates of the element row between 0.0 and 23.1 mm (see Figure 0.1).

The critical state parameters for such a material at that Temperature(115,1 C) and VMA (0.260) level are:

CRITICAL STATE MATERIAL PARAMETERS	
Slope elastic, κ	-0.01763
Intercept elastic, VMA_{κ}	0.2311
Slope plastic, λ	-0.2452
Intercept plastic, VMA_{λ}	0.7830
p' intersection	0.4125
q intersection	0.6669
VMA level intersection	0.2341
$\varepsilon_{sh}/\varepsilon_{vol}$ plastic deformation	0.7939

Table 0.3 The estimated Critical State material parameters for a material of 115.1 °C and an initial VMA value of 0.26. This material corresponds to the material of the lowest element row of simulation of the first roller drum pass of layer 2, lane A

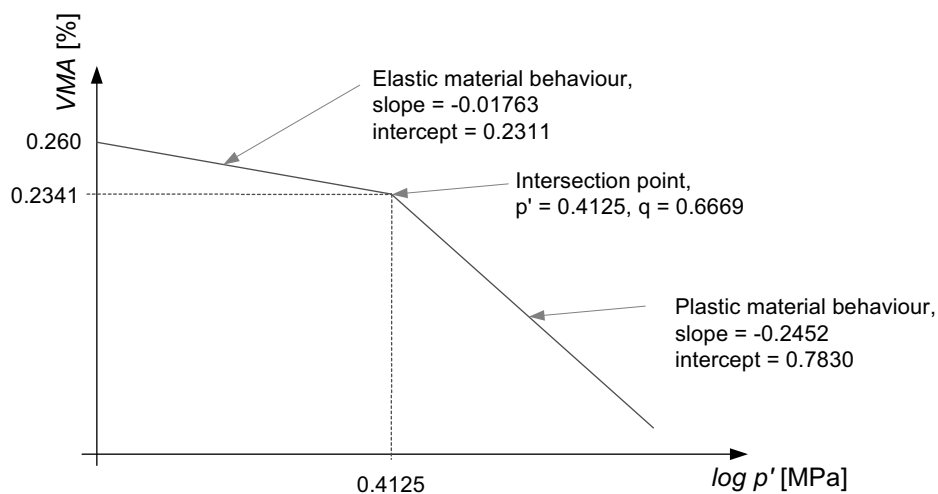


Figure 0.2 Illustration of the Critical State information for the DAC 0/11 at 115.1 °C and a VMA level of 0.261.

Based on the critical state information as expressed in Table 0.3 (position intersection point $p' = 0.4125$, $q = 0.6669$, direction of plastic flow $\varepsilon_{sh}/\varepsilon_{vol} = 0.7939$) the ellipse of the yield locus can be sized and shaped. By doing that use can be made of the formulae as described in appendix 4.2. In this particular situation the parameters A and B can be quantified on respectively, on 44.1 and 2.09. Further, the ellipse must be shifted along the p' axis to meet all criteria over a distance of p'_n . For this example p'_n is calculated on -0.3727 MPa. From the dimensions of the ellipse the eccentricity, EX, can now be calculated which is an input parameter for Rock. The eccentricity, EX, is calculated on $\sqrt{(3 \times B)/A} = 0.3773$.

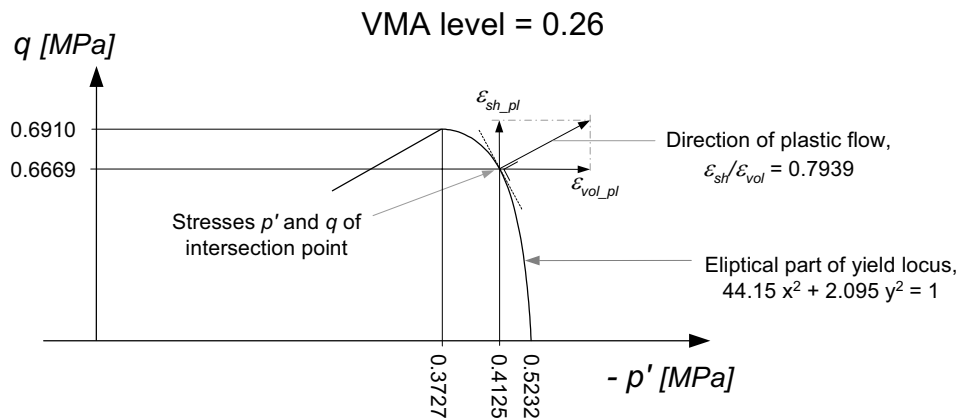


Figure 0.3 Positioning of the ellipse through the $p':q$ intersecting point.

As a next step a shear branch must be modelled. The shear branch is connected to the critical state point of the yield locus, which corresponds to the highest point (highest stress q) of the ellipse. Because the model of the shear branch was not so important for our research project (during a normal compaction process the stress state is on the wet side of critical, see section 2.5) the shear branch is modelled as a straight line. For the same reason the isotropic tension strength of the material, p'_{ten} , is relatively un-important, it was quantified on 0.15 times the isotropic compression strength, p'_{max} . p'_{max} was -0.5232 MPa so p'_{ten} becomes $-0.15 \times -0.5232 = 0.0785$ MPa.

Three Rock parameters that regulate the slope and position of the shear branch are p'_{bp} , q_{bp} and AA . The AA parameter regulates the slope of the shear branch. The position p'_{bp} , q_{bp} is here arbitrarily shaped half way the critical state point. This implies that $p'_{bp} = 0.1864$ MPa and $q_{bp} = 0.4056$ MPa. Calculation of the shear branch slope parameter (AA) can be done with parameter $A2$. The formulae for calculation of AA and $A2$ can again be found in appendix 4.2. Using these equations in our model leads to $A2$ and AA values of respectively 0.7037 and 1.00.

The parameter for hardening, $W3$, has to be shaped by trial and error from one element test run and comparing the results to known critical state behaviour. It proved that a $W3$ value of 12083 is suitable for the material at a temperature of 115.1°C .

The remaining variables E , ν and $W1$ (softening caused by shear) has not been calculated but fixed values were used for all calculations. Table 0.3 summarises all the Rock material parameters for a material of 115.1°C material temperature and 0.260 initial VMA level;

ROCK MATERIAL PARAMETERS	
<i>Current temperature</i> [°C]	115.1
<i>Initial VMA level</i> [-/-]	0.260
<i>E</i> [MPa]	200
<i>v</i> [-]	0.2
<i>W1</i> [-]	0.05
<i>AA</i> [-]	1.0
<i>EX</i> [-]	0.3773
<i>HP</i> [-]	1.0
<i>HB</i> [-]	1.0
<i>SBP</i> [Mpa]	0.1864
<i>TBP</i> [Mpa]	0.4056
<i>p' _{ten}</i> [Mpa]	0.0785
<i>p' _n</i> [MPa]	0.3727
<i>W3</i> [-]	12083

Table 0.4 The calculated Rock material parameters for a material of 115.1 °C and an initial VMA value of 0.260. This material corresponds to the material of the lowest element row of simulation of the first roller drum pass of layer 2, lane A.

Step 3.

Positioning of the free rotating roller drum related to the material.

During a normal asphalt compaction process the progression (in compaction) depends on the roller weight in combination with the characteristics (i.e. compactibility) of the material that is compacted. However, during a FEM simulation of the process, the procedure runs the other way around; compaction progress is fixed (the layer thickness reduction is pre-described) whereas the required rolling drum force becomes calculated. In the simulation input-file it must be specified what the position of the roller drum is related to the material. And, as a result of that, how far the roller drum is pushed into the material. The extent the material is plastically deformed in combination with the (pre-described) material specifications deduces what maximum stresses underneath the roller drum will be reached during rolling. This maximum stress, is not known in advance, it deduces, however, how far the material will recover elastically after the roller drum is passed. Therefore, the magnitude of elastic recovery is also not known in advance. This whole procedure, the process of coming to the correct layer thickness reduction, is therefore one of trial and error. As mentioned earlier DiekA has a feature to overcome this problem, to adjust the total layer thickness reduction on pre-described value. However, during our calculations this feature did not work. Further complications are that estimating the vertical roller drum position has to be done carefully. When the drum is positioned to deep “in” the material it can be that the calculation does not work. A too high positioning of the drum can result in only elastic deformations.

Step 4

Do a simulation while the (plastic) layer thickness reduction is overestimated, calculate the required rolling drum force.

Step 5

Do a simulation while the (plastic) layer thickness reduction is underestimated, calculate the required rolling drum force.

Step 6

Calculate from the previous two steps by linear interpolation which plastic layer thickness reduction should fit to the given rolling drum force and calculate the correct thickness.

Step 7

Judge if the calculated rolling drum force corresponds to the given rolling drum force and if this is not the case repeat the previous step until the correct rolling drum weight is obtained with enough accuracy.

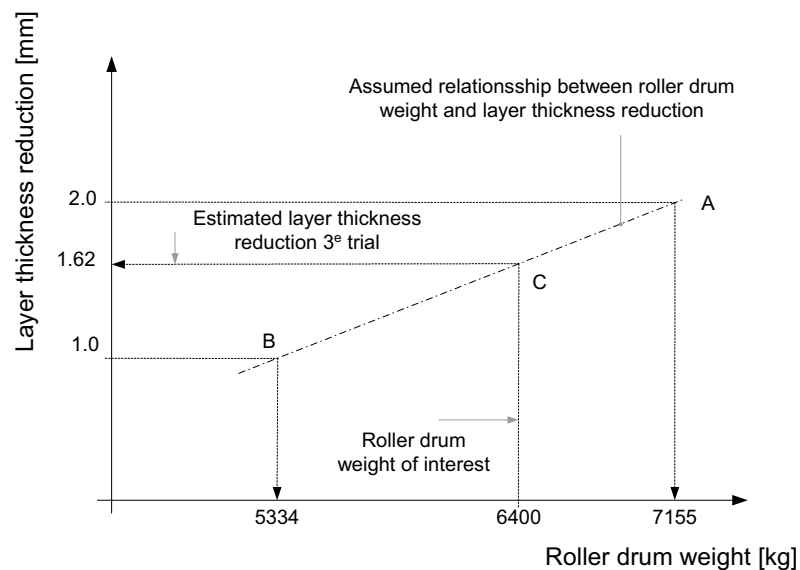


Figure 0.4 Interpolation procedure for the determination of the right roller drum weight related to measured layer thickness reduction. In this example 1.62 mm is the wanted layer thickness reduction.

During the steps 4 to 7 the correct relationship between layer thickness reduction and given roller weight can be obtained with an iterative procedure. This procedure is explained with help of Figure 0.4.

Example

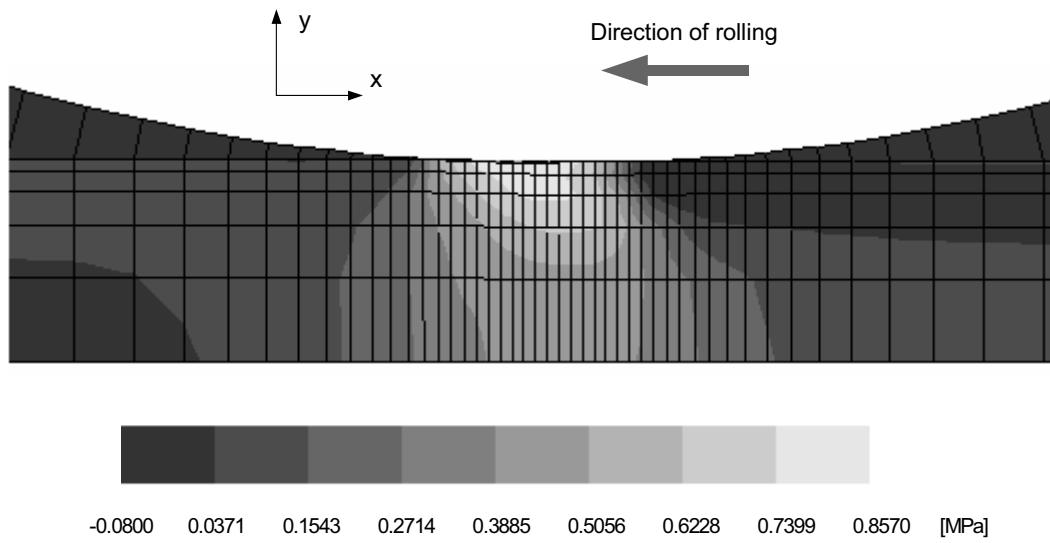
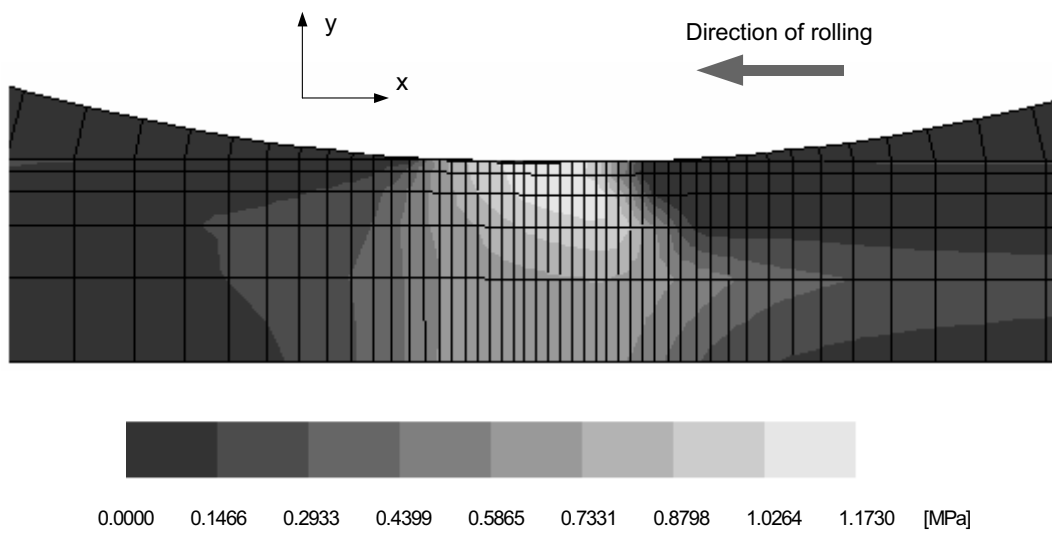
ITERATION PROCESS TO CORRECT LAYER THICKNESS REDUCTION		
Iteration step	<i>Y coordinate asphalt surface [mm]</i>	<i>Roller drum mass [kg]</i>
1	51.97	5334
2	51.83	7155
3	51.89	6403

Table 0.5 Iteration procedure for obtaining the correct layer thickness reduction. Target value of layer thickness reduction was from 52.29 mm (before applying roller pass) to 51.90 (after), simulation 3.5 on B lanes.

Step 8

An important control mechanism on FEM calculations is the visual check on the plausibility of the obtained stress and strain results. Most of them can be directly checked just after doing a run (i.e. without a conversion step). Here an example of the simulation of the first roller pass on the A lane of layer 2 will be given. It will be noted what particular details must be focussed on for checking the figures.

Items that have to be checked are; the stress and strain patterns inside/of the rolled material, the course of the free material surface, the penetration of the roller drum in the material (i.e. overlap), the particle tracing patterns and the length of the modelled material. If necessary and if the calculated results give cause for it, one or more model parameters should be tuned and subsequently the simulation procedure repeated. The different stress, strain, material deformation and material displacement patterns will be shown.

Stress patterns p' , q and xy inside the rolled material.**Figure 0.5** Isotropic normal stresses, p' , as a result of the first roller-drum pass 05 on lane B, layer 2.**Figure 0.6** Deviator stresses, q , as a result of the first roller-drum pass 05 on lane B, layer 2.

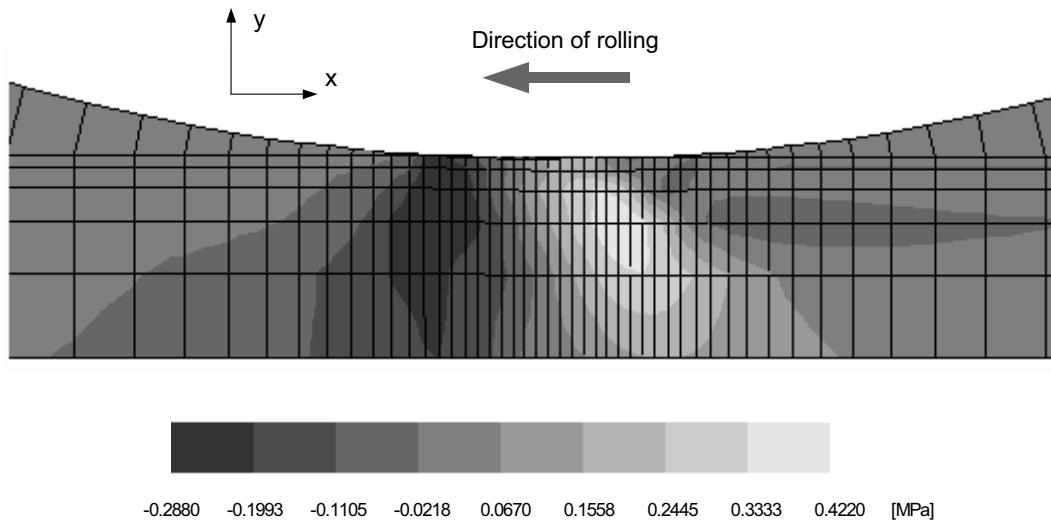


Figure 0.7 Shear stresses as a result of roller pass 05 on lane B, layer 2.

The simulated stress patterns inside the material as illustrated in the figures 0.1, 0.2 and 0.3 show that the major stress concentration (p' and q) occurs just underneath the contact interface roller drum - rolled material, high in the layer. The xy shear stress, as illustrated in Figure 0.7, changes from sign when the material is enforced underneath the rolling drum. At positions in front of the centre of the drum the shear stress (τ_{xy}) points in another direction related to positions behind the drum.

Strain patterns in the material.

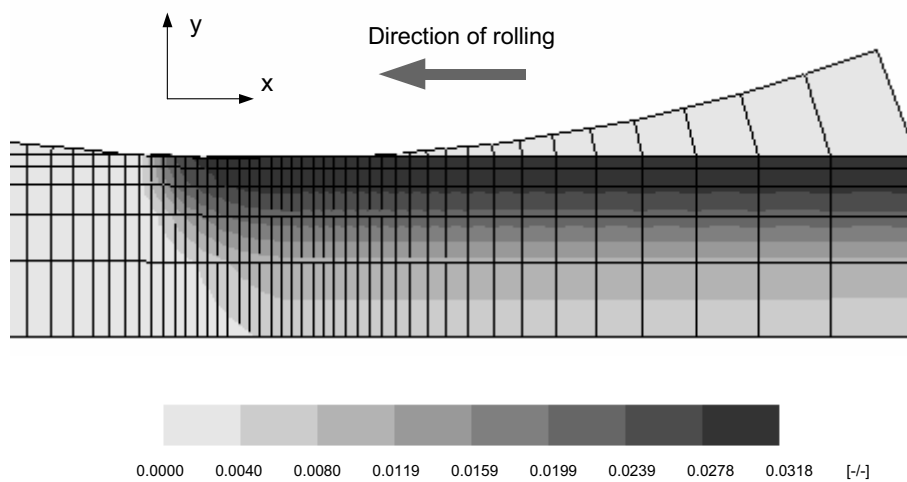


Figure 0.8 Irrecoverable volumetric strain as a result of roller pass 05 on lane B, layer 2.

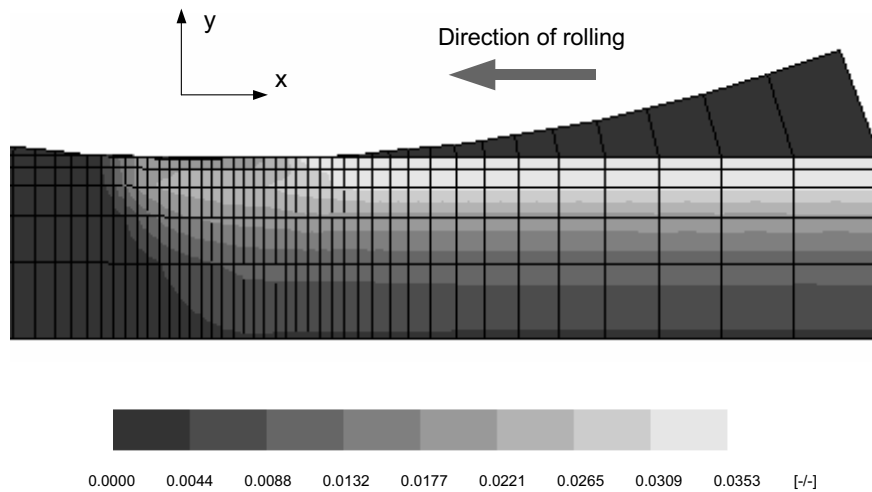


Figure 0.9 Irrecoverable deviatoric strain as a result of roller pass 05 on lane B, layer 2.

Figure 0.8 and Figure 0.9 indicate respectively the volumetric strain and shear strain achieved by FEM rolling simulations. The figures indicate that the biggest strains occur high in the layer, which is plausible because it concerns the simulation of the first roller pass on an initially homogeneously pre-compacted layer. It is possible that during later rolling drum simulations the majority of plastic deformation occurs deeper inside the layer. The strains do start around the roller drum and do continue in the downstream direction. Far upstream of the drum there is no plastic strain. Of course it concerns here “fresh” un-compacted material. One can also see that around the right vertical border there is no change in strain anymore, which appears to reason because otherwise it would indicate a too short modelled piece of material.

The free material surface and roller drum outline

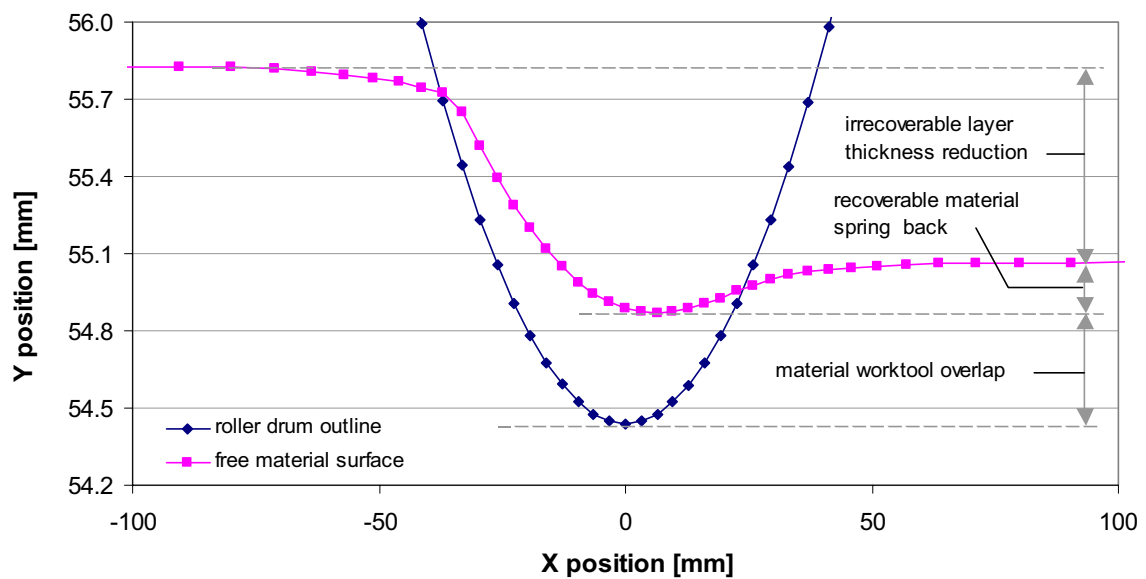


Figure 0.10 The free upper material surface of the HMA and the outline of the roller drum, pass 05, layer 2 lane B.

Figure 0.10 illustrates the position of the free material surface and the contour of the roller drum. The indications; a.) the way the free material surface flow's in front of and behind the drum, and, b.) the actual overlap between roller drum and rolled material.

a.) The gradually of flow of the free material surface informs about adjustment of contact stiffness related to the material stiffness. If such an adjustment is not acceptable it can deteriorate the accuracy of the calculated results. A poor adjustment would result in a swing of the free material surface from up to down around the average line. Also an incorrect distribution of the element mesh in horizontal direction may deteriorate the flow of the free material surface (e.g. too coarse mesh at positions where stresses highly vary).

b.) Figure 0.10 illustrates an overlap of roller drum and rolled material in-between of 0.4 to 0.5 mm. A too large overlap would deteriorate the representation of the roller drum stress pattern as is enforced on the layer. During this compaction research the overlap was limited on about 1.0 mm. However, the results indicated for these calculations show a limitation of the overlap on 0.4 to 0.5 mm would also be possible. The smaller the overlap the better the accuracy of the obtained results. On the other hand, a too small overlap (too stiff modelled contact) can result in numerical instability during the simulation.

Stresses p' and q

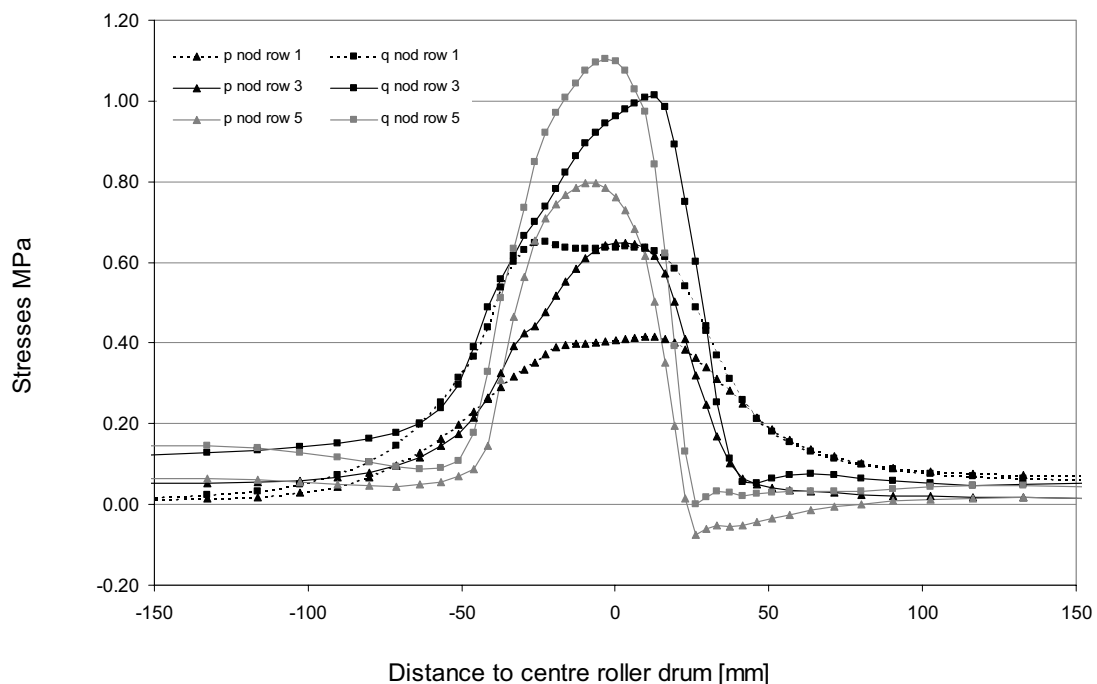


Figure 0.11 Isotropic normal compression stress, p' , and the deviator stress, q , at three depth levels inside HMA when it is rolled.

Figure 0.11 illustrates the path of stress level p' and q to which the material is applied as it is rolled. The figure illustrates the stress levels for three depths inside the layer; nodal row 1 at $y = 0.0$ mm, nodal row 3 at $y = 37.6$ mm and nodal row 5 at $y = 52.3$ mm. The figure that is high in the layer (nodal row 5) shows the stress levels are

relatively large and stresses are not spread over a large area in length direction. At the bottom of the layer stress levels are significantly reduced (with about a factor 1.75 till 2) but the stresses exists over a larger area. This mechanism indicates that the load enforced on the material is spread in the same way as is known for granular materials in general.

It can also be seen from the figure that the variations in p' and q became less then significant at y co-ordinates -150 and $+150$ mm. This implies that a modelled material length of 400 mm is sufficient. The figure indicates further that in particular at high positions inside the layer the deviator stress q is still increasing while the isotropic stress p' already declines (the stress paths as expresses in Figure 0.12 illustrate this too). This can indicate a sensible point of the HMA compaction process; a location of high q and low p' stress.

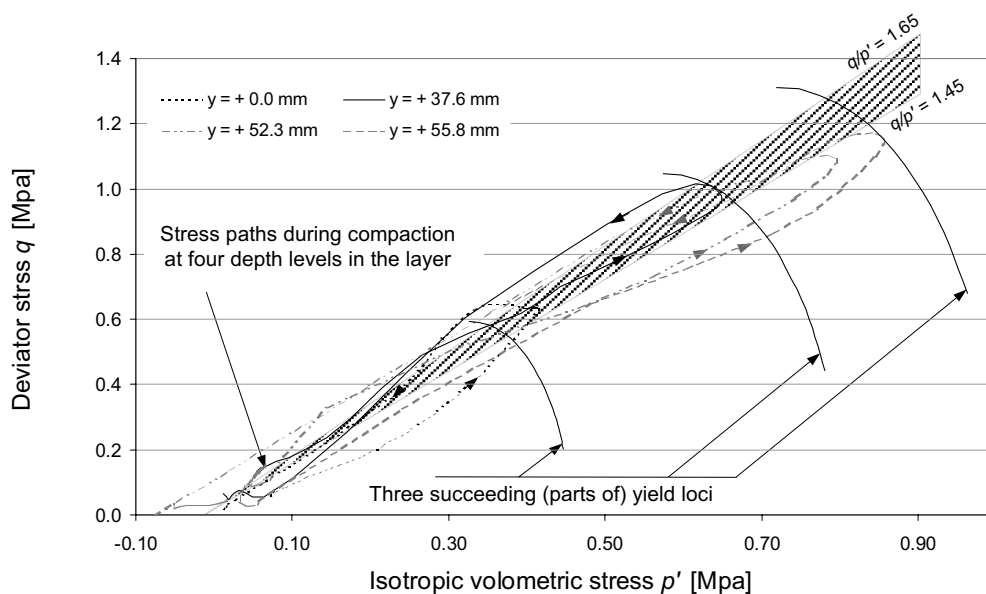


Figure 0.12 Stresses at four depth levels expressed in the $p':q$ plane together with three (parts of) yield loci.

Figure 0.12 indicates at what position (at what stress combination) the stress path hits the yield locus during rolling simulations compared to the stress conditions on the samples during the laboratory-measuring programme⁶. It would be favourable when the stress conditions during rolling proved to be not very different from the stress conditions during the material testing. The figure indicates that indeed the stress conditions were comparable. From the test results presented in chapter 3 it was concluded that during the laboratory measuring programme the q/p' ratio was in between 1.45 and 1.65 (or in between 1.52 and 1.65 when only the tests done with spring 2 are considered). This area is marked in the graph.

⁶ During the laboratory-measuring program, critical state parameters of the material were obtained. However during these tests, only a specific domain of stress conditions were enforced onto the samples.

Incremental material displacement

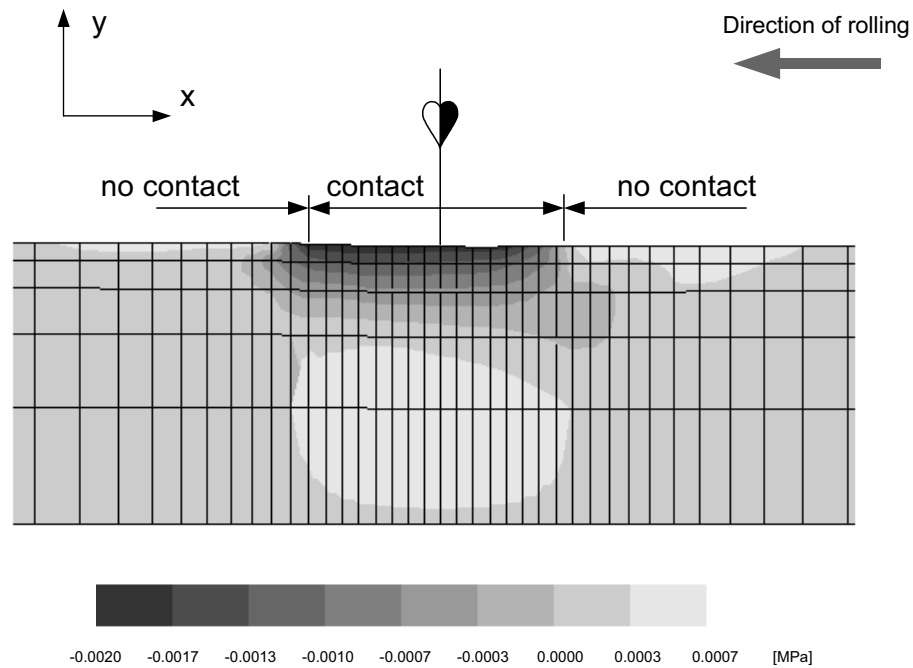


Figure 0.13 Incremental displacements in the x direction (i.e. horizontal material movement). A negative sign means movement in the rolling direction, a positive sign means movement reverse to the rolling direction. The enforced material displacement is 0.2 mm per step size in horizontal direction.

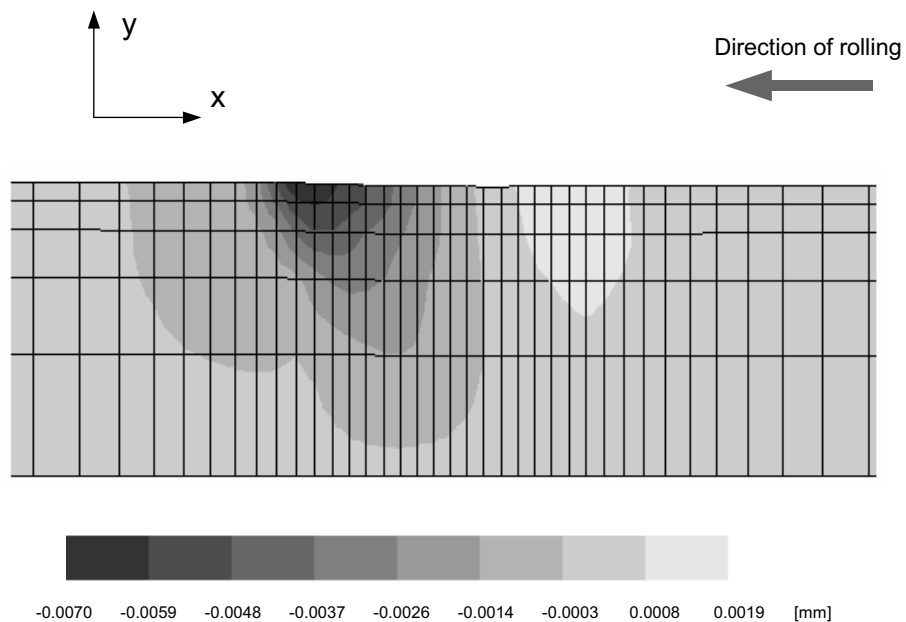


Figure 0.14 Incremental displacements in the y direction (i.e. vertical material movement). A positive sign means upwards material movement, a negative sign means movement downwards. The enforced material displacement is 0.2 mm per step size in horizontal direction.

Both figures 0.13 and 0.14 show the material displacement per loading increment for respectively the x and y direction. Figure 0.2 indicate that the biggest material

movement in the horizontal direction occurs around the rolling drum and in the direction of rolling (dark collared area). The figure also shows, on other locations (lighter collared areas) material movement slightly reverse to the rolling direction. This system looks plausible from the following point of view. Globally seen a road section that becomes rolled does stay in its position; it does walk in a horizontal direction. So there must be a balance in material movement. When there is movement in a certain direction (dark area) there must also be movement somewhere reverse to that direction.

Figure 0.14 indicates a vertical material movement downwards (dark area) just in front of the drum and a smaller movement upwards (lighter area) just behind the centre of the drum. Because the material becomes compacted the average material movement should be downwards. From the figure one can see that a strong concentration of the vertical movement is around the places where the drum touches the material and where this contact is lost.

Particle tracing

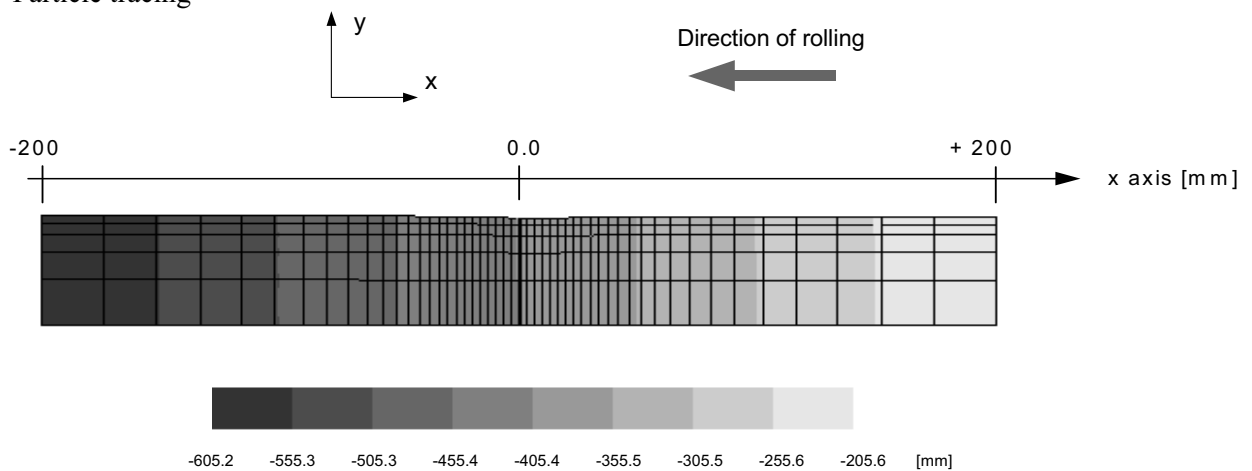


Figure 0.15 Particle tracing positions in the X direction.

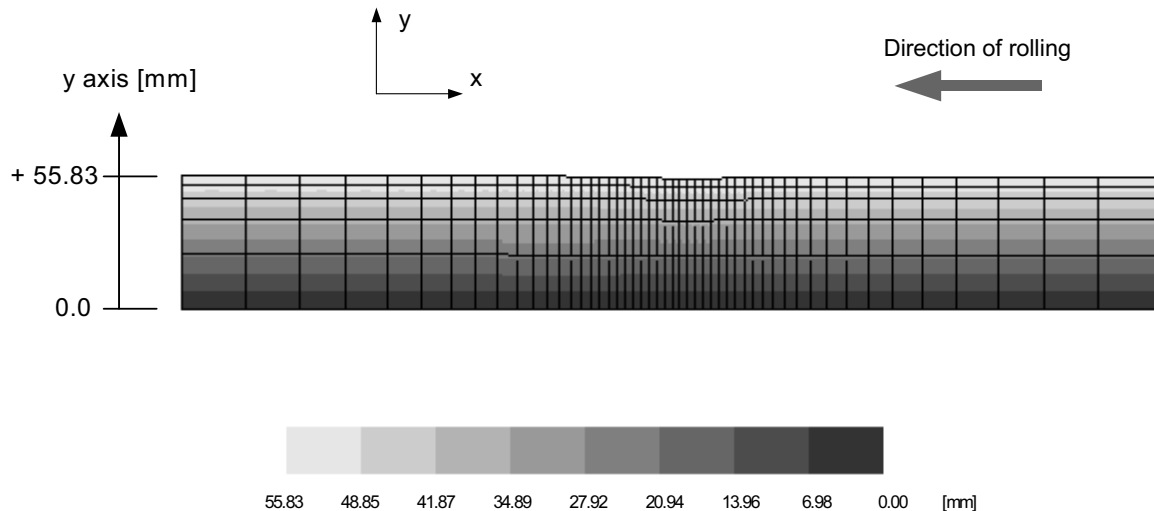


Figure 0.16 Particle tracing positions in the Y direction.

Figure 0.15 and Figure 0.16 indicate particle tracing in respectively the horizontal (i.e. x) and the vertical (y) direction. Particle tracing informs about the initial position of the material that is currently at that specific location. For example; the darkest area part in Figure 0.15 can be found in between the positions $x = -151.2$ and $x = -200$ mm. The legend show that this material came from in between $x = -605.2$ and $x = -555.3$ mm. This indicates that this material moved over a distance of $-605.2 - -200$ (or $-555.3 - -151.2$) = 405.2 mm. The same conclusion can be drawn for the lightest area. The global piece of material, local disturbances around the drum not considered, should move over around 406 mm because this was the pre-described boundary condition (for this calculation). The figure indicates that this happened.

Figure 0.16 indicates the particle tracing positions in the vertical direction. From the figure it can be seen that material that was initially at the top of the layer stays at the top and material that was at the bottom stays at the bottom just the way one expects. It would be strange that by rolling material that is initially at the bottom after rolling turns up at the top and v.v. The same view is held for material in between top and bottom. Both figures (0.15 and 0.16) indicate a neat stratification of the material and gradual transitions from one stage into another. They do not indicate incorrectness of the calculations.

Step 9

In step 1 the initial *VMA* level of the material was calculated (before rolling started). After doing the rolling pass simulation, the volumetric strain distribution in depth direction of the layer can be obtained from the output. This volumetric strain is required for calculation of the new *VMA* levels in depth direction of the layer. This “new *VMA* profile” will be used as input for the next rolling-drum pass simulation.

Example: The example will reflect the effect of volumetric strain at element rows 1 (i.e. from $y = 0.0$ mm to $y = 23.1$ mm), from the first applied roller drum pass (code 05) on B lane of layer 2.

Information obtained in step 1

In step 1 the following material information was calculated:

Density material after paving:	2068.0 kg/m ³
the Voids content;	HR _{INI} = 0.1440 -/-,
Bitumen content volumetric;	BIT _{INI} = 0.1172 -/-,
the initial VMA;	VMA _{INI} = 0.261 -/-.

Situation after the first roller drum pass (coded 05B)

As a result of the DiekA output for a specific roller pass the volumetric strain can be extracted at the six nodal points at different depths in the layer.

Material information.

Bulk density material after paving:
2068.0 kg/m³ (rel. to Marshall density 89%)

Calculated strains roller pass 05B element row 1,
 $\varepsilon_{vol} = 0.007943$ -/-

Bulk density after first roller pass at element row 1;
 $BD_{05} = 2068.0 / (1 - 0.007943) = 2085.0$ kg/m³

Voids percentage after first roller pass at element row 1;
 $HR_{05} = (1 - (2085.0 / 2416.6)) = 0.1370$ -/-

Bitumen content volumetric for element row 1:
 $Bit_{05} = (1 - HR) \times bit\ cont = (1 - 0.1370) \times 0.137 = 0.1182$ -/-

VMA of the material after 1 pass (05), element row 1;
 $VMA_{05} = HR + Bit = 0.1370 + 0.1182 = 0.2552$ -/-

A similar procedure must be applied in order to obtain the same “new material information” for the element layers 2 till 5. Material information about all element rows (i.e. 1 to 5) before and after applying a roller drum pass is summarised in Table 0.6.

RESULTS OF MATERIAL INFORMATION ROLLER PASS 05B					
<i>Element layer</i>	<i>1</i>	<i>2</i>	<i>3</i>	<i>4</i>	<i>5</i>
<i>Bulk density [kg/m³]</i>	2071.4				
<i>HR_{INI} [-/-]</i>	0.1429				
<i>BIT_{INI} [-/-]</i>	0.1174				
<i>VMA_{INI} [-/-]</i>	0.2603				
<i>ε_{vol} [-/-]</i>	0.007943	0.017042	0.026244	0.02633	0.030594
<i>Bulk density [kg/m³]</i>	2085.0	2107.3	2127.2	2127.4	2136.8
<i>HR₀₅ [-/-]</i>	0.1370	0.1280	0.1197	0.1167	0.1158
<i>BIT₀₅ [-/-]</i>	0.1182	0.1195	0.1206	0.1210	0.1211
<i>VMA₀₅ [-/-]</i>	0.2542	0.2474	0.2403	0.2377	0.2269

Table 0.6 Voids content, Bitumen content and VMA level before and after the first roller drum pass applied on layer 2 lane B.

Appendix O

A calculation to check the obtained roller forces

As can be seen in Figure 6.24 of Section 6.2 the rolling forces as calculated from the DiekA rolling simulations do not correspond to the real rolling drum weight. In this appendix the calculated rolling forces of the simulated passes 0.5 (the first roller drum pass in one direction) and 6.0 (after 6 roller passes) by means of DiekA will be compared to figures obtained by a rough calculation method. This all in an attempt to find the ground for the differences between the calculated roller-drum forces and the real ones.

The basic strategy during the following calculations is;

- Check the plausibility of the vertical stresses obtained by the FEM simulations to practical rule of thumb calculations.
- Calculate the force that is required for achieving the plastic part of the deformation.
- Calculate the force that is required for achieving the elastic part of the deformation and correction of the modelled, overestimated E value.
- Calculate the “corrected” total force and compare them to the force applied in reality.

General:

The roller drum weight of the used HAMM DV 6.42 was about 3.500 kg (i.e. 35.000 N). The roller drum was 1400 mm wide. This all implies that the roller drum loads⁷ the material with $35.000 / 1400 = 25 \text{ N/mm}$.

Roller pass 0.5B the first roller drum pass

The contact length as obtained from the rolling simulation was about 60 mm. The average contact stress between roller and rolled material can then be calculated on $25/60 = 0.42 \text{ N/mm}^2$.

If it is estimated that the peak stress is a factor 2 to 3 larger than the calculated average stress, the peak stress should be 2 to 3 times 0.42 is 0.83 to 1.25 N/mm^2 .

The maximum contact stress obtained from the simulation indicates 1.56 N/mm^2 . It can be concluded that the differences are not very large.

Further, from the simulation can be obtained that at a position where the vertical stress σ_{yy} is 1.56 N/mm^2 , the isotropic normal compression stress p' is about 0.66 N/mm^2 .

The ratio between σ_{yy} / p' is thus $1.56/0.66 = 2.36$.

When this factor is applied on the estimated peak stress of 0.83 to 1.25 N/mm^2 , the peak value of p' must have been; $(0.83 + 1.25) / (2 \times 2.36) = 0.44 \text{ N/mm}^2$.

⁷ For calculation of the roller drum load the assumption is made that the ends of the roller drums do not play a role, it is plausible that this contributes to an error in calculating the actual roller drum weight. In the calculation we use a load per mm over the whole width of 1400 mm.

When it is considered that plastic deformation of roller pass 0.5B started at a p' of 0.36 N/mm^2 , the plastic deformation in the peak zone area can be calculated. For this calculation use is made of the slope of the irrecoverable branch of the modelled material behaviour as obtained in chapter 3 (see also Figure 0.1).

$$\delta VMA = 0.25 \times (\log(0.465) - \log(0.36)) = 0.03 \text{ [-/-]}$$

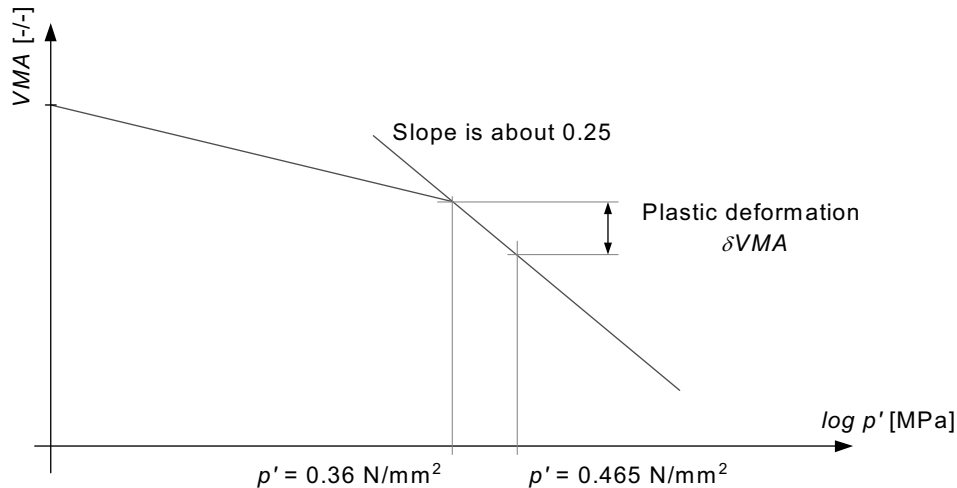


Figure 0.1 Estimating the plastic strain based on critical state information.

The initial VMA value was 0.26 so the volumetric strain is around $0.03/1.0 = 0.03 \text{ [-/-]}$ (3%). If it is further estimated that this strain in the peak stress region exists over about 30% of the height of the layer the average plastic deformation (relative layer thickness reduction) becomes $0.3 \times 0.03 = 0.01 \text{ [-/-]}$.

Compared to the layer thickness reduction that is prescribed for this roller pass (around 1 mm on 50 mm i.e. 0.02) this obtained strain by DiekA looks too large but is at least in the same order.

A rough guess of the force required for achieving this plastic deformation can also be made. From the figures that express plastic volumetric strain (Figure 0.2) it can be obtained over what length the material deforms plastic. For roller pass 0.5 this is over a length of about 39 mm (from $x = -39 \text{ mm}$ to $x = .0 \text{ mm}$). At that area the vertical stress is about 1.12 N/mm^2 . From these figures the vertical force for achieving the plastic deformation can be estimated; $1.12 \times 37.5 = 42 \text{ N/mm}$. The force that was calculated by means of the DiekA simulation (sum of elastic and plastic part) was 69 N/mm. The force for realisation of the elastic part of the deformation can then be calculated on $69 - 42 = 27 \text{ N/mm}$. When it is assumed that this force for achieving the elastic deformation must be around a factor 20 too large (because the E modulus as modelled is a factor 20 too large), the total roller drum force can be calculated on $42 + 27 \times 0.05 = 43.3 \text{ N/mm}$ (i.e. a vertical roller drum weight of 6062 kg).

The rolling drum force applied in reality was 25 N/mm so using this approximation an error still remains of about 73%.

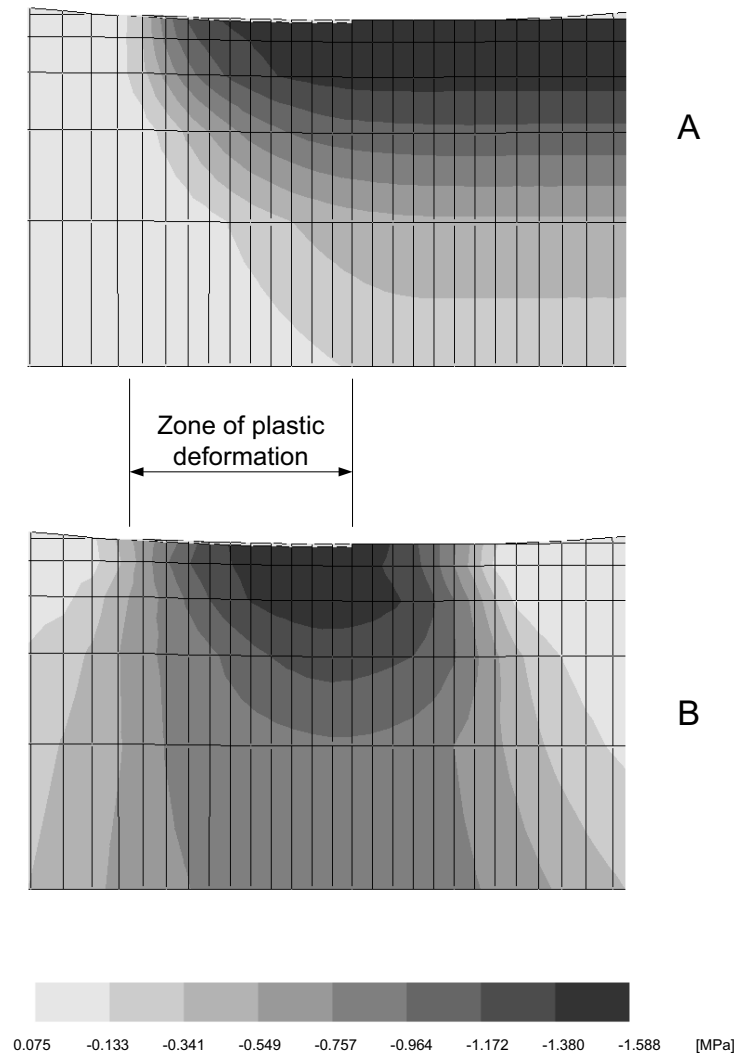


Figure 0.2 The volumetric strain (A) and the vertical stress (B) obtained from the DiekA simulation, pass 0.5B.

Roller pass 6.0B

For the succeeding roller drum passes it is more complex to estimate the contact stress during compaction. However, a similar procedure for calculating the rolling drum force was done. The vertical stress, σ_{yy} , in the zone where deformation is plastic is obtained on around 11.3 N/mm², see Figure 0.3. Note that this is totally outside the stress level⁸ used in the MHSM. The length of the zone of plastic deformation is 16.1 mm. The vertical force for achieving this plastic deformation can be estimated on $11.3 \times 16.1 = 182$ N/mm. The force that was calculated by means of the DiekA simulation (sum of elastic and plastic part) was 909 N/mm. Thus the force for realisation of the elastic deformation can therefore be calculated on $909 - 182 = 727$ N/mm. When it is assumed that this force for achieving the elastic deformation was around a factor 20 too large, the total roller drum force can be calculated on $182 + 727 \times 0.05 = 219$ N/mm. The rolling drum force in reality applied was 25 N/mm so there still exists an error of approx. factor 8.7, which is large. A roller drum force of 219 N/mm corresponds to a roller drum weight of 30.660 kg (30.6 tonne).

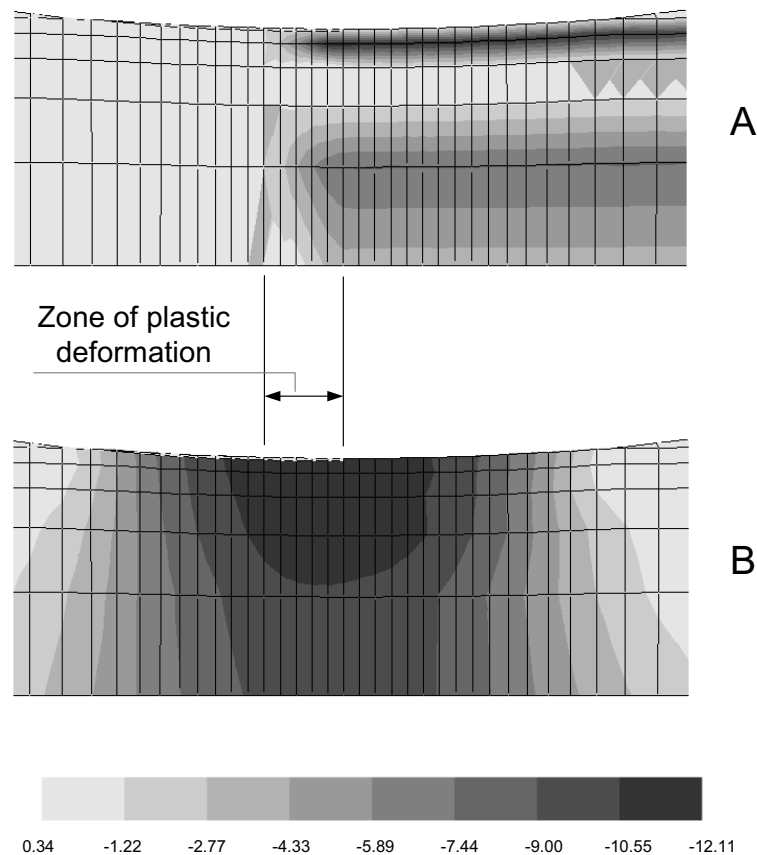


Figure 0.3 The volumetric strain (A) and the vertical stress (B) obtained from the DiekA simulation, pass 6.0B.

⁸ During the material measuring program the HMA material was loaded until about axial stresses of 3 to 4 MPa.

Because there still remains a large difference between the calculated roller drum force and reality (after the value was corrected for the too large E modulus) it is also expected that additional causes for the error must exist. Analysis of the stresses due to rolling indicate that the maximum stress in the plastic zone (i.e. 11.3 N/mm^2) of the simulation is much higher than reasonably can be expected based on a roller drum weight of 25 N/mm . A possible cause for this far too high stress might be illustrated with help of Figure 0.4. The average VMA value of the material before roller pass 6.0 was applied was about 0.205 [---] (obtained from test sections results). If, with respect to critical state principles, a recoverable line is depicted inside the $VMA:\log p'$ area, it can be seen that material with such a VMA level starts to behave plastic at a stress level, p' , of about 6.45 N/mm^2 . This is also a high value related to the vertical roller drum force of 25 N/mm . However, plastic deformation must occur in the simulation because the simulation is driven on a certain extent of plastic deformation (plastic layer thickness reduction). The fact that the material must be loaded to that (too) high stress level can probably be explained by the fact that the real $VMA:\log p'$ curve deviates from the critical state model line, illustrated in Figure 0.4.

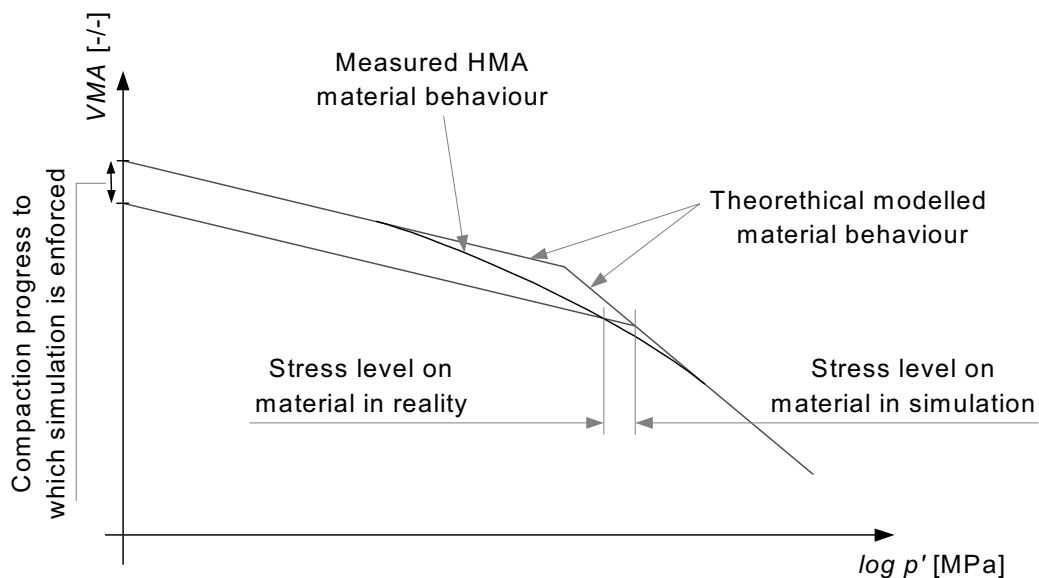


Figure 0.4 The difference in real and modelled material behaviour during plastic deformation.

List of codes and abbreviations

ALE	= Arbitrary Lagrangian Eulerian method
AVV	= the Transport Research Centre of the Dutch Ministry of Transport, Public Works and Water Management
BTDC	= Bitumen test data chart
CMC	= Critical moisture content
CRS	= Computational reference system
DiekA	= Name of the used FEM software
DAC	= Dense asphalt concrete
DE	= Divided Europe scenario
EC	= European coordination scenario
FEM	= Finite element method
HSM	= Hveem Stabilometer
HTM	= High temperature mixture
GC	= Global competition scenario
LT	= Layer thickness of asphalt
LBC	= Low bitumen content mixture
MTM	= Medium temperature mixture
MC	= Mohr Coulomb failure criterion
MRS	= Material reference system
MHSM	= Modified Hveem Stabilometer
REF	= Reference asphalt mixture
RM	= Mixture with more round sand
Rock	= Used material model within DiekA
SRS	= Spatial reference system
SP1	= Mixture tested at higher confining stiffness
VMA	= Voids in the mineral aggregate
VFB	= Voids filled with bitumen

List of symbols

A_{top_cap}	= Contact area top-cap sample
A_{pist}	= Piston area
A_{curr_rad}	= Current calculated radial sample area]
C	= a fixed value (gas equation)
C	= A value for the compactibility of a sample (C-value method)
C	= Factor for the roller type (rolling, Nijboer)
C_n	= Stiffness in normal direction of the contact element
C_t	= Stiffness in shear direction of the contact element

D	= Diameter of the roller drum (Nijboer)
D_o	= Initial density of the asphalt
E	= modulus of elasticity
F	= Rolling drum loading force on the material
F_{ax}	= Axial loading force on the sample
LT_N	= Layer thickness after roller pass N,
LT_∞	= Theoretical layer thickness after an infinite number of roller passes
LT_o	= Layer thickness before compaction starts
N	= Applied number of roller passes,
P_{oil}	= Measured oil pressure
H_{cur}	= Current sample height
P	= Weight of the roller drum (Nijboer)
P	= Pressure (gas equation)
P'	= Oil pressure in Stabilometer
p'_{int}	= Pressure of intersection point of the the bilinear (critical state) model
R_f	= Indicator for how far compaction is progressed (Nijboer)
R_{ini}	= Initial sample radius
R_{cur}	= Current sample radius
S	= The amount of compaction energy applied to a sample under compaction
V	= Volume in mm^3
VMA	= Voids in the Mineral Aggregate of a sample.
VMA_o	= Initial VMA value of the asphalt
VMA_κ	= (scaled) VMA value for recoverable material behaviour at $p' = 1$ MPa
VMA_λ	= (scaled) VMA value for irrecoverable material behaviour at $p' = 1$ MPa
VMA_I	= Average VMA value for starting a series of tests, also the scaling value
VMA_{int}	= VMA value of intersection point of the bilinear (critical state) model
S	= Estimated slope of the model
T	= Temperature in
T_{HMA_c}	= Current HMA material temperature
T_{air}	= Current air temperature
dT	= Temperature difference between the two objects
dx	= Distance between the two objects
e	= The volume of voids in a sample related to the volume of solids.
g_{ref}	= Reference deformation of the contact element in normal direction
h	= Thickness of the layer (Nijboer)
h_{ini_aver}	= Deduced average initial sample height
l	= Width of the roller drum (Nijboer)
t	= Time in minutes after spreading
q''	= Heat flux (indicator for amount of heat that is lost)
v	= The specific volume of a sample
t	= time in sec.
p'	= Effective isotropic normal compression stress (critical state)
q	= Deviator stress

α	= Factor representing the progression of the compaction (chapter 5)
α	= Thermal expansion coefficient of a material (chapter 3)
α_v	= Phase angle of loading signal
α_g	= Phase angle of deformation signal
δ_{ax}	= Measured axial sample deformation
δ_{rad}	= Measured radial sample deformation
δ_{pist}	= Piston displacement of the modified Hveem Stabilometer
δ_{ax}	= Axial deformation of the sample [mm]
δT_C	= Current difference between material and air temperature
δT_{INI}	= Difference between material and air temperature during paving
ε	= Volumetric strain of a sample
ε_{vol}	= Volumetric Strain
ε_{sh}	= Shear Strain
ε_{ax}	= Axial strain of a sample
ε_{rad}	= Radial strain of a sample
ε_{sh_pl}	= Plastic part of the shear strain
ε_{vol_pl}	= Plastic part of the volumetric strain
γ	= Factor between LT_o and LT_∞
γ	= Shear strain of a sample
η	= Viscosity of the (HMA) mass.
η_m	= The viscosity of the mass of the compacted mixture (Nijboer)
φ	= Obtained phase shift angle (complex modulus method)
φ	= Angle of internal friction (soil mechanics)
κ	= (scaled) Slope of irrecoverable material behaviour in the $VMA\text{-}log p'$ plane (critical state)
κ	= Thermal conductivity coefficient of the material (chapter 5)
λ	= (scaled) Slope of recoverable material behaviour in the $VMA\text{-}log p'$ plane (critical state)
μ	= Friction in the interface layer (between roller drum and rolled material).
ν	= Poissons ratio
ν	= Speed of the compactor (Nijboer)
ρ	= Density of a material or sample
ρ_{AS}	= The bulk density of a sample as a function of S
ρ_{A0}	= The bulk density of a sample at the start of the compaction process
$\rho_{A\infty}$	= The maximum achievable Density of a sample
σ	= Normal stress on a sample
σ_{ax}	= Axial stress on a sample
σ_{rad}	= Radial stress on a sample
σ_n	= Stresses in normal direction of the contact element
σ_{ref}	= Reference stresses in normal direction of the contact element.
σ_t	= Stresses in tangential direction of the contact element
τ	= Shear stress of a sample
τ	= Internal resistance of mixture (Nijboer)
τ_E	= Complex internal resistance (Gauer)
τ_{cb}	= Initial resistance of the bituminous mixture (Nijboer)

References

- Abd El Halim, 2004. <http://www.civeng.carleton.ca/~ahalim/amir.html>, 08-02-2004.
- Arand, W., 1972. *Verdichtungsgrad oder Hohlraumgehalt als Abnahmecriterium? (Compaction rate or voids content as control criterion?)*. Bitumen-Teere-Asphalt-Peche 23(7), 1972.
- Arand, W., 1974. *Verdichtung - mathematisch-analytisch betrachtet (Compaction, mathematical and analytical considered)* Bitumen-Teere-Asphalt-Peche, 25(11) 1974.
- Arand, W., 1985. *Compaction of classifying characteristics for asphalt mixtures. Proceedings of Third Eurobitume symposium*. The Hague, 11-13 September 1985.
- Arand, W., et al, 1987. *Arbeitsanlagen für die Bestimmung der Verdichtbarkeit von Walzasphalt mit Hilfe des Marshallverfahrens, (Operational instructions for deduction of the compactibility of asphalt by means of the Marshall compactor)*. Forschungsgesellschaft für Straßen und Verkehrswesen, Köln.
- Arquié, G., 1973. *Verdichtung van grond, (Compaction of soils)*. Wegen, 47(8) 1973.
- Asphalt Institute, 1989. *The Asphalt Handbook*. The Asphalt Institute, USA.
- Atkinson, J.H., 1993. *The Mechanics of Soils and Foundations*. McGraw-Hill, London.
- Barnes, G.W., 1995. *Soil mechanics, Principles and Practice*. Mc Millan, London.
- Böhmer, P., 1974. *Verdichtung Bituminösen Mischgutes beim Einbau mit Fertigern, (Compaction of bituminous mixtures during paving)*. Ph.D. thesis Universität Karlsruhe, Karlsruhe.
- Bossemeyer, H.R., 1966 *Temperaturverlauf beim Einbau von bituminösem Mischgut (The effect of temperature during pavement and compaction of bituminous mixtures)*. Ph. D. thesis, Technischen Hochschule Darmstadt, Darmstadt.
- Brekelmans, W.A.M., 1989. *A simulation method for the die compaction of granular materials*. Ph.D. thesis Eindhoven Technical University, Eindhoven.
- Bruce, B.A., et al, 1998 *An asphalt paving tool for adverse conditions*. Technical report, University of Minnesota, Minnesota?? (USA).
- CBS, 2003. <http://statline.cbs.nl/StatWeb/start.asp?lp=Search/Search>, 12-06-2003.
- C.R.O.W, 1995. *Standaard RAW Bepalingen 1995 (RAW Standard Conditions of Contract for Works of Civil Engineering Construction 1995)* C.R.O.W, Ede.
- Cronney, D. and P. Cronney, 1991. *The Design and Performance of Road Pavements*. McGraw-Hill, London (UK).
- Daines, M.E., 1985. *Cooling of bituminous layers and time available for their compaction*. TRRL, Crowthorne.
- Daines, M.E., 1986. *Cooling of bituminous layers and time available for their compaction. Proceedings of Third Eurobitume symposium*. The Hague, 11-13 September 1985. pp 237-242,
- Daines, M.E., 1995. *Tests for voids and compaction in rolled asphalt surfacing*. TRL Project Report 78, Crowthorne (UK).

- Di Benedetto, H. and Ch. de La Roche, 1998. *State of the Art on Stiffness Modulus and Fatigue of Bituminous Mixtures*. Bituminous Binders and Mixes, L. Francken, Spon, London (UK). RILEM Report 17, pp 135-180.
- Eekelen, S.J.M. van and P. van den Berg, 1994. *The Delfst Egg model, a constitutive model for Clay*. DIANA Computational mechanics '94, Kluwer, Dordrecht, pp 103-116.
- Figge, H., 1987. *Verdichtungs- und Belastungsverhalten Bituminöser Gemische, (Compactibility and mechanical behaviour of bituminous mixtures)*. Ph.D. thesis, Technische Hochschule Aachen, Aachen.
- Gauer, P.K., 1975. *Eine Analyse der Verdichtungswilligkeit und des Verformungswiderstandes von bituminösem Mischgut bei Verdichtung im Gyrator, (Analyses of the compactibility of a bituminous mixture and the resistance against deformation when compacted by means of a gyratory compactor)*. Ph.D. thesis, Technische Hochschule Darmstadt, Darmstadt.
- Geller, M., 1984. *Compaction Equipment for Asphalt Mixes. Placement and Compaction of Asphalt Mixtures*, American Society for Testing and Materials, Special Technical Publication 829, pp. 28-47. Wagner, Philadelphia.
- Head, K.H., 1980 *Manual of Soil Laboratory Testing*, Vol. 1. Pentech, London (UK).
- Hopman, P.C. and J.H. Dijkink, 1994. *Een functionele ontwerpmethod voor asfaltmengsels, (A functional design method for asphalt mixtures)*. CROW, publicatie 82, the Netherlands,
- Huet, C., 1963. *Etude par une méthode d'impédance du comportement viscoélastique des matériaux hydrocarbonés*, Thèse de Docteur Ingénieur, Faculté des Sciences de l'Université de Paris. Paris.
- Huschek, S., 1980. *Zum Verformungsverhalten von Asphaltbeton unter Druck, (The deformation behaviour of asphalt mixes under triaxial pressure)*. Ph.D. thesis, ETH Zürich, Zürich.
- Hveem, F.N. and H.E. Davis, 1950. *Some concepts concerning triaxial compression testing of asphaltic paving mixtures and subgrade materials*. A compilation of papers Presented at the First Pacific Area National Meeting, San Francisco, 10 october 1949 and Fifty-Third Annual Meeting, Atlantic City 28 june, 1950. pp 25-54, ASTM, Philadelphia (USA).
- Incropera, F.P. and D.P. DeWitt, 1996. *Fundamentals of heat and Mass Transfer*. John Wiley & Sons, New York (USA).
- Jacobs, M.M.J., 1995. *Crack Growth in Asphaltic Mixes. Ph. D. thesis Delft University of Technology, Delft*.
- Kezdi, A., 1969. *Handbuch der Bodenmechanik, (Handbook for soil mechanics)*. Verlag für Bauwesen, Berlin.
- König, F., 1969. *Verdichtung im Erd- und Strassenbau, (Compaction of embankments and roads)*. Bauverlag, Wiesbaden.
- Leech, D. and N.W. Selves, 1976. *Modified rolling to improve compaction of dense coated macadam*. TRRL Laboratory Report 724, Crowthorne (UK).

- Leech, D. and W.D. Powell, 1974. *Levels of compaction of dense coated macadam achieved during pavement construction*. TRRL Laboratory Report 619, Crowthorne (UK).
- Leech, D., 1979. *Trails of a modified specification for compacting dense roadbase and basecourse coated macadam*. TRRL Laboratory Report 891, Crowthorne (UK).
- Nijboer, L.W., 1942 *Onderzoek naar den weerstand van bitumen-mineraalaggregaat mengsels tegen plastische deformatie, (Research after the resistance of bitumen-aggregate mixtures against plastic deformation)* Noord Hollandsche uitgevers maatschappij, Amsterdam.
- Nijboer, L.W., 1948. *Plasticity as a factor in the design of dense bituminous road carpets*. Elsevier, New York.
- Min. v VWS, 1995. *Actuele wegenlijst, stand per juli 1995 (Current road list of July 1995)*. Ministerie van Verkeer en Waterstaat, The Hague.
- Min. v VWS, 1988-1991. *Tweede Structuurschema Verkeer- en Vervoer (Second Transport Structure plan)*. SDU, The Hague.
- Min. v VWS, 2000. *Nationaal Verkeer en Vervoersplan 2001 - 2020 (The Dutch Traffic and Transport plan for 2001 - 2020)*. Ministerie van Verkeer en Waterstaat, The Hague.
- Min. v VWS, 2001. *Kerncijfers personen vervoer 2001 (figures of the Dutch Traffic for 2001)*. Ministerie van Verkeer en Waterstaat, The Hague.
- Min. v VWS, 2002. *Jaarrapport verkeersgegevens 2001 (Annual report traffic figures 2001)*. Ministerie van Verkeer en Waterstaat, The Hague.
- Partl, M.N. and L. Francken, 1998 *Backgrounds of RILEM interlaboratory tests. Bituminous Binders and Mixes, L. Francken, Spon, London (UK)*. RILEM Report 17, pp 1-10.
- Paulmann, G., 1969. *Vorgänge und Gesetzmässigkeiten bei schlag- und gyratorisch verdichtetem bituminösem Mischgut, (Basic rules and procedures for blow- and gyratory-compaction of asphalt mixtures)*. Ph.D. thesis, Technische Hochschule Darmstadt, Darmstadt.
- Paulmann, G., 1970. *Verdichtungs Vorgänge und Verdichtungswiderstand bei bituminösen Mischgut (Compaction progression and compaction resistance of bituminous mixtures)*. Bitumen, no. 2, february 1970.
- Pike, D.C., 1972 *Compactibility of graded aggregates; Standard laboratory tests*. TRRL Laboratory Report 447, Crowthorn, Berkshire (UK).
- Powell, W.D. and D. Leech, 1982. *Standards for Compaction of Dense Roadbase Macadam*. TRRL Supplementary Report 717.
- Powell, W.D. and D. Leech, 1983. *Compaction of bituminous road materials using vibratory rollers*. TRRL Laboratory Report 1102, Crowthorne, (UK).
- Powell, W.D. et al., 1980. *Dense graded bituminous macadams: effect of mixture variables on compactibility*. Proceedings of International conference on compaction, Laboratoire Central des Ponts et Chaussées, Paris, 22 - 24 april 1980. Pp 457-462, Ed. Anciens ENPC, Paris.

- Renken, P., 1980. *Verdichtbaarheid van Asphaltbetongemischen und ihr Einfluss auf die Satndfestigkeit (Compactibility of asphalt mixtures and the effect of it on bearing capacity)*. Technische Universitat Carola-Wilhelmina, Braunschweig.
- Rietman, B., 1998. *DiekA manual, Release 5.0*, University of Twente, Enschede.
- Robberts, F.L. et al, 1996. *Hot Mix Asphalt Materials, Mixture design, and Construction*. NAPA, Lanham (USA).
- Roscoe, K.H. and J.B. Burland, 1968. *On the generalized behaviour of 'wet' clay*. Engineering Plasticity, J. Heyman and F.A. Leckie, Eds., Cambridge University Press, London (UK). pp. 535-609.
- Schofield, A.N. and C.P. Wroth, 1968. *Critical State Soil Mechanics*. McCraw-Hill, London.
- Schwartz, E.G., and A.R. Holland, 1969. *Determination of yield criterion for iron powder undergoing compaction*. *International Journal of Powder Metallurgy*, Vol. 5, pp 79.
- SCW, 1970. *Mededeling 24, Resultaten proefvakken 1967, Toepassing van de bandenwals (Record no. 24, Results test sections 1967, the use of pneumatic tired rollers)*. SCW, Arnhem.
- SCW, 1971. *Mededeling 26, Resultaten proefvakken 1968, Toepassing van de bandenwals (Record no. 26, Results test sections 1968, the use of pneumatic tired rollers)*. SCW, Arnhem.
- SCW, 1978. Record no. 3, *Compaction of thin asphalt layers*. SCW, Arnhem.
- Semmelink, Ch. J., 1991. *The effect of material properties on the compactibility of some untreated roadbuilding materials*. Ph.D. thesis, University of Pretoria, Pretoria.
- Shell, 1990. *The Shell bitumen Handbook*. Shell, Chertsey (UK).
- Swanson, R.C. et al., 1996. Effect of Asphalt Viscosity on Compaction of Bituminous Concrete. Highway Research Record, Vol. 117.
- SWOV, 2003. http://www.swov.nl/nl/kennisbank/25_mobimiteit/mobiliteit_per_jaar_voertuig_en_weg.htm, 09-10-2003.
- Ter Huerne, H.L. and M.F.A.M. van Maarseveen, 1996. *Het spanningsveld tussen uitvoeringsomstandigheden en kwaliteit (The field of tension between circumstances during construction and quality)*. Wegbouwkundige werkdagen 1996, pp 1299 - 1311. CROW, Ede.
- Ter Huerne, H.L., 1997. *Asfalteren bij duisternis en regen leidt tot minder goed wegdek (Paving of asphalt roads during adverse weather conditions results in reduced quality)*. *Wegen*, 71(4), april 1997, pp. 16-19
- Ter Huerne, H.L., 2000. *Possibilities for material characterisation and FEM simulation of compaction processes of asphalt pavements*. HERON, Vol. 45 no. 3, Delft.
- Teunissen, J.A.M., 1983. Internal notes used for development of the DiekA Rock model.
- Van den Boogaard, A.H., 1995. *Arbitrary Lagrangian Eulerian Analysis in DIANA*. TNO building and Construction Research report 95-NM-R1002 TNO, the Hague.

- Van den Boogaard, A.H., 1995. *Contact elements for geometrically nonlinear analysis*. TNO building and Construction Research report 95-NM-R1003.TNO, the Hague.
- VBW-Asfalt, 1997. *Gyratorworkshop. Een "nieuwe" laboratoriummethode voor het verdichten van asfalt, (Gyratory compactor workshop; a new laboratory method for compaction of asphalt)*. VBW-Asfalt, the Netherlands, no.1, march .
- Vermeer, P.A., 1980. *Formulation and analysis of sand deformation problems*. Ph.D. thesis, Delft University of Technology, Delft.
- VBW-Asfalt, 2000. *Asfalt in wegen en waterbouw, (Asphalt used for civil engineering purposes)*. VBW-Asfalt, the Netherlands.
- Verschuren, P., and H. Doorewaard, 1995. *Het ontwerpen van een onderzoek (The design of a research)*. Lemma, Utrecht.
- Vizi, L. and C. Büttner, 1981. *Verdichten von Asphalt im Strassenbau (Compaction of asphalt roads)*. Werner Verlag, Düsseldorf.
- Wood, D.M., 1990. *Soil Behaviour and Critical State Soil Mechanics*. Cambridge University Press, Cambridge.



Curriculum Vitae

Henny ter Huerne was born on the 12 April 1961 in Enschede, Netherlands. He studied according to the principles which were shaped by what is called “de Mammoet wet” in the Netherlands. He started with MAVO (equivalent to O-level) schooling, followed by MTS (technical school medium level, 1977-1980) and HTS (technical school higher level, 1980-1984). After military service (1984-1986) he studied Civil Engineering between 1986 and 1990 at Delft University of Technology (TU-Delft).

During his HTS master project he designed a bridge made of pre-tensioned concrete that crosses the Twente canal in the Eefde neighbourhood. During his military time he was a sergeant in the Genie (a bridge building division of the army). During the last period of his academic schooling he specialised in structural engineering. His masters project subject was to design, construct and engineer a double curved structural glass and steel roof. After his academic education he worked for three years at DHV as a consultant in the engineering of concrete and steel structures used for water supply and sewage systems. At the end of 1992 Henny started working at the Traffic and Transportation (T&T) group in the department of Civil Engineering at the University of Twente (UT). Because of his position inside the T&T group it was natural that his research was in the direction of “construction and maintenance of transport infrastructure”. Since the start of his job at UT he was involved in teaching topics such as: design of civil structures and infrastructure, mechanics of constructions and road and traffic engineering. He also coached a number of students doing practical training or their master thesis projects. During his time at the UT the author built up and maintained a joint co-operation with the RRL (Road and Railroad Laboratory) group of the TU-Delft.

Currently he works at the UT, but has moved from the T&T group to the Structural Engineering (BT) group. It is clear that inside this group his experience gives scope for structural engineering project research.